THE UNIVERSITY OF LIVERPOOL

Mo- Modified HZSM-5 Zeolite for the Dehydro-oligomerisation and Aromatisation of Methane in the Absence of Oxygen

Thesis submitted in accordance with the requirements of the University of Liverpool for the degree of Doctor in Philosophy

by

Chandra Mohan Sinnathambi

December 2005

Acknowledgements

I would like to thank my Supervisor Dr. JB Claridge, for his guidance and support throughout the major part of my PhD studies, Professors EG Derouane and Professor J Vedrine for their guidance during the first year of my PhD studies

I would also like to thank the technical staff of the Liverpool Centre for Material and Catalysis, especially Mr. Brian Townley, Steve Apter, Dr. Arthur Greene, Gordon Bostock, John Gilmore, Peter Halliwell and Paul Cross for their invaluable technical assistance and advice. Furthermore I would also like to thank the former as well as present students and Lecturers of the Liverpool Centre for Material and Catalysis with special mention to Drs. Elena Kozhevnikova, Tanya Stuchinskaya, Jaspal Kaur, Neil Winterton and Robin Whyman for their friendship and generous help during my studies. Also I would like to thank the other staff of the University of Liverpool who helped me either directly or indirectly.

I would like to thank Universiti Teknologi Petronas Malaysia, my sponsor and employer, for funding me throughout the full duration of my course. Not forgetting to mention the University of Liverpool for accepting me as a student.

Last but not least I would like to thank my family especially my wife, Devi, and my children Harren and Mira for their love, patience, sacrifice and for being a constant source of encouragement throughout the full duration of my PhD. course.

ABSTRACT

Methane dehydrogenation aromatisation (MDA) has been highly pursued since 1993 as a route of converting methane to aromatics. It is believed to proceed via a by bi-functional catalyst namely Mo modified HZSM where by methane is activated by the Mo carbide by dehydrogenation process and the intermediate species are oligomerised and dehydrocyclised over the acid site of the HZSM-5 zeolite. The aim of this study is to optimise catalytic activity with high yield and selectivity to aromatics and low coke yield and selectivity. This will include basic principles behind catalyst design, activation and stabilisation. The MDA analysis was carried out on a quartz micro reactor operating at 1 atm. and 700°C using an on-line GC and a list of catalyst characterisation equipments to explain the findings.

The optimum catalytic activities were investigated using methane on Mo modified HZSM5 (Si/Al =41). Mo wt % loadings used were 3, 5 and 10 prepared by wet impregnation of ammonium heptamolybdate on HZSM-5. The preliminary micro reactor test showed that a GHSV of 1500 h^{-1} was the optimum flow rate for the process.

Based on investigation on the hcp β-Mo_2C and fcc α-MoC_{1-x}, Mo loading of 10wt% is found to be the optimum catalytic loading for MDA for both. Re-dispersion of the MoO_3 species over the catalyst surface and into the channels of the zeolite or pore is governed by calcination. Based on this study for the hcp β-Mo_2C catalyst 600°C was the optimum calcination temperature while for the α-MoC_{1-x} it was 500°C.

Activation of the MoO_3 species results in the formation of hcp β-Mo_2C and fcc α-MoC_{1-x}, the active Mo carbide phase which is responsible for methane activation and follow different route of preparation. It was found the hcp β-Mo_2C catalyst has higher catalytic activity than the fcc α-MoC_{1-x} counterpart. This higher catalytic activity for the hcp β-Mo_2C is attributed by the higher coke deposition as compared fcc α-MoC_{1-x} which has lower coke yield and selectivity but higher aromatic yield and selectivity at lower calcinations temperature.

Catalytic activity and stability was found to be improved by co-dosing with CO onto both the hcp β-Mo_2C and MoC_{1-x} catalysts. CO dosing was found to prevent coke build up during MDA reactions. From this investigation, it was found CO dosing is more significant towards higher Mo loading of 10wt% rather than for the lower loading of 3wt%. The most suitable CO for the 10wt% α-MoC_{1-x} was 4 v/v%, while for 10 wt % hcp β-Mo_2C it is 12 v/v%

Glossary

AHM-	Ammonium Heptamolybdate
BAS	Bronsted Acid Sites
BET SA	Brunauer, Emmett and Teller Surface Area
Coke I	Inactive Carbon deposit or burn-off coke
Coke II	Carbon deposit associated with Mo carbide
GC	Gas Chromatography
GHSV	Gas Hourly Space Velocity
ICP AES	Inductive Coupled Plasma- Atomic Emission Spectroscopy
MDA	Methane Dehydro-aromatisation
MFC	Mass Flow Controller
nmr	Nuclear Magnetic Resonance
RSF	Relative Sensitivity Factor
ROF	Rate of Formation
R&C	Reduction and Carburisation
SA	Surface Area
Syngas	Synthesis Gas
TGA	Thermo Gravimetric Analysis
TOS	Time on Stream
TMI	Transition Metal Ion
XPS	X Ray Photoelectron Spectroscopy
XRD	X Ray Diffraction

TABLE OF CONTENT

CHAPTER 1 INTRODUCTION

1.1 Dependence on Liquid Petroleum

The chemical industries rely heavily on crude oil directly or indirectly, crude oil constitutes the main feedstock for many organic chemicals which stretch from laboratory to industrial scale [1].

One of the main sources of benzene in the world is produced via naphtha cracking or an ethylene cracker which in turn is directly dependent on crude oil. With the increasingly short supply and high demand for crude oil, the price is expected to remain above an average of US$40 a barrel for several years, forcing the petrochemical producers to seek for cheaper options [2]. The price for benzene has been rising steeply, at times commanding a premium price of US$500-600 per tonne above the price of naphtha [2].

Table 1.1 is based on the most recent data on conventional oil reserves of the world (on a regional basis) presented by Energy Information Administration (EIA), the Official Energy Statistics of the US Government [3]. The term 'oil' used in context includes crude oil, gas condensate and natural gas liquids. It should also be noted that the oil reserve for North America in column 3 excludes the 174.5 million barrels of sand oils. For validity of the data please refer to Appendix 1.

From the Table 1.1 It can be seen that all 3 independent surveyors show similar findings. It can be seen that the largest reserves are concentrated in the Middle East and shared between Saudi Arabia, Iran, Iraq, Kuwait and United Arab Emirates.

Table 1.1 World Proven Reserve of Oil (Oct. 2005)*[1]

	Billion Barrels		
	BP Statistical review[2] (Year End-2004)	OGJ[3] Jan 1 2005	World Oil [4] End 2004
North America	60.904	40.271	40.874
Central & South America	101.165	100.595	75.973
Western Europe	17.372	16.255	16.864
Eastern Europe & Former USSR	121.871	79.19	91.16
Middle –East	733.859	729.341	708.289
Africa	112.233	100.784	112.41
Asia & Oceania	41.1	36.246	36.244
WORLD	1,188.05	1,102.68	1,081.81

* Proved reserves are estimated quantities that analysis of geologic and engineering data demonstrates with reasonable certainty are recoverable under existing economic and operating conditions. (Refer to Appendix 1 for further details)

Figure 1.1 gives the average contribution by region of the proven oil reserve in the world. This is done by averaging the oil reserve between the 3 surveyors and normalising the contribution by each region.

From the Figure 1.1 it can be seen that Middle East contributes almost two third or 64.5% of the world proven oil reserve. The rest of the world which includes North America, South and Central America, Western Europe, Eastern Europe and Former USSR States, Africa and Asia & Oceania contributes 4.2, 8.2, 1.5, 8.6, 9.7 and 3.4% respectively.

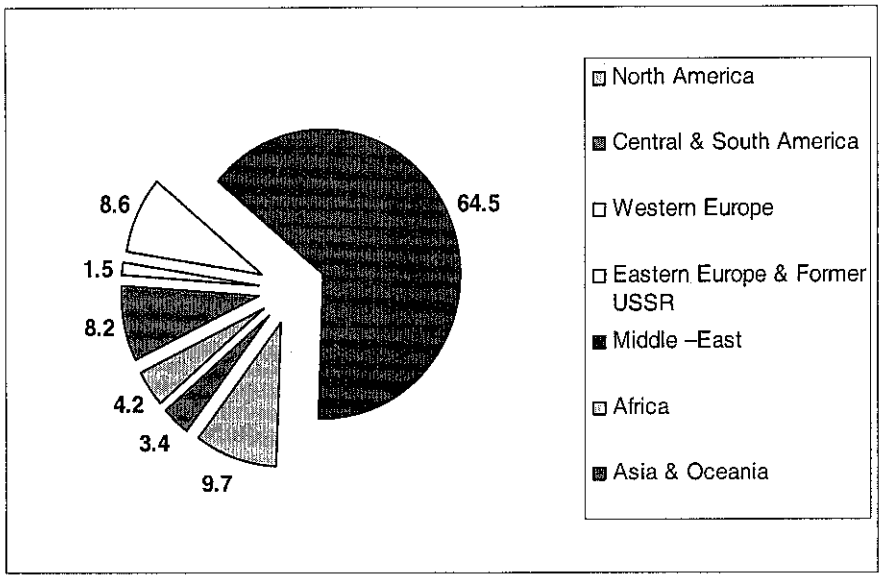

Figure 1.1 Distribution of World Proven Oil Reserve

A recent overview by Bentley [4] on the 'Global Oil and Gas Depletion' indicated that the world production of conventional hydrocarbons is experiencing an inevitable shortage which will soon be at physical risk. This is because the sum of conventional oil production from all countries in the world excluding the 5 main Middle East suppliers (Saudi Arabia, Iran, Iraq, Kuwait and United Arab Emirates) are near the maximum set by physical resource limits. With the above scenario, the call for conventional oil supply is now highly inclined towards the Middle East suppliers who have only limited spare operational capacity and it would be a matter of time before they too will run to depletion. To highlight this matter Bentley has created a pictorial figure on the current world situation on conventional crude oil consumption and available reserves compiled by Francis Harper (Manager, Reserve and Resources, BP) - 1999 resources based on industry (proven and probable) data and excludes crude oil yet to be discovered. The figure is illustrated by shaded circles placed at the respective region. The dark shade portion of the circle represents the crude oil that has been consumed and the light

colour portion is the available reserves. The above said figure is presented as Figure 1.2 below.

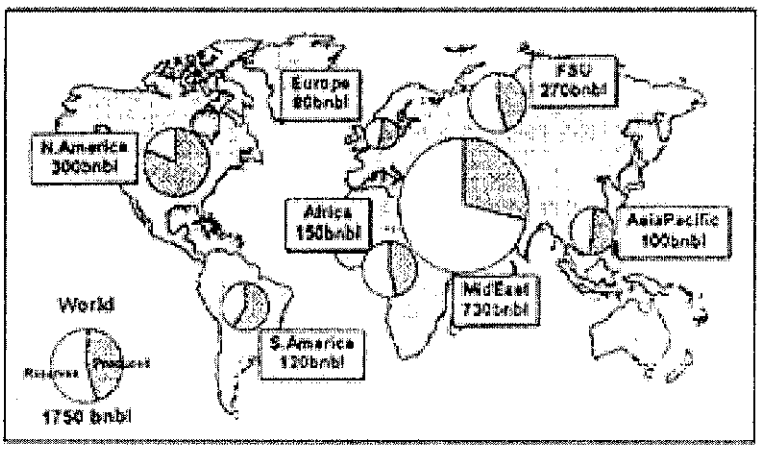

Figure 1.2 Global Conventional Crude Oil Distributions (Taken from Ref. 4)

Based on Figure 1.2, he concluded that the world is half way through its effected recoverable or conventional crude oil. This is essentially true for every region in the world except the Middle East, which has the advantage of potential control of its marginal reserves. As for North America it has consumed three-quarters of this natural resource. Africa, Asia Pacific and former USSR states are close to decline. Europe and South America have started the decline.

Campbell further expounded on the shortage of crude oil in a recent interview with Oil and Gas Journal [5], he divided the world endowment of conventional oil into 2 eras. He named them as the 'First and Second Half of the Age of Oil'. The first half is 150 years old and starts from the 1st oil wells drilled in Pennsylvania and the shores of the Caspian Sea in 1859 to 2005. This represents the mid-point of endowment of conventional oil depletion and is associated with peak production. The

downward trend after peak production is regarded as the 2nd half of the 'Age of Oil'. According to his calculation, the world has used up 49% of endowment of conventional oil which normally corresponds with peak production. The peak production is not particularly a significant event, but the relentless downward slope or 2nd half of the 'Age of Oil ' certainly is.

During 1st half period the world has enjoyed the abundant supply and cheap and convenient oil-based energy. This had a huge boom which resulted in rapid industrial expansion, transport, trade, agriculture and financial capital. The world population has expanded six-fold exactly in parallel with the 1st half of the 'Age of Oil'.

With the 2nd half of the 'Age of Oil' dawns, this period is marked by the decline in oil production and the transition is likely to be endowed with great tension and difficulties, particularly due to shortage of financial capital. Scope for further expansions will be tightly marked

The prospect of reducing the world's dependence on fossil fuels especially oil is problematic. Alternative energy technologies like nuclear, solar, hydroelectric, wind and geothermal energies do exist, but their current combine energy consumption is only 14% of the total energy consumption world wide [6]. Energy conservation is also a logical part of the solution, but as global energy consumption grows each year, development of certain alternative energy sources becomes increasingly important. Clearly it shows other viable options are needed.

This high reliance on crude oil could cause turmoil in the future economy of the world as highlighted by Campbell above [5]. OPEC's inability to control the ever rising prices of oil as a result of conflict in Iraq, high

level of Asian economy especially India and China, political turmoil in Venezuela has led to the recent peak in the price of crude oil.

1.2 Natural Gas

1.2.1 INTRODUCTION

Natural gas is now commonly believed to offer part of the solution to problems to relieve the strain on crude oil. At the moment natural gas is basically used for heating purposes and electric generation and to a lesser part in petrochemical sector. It is believed that natural gas will slowly take over from crude oil as the main building block for the chemical industry. In order for this transitional to take place from crude oil to natural gas, technology transfer from developed countries will be required to fulfil this need. This transition apart from relieving the strain on crude oil will also significantly improve environmental benefits locally, regionally and globally as it is a much cleaner substitute than crude oil. It should be the right direction taken as we head into the 21st Century.

1.2.2 NATURAL GAS RESERVES

The world's original endowment reserve for conventional gas in terms of energy value is probably the same as its endowment of conventional crude oil. Since less gas has been used so far as compared to crude oil, it is logical for the world to increasing turn to gas as the crude oil reserves declines [4].

Table 1.2 represent the world proven reserves of natural gas in terms of trillion cubic feet as released by the EIA of USA.

Table 1.2 World Proven Reserve of Natural Gas (Oct. 005)*[6]

	Trillion Cubic Feet			
	BP Statistical review [2] End-2004	CEDGAZ [5] Jan 1 2005	OGJ[3] Jan1 2005	World Oil[4] End 2004
North America	263.96	263.108	263.963	273.661
Central. & South America	250.595	243.956	250.52	241.355
Western Europe	178.305	217.929	182.487	177.828
Eastern Europe & Former USSR	2,081.43	2,043.75	1,964.16	2,836.73
Middle –East	2,570.79	2,589.65	2,522.13	2,542.69
Africa	496.43	498.83	476.509	500.759
Asia & Oceania	501.519	504.793	383.913	424.745
WORLD	6,343.03	6,362.04	6,043.677	6,997.77

* Proved reserves are estimated quantities that analysis of geologic and engineering data demonstrates with reasonable certainty are recoverable under existing economic and operating conditions. (Refer to Appendix 1 for further details)

From the Table 1.2 it can be seen that the major reserves of natural gas is distributed between the Middle East and the Eastern Europe and former USSR states.

A pie chart of the world distribution of natural gas is given in Figure 1.3 below. It is calculated by averaging the values presented by the 4 surveyors and normalising the contribution by each region.

From the same figure it can be seen that three quarter of the world natural gas comes from the Middle East and the Eastern Europe and former USSR states.

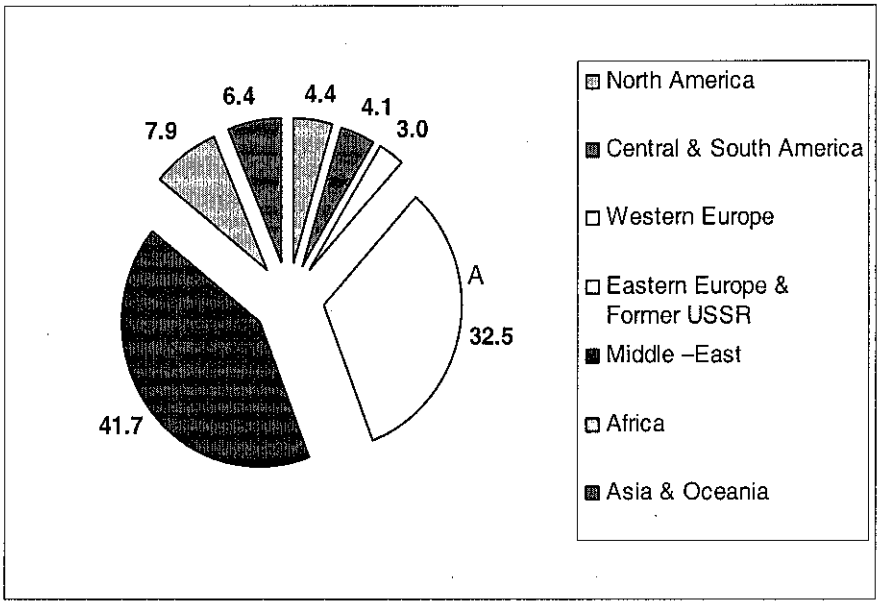

Figure 1.3 Distribution of Proven Natural Gas Reserve

1.2.3 THE GAS ECONOMY

The U.S. Geological Survey (USGS) periodically assesses long term production potential of worldwide petroleum resources which include oil, natural gas and natural gas liquids. They released a statement based on the recent USGS estimates (July 2005) [6], in the World Petroleum Assessment 2000 which disclosed that a significant volume of undiscovered natural gas reserve worldwide amounting to 4,301 trillion cubic feet. Of these 3,000 trillion cubic feet is located in 'stranded' reserves, usually located too far from pipeline infrastructure or population centres to make transportation of natural gas economical. This amounts to approximately double the worldwide cumulative consumption forecast from 2002 to 2025 based on estimates made in 2005(EO2005). These new natural gas resources are expected to be added over the next 25 years. With this addition more natural gas becomes available to further loosen the dependence on crude oil. Some of the strategies involved for increased utilisation of natural gas depend on price and

location, demand, construction cost, economics and political stability of the region. With the increasing price of the world depleting crude oil, natural gas looks more and more lucrative. In other words, the known gas reserves are enormous and keep on increasing with new discoveries. On the other hand, crude oil is over utilised and are depleting much faster rate due to limited discoveries.

1.2.4 METHANE

Methane or natural gas, a by-product usually associated with crude oil production, is considered as a liability as it is classified as a greenhouse gas. Certain contracts require that the producer takes the gas along with the liquid petroleum. Since capital and operational costs are high for methane utilisation, this creates a negative value for methane. To overcome this negative value some producers either re-inject, reduce production or flare or vent the gas. Flaring the gas creates environmental issue related to emission of green house gas. To overcome these obstacles, finding new methods of converting methane to chemical feed stocks or transportation fuels economically represents a considerable challenge.

Methane, the major component of most natural gas reserves is under utilised. The main utilisation of methane is in the domestic and industrial heating industries as well as in the generation of electric power. Methane although have low levels impurities as compared to crude oil, is still lacking behind the latter as a resource for chemical and liquid fuel.

The world's abundance supply of natural gas exceeds its demand. In order to increase the demand to match its ever growing supply, new markets should be created. These new markets can be created by continued technology innovation.

Driving force for technology innovation is the desire for less carbon-intensive and environment friendly cleaner fuels or feedstock. Other factors include cheap, plentiful supply, easy handling, transportable and economically viable feedstock. Looking at these factors, methane could fulfil most of the factors mentioned above; the main drawbacks are easy handling and transportation. This could be overcome by converting the natural gas into liquid fuel.

1.2.5 COMPOSITION AND USES

The main component of natural gas is methane. It can vary from 55% to 99.5% depending on location. Table 1.3 [7] shows a summary of the natural gas composition.

Table 1.3 Components of natural Gas (taken from Reference 7)

	CH_4	C_2H_6	C_3H_8	C_4H_{10}	C_5+	N_2/He	H_2S	CO_2
Holland	81.3	2.8	0.4	0.2	-	14.4	-	0.9
Italy	99.5	0.1	-	-	-	0.4	-	-
UK	92.6	3.6	0.9	0.4	0.3	2.2	-	-
Norway	90.9	5.9	1.1	1.1	1.1	0.6	-	1.5
S. Arabia	59.3	17.0	7.9	2.6	1.1	0.4	1.6	10.0
Iraq	55.7	21.9	6.5	3.9	1.2	-	7.3	3.0
Iran	76.1	11.1	6.1	2.2	1.1	-	0.3	3.1
USA	88.7	7.0	1.9	0.3	-	1.5	-	0.6

The main uses of natural gas previously were in the domestic and industrial heating industries and electric generation in power stations [3]. With the increase in quest for alternative fuel for crude petroleum, the natural gas has now paved its way into the manufacture of fuel

substitutes; renewable fuels, gas to liquid (GTL) synthetic fuel and ether. Other alternatives like compressed natural gas, liquefied petroleum gas, advance vehicle technology, fuel cells etc. will also contribute to the move away from crude petroleum [8]. Of the 3 main alternatives mentioned above, GTL is moving at a faster rate for the utilization of natural gas.

1.3 Indirect methods for methane Utilisation

1.3.1 GAS TO LIQUID (GTL)

GTL has become a synonymous with the Fischer Tropsch (FT) route for producing liquid fuels, petrochemicals and other products of natural gas. The route of GTL to higher value product is via synthesis gas (syngas). Figure 1.4 lists the GTL options [9].

1.3.1.1 Synthesis Gas Production

Methane can be converted to synthesis gas or syngas by indirect methods. Syngas is made up of a blend of carbon monoxide and hydrogen, which is the building block or the first step to various chemical processing. The hydrogen can be isolated for the manufacture of fertilisers like ammonia and urea or others like fuel cells. Methanol is the other key product from syngas. It can be converted to high value chemicals like formaldehyde, acetic acid and MTBE, a fuel additive. It is anticipated that these oxygenates will eventually serve many large fuel markets for instance, electric power, transport and domestic fuel markets. They can also extend the boundaries to become building blocks for gas based chemical industries.

The other option of syngas is the production of synthetic crude, which is becoming an increasingly global commercialisation activity. The leaders in this technology are;

1. Shell with their Shell Middle Distillate Synthesis (SMDS) commercialised plant at Bintulu , Malaysia.
2. Sasol with their extensive large scale experience with several coal-based FT process, Mossgas a Sasol licensee, has also GTL operational experience and
3. Exxon Mobil's Advance gas conversion technology 21st century (AGS-21).
4. Other players in this field include BP, Syntroleum , Conoco and Rentech, who have or are in the process of acquiring experience with large scale 70-400 barrel per day pilot plants.

GTL is a highly capital intensive process. Reducing process cost is a major obstacle for GTL and could be made attractive by improving existing technology. Other encouraging factors for GTL to be successful includes: ample resources from gas field located at low cost areas with adequate infrastructure, ample investment on project financing, accelerated capital recovery from short term deferred taxes, ample demand for products, reasonable high pricing for product and low gas pricing are some of the factors for encouragement for GTL projects.

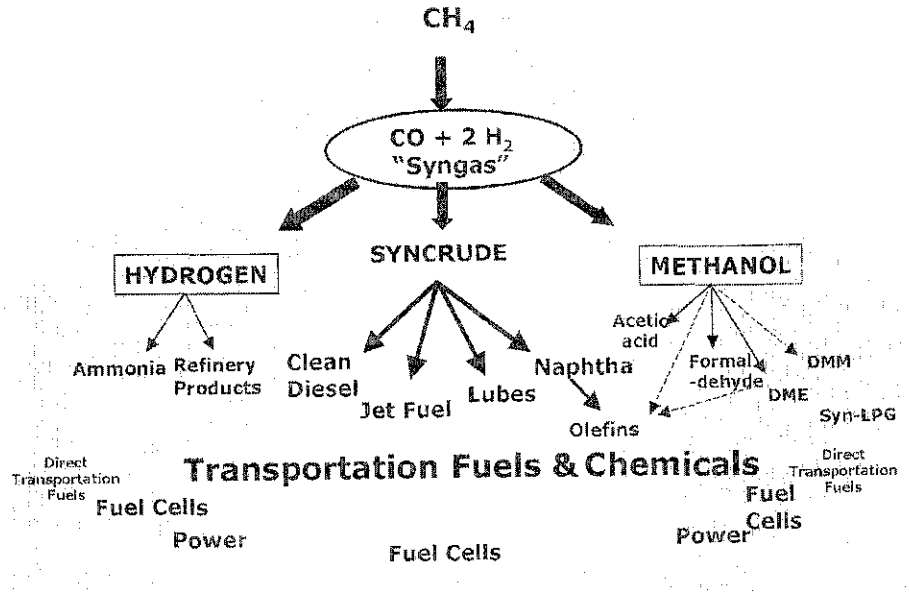

Figure 1.4 GTL Options (Taken from Ref. 9)

1.4 Direct Methods of Methane Conversion

Methane being the smallest and simplest hydrocarbon has posed many challenges to catalytic chemist on how to realize direct conversion of methane to versatile fuels and valuable chemical building blocks with selective bond breaking and forming. In the indirect method described above, the main problem was to overcome the thermodynamic constraints to break all four C-H bonds and reforming it into syngas ($CO+H_2$). This process requires huge amount of energy in breaking all four C-H bonds, then more energy is used to recreate similar C-H bonds. In the case of direct methane conversion, the scenario is completely different; here one or two of the C-H bond/s is/are selectively broken under oxidative or non-oxidative conditions and reconstructed to form oxygenated compounds like methanol and formaldehyde or recombined to form longer hydrocarbon chains which are valuable and versatile like aromatics.

In theory, direct methods should have a distinct economic advantage over indirect methods. Despite enormous efforts conducted via various approaches such as thermal, homogeneous or heterogeneous catalysis, photocatalysis and electrocatalysis, no known profitable or practical approach has been realized. To date, no direct methane conversion method has progressed beyond pilot plant scale. Further the product yield from this single pass mode is generally small and makes separation difficult and costly.

1.4.1 OXIDATIVE CONVERSION OF METHANE

Direct conversions of methane under oxidative conditions are more thermodynamically favourable than non-oxidative conditions. This led to well known study of oxidative coupling of methane (OCM) which bloomed in the mid-1980s till mid-1990 [10-14]. Despite numerous efforts, no catalyst could be found which could increase the C_{2+} yield beyond 25% and the C_{2+} selectivity higher than 80% [15], which represent one of the main criteria for industrialisation application of OCM, as such it led to the weakening interest of research. To date, this target has not been met and ethylene from surplus ethane derived from natural gas provides a more economical route for its production. Further OCM suffers from product separations, increase in exothermicity of the reaction and catalytic instability due to high reaction temperature.

In the biological domain, a major advance in the direct conversion of methane to oxygenates, methanol and formaldehyde via Methane Monooxygenase (MMO) enzyme under ambient condition poses a tough challenge in heterogeneous catalysis. Tanabe et al [16] has come up with a comprehensive review on this matter.

1.4.2 NON-OXIDATIVE CONVERSION OF METHANE

Thermodynamics do not favour the direct conversion of methane under non-oxidative conditions. Nevertheless, it has still attracted many researchers as an alternative approach to higher hydrocarbon synthesis [17-19]. Various metals e.g. Co, Ru or Pt catalysts have been known to chemisorb methane at moderate temperature and be decomposed to carbon and hydrogen at elevated temperatures. With the above knowledge and to overcome the unfavourable thermodynamic conditions, Amariglio et al [19] and van Santen et al. [20], two different research groups, almost simultaneously reported a 'two-step' process involving a low temperature non-oxidative oligomerisation of methane. Unfortunately, both the groups disagree on the exact mechanism of the oligomerisation. Amariglio et al [21-26] based on their study on the 'two-step' process on Pt (including EUROPT-1), Ru and Co under isothermal conditions suggested that methane broken down to carbonaceous deposit during the 1^{st} step chemisorption, forms a C-C bonding with the H-deficient CH_x and then is saturated by the hydrogen (1^{st} step chemisorption) in the 2^{nd} stage and removed from the surface.

van Santen et al. suggested that methane dissociates into carbide and H_2 on the precious metal catalyst in the 1^{st} stage, followed by the carbide being hydrogenated by H_2 to produce the higher hydrocarbon. It was also suggested that the C-C bond formation in the 2^{nd} stage is similar to that occurring in the Fischer-Tropsch reaction [27, 28]

Despite substantial research on the 'two-step' non-oxidatative process [21-34] or the 'one-step methane homologation, the stumbling block was the low efficiency to further develop it into a commercial process. In order to overcome the 'two-step' process, multifunctional catalyst based on multi-component catalysis were suggested by many researchers. Mitchell and Wanyhorne filed a patent [34] claiming that if methane was

passed over a multicomponent catalyst made up of a precious metal together with a group VIB and IIA metal at 977K (604°C) benzene could be detected in the product.

Plasma excitement has also been investigated to overcome thermodynamic limitation and to improve yield and methane conversion over non-oxidative conditions [35,36]. Here again, the main drawback is the low energy efficiency to overcome the thermodynamically unfavourable reaction.

1.4.2.1 Methane DehydroAromatization (MDA)

Under non-oxidative conditions, methane transformation to aromatics are much more favourable thermodynamically than to olefins as shown in Figure 1.5. These results were compiled by Xu et al [35] derived from several catalytic tests conducted by either a pulse or a flow reactor [36-40].

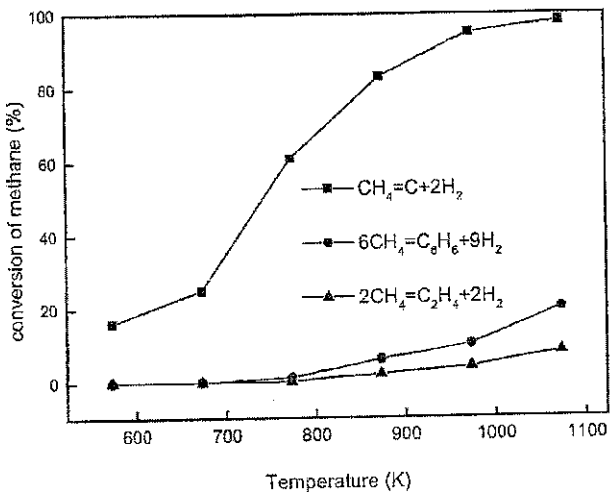

Figure 1.5 Thermodynamic of Direct Conversion of Methane under Non-oxidative Conditions (Taken from Ref. 36)

Since Wang et al (41) reported a direct conversion of methane by a non-oxidative aromatisation over HZSM-5 zeolite catalyst modified with transition metal ions (TMI), considerable interest has been generated in this potential route. Since than, many research groups in particular, those of Solymosi, Lunsford, Ichikawa, Iglesia and the Chinese groups of Xu and Lin etc. have shown much interest in these type of reactions and have made encouraging progress. Anderson [42] calculated the molar equilibrium compositions for MDA between 200-1000°C using Outokumpu HSC software, found that below 400°C negligible methane conversion is expected. Using similar method employed by Wang et al [41], he found that an approximate methane conversion of 12% can be obtained at 700°C. The theoretical product distribution was found to be dominated by an equimolar quantity of benzene and naphthalene with small amounts of ethylene and trace amounts of ethane and toluene. They also found huge amounts of hydrogen produced from the MDA reaction.

1.4.2.2 Introduction to MDA Reaction [43-46]

The following section describes a general reaction that occurs in a MDA reaction. In the preparation of Mo/HZSM-5 via impregnation of HZSM-5 by ammonium heptamolybdate tetrahydrate [$(NH_4)_6Mo_7O_{24}.4H_2O$], the Mo species in the form of $Mo_7O_{24}^{6-}$ locate themselves on the external zeolite surface during the impregnation stage. On calcinations at specific temperature, the $Mo_7O_{24}^{6-}$ species decomposes to MoO_3 crystallites and some of them migrate into the zeolite channels and interact with and replace a H^+ of the OH group found at the Bronsted acid sites.

On the introduction of methane, the Mo species is reduced by methane to form the active Mo-carbide at the same time deposition of carbonaceous coke occurs. During the initial part of this period, no hydrocarbon was produced, the main products were CO, CO_2 and H_2O. This constitutes the induction period. The end of the induction period is marked by the

appearance of ethane, ethylene and benzene (the first of the hydrocarbons). It is interesting to note that at the end of the induction period, CO_2 and H_2O product almost completely disappear with CO decreasing with time on stream (TOS). This will be discussed in detail later. The Mo-carbide provides the active site for methane activation where ethylene is formed. The ethylene is subsequently converted to benzene and higher aromatics at the Bronsted acidic sites. With TOS, the carbonaceous deposit increases and eventually deactivates the catalyst [43-46].

The products obtained from MDA contain a mixture of light aliphatic (ethylene and ethane), aromatics (benzene, toluene and naphthalene) and potential amount of hydrogen. Molybdenum modified HZSM-5 prepared by impregnation with ammonium heptamolybdate at room temperature with Mo loading of 2-6 weight % is considered as the best catalyst precursor. The precursor is calcined in air between 500 to 700°C for one to several hours. The calcined precursor is then activated between 600 to 750°C under a stream of methane or a mixture of methane/hydrogen to produce the final reduced catalyst. It is generally accepted that the active components of the catalyst are the Mo-carbide (α or β form) and HZSM-5, an example of a bifunctional catalyst. Methane can then be converted to the desired product at 700 to 850°C. The reaction is believed to proceed via initial formation of ethylene, which is further transformed to benzene, and on further condensation, benzene is transformed to naphthalene and higher aromatics and carbonaceous deposit. It is this carbonaceous deposit that causes the rapid deactivation of the catalyst due to coking. Recent work in the LCIC [42] has shown that Mo-carbide is the main component for high stability at high temperature. HZSM-5 with a Si/Al ratio of 40 is one of the best choices for support. Catalyst activation is best carried out under a mixture of 10:1 H_2/CH_4 at 700°C or

10;1 C_4H_{10}/CH_4 ratio. Co-feeding carbon monoxide increases catalytic stability at maximum conversion.

1.4.2.3 Advances in MDA Reaction

Xu and Lin[43] reviewed the latest advances in MDA reaction recently. In this review, they came up with four categories where research works in MDA are primarily focussed on. These areas are:

1. Modification of the Mo/HZSM-5 catalyst and optimisation of reaction conditions
2. Study of interaction between the TMI component and the zeolite support
3. Active sites(or active phases) and reaction mechanisms
4. The formation of carbonaceous deposits and their role in the reaction.

Based on their works a summary of their findings are given below.

- **Modification of the Mo/HZSM-5 catalyst and optimisation of reaction conditions:-**

  Xu et al[43] suggest that many researchers agree the best catalyst for this reaction is Mo/ HZSM-5 zeolite. This is usually prepared by impregnation of ammonium heptamolybdate tetrahydrate $[(NH_4)_6Mo_7O_{24}.4H_2O]$ on H-ZSM-5 and is believed to be the best route in preparation of the above catalyst. Xu et al. and Lin et al. [43] agree that impregnation of Mo is claimed to have higher catalytic activity and shorter induction period than those prepared by solid state ion exchange methods [47-50]. Furthermore for the impregnated catalyst, the TMI are usually located at the external surface and only a fraction of them diffuse into the channels of the zeolite.

Xu et al.[51,52] also found that loading a 2nd metal component like Ru, Pt, W, Zr, Co, Fe and Cr can enhance the reactivity and/or stability of the catalyst, but addition of V, Li and P has the opposite effect. Loading of 2nd metal component by impregnation should be done after the Mo loading. Loading with Pt can significantly reduce the coke deposit thus improving catalytic stability as shown by Chen et al [53]. Ru addition on the other hand has shown to improve the reduction of the Mo species and the dehydrogenation of methane. As a result both methane conversion and aromatic formation increases. [54]. Addition of Fe or Co increases the rate of formation of aromatics and reduces the selectivity of coke [55].

Optimisation of reaction conditions like pre-treatment atmosphere [49,52,56] and temperature [54,57,58], reaction temperature [47,56], pressure [47,59], methane space velocity [48,50,57,59]and regeneration [49,58] has shown to influence catalytic performances.

- **Study of interaction between the TMI component and the zeolite support:**

  In the MDA reaction methane is the sole reactant and Mo/HZSM-5 is the active catalyst. It is believed that the Mo species is high dispersion on/in the zeolite as a result of its interaction with the Bronsted acid site of the HZSM-5 zeolite. In other words, the driving force for Mo species dispersion is the acid sites of the zeolite. This kind of interaction increases with increase in Mo loading and/or calcination temperature. With too high Mo loading and/or calcination temperature, the Mo species may extract the framework Al to form extra framework Al followed by $Al_2(MoO_4)_3$ which is detrimental for MDA reaction [60].

Addition of a Mo and/or a 2nd metal component changes the acid sites by decreasing the strong acid sites and increasing the moderate strength ones [48,51,52,57].

- **Active sites (or active phases) and reaction mechanisms**

  Two fundamental issues remains unresolved in the literature; namely
  - the state and location of the active form of Mo, and
  - the mechanism of reaction

Some of the highlights are discussed below:
Solymosi et al. [61-63] based on XPS technique of spent catalyst claim Mo_2C as the active species. Lunsford et al.[64,65] however based on their study on supported and unsupported Mo_2C concluded that besides Mo_2C, oxygen deficient MoO_2 may also be responsible for the methane activation. Lunsford et al. [64,65] also found that during the initial induction period, CH_4 reduces the Mo^{6+} in the zeolite into Mo_2C accompanied by carbonaceous deposits. On pre-treating the calcined catalyst with a CH_4/H_2 mixture at 700°C, they noticed that the Mo^{6+} ion is reduced to Mo_2C and the induction period can be almost eliminated by this process. They also showed that the pre-formed Mo_2C without coke deposit on the other hand needs the induction period for MDA reaction.

Based on these observations, they suggested that coke modified Mo_2C may be the active species in the formation of ethylene.

Ichikawa et al. using Mo K-edge EXAFS and TG/DTA/MASS/FT-IR techniques [66-69] tried to characterise the active phase and elucidate the mechanism of MDA reaction and proposed the following mechanism as shown in Equation 1.

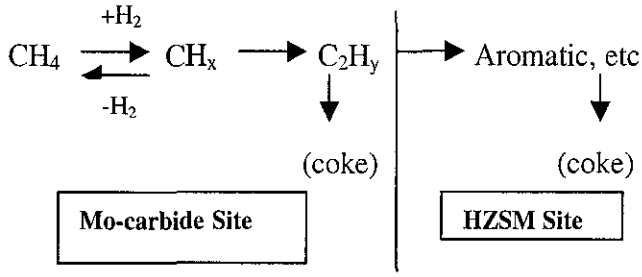

Equation 1

Based on their study, they reveal that Mo oxide supported on the zeolite is endothermically converted to Mo_2C clusters under methane atmosphere. This Mo_2C then initiates the methane aromatisation to benzene and naphthalene at 600-900°C. They suggested that methane dissociates on the Mo-carbide or oxycarbide cluster site supported on HZSM-5 having optimum Bronsted acidity to form CH_x (x >1) and C_2-species being the primary intermediate. The C_2-species is than oligomerised to benzene and naphthalene aromatics at the interface of Mo_2C and HZSM-5 zeolite having the optimum Bronsted acidity.

Iglesia et al.[70] investigated the structure and density of Mo species in Mo/HZSM-5 before, during and after MDA reaction using XAS, TPO and isotopic exchange of D_2 with OH groups methods reveal that methane reaction causes $Mo_2O_5^{2+}$ dimers to be formed as a result of concurrent regeneration of Mo species with bridging OH groups. These catalytic inactive $Mo_2O_5^{2+}$ dimers are activated in contact with CH_4 by reduction and carburisation to form active MoC_x (pore diameter of HZSM-5 being 0.6-1.0 nm) clusters required for MDA reaction. MoC_x is believed to be responsible for C-H bond activation and initial C-C bond formation and the acid sites for oligomerisation and cyclisation of C_{2+} hydrocarbon to form stable aromatics.

Based on the above discussion, it is clear that most researchers in the area agree that Mo-carbide or oxycarbide is responsible for the conversion of methane to ethylene. Ethylene is then converted to benzene and higher

aromatic products over the acidic sites within the channels of the zeolite [71].

- **The formation of carbonaceous deposits and their role in the reaction**

The heavy carbonaceous deposits formed during the MDA present a major obstacle for better understanding of the reaction and process development. Lunsford et al [71] using XPS technique identified 3 surface carbon species formed on spent catalyst. They named them as;

- species A- a graphitic-like carbon mainly present in the zeolite channels
- species B- a carbidic like carbon in Mo_2C and is mainly located on the outside surface of the zeolite
- species C- a hydrogen-poor sp^2 type or pregraphitic type mainly present on the outer surface of the zeolite. This species increases with TOS and gradually covers both the external surface as well as the Mo_2C phase. It is the one responsible for catalytic deactivation of Mo/HZSM-5 during MDA reaction.

Xu et al [72,] classified the carbonaceous deposit of Mo/HZSM-5 by nmr into 2 types, one located on the acid sites and the other on the partially reduced Mo species. They believe that the former as being the inactive or unreactive carbon deposit which leads to the decrease in acid sites amounts and is responsible for catalytic deactivation and the latter is responsible for methane activation and effectively transform from carbine-like species and/or carbide species to ethylene.

Xu, Bao and co-workers [73] studied the effects contact time in MDA reaction. They analysed the carbonaceous deposit created by MDA

reaction and concluded that the various forms of the deposit play different roles. The Mo_2C and/or MoO_xC_y formed during the induction period may be responsible for methane activation. Species B is formed as the end of the induction period on the Mo_2C and/or MoO_xC_y is responsible for the formation of the C_{2+} intermediate and species C coke is responsible for catalytic deactivation. They agreed that the Mo_2C shows some precious metal properties as previously shown by Boudart et al [74].

The suppression of carbonaceous deposit formed during MDA reaction is intensively studied with a number of results published. Addition of CO or CO_2 to the methane feed and increasing methane pressure is claimed to have enhanced catalytic stability [69,75,76]. The unique role of CO was investigated using ^{13}CO tracer experiment by Ichikawa et al [69,75]. They suggested that the CO dissociates on the Mo sites to form the active CH_x species. The dissociated oxygen species from CO might react with the surface inert carbon species to regenerate the CO which suppresses coke build up on the catalyst.

Another effective way of enhancing the activity and increasing the stability of the Mo/HZSM-5 is to adjust the Bronsted acid sites and its distribution on/in the parent zeolite This can be done by treatment of parent zeolite by steam dealumination, dealumination by acid solution or silanization with large size Si-containing molecules [73-75]. Results from this reduction of Bronsted acid site suggest that although it is necessary for MDA reaction, excess is detrimental for the reaction since they promote coke formation.

Iglesia et al[70] claim that selective silanation of external acid sites on HZSM-5 using large organosilane molecule, the acid content as well as number of MoO_x species could be reduced on the external surface.

For methane aromatisation using Mo/MFI zeolite, a number of facts have been established:

- It is generally agreed that the catalytically active form Mo is reduced and most likely in the form of Mo-carbide (Mo_2C) which is active for the reforming reactions. Two structural forms of Mo_2C (α-MoC $_{1-x}$ and β-Mo_2C) have been identified which are believed to be the active catalyst.
- HZSM-5 zeolite is believed to be the best support and provides the acidic sites (Bronsted acid sites) for ologomerisation reaction.
- Mo/HZSM-5 prepared by impregnation of ammonium heptamolybdate tetrahydrate [$(NH_4)_6Mo_7O_{24}.4H_2O$] on H-ZSM-5 is believed to be the best route in preparation of the above catalyst.
- Mo_2C can be prepared by calcination under air at 600°C followed by methane activation at 500 to 750°C is believed to produce the most efficient catalyst for the reaction
- Highest conversion recorded for methane is between 7 to 10% at 700°C as compared to equilibrium conversion of 12.5%
- Methane aromatisation proceeds via bi-functional catalysis. Methane is activated at the Mo-carbide sites to form CH_x and C_2 species which then may migrate to the interface of the ZSM-5 acidic support. Here, C_2 species are dehydro-aromatised to intermediates to benzene. Furthermore condensation converts benzene to naphthalene and higher aromatic and carbonaceous deposit.
- The catalyst is deactivated by carbonaceous material deposit. Results have shown that co-feeding CO delays or stabilises the deactivation of the catalyst.

1. 5 Objective and Scope of the Research Thesis

MDA is a promising route for the production of aromatics from methane. The key in obtaining good catalyst activity is by optimising the process variable by finding optimum balance between dehydrogenating and acid functions.

The main objective of this thesis is to optimise catalytic activity or increase methane conversion with high selectivity towards aromatic namely benzene and naphthalene, with low coke formation and improve catalytic stability.

The scope of the present PhD thesis uses Mo/HZSM-5 catalyst prepared by impregnation of ammonium heptamolybdate tetrahydrate $[(NH_4)_6Mo_7O_{24}.4H_2O]$ on HZSM-5. The feed employed for this project is methane. The catalyst loading studied is between 3 and 10 Mo wt %. The investigations were directed to optimisation of process variables in order to improve catalyst activity and stability.

A range of analytical and characterisation techniques are used to characterise catalyst and quantify reaction products. These include gas chromatography, inductive-coupled plasma–atomic emission spectroscopy, thermal gravimetric analysis, surface area and pore volume and diameter determination, elemental analysis etc.

The experimental details, results obtained, discussion, and calculations used are presented in Chapters 2 to 7, followed by a general conclusion in Chapter 8.

1.6 Chapter 1 References

1. Morrison, R.T., and Boyd, R.N., in 'Organic Chemistry' , 5th Edition, Allyn and Bacon Inc., p 92 &537 (1987)
2. Milmo S., Chem. World. Vol 2/No.11(2005) 36
3. http://www.eia.doe.gov/emeu/international/reserves.html
4. Bentley, R.W., Energy Policy 30 (2002)189
5. Campbell, C.J., Oil and Gas J., 103 (2005) 24
6. http://www.eia.doe.gov/oiaf/ieo/nat_gas.html
7. Villa, P.L., and Ragagna, S., S Proc. NATO ASI on 'Progress and Challenges in Alkane Activation and Functionalisation' (Derouane E.G., Haber J., Lemos F., Ribeiro, R.R. and Guisnet, M., Eds.), Villamoura, Portugal, May 1997; Kluwer Pub., Dordrecht
8. Higgins, T., World Refining, Vol 3/ No. 4, (2003) Syntroleum Pub. 4
9. Fleisch, T.H., Sills, R.A. and Briscoe, M.D., J Nat Gas Chem Vol 11/ No.1-2 (2002) 1-14
10. Lee, J.S and Oyama, S.T., Catal. Rev. – Sci. Eng., 30, (1988) 249
11. Keller, G.E., and Bhasin, M.M., J. Catal., 73 (1982) 9
12. Hutchings, G.J., Scurrell, M.S., Woodhouse, J.R., Chem. Soc. Rev., 18 (1989) 251
13. Lunsford, J., Catal. Today 6 (1990) 235
14. Krylov,O.V., Catal. Today 18 (1993) 209
15. Kuo,J.C.W., Kresge, C.T., and Palermo, R.E., Catal. Today 4 (1989) 4
16. Tanabe, K., Teng, Y., Takermoto, T., Suzuki,E., Banares, M.A., Pena, M.A., and Fierro, J.L.G., Catal. Rev. 44 (2002) 1.
17. Periana, R.A., Taube, D.J., Evitt, E.R., Loffler, D.G., Wentrecek, P.R., Voss, G., and Masuda, T., Science 259 (1993) 340
18. Periana, R.A., Taube, Gamble, S., Taube, T., Satoh, T., and Fujii,H., Science 280 (1998) 560

19. Belgued, M., Pareja, P., Amariglio, A., and Amariglio, H., Nature 352 (1991) 789
20. Koerts,T., Deelen, M.T.a.G., and van Santon, R.A., J. Chem. Soc. Chem. Commun. (1991) 1281
21. Pareja, P., Amariglio,A., Belgued,M., and Amariglio, H., Catal. Today 21 (1994) 423
22. Amariglio,H., Pareja, P., and Amariglio, A., Catal Today 25 (1995) 113
23. Amariglio, H., Belgued, M., Pareja, A., and Amariglio, A., Catal. Lett. 31 (1995) 19.
24. Belgued, M., Amariglio, A., Pareja, H., and Amariglio, H., J. Catal. 159 (1996) 441
25. Belgued, M., Amariglio, A., Pareja, H., and Amariglio, H., J. Catal. 159 (1996) 449
26. Belgued, M., Amariglio, A., Lefort, L., Pareja, H., and Amariglio, H., J. Catal. 161 (1996) 282.
27. Koerts,T., Deeelen, M.T.A.G., and van Santen, R.A., J. Catal. 138 (1992) 101
28. Koerts,T., and van Santen, R.A., J. Mol. Catal. 74 (1992) 185
29. Koerts,T., Leclercq, P.A., and van Santen, R.A., J. Am. Chem. Soc. 114 (1992) 7272
30. Solymosi, F., Erdohelyi, A., Cserenyi, J., and Felvegi, A., J. Catal. 147 (1994) 272
31. Solymosi, F., and Cserenyi, J., Catal. Lett. 34 (1995) 343
32. Guczi, L., Sarma, K.V., and Borko, L., J. Catal. 167 (1997) 495
33. Wu, M., Xu, Q., and Goomdan, D.W., J. Phys. Chem. 98 (1994) 5104
34. Mitchell III,H.L., and **Wanyhorne,** R.H., US Patent 4,239,658, (1980)
35. Xu, Y., Bao, X., and Lin, L., J. Catal. 216 (2003) 386

36. Kado, S., Sekine, Y., and Fujimoto, K., Chem. Commun. (1999) 2485
37. Zhu,A., Gong, W., Zhang, X., and Zhang, B., Sci. China 43 (2000) 208
38. Thanychotpaiboom, K., Chavadej, S., Caldwell, S., Lobban, L.L., and Mallinson, R.G., React. Kinet. Catal. 44 (1998) 2252
39. Onoe, K., Fujie, A., Yamaguchi, T., and Hatano, Y., Fuel 76 (1997) 281
40. Xu, Y., Tian, Z., Xu, Z., Ziu, A., and Liu, L., Stud. Surf. Sci. Catal. 136 (2001) 75
41. Wang, L., Tao, L., Xie, M., Xu, G., Huang, J., Xu,Y., Catal. Lett. 21 (1993) 35
42. Anderson ,J.R., Phd Thesis, University of Liverpool, UK (2001)
43. Xu,Y., and Lin, L., Appl. Catal. A. 188 (1999) 53
44. Xu, Y., Bao, X., and Lin, L., J. Catal. 216 (2003) 386
45. Shu, Y, and Ichikawa, M., Catal. Today 71 (2001) 55
46. Lunsford J.H., Catal. Today 63 (2000) 165
47. Wang, L., Tao, L., Xie, M., Xu,G., Huang,J., and Xu,Y., Catal. Lett.21 (1993) 35
48. Chen. L., Lin, L., Xu, L., Li, X., and Zhang,T., J. Catal. 157 (1995) 190
49. Xu,Y., Liu,S., Wang,L., Xie, M., and Guo,X., Catal. Lett. 30 (1995) 135
50. Wong,S., Xu,Y., Liu,L., Wang, X., and Guo,X., Appl. Catal. A. 136 (1996) 7
51. Wang,L., Xu,Y., Xie, M., Liu,S., and Tao,L., Stud. Surf. Sci. Catal. 94 (1997) 495
52. Wang,L., Xu,Y., Wong,S., Cui,W., and Guo, X., Appl. Catal. A. 152 (1997) 173
53. Chen,L., Lin,L., and Xu,Z., Catal. Lett. 39 (1996) 169

54. Shu,Y., Xu,Y., Wong, L., Wang, L., and Guo,X., J. Catal. 170 (1997) 11
55. Liu,S., Dong,Q., Ohnishi,R., and Ichikawa,M., Chem. Commun. (1997)1455
56. Solymosi,F., Szoke,A., and Cserenyi, J., Catal. Lett. 39 (1996) 157
57. Solymosi,F., Szoke,A., and Cserenyi, Appl. Catal. A. 142 (1996) 361
58. Xu,Y., Shu,Y., Liu,s., Huang, J., and Guo, X., Catal. Lett. 35 (1995) 233
59. Xie,M., Yang,X., Chen,W., Tao,L., Wang,L., Xu,G., Wang, L., Xu,Y., Liu, S., and Guo,X., Stud. Surf. Sci. Catal. 105 (1997) 869
60. Xu,Y., Liu,W., Wang,L., Wong, S., and Guo,X., Catal. Lett. 40 (1996) 207
61. Solysomi, F., Erdohelyi, A., and Szoke, A., Catal. Lett. 32 (1995) 43
62. Szoke, A., and Solymosi, A., Appl. Catal. A. 142 (1996) 361
63. Solymosi, A., Cserenyi, J., Szoke,A., Bangsagi, T., and Dszko, A., J. Catal. 165 (1997) 150
64. Wang, D., Lunsford, J.H., and Rosynek, M.P. Top. Catal. 3 (1996) 289
65. Wang, D., Lunsford, J.H., and Rosynek, M.P. J. Catal. 169 (1997) 347
66. Liu, S., Wang,L., Ohnishi, R., Ichikawa, M., J. Catal. 181 (1999) 175.
67. Wang, L., Ohnishi, R., Ichikawa, M., Catal. Lett. 62 (1999) 29.
68. Wang, L., Ohnishi, R., Ichikawa, M., J. Catal. 190 (2000) 276.
69. Liu, S., Wang, L., Dong, Q., Onishi, R., Ichikawa, M., Stud. Surf. Sci. Catal. 119 (1998) 241.
70. Ding, W., Li, S., Meitzner, G.D Iglesia, E., J. Phys. Chem. B105 (2001) 506.
71. Weckhuysen, W.M., Rosynek, M.P. and Lunsford, J.H., Catal. Lett. 52 (1998) 31
72. Jiang, H., Wang, L., Cui, W., and Xu, Y., Catal. Lett. 57 (1999) 95

73. Shu, Y., Ma,D., Su, L., Xu, Y., and Bao, X., Stud. Surf. Sci. Catal. 136 (2001) 27
74. Lee, J.S., Oyama, S.T., and Boudart, M., J. Catal. 106, (1987) 125
75. Liu, S., Wang,L., Dong,Q., Onishi,R., and Ichikawa, M., Chem. Commun. (1998) 1217
76. Lu, Y., Ma, D., Xu, Z., Tian, Z., Bao, X., and Lin,L., Chem. Commun. (2001)2048
77. Ma, D., Lu,Y., Su,Z., Xu,Z., Tian, Z., Xu, Y., Lin, L., and Bao,X., J. Phys. Chem. B 106 (2002) 8524

CHAPTER 2 EXPERIMENTAL

2.1 Catalyst Preparation

2.1.1 PREPARATION OF HZSM-5

NH_4ZSM-5 with a Al/Si ratio of 41 was obtained from Zeolyst International (batch number = CBV8014G). NH_4ZSM-5 was then dried at 150°C in an oven overnight. It was then cooled in a desiccator without desiccant for an hour before being calcined. Calcination in air was performed to convert the NH_4ZSM-5 to its acidic form i.e. HZSM-5.

$$NH_4\text{-ZMS-5} \longrightarrow NH_3 + \text{H-ZSM-5}$$

This was done by heating the NH_4ZSM-5 zeolite packed in a porcelain boat and placed in a quartz tube reactor fed by a constant air flow rate of 12 ml/min. The zeolite was then heated at a constant heating rate of 5°C/min to 600°C and held at this temperature for 4 hours before being allowed to cool to room temperature at a rate of 10°C/min.

2.1.2 PREPARATION OF MoO_3/HZSM-5

The weight % of Mo in research papers is either quoted as wt% Mo metal or wt% MoO_3. Since neither Mo metal nor MoO_3 is the active species, it is arbitrary which one is used. The wt % used in this study refers to Mo metal wt % supported on HZSM-5 assuming that MoO_3 is the final phase produced.

In this study 3, 5 and 10 wt% Mo/HZSM-5 are prepared by wet impregnation of ammonium heptamolybdate tetrahydrate $\{(NH_4)_6Mo_7O_{24}.4H_2O\}$ (AHM) onto H-ZSM-5. The AHM used in this study is of A.C.S. reagent grade obtained from Aldrich with formula weight 1235.86 and density of 2.498 and is the source of Mo. For further details on the preparation refer to Chapter 3.

2.1.3 CALCINATION

The powdered zeolite was packed loosely in porcelain boat and placed in a horizontal quartz tube reactor fed by a constant air-flow of 12 ml/min. This zeolite was then slowly heated up from room temperature to 400°C at a constant heating rate of 10°C/min. The calcination heating cycle for this zeolite is given in Figure. 2.1. At 400°C the temperature was maintained for 2 hours before being increased to 600°C. This was done to slowly remove excess water formed during the reaction and avoided zeolite dealumination due to steaming. Dealumination can result in reduced number of Brønsted acid sites and produce octahedrally coordinated extra-framework aluminium. After 2 hours at 400°C, the temperature was then slowly raised to 600°C at constant rate of 5°C/min and kept overnight at this temperature to complete the transformation and at the same time remove any other excess water that might be present. It was then allowed to cool to room temperature at a constant rate of 10°C/min. The zeolite was stored in a desiccator without desiccant .

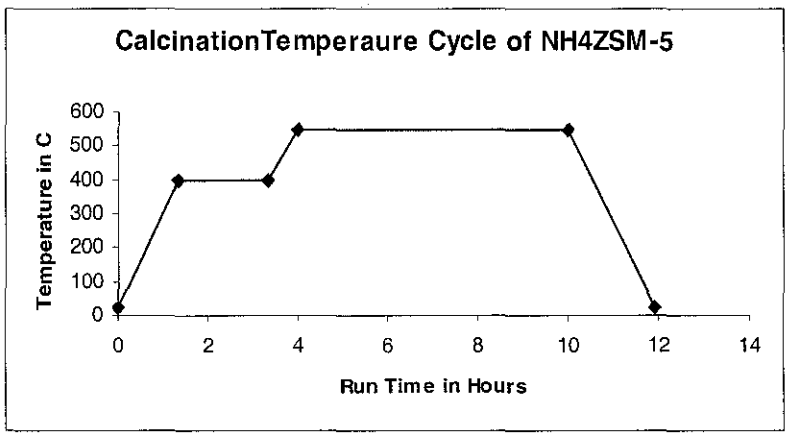

Figure 2.1 Calcination Temperature Cycle for MoO_3/HZSM-5

2.1.4 PELLETIZATION OF CALCINED MoO_3/HZSM-5

The cool calcined powder was further ground in a glass mortar and pestle. It was then introduced into a pellet maker and pressed into pellets

under a pressure of 8 tons. Again the pellets were crushed by the pestle and mortar and sieved to a particle size of 250-425μm (40-60 mesh).

2.2 Micro-reactor set-up

Catalyst testing was carried out in a fixed bed continuous plug flow micro-reactor system which was constructed for this specific purpose (see Figure 2.2). The micro-reactor system can be divided into 3 main sections:

2.2.1 GAS DELIVERY SYSTEM

Gases were delivered to the Brooks 5850S Smart Mass Flow Control (MFC) via 1/8 inch stainless steel pipes from gas bottles stored in gas cupboard. Each of the gases used was supplied to individual MFC which is protected by a 7 micron filter and non-return valve. Every 4 MFC in turn was controlled by a Brooks 0154 Microprocessor unit (BMpU). Each gas supplied to the MFC was independently calibrated using a Varian Intelligent Digital Flow Meter. The BMpU controls the gas flow via the MFC to the reactor inlet which in turn is protected by a 10 bar security check valve. All gas lines to the reactor inlet are made of 1/8 inch stainless steel tubing.

2.2.2.1 Gases

All gases used in the following reactions which includes catalyst calcination, activation and reaction or analysis were supplied by British Oxygen Company. These gases include: air, hydrogen, helium, (all UHP grade), n-ethane, n-butane, carbon monoxide (all N2.0 grade). Methane and argon, the primary feed gas, was specially prepared by mixing 97.0 vol % of 99.95% methane and 3 vol% of 99.995% argon). Calibration gases (Scott Specialty Gases) supplied by Sulpelco comprising of acetylene,

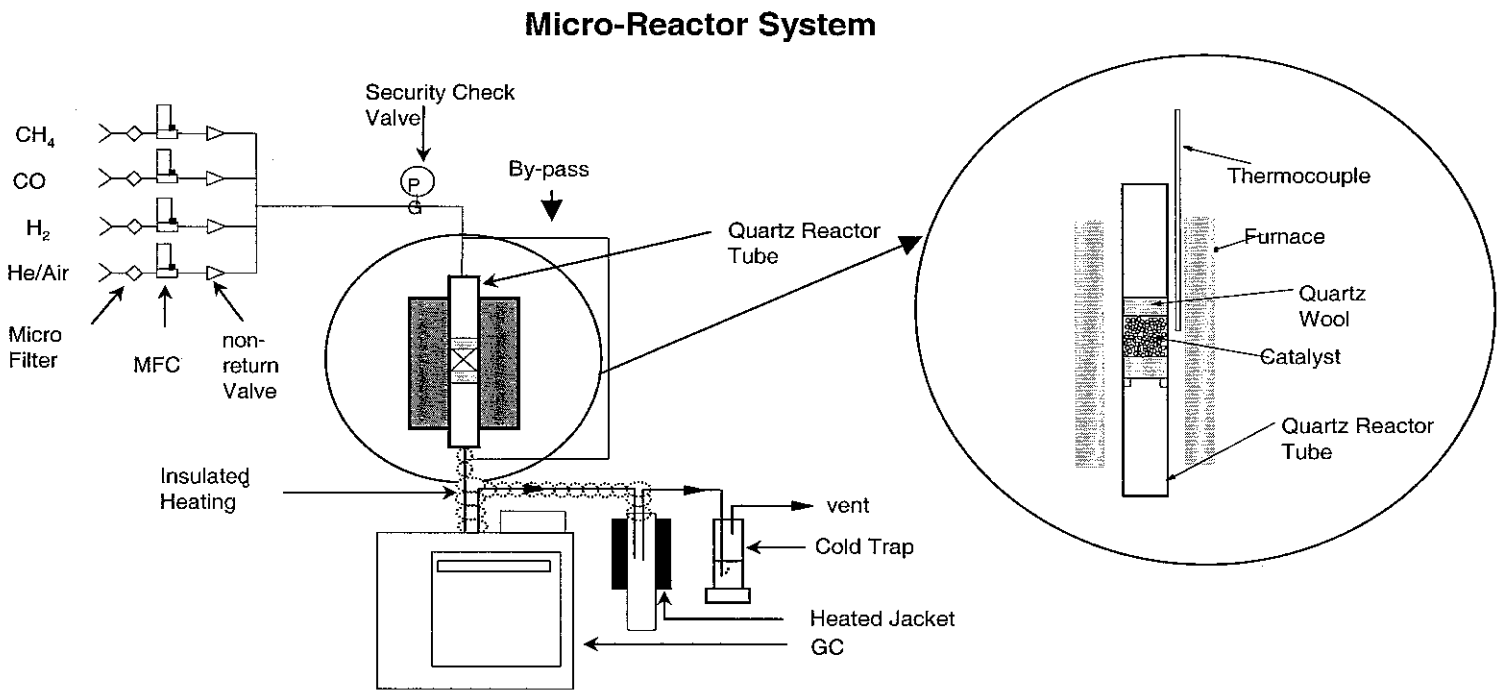

Figure 2.2 Micro Reactor Set-up System for MDA

carbon dioxide, carbon monoxide, ethane, ethylene, methane (1.0 mole % each) and balance nitrogen were used for identification, calibration and quantification of product gases in the GC. 0.5 vol % benzene in helium was specially supplied by British Oxygen Company (BOC), was also used for calibration and quantification purposes. Both the calibration gases and primary feed (methane and argon) come with a calibration certificate.

2.2.2 CATALYTIC REACTOR SYSTEM

The catalytic reactor is the heart of the reactor system. This is where all the chemical reactions take place. The reactor tube is made of a 9mm I.D. (12mm O.D.) and 40 cm length quartz tube sealed with ½ inch teflon ferrules and PTFE tape. At the centre of the tube a 3-prong indention is purposely introduced to hold the catalyst bed. A weighed amount of catalyst is sandwiched between 2 layers of 0.5mm thick quartz wool (top and bottom) above the 3-prong indentation. The quartz tube reactor in turn is heated with a Carbolite MFT furnace fitted with a Eurotherm 254 CH155555 controller. The furnace has a 30cm tube length with a 25cm heating zone and a uniform thermal zone of 9cm. The temperature at the centre of the catalyst bed is monitored by a type-K thermocouple (+/- 5°C). The thermocouple is positioned at the centre of the catalyst bed and placed outside between the furnace tube and the quartz tube wall. The temperature difference between the quartz reactor and inner furnace wall was found to be insignificant. The quartz reactor tube is positioned as such that the catalytic bed is at the centre of the furnace tube. The exposed parts of the reactor tube are insulated with Koa wool plug at either end of the furnace.

The outlet of the reactor tube is fitted with 1/16 inch stainless steel tubing sealed to the quartz reactor using ½ inch teflon ferrules and PTFE tape. This section is heated to 250°C by tripled wrapped Isopad ITH-75

heating tape insulated with Dalfratex tape. From the exit line of the reactor the 1/8 inch stainless steel tubes end up at the on-line gas chromatograph (GC).

2.2.3 PRODUCT ANALYSIS SYSTEM

The gas product analysis system is made up of an on-line GC and exhaust system. A Varian 3800 GC equipped with a PC-based Star 4.5 data handling software was utilised for purpose of product analysis. The GC is fitted with a 10 and 6-port gas sampling valves, Flame Ionisation Detector (FID) and a Thermal Conductivity Detector (TCD). The FID basically is used to separate all the hydrocarbons, while the TCD is used to separate CO, CO_2, and C_1 and C_2 hydrocarbon.

2.2.3.1 Columns

The columns used consist of a Phase Sep Porapak Q (80-100 Mesh, 12 feet , 1/8 inch O.D. , 2mm I.D.), and a Molsieve 5A (6ft, 1/8 in O.D , 2mm I.D) packed columns joined in series to end at the TCD outlet. To the FID end, a GSGasPro 60m with 0.32 I.D capillary column is connected. These columns are used for physical separation of the gaseous products.

2.2.3.2 Detectors

Two different types of detectors (flame ionisation and thermal conductivity detectors) were housed in the GC. They were configured in parallel so that simultaneous detection of chemical species was made possible.

Flame Ionisation Detector or FID is used to measure the concentration of hydrocarbon within a sampled gas. It is very robust and easy to use. It also has a high sensitivity, a large linear response range with low noise level, but unfortunately, it destroys the sample.

Methane, ethylene, ethane, carbon monoxide and carbon dioxide were detected by a Thermal Conductivity Detector or TCD. TCD is a universal, concentration sensitive, non-destructive detector. It measures the thermal conductance of a gas sample by monitoring the resistance of two identical heated resistors placed in the path of two different gas flow channels, i.e. sample and reference channel. A wheatstone bridge is used to balance the resistance. As small concentrations of analyte are eluted from the column to the sample channel, changes in thermal conductivity between these 2 identical resistors (sample and reference channel) are measured.

The concentration of each product appears as peak on the chromatogram. Area under the peak is divided by their respective Relative Sensisivity Factors (RSF) to give the true number of counts. The RSF were obtained from the calibration of each gas [1].

2.2.4 GAS CHROMATOGRAPHY CONFIGURATION

Figure 2.3 shows the GC configuration used for MDA product detection. The product stream flows through a 10-port gas-sampling valve located in the front injection-heating block. Two sampling tubes whose capacity being 50µl and 250µl were connected to the front end of the GasPro capillary and packed Porapak columns respectively, while the other ends are attached to this 10-port valve. Figure 2.4 gives a schematic diagram of the set-up. Switching of the valve results in dual injection of 50µl into the 60metre GS GasPRo column ending at the FID end and a 250µl injection into the Porapak and MoleSiev packed column ending at the

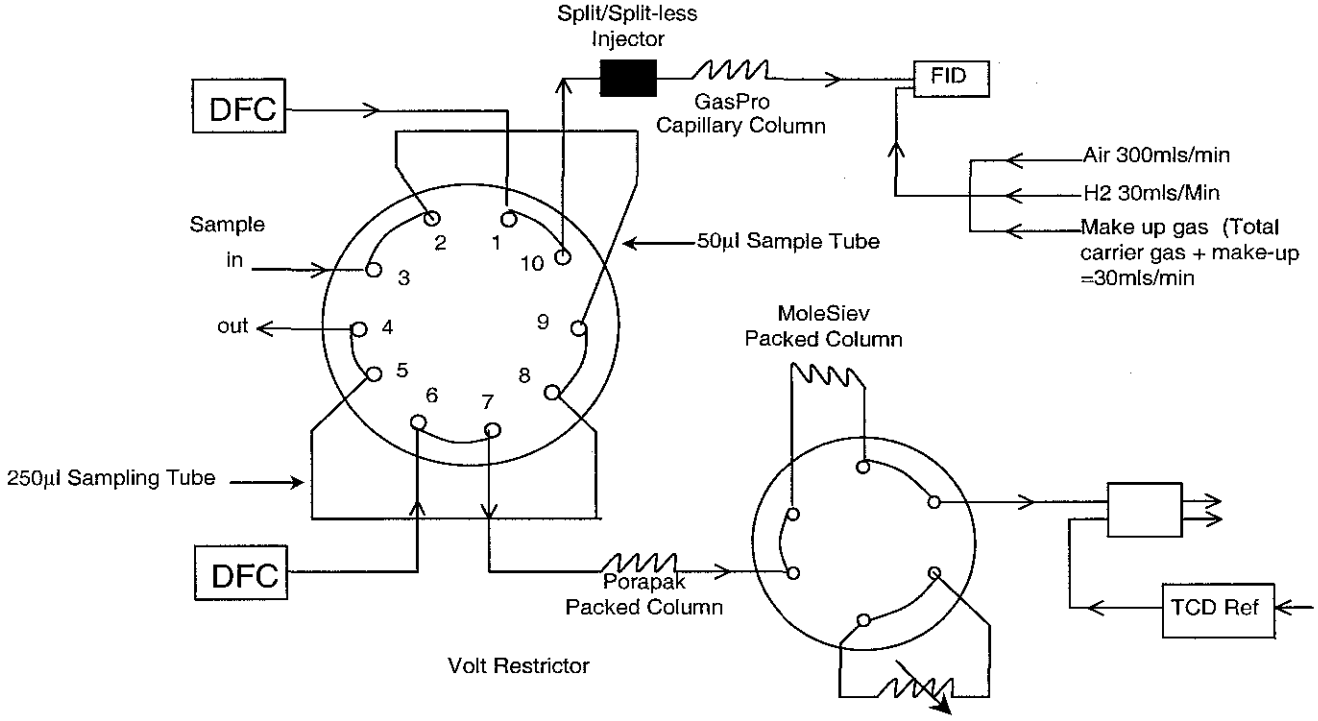

Figure 2.3 GC Configuration

TCD end. As for the 6-port gas sampling valve no switching is activated so as the packed columns of Porapak and MoleSiev aligned in series and ends at the TCD end. Sample injection is time programmed to dwell for 0.2 min, after which flow condition returns to initial mode.

2.2.5 GENERAL GC OPERATING CONDITION

The general GC operating condition is given in Table 2.1

Table 2.1 Gas Chromatograph Operating Conditions

Operating Units	Operating Parameters	Operating Conditions
Column Oven Temperature Programming	Column Stabilisation Time	10.0 mins
	Initial Column Temp.	80°C
	Initial Column Temp. Time	0.5 min
	Second Column Temp.	175° C
	First Ramp Rate	20.0°C/min
	2nd Column Temp. Hold Time	2.0 mins
	Final Column Temp.	250°C
	Final Ramp Rate	20.0°C/min
	Final Column Temp. Hold Time	30 mins
Oven Valve Temp	Midle Valve Oven Temp.	200°C
TCD Settings	TCD Temp.	250°C
	TCD Filament Temp.	350°C
	TCD Range	0.5
FID Settings	FID Temp.	275°C
	FID Range	11
	FID Split Ratio	10:1
	FID Attenuation	2

The packed column's back pressure and set at 46.0 psi initially and was held here for 0.5 min. After 0.5 minute, it was timed programmed to 60.0 psi at a rate of 2.9 psi/min. and held at this rate until the end of the GC cycle. A flow rate of 25ml/min gas flow was balanced with the TCD reference flow.

The GasPro capillary column on the other hand, the head pressure was set at 29.0psi with a flow rate of 3.9 ml/min at 80°C. This condition was observed to give the optimum product separation especially the heavy hydrocarbons. The injection port of the FID consists of a split/split-less injection mode. Product was injected in the split mode giving a split ratio of 10:1 so as to prevent 'flooding of column' .

2.2.5.1 Identification of Products

From the TCD data, argon, methane, carbon monoxide and carbon dioxide were easily separated. Table 2.2 gives the retention times for the products eluted through the columns pack column section consisting of a Phase Sep Porapak Q (80-100 Mesh, 12 feet , 1/8 inch O.D. , 2mm I.D.) and a Molsieve 5A (6ft, 1/8 in O.D , 2mm I.D).

Table 2.2 Product Identification From GC Retention Times

Product	Retention Times (mins)		RSF	
	TCD	FID	TCD	FID
Argon	1.78	-	1.00	-
Carbon monoxide	2.07	-	0.90	-
Methane	2.43	2.65	1.00	0.97
Carbon dioxide	4.80	-	0.90	-
Ethane	5.08	2.80	-	1.0
Ethylene	-	3.08	-	1.02
Propane	-	4.30	-	1.06
Butane	-	5.80	-	1.06
Benzene	-	11.10	-	1.12
Toluene	-	17.40	-	1.07
Para Xylene	-	22.80	-	1.07
Artho Xylene	-	26.30	-	1.07
Meta Xylene	-	27.60	-	1.07
Naphthalene	-	31.86	-	0.68

At the FID end, a GSGasPro 60m with 0.32 I.D capillary column was able to separate the hydrocarbon gaseous products which includes, methane, ethane, ethylene, propane, butane, benzene, toluene, xylene (alpha, meta and para) and naphthalene. Refer to Table 2.2 for the retention times.

2.2.5.2 GC Calibration

Quantification measurements in GC are based on the peak area generated by each component in a solution or mixture. Equal peak areas exhibited by different components do not necessarily mean equal composition or quantity. Each component has different response to different carrier. Individual peak area was divided by its respective RSF to obtain a comparable value.

2.2.5.3 Quantification of Data

The primary reactant introduced into the GC was quantified at the TCD terminal. The primary reactant used was methane with argon as internal standard which was specially prepared by British Oxygen Company (BOC) for this reaction. Argon, the internal standard in this reaction is non reactive. It was used to determine the methane consumed in the reaction by back calculation method.

Using Ar as the internal standard quantification of product and feed is more consistent. For the on-line measurement for methane conversion, selectivity and rate of formation calculation was based on Masaru Ichikawa et al [2] and Anderson [3].

The calculation is based on the principles of carbon mass balance. By measuring the total inlet gas flow rate into the reactor, the total outlet gas flow rate from the reactor can be accurately determined. Based on this concept, they derived a calculation method to determine methane

conversion and hydrocarbon product selectivity. The carbon deposit or coke here is expressed as total methane consumed and include undetected heavy aromatics, amorphous carbon and graphitic carbon on the catalyst and others which are trapped in the transfer lines. Based on this concept they produced the calculation given as below.

Since Ar is non-reactive in this reaction the mole fraction of Ar should be consistent in both the inlet and outlet flow rate of the reactor.

Thus it follows:

$$F^{inlet} X_{Ar}^{inlet} = F^{outlet} X_{Ar}^{outlet} \qquad \text{Equation 1}$$

Where F^{inlet} and F^{outlet} represent the flow rate of feed in and out of the reactor.

Whereas X_{Ar}^{inlet} and X_{Ar}^{outlet} represent the mole fraction of argon inlet and outlet flow respectively.

Since the methane is the only reactant in the feedstock which is consumed, conversion can be accounted on the basis of consumption of methane in this reaction. Thus it follows:

$$Conversion = \frac{F^{inlet} X_{methane}^{inlet} - F^{outlet} X_{methane}^{outlet}}{F^{inlet} X_{methane}^{inlet}} \qquad \text{Equation 2}$$

Equation 2 can be further simplified as:

$$= 1 - \frac{X_{methane}^{outlet} X_{Ar}^{inlet}}{X_{methane}^{inlet} X_{Ar}^{outlet}} \qquad \text{Equation 3}$$

The hydrocarbon product ($S_{product}^{carbon}$) in the gas phase can be further exploited from equation 2 and 3 and $N_{product}^{carbon}$ is the carbon number of the product.

$$S_{product}^{carbon} = \frac{F^{outlet} X_{product}^{outlet} N_{product}^{carbon}}{F^{inlet} X_{methane}^{inlet} - F^{outlet} X_{methane}^{outlet}} \qquad \text{Equation 4}$$

Simplification of equation 4 results in:

$$= \frac{X_{Ar}^{inlet} X_{product}^{outlet} N_{product}^{carbon}}{X_{Ar}^{outlet} X_{methane}^{inlet} - X_{Ar}^{inlet} X_{methane}^{outlet}} \qquad \text{Equation 5}$$

The coke or carbon deposit on the catalyst can be determined by:

$$\text{Coke} = 1 - \sum S_{product}^{carbon} \qquad \text{Equation 6}$$

The rate of formation of a particular product can be calculated from results obtained from % product selectivity, % conversion, flow rate and weight of catalyst used. Flow rate is expressed in nL/sec and catalyst in gram.

From the ideal gas equation

$$PV = nRT \qquad \text{Equation 7}$$

$$n = \frac{PV}{RT} \qquad \text{Equation 8}$$

Mole is expressed in nmol methane per second (nmol CH_4 s^{-1})

$$R^{formation} = \frac{C^{\%methane} S^{\%product} F^{methane}}{10000 M^{catalyst}} \qquad \text{Equation 9}$$

Where R, C, S, F and M is rate of formation, conversion, selectivity, flow rate and mass of catalyst respectively. The final unit is nmolC/g.sec.

It is necessary to divide by 10000 to convert % to real numbers.

2.3 Mass Transfer Limitation

Catalyst testing of the Mo- modified HZSM-5 zeolite for the dehydro-oligomerisation and aromatisation reaction of methane in the absence of oxygen was carried out in a continuous flow micro reactor system. The outlet of the micro reactor is connected to the inlet of the gas

chromatography (GC) via heated traced lines. The product obtained was evaluated using an on-line GC.

Mass transfer limitation effects in any catalytic process should be minimised in order to obtain realistic intrinsic reaction rates. The most common mass transfer limitation factor arises usually from packing and particle size of the catalyst or in some the type of reactors. In heterogeneous catalytic systems, these mass transport limitation results in the evolution of temperature and concentration at the boundaries of the two phases i.e. the catalyst surface and reactant and/or products end or the reactor wall and packed catalyst. These constraints give rise to interphase (external) as well as intraphase (internal) gradient limitations. These limitations must be negligible or eliminated to avoid any deviation from ideal behaviour, thus enabling intrinsic reaction rates to be determined quite accurately.

Interphase (external) gradient limitation is usually associated with the volume or mass of the catalyst bed as opposed to the flow of the reactant through this bed in a batch or continuous reactor system. Diagnosis test can be conducted by fixing GHSV and varying the catalytic bed volume or weight. Deviation in the flow rate or conversion at similar conditions and environment indicates that the system is limited by external diffusion.

In the case of Intraphase (internal) gradient limitation which is closely associated with the catalyst particle size and the flow of the reactant through the reactor system. Here the catalyst weight or volume is kept constant together with GHSV fixed at reasonable conversion or flow. Any deviation observed renders the system as limited by internal diffusion.

Diagnosis studies conducted with a fixed GHSV of 1000 h^{-1} at 700°C and 1 atmosphere by Anderson [2] shows that the system is not limited by interphase (external) nor intraphase (internal) gradient limitations for similar reaction testing conditions if the particle size of the catalyst lies between 250 to 425 μm and catalyst weight lies between 0.2 to 0.7g. In all further tests conducted hereafter, the catalyst particle size was fixed at 250 to 425μm and the quartz reactor was used.

2.4 Characterisation Techniques

2.4.1 NITROGEN ADSORPTION

BET and Langmuir specific surface area and pore properties measurements were obtained from volumetric nitrogen adsorption using a Micromeritics ASAP-2010 instrument equipped with PC based V1.01 software.

Approximately 0.10 to 0.15g of catalyst was weighed into a sample tube. The sample was heated to 90°C and out-gassing slowly to 80 mm Hg. After this stage the out-gassing was carried out at a fast setting to reach 10 mm Hg. The sample was then heated up to 250°C and maintained at this temperature for 0.5 hour. Following out-gassing, the samples were cooled to ambient temperature. The sample and sample tube was transferred to the analysis section. The analysis was carried out at 77K (-196°C) by a fixed increment of nitrogen dosages onto the sample. A physical isotherm thus built up is used to plot a straight line according to the method proposed by Brunauer, Emmett and Teller [4] Equation 2 shows the BET equation.

$$\frac{P}{V(Po - P)} = \frac{1}{V_m C} + \frac{(C - 1)}{V_m C} \bullet \frac{P}{Po} \qquad \text{Equation 10}$$

Where :

V is the volume adsorbed at Pressure P

V_m is the volume of gas required to form an adsorbed monolayer
Po is the saturated vapour pressure of the gas at 77K
C is a constant that reflects the difference in heat of adsorption between the 1st and the 2nd adsorbed monolayer.

From the straight-line plot, V_m is calculated which is used to determine the surface area assuming that a molecule of nitrogen occupies $0{\cdot}162nm^2$. The extent of microporosity can be estimated from the t-plot method derived by Lippens and de Boer [3]. The method plots the volume of nitrogen adsorbed against the statistical thickness (t) of the adsorbed layer calculated from a universal reference isotherm (in this case Harkins and Jura). Equation 3 shows the Harkins and Jura equation.

$$T= [13.9900/0.0340 - \log (P/Po)]^{0.5} \qquad \text{Equation 11}$$

Where:
T is the statistic thickness in Å
P/Po is the relative pressure
Thickness range 1.5 to 3.4 Å (for extrapolation)
Another measure of the porosity can be estimated from the BJH Desorption Cumulative Pore Volume [5].

2.4.2 THERMOGRAVIMETRIC ANALYSIS (TGA)

Thermogravimetric Analysis using a Perkin Elmer TGA-7 thermo gravimetric analyser was employed. TGA measures the changes in weight of a material heated at constant heating rate under a controlled environment (He, N_2, air, etc). The controlled environment in this study was air which was used to monitor the decomposition and phase changes in fresh catalysts, as well as the amount and nature of coke deposits and carbidic species on deactivated catalysts.

Measurement is made by weighing approximately 20 mg of sample placed in a platinum crucible hung from a microbalance. The sample was heated to about 30°C and maintained at this temperature for 2 minutes. The temperature was then ramped to 700°C at a constant rate of 10°C/min under an air environment with a constant flow rate of 20ml/min.

2.4.3 X-RAY DIFFRACTION ANALYSIS

Powder XRD is a very important technique for the qualitative and quantitative characterisation of zeolites. The diffraction pattern is characteristic of the material analysed and can act as a 'fingerprint' for identification of the phases present.

XRD diffraction patterns were obtained at room temperature using a Siemens D5005 diffractometer (CuK_α radiation, step-size 0.014°). Diffractograms were recorded for 2θ values ranging from 10 to 80° with a scanning rate of 0·05 s/step. The carbide region (2θ = 30-50°) is of particular interest. The diffraction pattern was then transferred to PC and was analysed using Xpert Plus software.

2.4.4 ELEMENTAL ANALYSIS

Elemental analysis is an important quantitative tool to determine the elements of carbon, hydrogen and nitrogen in organic compounds [6]. The elemental analysis was carried out using the Thermo EA Flash 112 using Eager 300 soft ware

About 1.0 mg sample was accurately weighed by a precision microbalance and placed into a tin capsule and sealed. The tin sample capsule was then placed sample rack above a heated reactor tube maintained at 1030°C with a constant He flow. The sample capsule is

than automatically introduced into the heated reactor tube. On introduction of the sample capsule, the reactor tube is temporarily enriched with pure oxygen to flash combust the sample. The carbon, nitrogen and hydrogen are subsequently converted to CO_2, NO_x and H_2O respectively during this flash combustion process. The tail gas from the reactor tube then passes through a reduction tube filled with fine Cu turnings, which acts as trap and reduces the NO_x into N_2. The reduced gas then is directed into a packed GC Porapak column maintained at 100°C, where the N_2, CO_2 and H_2O are separated before being finally being detected by TCD. The software than quantifies the products into total C, H and N.

The elemental microanalysis were obtained by submission of samples to the analytical laboratory of the University of Liverpool.

2.4.5 INDUCTIVE COUPLED PLASMA- ATOMIC EMISSION SPECTROSCOPY (ICP-AES)

ICP-AES is bulk technique for multi-element detection which includes metals and metalloids at ultra trace, trace, minor and major concentration levels [6]. Inert gases and some prominent non-metals like C, H, O and N are not detected by ICP-AES.

ICP-AES utilises plasma, an electrically neutral, highly ionized gas that consists of ions, electrons and atoms. The plasma used is normally pure argon or helium which is heated to 8,000K by means of high frequency electric or magnetic fields. The plasma acts as a carrier for sample solutions making them completely atomised for easy detection. A schematic of a typical ICP-AES is given in Figure 2.4

The ICP-AES was carried out on a Spectro Ciros CCD emission spectrometer. The results obtained is by submission of samples to the analytical laboratory of the University of Liverpool.

2.4.5.1 Sample Preparation and Digestion

The sample preparation and digestion for the ICP-AES analysis was carried out in a Microwave Accelerated Reaction System using MARS5 V047917 Software. The procedures are as follows:

1. 20 mg. of the sample is weighted accurately into a PTFE crucible.
2. To the sample an acid mixture of 10ml conc. nitric acid, 2ml hydrofluoric acid and 2 ml of hydrochloric acid is added. All the acid used in the acid mixture is of spectroscopy grade.
3. The PTFE crucible is than secured by kervlar sleeve to prevent explosion.
4. The secured vessel is then sat in an industrial microwave oven together with a control vessel for maintaining the temperature and pressure in the vessel at 220°C and 600 psi.
5. The microwave is than time and temperature programmed to heat the sample from room temperature at a ramp rate of 20°C/min to 180°C. Here the temperature is maintained for 10 mins, before being cooled to room temperature and allowed to settle for 10 minutes before being open.

Note: It is important that the sample is clear and has no traces of sediments; if not procedures 2 to 5 have to be repeated.

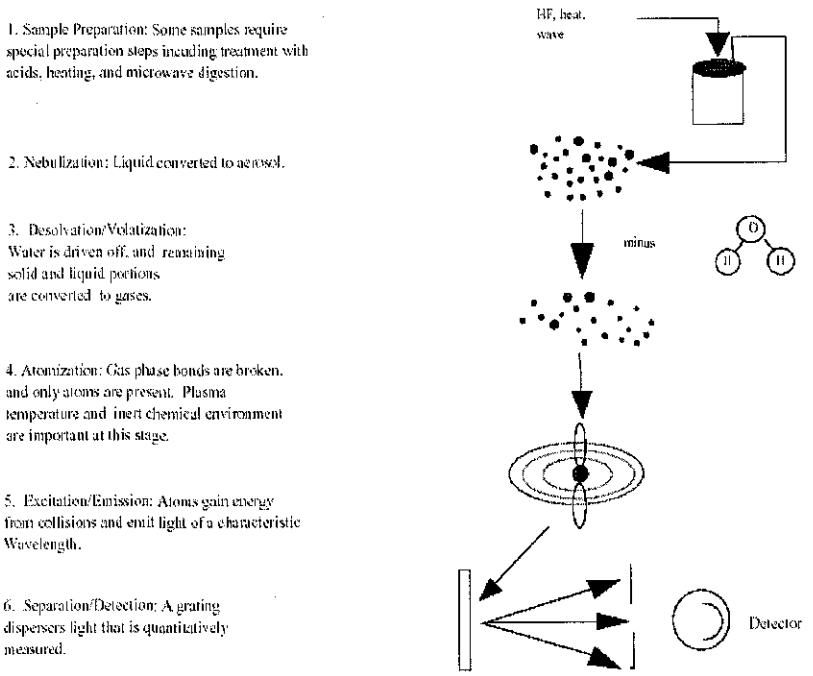

Figure 2.4 Schematic for ICP-AES (Extract taken from Ref7)

2.5 Reference Chapter 2

1. Dietz, W.A., J Gas Chrom., 70 (1967) 68
2. Lin, S., Dong, Q., Ohnishi, R., and Ichikawa, M., Chem. Commum., (1997) 1455Anderson, J.R., PhD Thesis, University of Liverpool, UK (2001)
3. Gregg, S.J., and Sing, K.S.W., Adsorption Surface Area and Porosity, Academic Press, London, 1982
4. Barret, E.P., Joyner, L.G., and Halenda, P.P., J. Am. Chem. Soc. 73 (1953) 373
5. Mendham, J., Denney, R.C., Barnes, J.D., and Thomas, M.J.K., Vogel's Textbook of Quantitative Chemical Analysis, Pearson Education Ltd., 2000
6. http://www.mrl.ucsb.edu/mrl/centralfacilities/chemistry/icp.pdf

CHAPTER 3 PRELIMINARY TESTING

3.1 Introduction

The main objective of many researchers in DMA catalysis is to improve reactivity, stability and selectivity of aromatics. For MDA reaction, it has been accepted by most researchers in this area that Mo/HZSM-5 zeolite prepared by impregnation is the best catalyst [1-4]. Furthermore, the importance of the channel structure and acidity of the HZSM-5 zeolite, as well as the valence and location of Mo species are crucial factors in catalytic performances [3].

The active catalyst for the title reaction is believed to be bifunctional in nature. The AHM (Mo precursor) impregnated is converted to MoO_3 by calcination which is then transformed to Mo-carbide by an activation mixture. Methane is converted to aromatics at specific reaction conditions by the Mo-carbide and Bronsted acid sites of the zeolite [3,4].

Having done a comprehensive literature search (please refer to Chapter 1 and references 1-7), a set of preliminary conditions were selected to choose the most desirable gas hourly space volume (GHSV) for the methane feed.

3.2 Experimental

3.2.1 MICRO-REACTOR OPERATION

Methane dehydro-oligomerisation and aromatisaton (MDA) reactions are commonly performed in a flow micro-reactor on a batch scale at atmospheric pressure. The reaction temperature commonly used is 700°C, and the catalyst is Mo loaded on HZSM-5 zeolite. The Mo content can vary from 2 to 10 wt% on the catalyst HZSM-5 support. The most common feedstock is undiluted methane or methane with a fixed volume of non-reactive internal standard such as argon or nitrogen [2,8-

10]. In the present study, 3 vol % Ar (internal standard) in methane (main reactant) was used. Ar is selected as a control as it is inert in MDA reaction. Assuming that the volume % of Ar and methane is fixed, any irregularity in the methane flow rate can be re-checked by Ar flow as it a control in this reaction. The calculation method employed by Ichikawa et al [9] was used to constantly monitor the methane flow rate/concentration at the inlet as well as the outlet of the reactor. Refer to Chapter 2 subsection 2.2.5.3 for a more detailled explanation.

The catalyst in the present study is the β-form of 3 wt% Mo modified HZSM-5. Calcination was carried out ex-situ under air as described in section 2.1 of chapter 2. The MDA reaction is conducted in a quartz micro reactor (section 2.2 of chapter 2) as described below.

0.3 grams of calcined catalyst was introduced into the quartz reactor tube with an i.d of 10mm and length of 450mm. The catalyst sandwiched between about 0.2g of quartz wool, placed at the mid section of the reactor supported by internal protrusion groves (Figure 2.2 of Chapter 2). To the calcined catalyst in the reactor, helium is introduced by Brooks Mass flow controllers at a flow rate of 12.5 ml/min (GHSV 2500h^{-1}). The catalyst was then heated to the first ramp stage of 400°C at a constant rate of 10°C/min and was dwelled at this temperature for 0.5 hour. This represents the drying stage. Here most of moisture that may be present in the catalyst or the system is removed. Moisture present may influence increase in mobility of the Mo species present in the catalyst causing it to agglomerate resulting in sintering of the catalyst and/or volatilisation [10].

After the drying stage, the temperature was held for a further 10 minutes at 400°C to accommodate a change in medium from helium to a mixture of 3% v/v argon (control) in methane with the same flow-rate of 12.5

ml/min. The temperature was then ramped to the second stage of 700°C at a constant ramp rate of 5°C/min under Ar/CH_4 mixture and held here for an hour. This is basically to activate the catalyst since MDA reaction has an induction period [1, 11-13]. At this stage the reduction and carburisation of the MoO_3 takes place where it is converted to the β-form of Mo-carbide [10], the active Mo site.

At 700°C, at the end of the reduction and carburisation stage, the mixture was switched off and replaced by a 2nd helium purge with a reduced flow rate of 7.5 ml/min and held at this temperature for 10 minutes. This is done so as to remove any contaminants or deposition that may be present before preparation for the final reaction stage. After 10 minutes, the helium purge is replaced by the main reactant. (3%v/v Ar in CH_4), at fixed and required flow rate for the GHSV study.

After the induction period, the first 10 minutes-products from the reaction stage is piped via the outlet of the reactor to an on-line GC for identification and quantification. GC data obtained from the reactor products were transformed to results of conversion, selectivity and rate of product formation based on the calculation section 2.2.5.3 of Chapter 2. After the 1st 10 minutes-product, the GC was automated to analyse further reactor products on an hourly basis up to 20 hours inclusive, continuously. The reactor's inlet and tail products for each hour were recorded, tabulated, analysed and transformed to the required results mentioned above using Microsoft Excel spreadsheet software program.

At the end of the 20 hours (reaction stage) the heating was discontinued and the reactor was allowed to cool to room temperature. At this stage methane was replaced by a 3rd helium purge flowing at 12.5 ml/min.

The spent catalyst was then removed from the reactor and placed in a 5 ml glass vial for further catalytic investigation.

The above procedure was used as a basis for further methane dehydro-oligomerisation and aromatisation reaction.

3.2.2 EFFECT OF GAS FLOW

Hourly space velocity quoted in literature for this type of reaction varies from GHSV 800 to 4500 h^{-1}[3-6]. As for the reaction temperatures, they are usually measured between 650 to 900°C [4, 7]. The main criterion for optimisation in this study is methane conversion, good selectivity for aromatics with special reference to benzene and naphthalene, low carbon deposition or lower catalyst decay.

To start off the study, effects of space velocity on methane conversion were analysed. Most authors believe that a GHSV of 800 to 1500 h^{-1} is optimum [3-6]. In this study the GHSV investigated were from GHSV 800 to 2500 h^{-1}. Six GHSVs were selected which include 800, 1000, 1200, 1500, 2000 and 2500 h^{-1}. Reaction time on stream (TOS) was fixed for 20 hours. This excludes the catalyst activation time of one hour, see above. The flow rates of methane were conducted between 5.0 to 12.5 ml/min to reflect the GHSV 800 to 2500 h^{-1} respectively.

For each of the different GHSV studied, the methane conversion, product yield % and rate of formation was calculated as in subsection 2.2.5.3 of Chapter 2. The desirable products include the aromatics, especially benzene and naphthalene (main fraction), and toluene and xylene (minor fraction) and the aliphatics namely ethane and ethylene. As for the undesirable product i.e. carbon deposition or coke, this was calculated based on the difference between the total methane conversion and the measured products (aromatic and aliphatic). The coke also includes the

carbon consumed to form β - Mo_2C, the active catalyst for MDA reaction, condensable products remaining in the zeolite channels or trapped in the transfer line and other undetected component.

3.2.3 CATALYTIC CHARACTERISATION

The freshly calcined, activated and the spent catalyst were analysed by catalyst characterisation unit (please refer to section 2.4 Chapter 2). XRD (powder) was used to monitor the change in structure if any. As for the catalyst support, surface topography and channel network were analysed by micrometric surface analyser. Mo content was also monitored by ICP-AES to check for loss. Carbon deposition and hydrogen content on the catalyst were determined by elemental analysis to cross check GC data. Kinetic data like catalyst activation energy and deactivation rate was also calculated from TGA data in the process to have a better selection of the optimised GHSV.

3.3 Results and Discussions

3.3.1 METHANE CONVERSION

In order to distinguish the most suitable GHSV for reaction yield and methane conversion the average for the first 10 hours (1^{st} -10^{th} hour) followed by the second 10 hours (11^{th} to 20^{th} hour) for the various GHSV were calculated. Averaging for 10 hours was done so as to have a better understanding of the reaction yield and cumulative rate of formation trend. The 1^{st} 10 hours will be grouped in curve A and the 2^{nd} 10 hours in curve B hereafter unless stated otherwise. These two curves were chosen so as to monitor changes if any, in variation towards conversion or production trends with time on stream (TOS). Averaging was done so as to have more consistent values. The following analysis was done using 3wt% Mo impregnated on HZSM-5 catalyst at a reaction temperature of 700°C with variation GHSV as mentioned above.

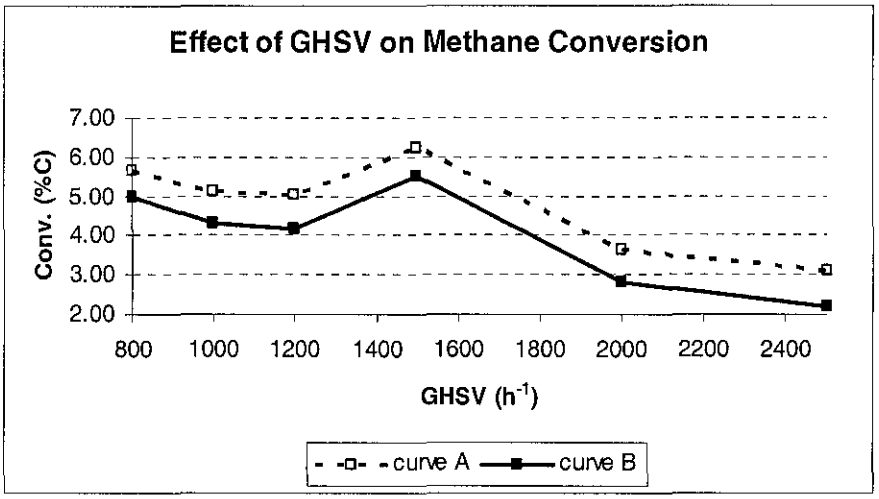

Figure 3.1 Effect of GHSV on Methane Conversion on 3wt% Mo/HZSM-5

Figure 3.1 depicts the methane conversion on 3wt% Mo/HZSM resulting from varying the GHSV from 800 to 2500 h^{-1} and fixing all the other process conditions. Methane conversion is based on the carbon conversion. The methane conversion in this study represents a general criterion on the catalyst activity.

From Figure 3.1 it can be seen that both curve A and B have similar trend towards the GHSV investigated from 800 to 2500 h^{-1}. The main difference between the 2 curves is in the numerical value; curve A has a higher methane conversion rate than curve B and a general drop of less than 1% methane conversion is observed throughout the whole GHSV studied between the 2 curves. This shows that the conversion decreases with time on stream (TOS).

From Figure 3.1 it can be seen that GHSV 1500 and 800 h^{-1} seem to give better methane conversions than the rest. The optimum methane conversion is observed at GHSV 1500 h^{-1}. On increasing the GHSV from 800 to 1200 h^{-1} methane conversion is observed to decrease gradually.

On further increase of GHSV to 1500 h^{-1} the methane conversion suddenly increases to its optimum value recorded in this study. After GHSV 1500 h^{-1}, methane conversion drops with further increase in GHSV. Other researchers have also reported similar findings where the optimum methane conversion is in the vicinity of 1500 h^{-1}. Xu and Lin [2] in summary for MDA reaction show that 800, 1440 and 1500 h^{-1} are the favourite GHSV used by most MDA researchers. They also suggested in selecting the optimum methane conversion, there should be a balance between the Mo active sites and the Bronsted acid sites. Liu and Xu [14] suggest that 60% of the BAS of parent HZSM-5 zeolite should be retained on Mo modified catalyst in order to have good methane conversion.

It is also interesting to note that the catalytic activity also deteriorates with TOS by definition. It is generally agreed that the catalytic deactivation in MDA type reaction is mainly due to coke deposition [15-19]. This catalytic deactivation may be brought about as a result of inhibition of the product leaving the catalyst surface due to their strong adsorption and slow desorption properties, and their slow diffusion within the channels resulting in condensation of the product on or within the catalyst[20]. Other possible reasons may be a change in catalytic surface or bulk properties [21] may effect catalytic deactivation.

3.3.2 ELEMENTAL COMPOSITION

In order to further understand whether catalytic activity decreases due to changes in the catalytic composition or structure with changing GHSV and TOS, catalyst characterisation tests were conducted as described in section 2.5 of Chapter 2.

The elemental content for Mo, Al and Si of the spent catalyst determined by ICP-AES as described in section 2.5.4 of Chapter 2 are tabulated in

Table 3.1. Both the respective elemental contents and ratio are calculated on a weight % basis.

Table 3.1 Elemental Distribution from Spent 3wt% Mo/HZSM-5

GHSV	Weight %			Weight Ratio	
	Mo	Al	Si	Mo/Al	Si/Al
Zeolite	0	0.96	39.68	-	41
Fresh Calcined	2.24	0.85	35.12	2.6	41
Activated	2.21	0.85	34.5	2.6	41
800	2.09	0.80	32.7	2.6	41
1000	2.11	0.81	34.2	2.6	42
1200	2.12	0.82	34.1	2.6	42
1500	2.14	0.83	33.7	2.6	41
2000	2.11	0.82	33.7	2.6	41
2500	2.09	0.80	32.9	2.6	41

Table 3.1 shows the experimental elemental distribution of Mo, Al and Si of the parent zeolite support, impregnated Mo/HZSM-5 which include the freshly calcined and the activated β- Mo/HZSM-5, and the spent catalyst (20 hours TOS) at various GHSV values.

The zeolite support used in this study had a Si/Al ratio of 41. This was performed so as to investigate loss if any, on the main catalytic component.

It can clearly be see that the Mo content of the activated, calcined and spent catalysts after different GHSV treatment show no appreciable changes in its content and are within the acceptable error of the ICP analyser. This is in agreement with Borry et al [20] who pointed out that if the catalyst are prepared and calcined at the right conditions whereby there is strong interaction and bonding between the Mo active species and the Al from the zeolite framework, loss of these catalytic

components can be minimised. This statement is further strengthened by the fact that Mo/Al elemental ratio for the whole series is always maintained at 2.6 although there is a small variation of Mo and Al elemental content. This is also observed for the Si/Al elemental ratio, which is maintained between 41 and 42 for the whole range of catalyst analysed. Individual variation of Mo, Si and Al may be due to the presence of other components mainly coke and condensable hydrocarbon on the catalyst. The Si/Al and Mo/Al weight ratio eliminate this variable from the analysis. These results clearly indicate the catalyst does not deactivate based on loses of its metallic content as a result of variation of GHSV or TOS after 20 hours.

3.3.3 X-RAY DIFFRACTION ANALYSIS

The next question that should be addressed is the structure competent of the catalyst. To further understand the structure integrity of the catalyst, (powder) XRD analysis on the activated as well as the spent catalysts were compared. Figure 3.2 represents this comparison. From this figure, it can be clearly seen that there is no structural distortion or any appreciable change in the structure of the studied catalysts. This clearly indicates that GHSV has no effect on the structure of any of the catalyst studied. This is in agreement with studies by Zhong et al [8].

From the information derived above, it suggests that neither the structure nor the catalytic components are altered with variation of GHSV or with increased TOS. But catalytic activity namely methane conversion **DOES** change with variation of GHSV and TOS. The next stage of investigation will be directed to product yield analysis.

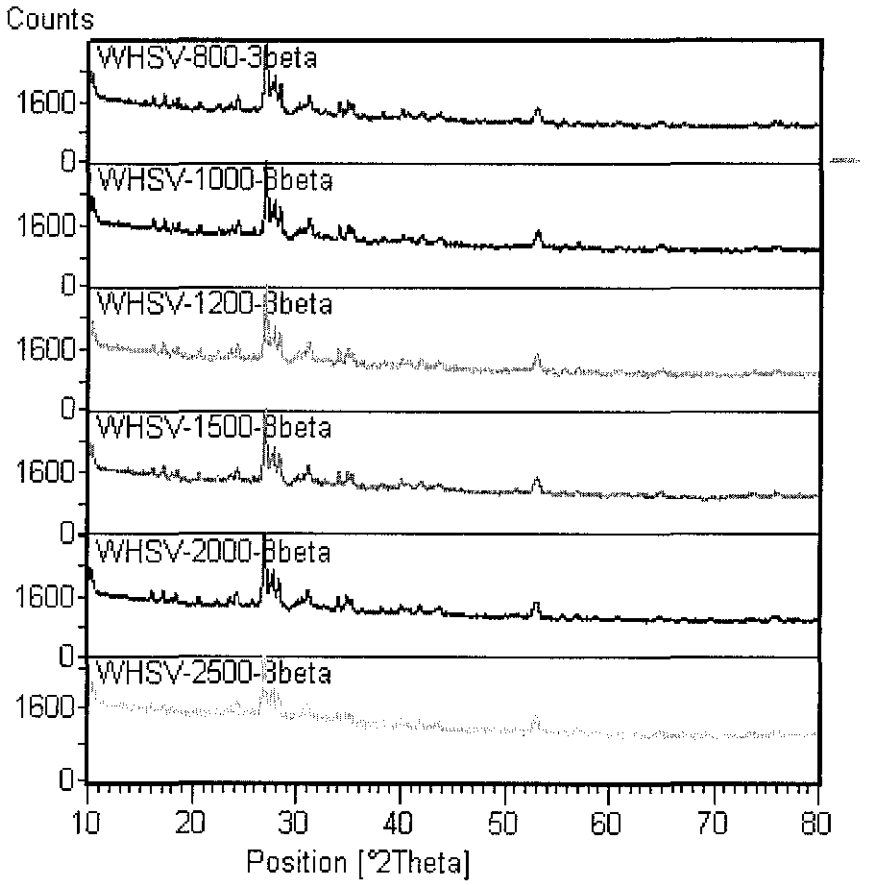

Figure 3.2 Powder XRD Pattern of 3wt% Mo/HZSM-5 Spent Catalyst at Various GHSV

3.3.4 MDA PRODUCT ANALYSIS

The product analysis can be classified under three main groups namely aromatics, aliphatic and coke. The desirable products in this reaction are the aromatics, the undesirable product coke which is basically made up of carbon deposit and heavy aromatics, which condense on/in the catalyst. The aliphatic on the other hand is a less valuable by-product.

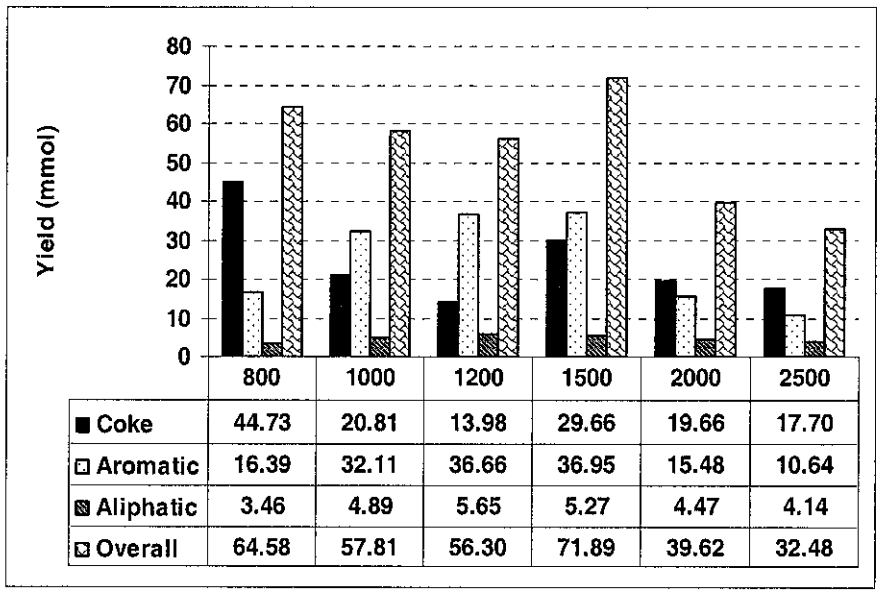

	800	1000	1200	1500	2000	2500
Coke	44.73	20.81	13.98	29.66	19.66	17.70
Aromatic	16.39	32.11	36.66	36.95	15.48	10.64
Aliphatic	3.46	4.89	5.65	5.27	4.47	4.14
Overall	64.58	57.81	56.30	71.89	39.62	32.48

Figure 3.3 Effect of GHSV on Product Yield Distribution

Figure 3.3 highlights the findings of the product yield distribution of carbon deposit, aromatic, aliphatic and the overall or total product yield in the form of a bar chart. The individual product yield is calculated from the average rate of formation yield of the respective product obtained over a 20 hour TOS.

From the Figure 3.3, it can be noticed that the rate of formation of MDA products or catalytic activity is the highest between for GHSV 800 to 1500 h^{-1}, after GHSV 1500h^{-1} the catalytic activity decreases very steeply with GHSV 2500 h^{-1} recording the lowest catalytic activity and GHSV 1500 h^{-1} the highest for the entire series. From the same figure, GHSV 800 h^{-1} has the highest and GHSV 1200 h^{-1} the lowest coke yield. In the case of aromatic from Figure 3.3, it can be seen that highest yield is observed at GHSV1500 h^{-1} and the lowest at GHSV 2500 h^{-1}.

The aliphatic fraction, although the minor product in MDA reaction, is important because of its precursor role in the production of aromatics.

From Figure 3.3 it can be seen that the aliphatic content increases with increase in GHSV in general. The highest aliphatic yield is at GHSV of 1200 $h^{-1}$and the lowest is at 800 h^{-1}.

Table 3.2 Effect of GHSV on MDA Product Selectivity

GHSV (h^{-1})	800	1000	1200	1500	2000	2500
Coke (%)	69.3	36.0	24.8	41.3	49.6	54.5
Aromatic (%)	25.4	55.5	65.2	51.4	39.1	32.8
Aliphatic (%)	5.4	8.5	10.0	7.3	11.3	12.7

Table 3.2 shows the product selectivity calculated from Figure 3.3. From the same table, it can be seen that with increase in GHSV from 800 to 1200 h^{-1}, a decrease in coke selectivity is observed. From GHSV 1200 to 2500 h^{-1} the coke selectivity increases with further increase in GHSV. It is interesting to note that the product selectivity for both coke and aromatic follows a reverse trend which suggests that coke and aromatics have a similar intermediate [2].

The aliphatic product selectivity on the other hand seems to increase in general across the board, the only deviation is at GHSV 1500 h^{-1}, and the selectivity reduces to 7.3% from 10.0% at 1200 h^{-1}.

To summarise the findings from Figure 3.3 and Table 3.2, it can be seen GHSV 2000 and 2500 h^{-1}, are least promising of the whole study and will not be considered for further selection.

Good catalytic activity is observed between GHSV 800 to 1500 h^{-1}. This is in agreement with the review by Xu and Lin on recent MDA advances [2], where they found that GHSV 800, 1440 and 1500 h^{-1} are favourites among MDA researchers. Between GHSV 800 to 1500 h^{-1}, it can be seen that GHSV 800 h^{-1} has the highest coke yield and selectivity, the lowest aromatic yield and selectivity and the 2nd highest catalytic activity. These

observations make GHSV 800 h^{-1} unsuitable for selection. GHSV 1000 h^{-1} although better than 800 h^{-1}, it is much less promising than either 1200 or 1500 h^{-1}.

This leaves GHSV 1200 and 1500 h^{-1} which show promising prospects for selection for optimised GHSV. Comparing between the two, GHSV 1200 h^{-1} has the lowest coke yield and selectivity, highest aromatic selectivity and almost similar aromatic yield as that of GHSV 1500 h^{-1}. As for the catalytic activity, it is much lower than 1500 h^{-1}. GHSV 1200 h^{-1} catalytic activity is about 78% of that of GHSV 1500 h^{-1}. In the case of GHSV 1500 h^{-1}, it has the highest catalytic and aromatic yield and 2nd highest coke yield. Based on these observations, it can be seen that both GHSV 1200 and 1500 h^{-1} show good selection for GHSV, but GHSV 1500 h^{-1} has a slight edge in that it has the higher catalytic and aromatic yield.

3.3.5 ALIPHATIC PRODUCT

3.4.5.1 Ethylene and Ethane

The debate on the primary product of the MDA reaction has been inconclusive. The argument between ethylene and ethane as the main primary product was discussed and demonstrated in the paper by Xu and Lin [2]. Many researchers in this area suggest that ethylene [16,17,20] is the primary product which further undergoes polymerises to form benzene and higher aromatics.

Figure 3.4 shows the effect of ethane and ethylene yield with varying GHSV over 20 hours TOS.

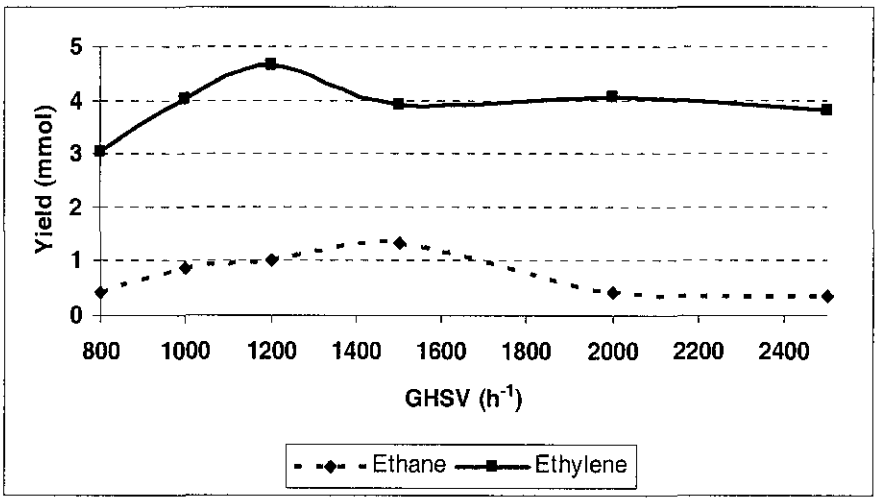

Figure 3.4 Effect of GHSV on the Yield of Ethylene and Ethane

From the above observation from Figure 3.4, it can be suggested that both ethane and ethylene may not have a common intermediate, because both follow a similar yield pattern. The main difference is in the yield produced, ethylene has a much higher yield than ethane on an average ratio of 7:1. This observation may be one of the reasons for the debate which is inconclusive as to whether ethylene or ethane is the primary product of the MDA reaction [2].

Figure 3.5 on the other hand represents the ethylene and ethane % selectivity. This values is calculated based on the % of ethylene and ethane obtained from the yield of aliphatic fraction at the specific GHSV.

From the Figure 3.5, it can be seen that both % selectivity of ethylene and ethane follows a different pattern, decrease in ethylene results in increase in ethane and vice-versa.

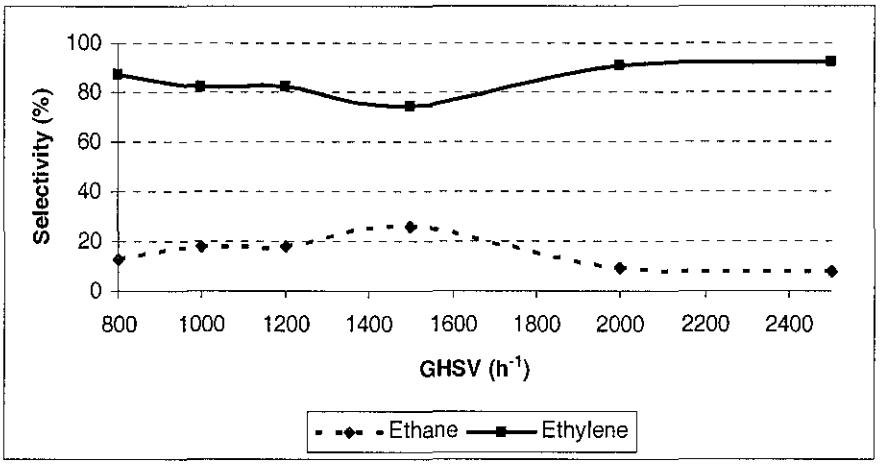

Figure 3.5 Effect of GHSV on the Selectivity of Ethylene and Ethane

The observation on the yield in Figure 3.4 shows a different pattern as compared to Figure 3.5 which shows the % selectivity of ethylene and ethane of the aliphatic fraction. From Figure 3.5, it can be seen that both ethane and ethylene have a different selectivity pattern. Increase in one component results in the decrease in the other, suggesting both of them may be part of a common intermediate. To further substantiate this finding, measurements at higher GHSV and lower conversion will be required.

3.3.6 AROMATIC FRACTION

The main priority for this study is the optimisation of aromatics especially benzene and naphthalene. Formation of aromatics are more favoured over ethane based on thermodynamic conditions proposed for MDA reaction as discussed in product selectivity above and in subsection 1.4.2.1 of Chapter 1.

The aromatics can be broadly classified into 3 main components, namely benzene, naphthalene, (the major fraction) and toluene and xylene (the minor fraction). Figure 3.6 represents the average cumulative yield of aromatics. This was derived by calculating the average rate of formation

of each group at designated GHSV and multiplying it with 20 hours. This then is taken as the cumulative yield of each group at the respective GHSV. It should be noted that the minor product fraction xylene was only detectable at GHSV 800h^{-1}. At all other GHSVs, it was undetected. Further the minor component yield is represented by the secondary y-axis.

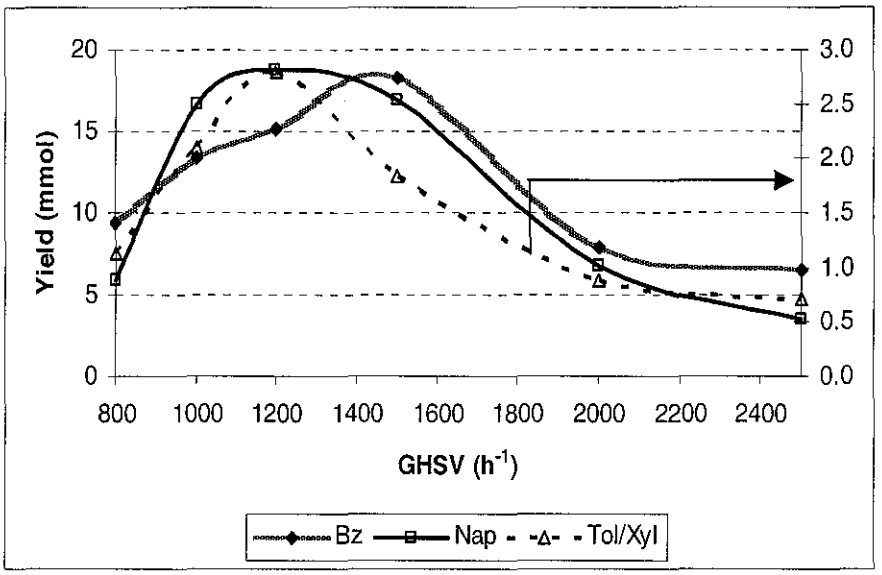

Figure 3.6 Effect of GHSV on Aromatic Fraction Yield

From Figure 3.6, it can be seen that GHSV have great influence on the yield of aromatics fraction. At GHSV 800 h^{-1} the yield or selectivity towards benzene is higher than that of naphthalene. Between GHSV 1000 to 1200 h^{-1}, the naphthalene selectivity is higher than that of benzene, but after GHSV 1500 h^{-1} the benzene selectivity is higher than that of naphthalene.

In the case of benzene, the yield rises from GHSV 800 to 1500 h^{-1} very sharply and peak at GHSV 1500 h^{-1}. After GHSV 1500 h^{-1} there is a drastic drop in benzene yield with increasing GHSV. GHSV 2000 and 2500 h^{-1} encounter a drop of 57 and 64% respectively lower than that at GHSV 1500 h^{-1}.

The naphthalene yield on the other hand rises sharply from GHSV 800 to 1000 h^{-1}. From GHSV 1000 to 1200 h^{-1} the increase in naphthalene is more gradual, and it peaks at 1200 h^{-1}, before gradually dropping at GHSV 1500 h^{-1}. After GHSV 1500 h^{-1}, the drop in naphthalene yield is more drastic with further increase to 2000 and 2500 h^{-1}.

The main difference between the benzene and naphthalene yield is the GHSV value for maximum yield. For benzene it is at GHSV 1500 h^{-1}, whereas for naphthalene it is at 1200 h^{-1}.

In the case of the minor aromatic fraction, toluene and xylene, its yield increases very sharply from GHSV 800 to 1200 h^{-1}, after GHSV 1200 h^{-1}, the yield drops very sharply with further increase in GHSV with the lowest at 2500 h^{-1}.

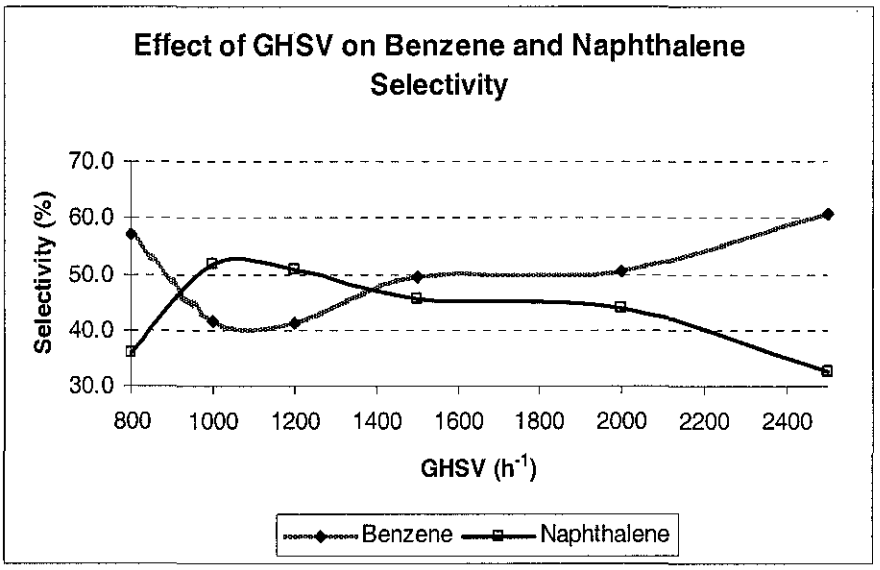

Figure 3.7 Effect of GHSV on Benzene and Naphthalene Selectivity

The % selectivity of the aromatic component with GHSV is shown in Figure 3.7. This is based on the % selectivity of the aromatic component

against the total aromatic fraction at the specific GHSV. In this figure only benzene and naphthalene will be considered.

From Figure 3.7, it can be seen that increase in GHSV results in increase in benzene selectivity in general or in other words decrease in GHSV results in increase in naphthalene selectivity. At GHSV 800 h^{-1}, it can be noticed that the benzene selectivity is higher than the naphthalene selectivity. This is odd because based on the general observation, benzene selectivity increases with increasing GHSV. This exception may be due to part of the aromatic fraction in particular naphthalene being condensed on the catalyst due to higher contact time at GHSV 800 h^{-1}. Further the coke yield was the highest for the various GHSV studied as observed in Figure 3.3. This increase in coke content may have arisen from naphthalene condensation on the catalyst. Between GHSV 1000 to 1200 h^{-1}, the selectivity towards benzene and naphthalene remains consistent, but after GHSV 1500 h^{-1}, the selectivity towards benzene is higher than that towards naphthalene.

In order to understand why benzene selectivity increases with GHSV, let it be assumed that benzene is the precursor for naphthalene, toluene and xylene as suggested by Lunsford et. al [17]. At lower GHSV the contact time is increased, this results in higher conversion of benzene to higher aromatic homolog namely naphthalene. With increase in GHSV, the contact time decreases as a result less naphthalene is produced.

From the above observations, since benzene being the more valuable aromatic, GHSV 1500 h^{-1} should be the ideal choice.

3.3.7 COKE

Carbon deposition especially in the form of Mo_2C is important at the initial stage of MDA reaction because it is the active component of the

said reaction [1-6], this importance will be discussed in greater detail in the catalytic activation section. Coke is undesirable when it builds up excessively because it leads to catalytic deactivation, yet it is important due to its impact on the MDA reaction with reference to Mo-carbide. It has been universally accepted that the main culprit for the deactivation of the catalyst in MDA reaction is due to coking and carbon deposition [2]. If coke deposition can be controlled, catalytic deactivation can be minimised, resulting in a very stable catalyst.

The main cause of catalyst deactivation in MDA is due to the deposition of coke [10,15-19]. It will be interesting to evaluate some kinetic data on the rate of coke deposition on the catalyst. Before embarking into the kinetic study, it important that we understand the nature and distribution of the carbonaceous deposit on/in the Mo modified HZSM-5 zeolite.

Since MDA reaction is activated by carbon deposition in the form of Mo-carbide, the importance of carbon species were further investigated.

Based on studies of Lundsford et al [17] using XPS, they observed that there are 3 different types of carbon deposit present on the catalyst. They named them species A, an adventitious or graphitic like carbon located mainly in the zeolite channel. Species B, a carbidic-like carbon present in Mo_2C and Species C, a hydrogen deficient sp carbon or pre-graphitic type found on the outer surface of the catalyst. According to them [17] species C is the one responsible for the gradual deactivation of the catalyst.

Aided by these findings, Lie et al [18] formulated a quantitative tool using TGA to calculate the carbonaceous deposit. Based on their study, they attributed weight loss below 260°C is due to desorption of adsorbed water molecules. A gain in weight was observed between 260 to 380°C is

observed. This they claim is the reaction between Mo_2C and/or $Mo_2O_xC_y$ and oxygen. From 380 to 700°C, decrease in weight was observed. This they related to burn-off coke. From this study, they suggested that the total amount of coke can be divided into 2 different parts, i.e. Coke I which is the burn-off coke and Coke II, coke associated with Mo_2C or $Mo_2O_xC_y$.

Based on the above understanding, they derived a set of formulae for Coke I and Coke II.

$$\text{Coke I} = \frac{M2 - M3}{M3} X1000 \qquad \text{Equation 1}$$

$$\text{Coke II} = \frac{M2 - M1}{M3} X \frac{m4}{2m5 - m6} X1000 \qquad \text{Equation 2}$$

$$\text{Total Coke} = \text{Coke I} + \text{Coke II} \qquad \text{Equation 3}$$

Where

M1 = % weight loss below 260C

M2 = % weight gain between 260 to 380C

M3 = % weight loss between 380 to 700C

m 4 = Molar weight of carbon

m5 = Molar weight of MoO_3

m6 = Molar weight of Mo_2C

In the present study, a Perkin-Elmer TGA 1700 was used. 20mg of the coked sample was heated from 30 to 700°C at a ramp rate of 10°C/min in air with a flow rate of 3 ml/min. A TGA profile was recorded based on weight loss/gain versus temperature change during this period of study.

The TGA method used the calculations derived by Lie et al [18] as described above. It should be noted that from the TGA calculations, 2

types of coke are presented. This includes coke I, which represents the lost in weight of the spent catalyst form 260 to 360°C, whereas coke II is the loss between 360 to 700°C. The combination of coke I and II results in total coke in this group. The results of these calculations are presented in Table 3.3 below. As a basis of comparison, the coke yield calculated from MDA and total coke from elemental analysis were also compared and is shown in Table 3.4 below.

Table 3.3 Carbon Deposition Based on TGA Studies

Unit	mg per gram catalyst				
Anal. Method	TGA			MDA	Ele. Anal
Type	Coke I	Coke II	Total Coke	Total Coke	Total Coke
800	153.0	0.141	153.2	178.9	159.22
1000	94.4	0.142	94.5	83.2	107.1
12000	71.1	0.142	71.2	55.9	87.1
1500	118.4	0.141	118.5	118.6	119.1
2000	84.6	0.143	84.7	78.6	103.2
2500	74.3	0.143	74.4	70.8	102.2

From the TGA results in Table 3.3 it can be seen that coke II is the minor coke species present in the spent catalyst and is observed to be unaffected by GHSV. The maximum difference between the various GHSV is less than 2%, which is within the TGA specification.

Coke I on the other hand is the major coke species on the spent catalyst. On comparing between the 2 coke species, coke I is 52 to 108 % higher than coke II. It is coke II which is affected by changing GHSV. From Table 3.3, it can be seen at GHSV 1200 h^{-1} has the lowest coke I species while GHSV 800 h^{-1} has the highest. GHSV 800 h^{-1} produces 215% more coke than 1200 h^{-1} and 125% more than GHSV 1500 h^{-1}. The findings follow a similar pattern observed from MDA coke yield in section 3.3.4.

From the observation above, it can be seen that coke II species is not influenced by variation of GHSV. This species is important as it is responsible for methane activation [17] and it is formed during the activation and induction phase of the fresh catalyst. Since coke II is associated with Mo active species, it also may indicate that only limited amount of this coke species is permissible around the Mo vicinity.

Coke I on the other hand varies with GHSV. According to Lin et al. [19], these species are usually present on the surface of the catalyst. The influence of coke I deposition on the surface with varying GHSV is closely associated with contact time between the catalyst and the feed. The contact time for GHSV 800 h^{-1} is 4.5sec/g cat whereas GHSV 2500 h^{-1} has 1.44sec/g cat. When the contact time increases, the catalytic activity should also increase. Judging on this statement GHSV800 h^{-1} should have the highest and GHSV 2500h^{-1} the lowest coke I yield of the 5 analysed. This is true for GHSV 800 h^{-1} but not true for GHSV 2500 h^{-1}. In fact from Table 3.3, the lowest coke I yield is observed for GHSV 1200 h^{-1}.

To understand the above observations, a study on its surface properties is essential; this is discussed in greater detail in surface properties sub section below (3.4.4.3).

Table 3.4 evaluates the 3 different methods used to calculate the total coke content. The methods used includes TGA, elemental analysis and product yield from MDA reaction (section 3.4.4) above.

The TGA method used for the comparison is reproduced from Table 3.3 above. As for the other total coke content method from MDA product yield as in section 3.4.4 above, the coke yield in mmol was converted to mg using mole wt. of coke as 12 and the catalyst weight of 0.30g to make

the results comparable with total coke derived by TGA. The 3rd coke content is based on elemental analysis as described in section 2.4.4 in Chapter 2. It should be noted that the total coke yield is used for comparison purpose only.

Table 3.4 Effect of GHSV on Total Coke

	Total Coke (wt %)		
GHSV	**TGA**	**MDA**	**Ele. Anal.**
800	**15.32**	**17.89**	**15.92**
1000	**9.45**	**8.32**	**10.71**
1200	**7.12**	**5.59**	**7.71**
1500	**11.85**	**11.86**	**11.91**
2000	**8.47**	**7.86**	**9.42**
2500	**7.44**	**7.08**	**9.12**

From Table 3.4, it can be seen that in general the trend for total coke is the same in all 3 methods used. In general TGA gives the lowest and elemental analysis gives the highest total coke value. The highest difference between the total coke between TGA and MDA varies by 21% and that between TGA and elemental analysis is 23%.

The TG data can also be used to obtain the activation energy for oxidation of coke on the Mo/HZSM-5 catalyst. Xu et al [18] developed this kinetic data based on a few assumptions. They express oxidation of coke burn-off as

$$C(s) + O_2(g) \rightarrow CO_2(g) \qquad \text{Equation 4}$$

Further they assume that the oxidation of coke as a first order reaction with respect to coke, and the value of E/RT is in the range of 20 to 60. This assumption was based on studies by Querini et al[23]. Querini et al looked at coke as tri-dimensional structure. Coke exhibits a reaction

order increasing from close to zero to approaching 1 as the oxidation reaction proceeds. This is because reaction is a gas-solid reaction and it is proportional to solid surface area. Large surface coke particles decrease in size very slowly (reaction order for coke close to zero) at the early part of the burning order to generate similar surface area coke particles (reaction order for coke approaches 1). Based on their analysis coke reaction order is thought to approach 1 when the temperature is higher than 387°C.

They then proceed to simply the formula based on studies by Querini et al[23] and Tian et al. [18] as.

$$\ln\left(\frac{-\ln C}{T^2}\right) = \ln\left(\frac{AR}{\beta E}\right)\left(1-\frac{2Rt}{E}\right)-\left(\frac{E}{R}\right)\frac{1}{T} \qquad \text{Equation 4}$$

where,

C = amount of coke present (wt %)

T = temperature

β = heating rate (C/min)

A = pre-exponential factor

E = activation energy of the oxidation of coke

A linear relationship can be obtained between the values of $\ln\left(\frac{-\ln C}{T^2}\right)$ versus $\frac{1}{T}$. The activation energy can be calculated from the slope of the straight line.

$$\text{Slope} = \frac{-E}{R} \text{ where R= 8.314 J/mol-K}$$

Equation 5

Based on the above assumption, the results are tabulated in Table 3.5 which lists the change in activation energy resulting from coke burning-

off, calculated from TGA data with changing GHSV. Activation energy is the minimum energy required for reaction to overcome energy barrier to formation of products. Activation energy for GHSV of $800h^{-1}$ to 2500 lies between 93 to 102 kJ /mol. This accounts for less than 10 % difference between them. As for the starting temperature for coke reaction order 1 is unaffected by GHSV. This may suggest that coke species are unaffected by GHSV. The activation energy required to burn-off coke from an acid solid is 114kJ/mol [24].

Table 3.5 Activation Energy Versus Variation of GHSV

GHSV (h^{-1})	Activation Energy (kJ/mol)	Starting Temp. (°C)
800	95.1	465
1000	94.3	465
1200	93.48	460
1500	93.20	466
2000	101.65	460
2500	101.65	462

In the above test, the activation energy lies between 93.2 to 101.7 kJ/mol. This is well below the burn-off coke from acidic solid (114 kJ/mol). Based on this information it can be assumed that most of the coke are not only located on the acidic solid, but also on the on the boundaries between the Mo-carbide and the Bronsted acid sites. This results obtained is similar to the findings by Xu et [18] who used 6Mo/HZSM-5 catalyst.

3.3.8 SURFACE PROPERTIES

To further understand how the coke deposition interferes with the product distribution, a study of the catalyst surface area, pore volume and size was studied using a Micrometric ASAP 2000 surface analyser as per method in Chapter 2. The results are tabulated in Table 3.6. The parent

zeolite is taken as control and compared to the freshly activated and spent (at different GHSV) catalysts.

Surface area, pore volume and pore size are important properties in catalysis because they determine the dispersion of active sites present in/on the catalyst, the accessibility of the active sites to the reactants and the ability to facilitate transport of products out of the catalyst to the bulk flow. For the surface area, the BET surface area (SA_{BET}) and the t-plot external surface area (SA_{Ext}) were chosen. For the pore characterisation the BJH (PV_{BJH}), pore volume and pore diameter (Pd_{BJH}) were investigated.

Table 3.6 Surface Properties of 3Mo/HZSM-5 Catalyst

GHSV (h^{-1})	*HZSM-5*	*Activated*	*800*	*1000*	*1200*	*1500*	*2000*	*2500*
SA_{BET}(m^2/g)	**399**	**381**	**206**	**210**	**220**	**221**	**184**	**171**
SA_{Ext} (m^2/g)	**150**	**139**	**45**	**56**	**54**	**52**	**48**	**49**
PV_{BJH}(cm^3/g)	**0.22**	**0.20**	**0.14**	**0.15**	**0.16**	**0.16**	**0.15**	**0.15**
Pd_{BJH} (nm)	**72.44**	**84**	**147**	**137**	**128**	**130**	**135**	**139**

From Table 3.6 it can be seen that fresh activated 3βMo/HZSM-5 loses about 4.5% of its BET SA compared to the parent HZSM-5, whereas the spent catalyst loses 45 to 57%. The highest loss is for spent catalyst with GHSV 2000 and 2500 h^{-1}. Between GHSV 800 to 1500 h^{-1}, the loss is more or similar. As for the external SA, the loss is much higher than the BET SA. This observation is expected as it is shown that coke deposition is mainly concentrated on the external surface of the catalyst. The loss varies between 7% for the activated to 63 to 70% for the spent catalyst when compared to the parent zeolite.

BJH pore volumes represent the meso pore and inter-catalyst volume. From Table 3.6, it can be seen that the freshly activated catalyst loses about 9% compared to the parent HZSM-5, whereas the spent catalyst on the other hand loses about 27.3 to 36.4%. Although the loss is quite minimal in terms of actual number, the highest loss among the spent catalyst is shown by GHSV 800 h^{-1} which also has the highest coke content of those studied. The decrease in pore volume may suggest pore blockage by coke deposition.

From Table 3.6, it can be seen that the pore diameter is enlarged in all the spent catalyst as compared to either the freshly activated or parent catalyst. The freshly activated catalysts pore diameter increased by 16%, while the spent catalysts increased by a massive 77 to 103% above the parent zeolite. This increase in pore size diameter may suggest that either a partial collapse or blockage of the pores has occured [25] by the spent catalyst. The highest increase is for GHSV 800 h^{-1} and the lowest is for 1200 $h^{-1}$for the spent catalyst. It is also interesting to note that the coke content is highest at GHSV 800 h^{-1}, and lowest at 1200 h^{-1} as shown in Figure 3.1 and Tables 3.3 and 3.4. The above observation and the XRD scan in Figure 3.2 supports variation in GHSV induce partial blockage rather than partial collapse of the pores. XRD scan in Figure 3.2 shows no significant change in structure of the spent catalyst as compared to the parent HZSM-5 zeolite.

From the above observations, it can be suggested that the deposition of coke is basically on the external surface and inter pore structure of the catalyst, as it can be seen that the external SA is more affected than BET SA. With higher GHSV like 2000 and 2500 h^{-1} higher external surface loss is observed. This may suggest that the coke deposition is concentrated more towards the mouth of the pores than those with lower GHSV. This can be accompanied by a reduction in catalytic activity due

to the inaccessibility of reactant to active sites as seen in Figure 3.1 above. This observation is also supported by the lower coke deposit at GHSV 2000 and 2500 h^{-1} as compared to 800 h^{-1}. This suggests that GHSV has minimum impact on structure collapse as compared to pore related blockage as seen above.

3.4 Conclusions

GHSV has a great influence on MDA reaction. It dictates methane conversion, rate of formation or yield of aromatic product and carbon deposition. GHSV does not affect the structure of the catalyst based on powder XRD studies.

For a MDA reaction, optimisation of aromatic especially benzene and naphthalene is the main criteria. High carbon deposition, the main cause of catalytic deactivation is the least desirable product. It is also noticed that carbon deposition is the detrimental factor of MDA reaction. This is because it is crucial for the formation of Mo_2C, which activation the MDA catalyst. Too much of it deactivates the catalyst by blocking pore access of the reactant and product to the active site and also deactivates the catalytic active sites leading to low aromatic yield.

Of the GHSV of methane studied, both GHSV 1500 and 1200h^{-1} shows promising results. The main difference between these 2 GHSV is than the former is more reactive than the latter. As such GHSV 1500 h^{-1} will be a better candidate to further optimisation reactions.

3.5 Chapter 3 References

1. Anderson, J.R. PhD Thesis. University of Liverpool, UK (2001)
2. Xu, Y., and Lin l., Appl. Catal.A 188(1999) pp53-67
3. Chen, L., Lin, S., Xu, Z., Li, X., and Zhang, T., J. Catal. 157 (1995). 190
4. Xu, Y., Liu, S., Wang, L., and Guo, X., Catal. Lett. 30 (1995) 135
5. Solymosi, F., Szoke, A., and Cserenyi, J., Appl. Catal. A 136 (1996) 361
6. Xie, M., Yang, X., Chen, W., Tao, L., Wang, X., Xu, G., Wang, L., Xu,Y., Liu, S., and Guo, X., Stud. Surf. Sci. Catal. 105 (1997) 869
7. Solymosi, F., Szoke, A., and Cserenyi, J., Catal. Lett. 39 (1996) 157
8. Zhong, J.Z., Long, M.A., and Howe, R.F., Catal. Today 44 (1998) 293
9. Liu, S., Dong, Q., Ohnishi, R., and Ichikawa, M.. Chem. Commun.. (1997) 1455
10. Wang, D., Lunsford, J.H., and Rosynek, M.P., J. Catal. 169 (1997) 347
11. Wang, L., Us, Y., Wong, S., Cui, W., and Guo, X., Appl. Catal. A 152 (1997) 173
12. Us, Y., Shu, Y., Liu, S., Huang, J., and Guo, X., Catal. Lett.35 (1995) 233
13. Shu, Y., Us, Y., Wong, S., Wang, L., and Guo X., J. Catal. 170 (1997) 11
14. Liu, W., and Xu, Y., J Catal. 185 (1999) 386
15. Juang, H., Wang, L., Cui ,W., and Xu, Y., Catal Lett. 57 (1999) 95
16. Liu, S., Wang, L., Ohnishi, R., and Ichikawa, M., J. Catal. 181 (1999) 175
17. Weckhuysen, B.M., Rosynek, M.P., and Lunsford, J.H., Catal Lett.52 (1998) pp31-

18. Liu, H., Li, T., Tian, B., and Xu, Y., Appl. Catal. A 213 (2001) 103
19. Xu,Y., Bao, X., and Lin, L., J.Catal 216 (2003) 386
20. BorryIII, R.W., Kim, Y.H., Huffsmith, A., Reimer, J.A., and Iglesia,E., J.Phys. Chem. B (1999) 5787
21. Ding, W., S.Li, Meitzner, G.D., and Iglesia, E., J. Phys. Chem. B 105 (2001) 506
22. Derouane-Abd Hamid, S.B., Anderson, J.R., Schmidt, I., Bouchy, C., Jacobsen, C.J.H., and Derouane, E.G., Catal Today 63 (2000) 461
23. Querini, C.A., and Fung, S.C., Catal. Today 37 (1997) 277
24. Zhuo, R., Tan, C., and Cheng, C., Petrochem. Technol (Chinese) 21 (1992) 815.
25. Li, Z., Gao, L., and Zheng, S., Appl. Catal A. 236 (2002)163

CHAPTER4

OPTIMISATION OF PROCESS VARIABLES

4.1 Introduction

In the previous Chapter, the initial micro-reactor testing was done to have a better understanding of the MDA reactions. The catalyst evaluation tests were closely tailored to the more conventional methods used and established by Wang et al in 1993 [1] and summarised by Lin et al[2]

In the present chapter, the effect of Mo loading, calcination and activation temperature together with carburisation and reduction gas mixture will be investigated

4.2 Mo loading

Solymosi [4] and Lunsford [5] claim that the above reaction proceeds with an initial induction period. During this induction period, the reduction of Mo^{6+} to a lower oxidation state takes place. The early part of the induction period on contact with methane resulted in the formation of carbon deposit, with the release of CO, CO_2 and H_2O. The end of the induction period is followed by the carburisation, where most of the MoO_3 are converted to Mo-carbides which are marked by the first formation of ethylene, ethane and benzene. After this period, the selectivity of benzene increases to about 60-65% and methane conversion of 7-12% resulted during steady state [4,5].

To improve catalytic reactivity, Howe et al. [6] in their studies suggested that; achieving maximum dispersion of active Mo species on/within the zeolite pores, optimising the acidity (which is closely related to the dispersion of the Mo species) and coke formation are critical. From their

observations, they noticed a remarkable interaction between the Mo species and the HZSM-5 zeolite which caused the Mo species to be well dispersed on/in the zeolite. This kind of interaction increases with increase in Mo loading and/or calcination temperature. Therefore optimisation of Mo loading and/or calcination temperature are crucial, because too low will have minimum interaction and low methane conversion, while too high will result in extraction of framework aluminium to form extra-framework Al first and then $Al_2(MoO_4)_3$ which are inactive [7].

4.2.1 EFFECT OF Mo LOADING

Since the spreading and interaction of the active Mo species are controlled by the Mo loading and calcination temperature, an investigation will be carried out to find the optimum Mo loading (within the study range), required to increasing catalytic activity. Most of the research work done on Mo loading ranges from of 2 to 15 wt% [8-12].

Knozinger et al [12] proposed that MoO_3 spreads on the Al_2O_3 surface via an 'unrolling carpet' mechanism until it reaches AlO_x sites, where they anchor and become immobile [13]. This process decreases the surface energies. After the external surface areas are completely covered with MoO_3 layers, further spreading cannot decrease the surface energy. Iglesia et al [13] using physical mixture of MoO_3 and HZSM-5 in their study showed, that the threshold for monolayer of MoO_3 on the zeolite is 4 wt% Mo element. (ZSM5 used had a SA of $24m^2/g$). Greater than 4 wt% Mo will result in sublimation (Figure 4.1). Iglesia et al [13] also pointed out, that for Mo loading of greater than 4 wt%, sublimation of Mo can be avoided by good calcination technique, whereby the Mo active species are bonded strongly with the Al species of the zeolite framework. The threshold for monolayer

Mo dispersion according to Lin et al [9] is 5g of Mo per 100g of HZSM-5 zeolite (SA 360m^2/g) using AHM and HZSM-5 impregnation technique. The MoO_3 species are usually adsorbed on the external surface of the zeolite during impregnation. On calcination the MoO_3 species migrates over the external surface and some may find its way into the pores to the Bronsted acid sites, which is the driving factor for migration of the MoO_3 species [6,12-14].

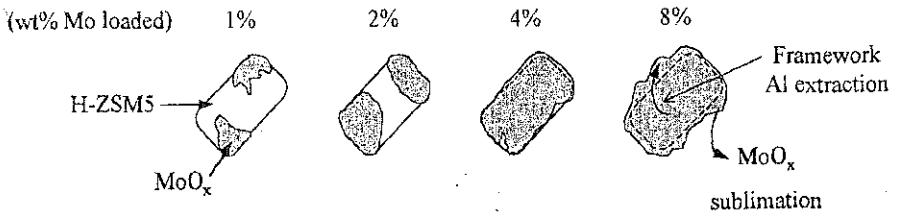

Figure 4.1 Effect of Mo Migration with Mo Loading (From Ref. 12)

In this study, Mo loadings of 10, 5 and 3 wt % are prepared by similar methods as described in Chapter 2 section 2.1. The catalytic evaluation tests carried out will be similar to that described in the previous chapter.

For the purpose of simplicity, the catalyst evaluated will be named as 10MoBM, 5MoBM and 3MoBM to represent the different Mo loading of 10, 5 and 3 wt % respectively. The above abbreviation for the catalyst in study will hold unless stated otherwise.

4.2.2 EXPERIMENTAL

In order to have a better understanding of the effect of Mo loading on catalytic reactivity, a series of tests were conducted. This include the catalytic evaluation study, catalytic characterisation study of the uncalcined , calcined, freshly activated and spent catalyst were done. Abbreviations such

as 'uncal', 'cal', 'act', and're' will be used to denote the catalyst state for the uncalcined , calcined, freshly activated and spent catalysts respectively. The catalyst characterisation tests conducted will strictly follow as per methods described in Chapter 2 section 2.4 unless specified otherwise. The calcination temperature will be 600°C.

4.2.3 RESULTS AND DISCUSSIONS

4.2.3.1 Methane Conversion

Figure 4.2 highlights the effect of Mo loading on methane conversion based on carbon number wt % conversion for 3MoBM, 5M0BM and 10MoBM over a 20 hours TOS. The initial methane conversion (1st 10 min) reading is not taken into account because it does not give representative information on the overall conversion. Thus methane conversions recorded hourly from the 1st to the 20th hours inclusive will be analyzed.

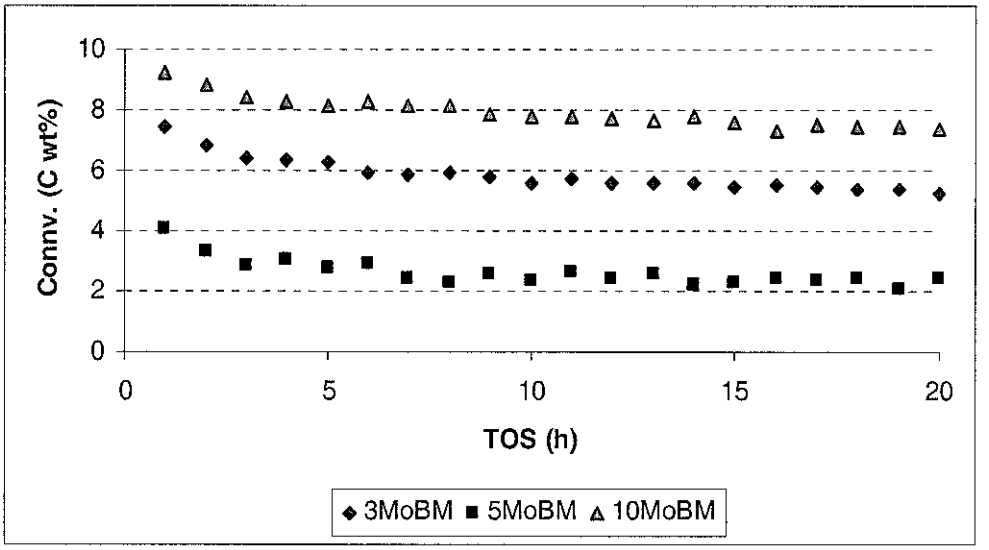

Figure 4.2 Comparison of Methane Conversion against Mo Loading

From Figure 4.2, it can be seen that 10MoBM has the highest methane conversion, followed by 3MoBM and 5MoBM respectively. The average

methane conversions for 3MoBM, 5MoBM and 10MoBM are 5.9, 2.6 and 8.0 C wt % respectively. Methane conversion between 5.7 and 8 C wt% which could be sustained for more than 16 hours using 2 wt% Mo, with a Si/Al ratio of 55 and 25 respectively were claimed by Solymosi et al [4] and Lunsford [5]. For the present study average difference of 5.4 C wt% methane conversion are observed between the best (10MoBM) and the worst (5MoBM) catalysts of this study.

Anderson [15], for his 10Mo-HZ-40(MH) catalyst recorded a drop of 27.5% from the 1st to the 20th hours (8.0% and 5.8 C wt %). Anderson's 2Mo-HZ-40(MH) on the other hand, produced a lower methane conversion of 6.5 on and 4.8 C wt% on the 1st and 20th hour respectively. This represents a drop of 26.2% over 20 hours. This indicates that, both his catalyst experience almost similar drop in activity over 20 hours TOS.

The result from the present study differs from that of observed by Anderson [15]. 10MoBM experiences a drop of 20% (9.25 to 7.36 C wt%), 5MoBM loses 48% (4.05 to 2.09 C wt%) and 3MoBM loses 30% (7.47 to 5.22 C wt%) between the 1st and 20th hour of methane conversion. This indicates that catalytic deactivation is not consistent with TOS with different Mo loading.

4.2.3.2 MDA Product Analysis

The main products as a result of methane conversion above are aromatics, aliphatics and coke. It should be noted that, the coke in the present study include carbon deposit or any heavy aromatic which might condense on the catalyst or on transfer lines and any other loss in methane during the MDA

reaction. The same description on composition for the three different product groups applies as in Chapter 3.

Table 4.1 is derived from the yield of each of the individual group of product over a time span of 20 hours. Product yields on a carbon number basis were calculated, based on the average rate of formation in nmol per sec for each hour as in sub heading 2.2.5 of Chapter 2. The results obtain were then multiplying with 20 hours to generate the overall yield in mmol for each group over 20 hours TOS. The numbers in bracket represent the % selectivity for each product fraction of the respective catalytic group.

Table 4.1 Catalytic Product Yield Over 20 Hours Time on Stream

Catalyst Type	Yield mmol Conversion over 20 hours TOS			
	Coke	Aromatic	Aliphatic	Total Conv.
3MoBM	29.66 (41.2 %)	39.95 (55.5 %)	5.27 (7.3 %)	71.89
5MoBM	18.95 (59.4 %)	9.84 (30.9 %)	3.1 (9.7 %)	31.89
10MoBM	32.81(33.8 %)	61.85 (63.7 %)	2.5 (2.6%)	97.16

Of the three catalyst studied, it can be seen from Table 4.1 that, 10MoBM has the highest catalytic activity which is 135 and 305% higher than 3MoBM and 5MoBM respectively. 10MoBM also has the highest aromatic yield and selectivity of the three compared. Due to its high catalytic activity, 10MoBM also has the highest coke yield, but the lowest coke selectivity of the three compared. The selectivity towards aromatics is 65.2%, which is much higher than for coke (33.8%). 10MoBM produces 155 and 111% more aromatic and coke respectively than that of 3MoBM.

5MoBM on the other hand has the lowest yield for both aromatics and coke. It has the highest product selectivity towards coke, which may be the main cause of deactivation resulting in poor catalytic activity.

3MoBM has moderate conversion for coke and aromatics, but slightly higher selectivity to aromatics (55.5%) than coke (41.2%).

The aliphatic yields for all three catalysts are below 10% of the overall yield. Based on Table 4.1, it can be seen that aliphatic yield increased with increase in Mo loadings, which are different from the aromatics and coke yields.

4.2.3.3 Coke Analysis

Figure 4.3 depicts the rate of formation in nmol per g cat per sec of coke with TOS. From this figure, it can be seen that 3MoBM has an initial higher activity for coke than either 5MoBM or 10MoBM. The coke for 3MoBM is more or less stable throughout the 20 hours TOS. 5MoBM also seem to follow the same trend as 3MoBM, but the rate of formation of coke for 5MoBM is much lower than 3MoBM.

10MoBM on the other hand, follows an entirely different carbon activity. The initial carbon activity starts very low and with TOS increases drastically from 1^{st} to 5^{th} hour. After the 5^{th} hour the carbon activity stabilizes. At this stage it has similar ROF for coke as that of 3MoBM and 5MoBM. This observation supports the higher methane conversion for 10MoBM compared to 3MoBM. Since carbon deposition is one of the major contributors to catalytic deactivation, 10MoBM has a major advantage of having lower coke deposition at the initial stage as compared to either 3MoBM or 5MoBM. In

other words, catalytic deactivation for 10MoBM starts at a much latter period when compared to either 5MoBM or 3MoBM.

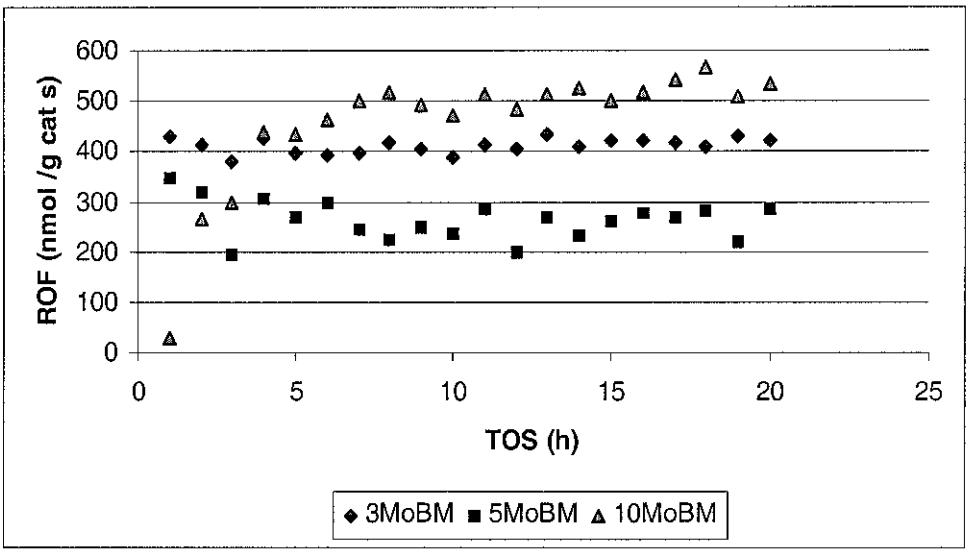

Figure 4.3 Rate of Coke Deposition with Time on Stream

4.2.3.4 Coke Species

To further understand the nature of the carbonaceous deposit formed on the Mo/HZSM-5, TGA and elemental analysis were carried out. Please refer to Chapter 2 sub-section 2.4.2 for further experimental details. The kinetic data presented in the same table is in accordance with Xu et al [14] technique.

Table 4.2 Carbon Deposit Analysis Based on TGA

	Coke I (mg/g)	Coke II (mg/g)	Act Energy (kJ/Mol)	Total Coke (wt%)
3MoBM-Act	**2.4**	**0.142**	**100.4**	**0.26**
3MoBM-Re	**98.9**	**0.151**	**93.20**	**9.91**
5MoBM-Act	**2.8**	**0.221**	**100.5**	**0.32**
5MoBM-Re	**68.1**	**0.254**	**95.6**	**6.84**
10MoBM-Act	**3.4**	**0.363**	**100.5**	**0.38**
10MoBM-Re	**111.1**	**0.401**	**98.8**	**11.15**

Tables 4.2 represent the type of cokes present on the reacted catalysts. Coke I, coke II and activation energy are derived based on TGA as in Chapter 3 subheading 3.4.4.2. Coke I represents the burn-off coke. Coke II represents the coke present with the Mo-carbide which is important for methane dehydrogenation. Activation energy also gives some information on the nature of the coke species. Total coke is the sum of coke I and coke II from TGA analysis.

From Table 4.2, it can be noticed that coke II of the activated catalyst is the smaller fraction of the total coke content. Coke II increased with increase in Mo loadings from 6 to 11% and is represented by 0.14, 0.22 and 0.38 mg/g cat for 3MoBM, 5MoBM and 10MoBM respectively. This increase although marginal, may be explained by the observations made by Xu et al [14]. Based on their studies on the TPH and $TPCO_2$ profiles on coked catalyst, they noticed that high Mo loadings resulted in large MoO_x particles being easily reduced into Mo_2C and/or MoO_xC_y.

In the case of spent catalyst, the coke II in 3MoBM, 5MoBM and 10MoBM increases by 6.3, 14.9 and 10.5% respectively when compared to the respective activated catalyst. This extra build up of coke II may hinder passage of reactant to active site. To recollect, coke II is associated with Mo and is responsible for methane activation and the production of aliphatic fractions. Based on this input 3MoBM should have the highest aliphatic yield and 5MoBM the lowest. Referring to Table 4.1, it can be seen that 3MoBM does have higher yield than the other 2 catalysts, but 10MoBM has a lower yield than 5MoBM. This may be because of better dispersion of Mo active sites in 10MoBM than in 5MoBM, as observed in catalytic activity in

Table 4.1. It can also be interpreted as higher consumption of the aliphatic fraction to produce aromatics [4, 5] for 10MoBM in the MDA reaction.

For the freshly activated catalysts, an increase in Mo loading results in a marginal increase in coke I. The same is not true for the spent catalyst. 10MoBM and 3MoBM have high coke I yield (111.1 and 98.9 mg/g cat respectively), whereas 5MoBM have a much lower value of 68.1 mg /g cat. The lower coke I for 5MoBM may be attributed by the poor catalytic activity due to reduced access of the reactant to active Mo sites as explained above. In the case of 10MoBM and 3MoBM, the former has a higher coke I yield than the latter. This observation is similar to the findings of Xu et al[14], whereby they noticed that with lower Mo loading, most of the graphitic like coke species (coke I) are located on the Bronsted acid sites (BAS), and with higher loadings most of coke1 are located on the complex of Mo_2C and BAS

.

The activation energy for the freshly activated and spent catalysts varies by less than 10%. For the freshly activated catalyst the value lies between 93.2 and 98.8 kJ/mol, whereas for the reacted catalyst it is between 100.4 and 100.5 kJ/mol. This indicates that the coke species present on the catalysts studied are similar in nature. Mo loading does not alter the nature of coke species deposit during MDA reactions.

Table 4.3 Total Coke from Different Analysis Methods

	Total Coke (wt %)			
GHSV	**TGA**	**MDA**	**Ele. Anal.**	**Average**
3MoBM	**9.91**	**10.68**	**10.56**	**10. 38**
5MoBM	**6.84**	**6.82**	**6.84**	**6.83**
10MoBM	**11.15**	**11.81**	**10.95**	**11.30**

The total coke wt % from TGA as in Table 4.2, were compared to those obtained from elemental analysis. The yields obtained from MDA are

showed in Table 4.3. Based on this comparison, it can be seen that the trends are similar with the maximum difference between them being less than 7 %. The accuracy is in accordance to repeatability of the 3 techniques used.

4.2.3.5 Aromatic Product

Aromatic content is main and next area of study in the catalyst evaluation. It is also the main component to be optimised in the title reaction. As in the previous chapter both benzene and naphthalene make up the main components in the aromatic content with some contribution from toluene and xylene.

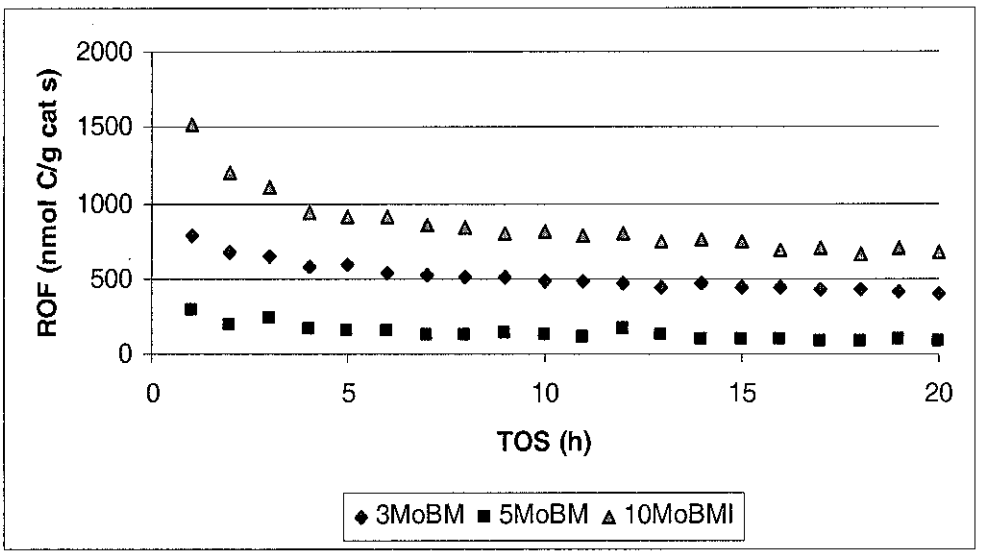

Figure 4.4 ROF of Aromatic Product versus Mo Loading

Figure 4.4 depicts the rate of formation of aromatics over a 20 hours period time on stream. From the same figure, it can be seen that all 3 catalysts have similar ROF pattern. From the 1st hour to the 4th hour TOS, there is a slow decrease in aromatic yield which becomes almost constant thereafter. The main difference between the three lies in the ROF of the aromatic yield. 10MoBM has the highest average yield of 859 mmol/g cat, which is 380%

higher that of 5MoBM (136.6 mmol/g cat.) and 260% higher than 3MoBM (226.3mmol/g cat).

4.2.3.6 Aliphatic Product

Another product resulting from the MDA reaction is the aliphatic product. It basically consist of ethane and ethylene. It is considered to be the precursor of the aromatic product [4-8]. It is believed to be converted to aromatics at the Bronsted acid sites of the HZSM-5 zeolite [4-8].

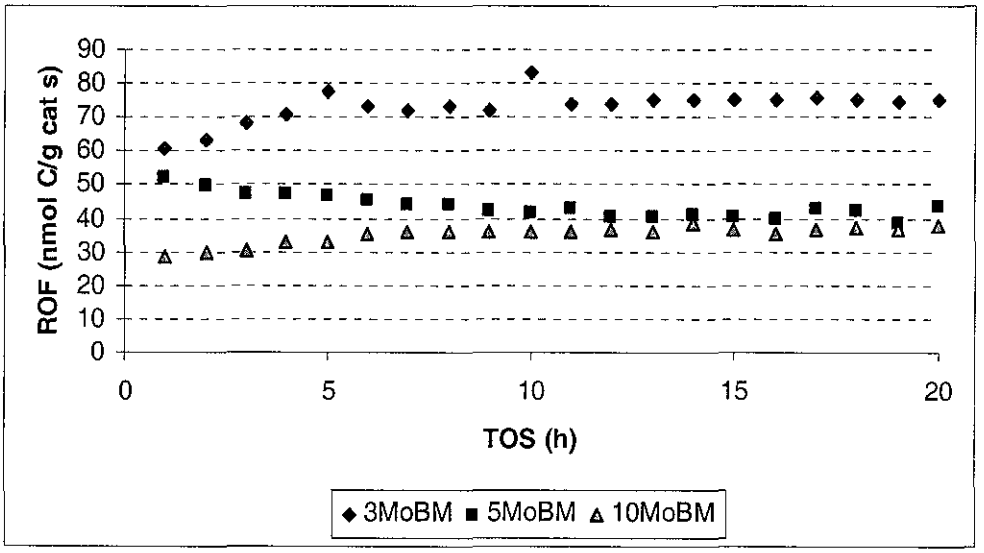

Figure 4.5 ROF of Aliphatic Product versus Mo Loading

Figure 4.5 depicts the rate of formation of this aliphatic component in the MDA reaction. From this figure, it can be seen that unlike the rate of formation of carbon and aromatic, the aliphatic component makes up a smaller portion of the product distribution

From Figure 4.5, it can be seen that both 3MoBM and 10MoBM have similar ROF pattern. The initial ROF for both 3MoBM and 10MoBM starts at a lower value and increases gradually until 5 hours TOS, thereafter it

remains constant. The main difference between 3MoBM and 10MoBM is that the former has a higher ROF for aliphatic fraction than the latter. In the case of 5MoBM it follows a different ROF pattern; it starts with an initial higher value and gradually decreases with TOS until 10 hours, thereafter it becomes constant.

On comparing Figure 4.4 and 4.5, it can be seen with a decrease in aliphatic fraction (Figure 4.5), an increase in aromatic fraction (Figure 4.4) results. This may suggest that decrease in aliphatic component is a result of the former being converted to the more desirable aromatic product. It should also be noted that reduction in aromatic conversion could also be brought about as a result of zeolite channel collapse or blockage by coke deposition. This effect can hinder the passage of the inlet aliphatic or the outlet of the aromatic product, which may eventually result in condensation into heavy aromatic products on the catalyst leading to deactivation of the catalyst. Another possible reason may be due to reduction in active BAS which may have been deactivated or destroyed during the MDA reaction condition. This may explain the variation between the ROF for aromatic and aliphatic between 3MoBM and 10MoBM, i.e. both have similar ROF but different yield pattern.

It is a well documented fact that Mo/HZSM-5 is a bi-functional catalyst. Mo-carbide of the Mo/HZSM-5 initiates methane activation with the formation of ethylene and ethane. BAS of the zeolite aromatises this aliphatic component into mainly benzene and naphthalene. Based on these assumptions, aromatization reaction are favoured by well dispersed Mo-carbide species and at the same time its close proximity to a BAS [4-6]. This may explain the high catalyst activity for 10MoBM [5]. Increase in aromatic

production will occur provided the catalyst have very efficient pathways to disseminate the products formed, failing which, will result in build-up high aromatic product which will further aromatize to heavier aromatics and block zeolite pathways resulting in catalytic deactivation. This is apparent from the results obtain in the catalyst evaluation studies whereby 10MoBM has better aromatic and coke yields as compared to 3MoBM or 5MoBM. The increase in coke yield may be due to pathway being disturbed or partially blocked. This will be further investigated in the catalyst characterization experiments.

4.2.3.7 Aromatic Fraction

Since the main purpose of the MDA study is the optimization of aromatic component, it will be interesting to see how the aromatic product yield changes with Mo loading.

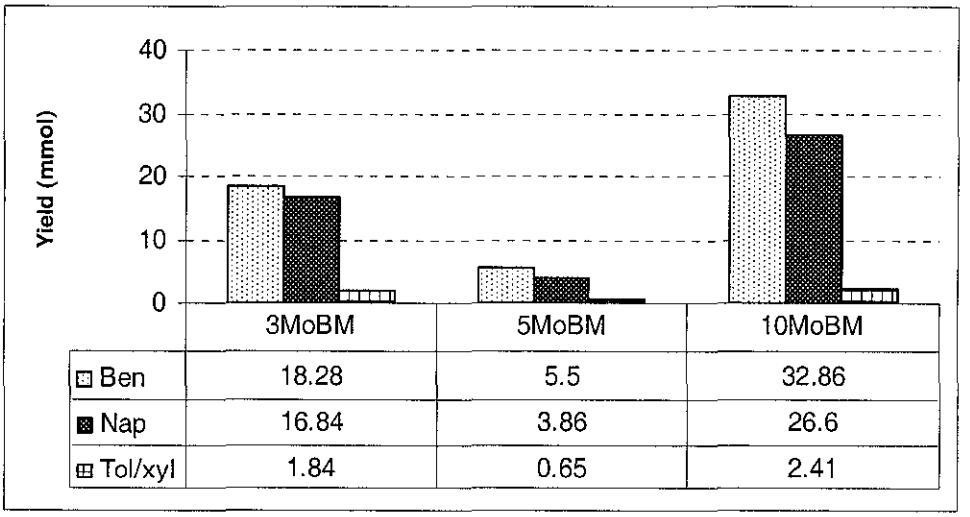

	3MoBM	5MoBM	10MoBM
Ben	18.28	5.5	32.86
Nap	16.84	3.86	26.6
Tol/xyl	1.84	0.65	2.41

Figure 4.6 Aromatic Fraction Yield Vs Mo Loading

The aromatic product in this study is basically made up of benzene and naphthalene, the minor products being toluene and the xylene isomers. Therefore the aromatic product will be divided into 3 main groups which

include benzene, naphthalene and others (toluene and xylene isomers). The average yield in mmol for each individual component was calculated over a 20 hours TOS and is shown in Figure 4.6.

From Figure 4.6, it can be seen that for all three catalysts, benzene fraction is the more prominent. The selectivity for benzene in general is higher at higher Mo loadings, whereas that of naphthalene decreased with higher Mo loadings. From Figure 4.6, the benzene selectivity for 3MoBM, 5MoBM and 10MoBM are 49.5, 54.9, and 53.1 % respectively and that of naphthalene are 45.6, 38.6 and 43.0 % respectively. From the benzene selectivity in Figure 4.6, it can be noticed that there is a slight drop of 1.8% in its selectivity from 5MoBM to 10MoBM, whereas for naphthalene an increase of 4.4% is observed. This discrepancy at 5MoBM may be due to its poor catalytic activity.

4.2.3.8 Deactivation Rate

The deactivation rate constant (k_d) will give a better understanding on the stability of the catalyst studied. Wang et al [20] came up with a deactivation curve based on the approach of Levenspiel [21]. The deactivation curve was derived by plotting the natural logarithm of the rate of formation of benzene against reaction time or TOS and it is represented in Figure 4.1.7. The slope of the curve gives the negative deactivation constant ($-k_d$). It is important to note that the deactivation rate is independent of the reaction concentration.

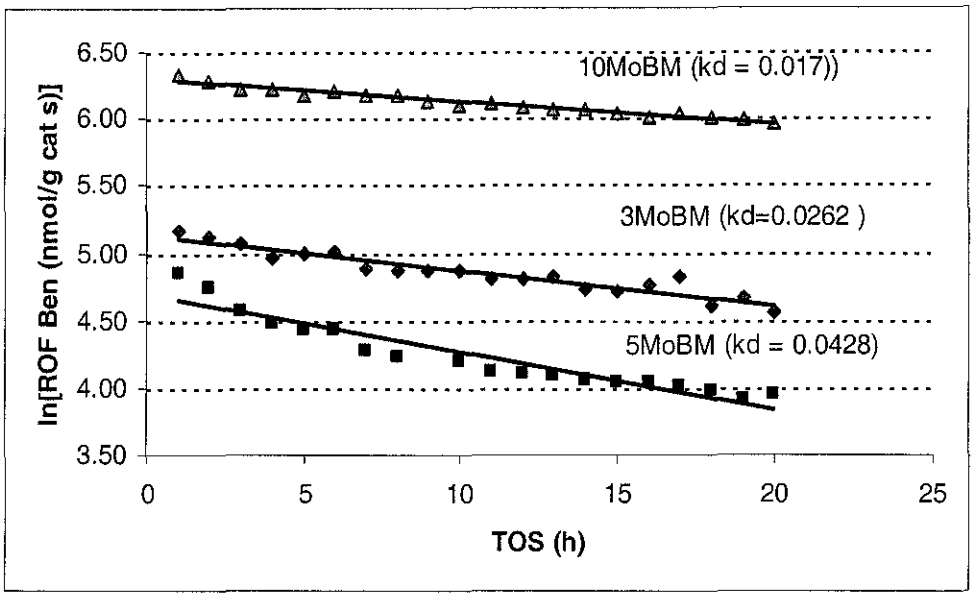

Figure 4.7 Catalytic Evaluations on the Rate of Deactivation Constant

From Figure 4.7 it can be seen that 10MoBM has the lowest deactivation rate constant, followed by 3MoBM and 5MoBM. The k_d of 3MoBM and 5MoBM are 1.5 and 2.5 times greater the 10MoBM respectively. This shows that 10MoBM is the more stable catalyst than either 3MoBM or 5MoBM, and 3MoBM is more stable that 5MoBM. This finding support of catalytic evaluation discussed above.

4.2.3.9 Surface Properties

To further understand the variation of product formation and its impact on catalyst deactivation, the changes in the surface properties with phase changing from calcination, to activation and finally to the reacted catalyst and its affect to Mo loading is investigated.

Table 4.4 Changes in Surface Properties Versus Mo Loading

$S_{BET}(m^2/g)$			
	Calcined	**Activated**	**Reacted**
3MoBM	372.5 (**- 7%**)	381.0 (**- 4%**)	204.6 (**-49%**)
5MoBM	239.1 (**-40%**)	340.7 (**-15%**)	227.6 (**-43%**)
10MoBM	193.0 (**-52%**)	287.3 (**-28%**)	274.3 (**-31%**)
HZSM-5	398.8		
S_{Ext} (m^2/g)			
3MoBM	139.0 (**- 7%**)	138.8 (**- 7%**)	49.7 (**-67%**)
5MoBM	85.53 (**-43%**)	128.4 (**-14%**)	62.21 (**-58%**)
10MoBM	65.83 (**-56%**)	104.2 (**-30%**)	93.15 (**-38%**)
HZSM-5	143.8		
$V_{BJH}(cm^3/g)$			
3MoBM	0.206 (**-6 %**)	0.211 (**- 4%**)	0.168 (**-23%**)
5MoBM	0.181 (**-17%**)	0.186 (**-15%**	0.186 (**-15%**)
10MoBM	0.127 (**-41%**)	0.122 (**-44%**)	0.139 (**-37%**)
HZSM-5	0.217		
$V_{mic}(cm^3/g)$			
3MoBM	0.103 (**- 9%**)	0.108 (**- 4%**)	0.069 (**-39%**)
5MoBM	0.069 (**-39%**)	0.094 (**-17%**)	0.073 (**-35%**)
10MoBM	0.059 (**-48%**)	0.082 (**-27%**)	0.081 (**-28%**)
HZSM-5	0.113		
d_{BJH} (nm)			
3MoBM	25.63 (**-65%**)	73.44 (**+1%**)	129.74 (**+79%**)
5MoBM	29.57 (**- 59%**)	69.67 (**- 4%**)	114.3 (**+58%**)
10MoBM	26.77 (**-63%**)	58.49 (**-19%**)	63.4 (**-12%**)
HZSM-5	72.44		

Table 4.4 list these changes mentioned above. The selected surface properties include BET surface area [$S_{BET}(m^2/g)$], external surface area [S_{Ext} (m^2/g))] calculated from t-plot, BJH average pore volume [$V_{BJH}(cm^3/g)$], average micro-pore volume [$V_{mic}(cm^3/g)$] calculated from t-plot, and BJH

average pore diameter [d_{BJH} (nm)]. The values in parenthesis give the average % changes in the individual properties studied in comparison with the parent HZSM-5 catalyst (Si/Al ratio 41).

From Table 4.4 it can be seen that the BET SA decreases with increasing Mo loading during calcination. 3MoBM records the smallest decrease (-7%) as compared with 5MoBM (-40%) and 10MoBM (-57%). Similar observations are also noticed for the external SA and micro pore volume measurement of the calcined catalyst.

The decrease in BET SA observed above (calcined catalyst) may be attributed to the bulky MoO_3 species, which adsorb mainly on the outer surface of the catalyst [6,12-14]. With calcination these bulky MoO_3 species tend to migrate over the external surface and some find its way into the pores or channels of the zeolite [4-6]. These migrations are driven by the driving force to anchor with the BAS present at the pores and channel of the zeolite. In the process some of the MoO_3 species are deposited in the channel mouth of the zeolite. As a result the BET SA, external SA and micro-pore volume decreases with increasing Mo loading.

Increase in average pore diameter may indicate structural collapse, whereas decrease in BJH pore volume suggest partial blockage of pore or inter catalyst channels. In the case of the calcined catalysts, it can be seen that there are decreases in both the pore volume and pore diameter. This suggests that increase in Mo loading and calcination temperature result in partial blockage in the zeolite channels enduring minimum structural damage.

The BET SA increases from the calcined phase to the activated phase of the catalyst. During this transformation the bulky anchored MoO_3 species are converted to the smaller and orderly structured Mo-carbide species with some further migration of Mo species into the channels with higher loadings [5]. Increases by about 3% for 3MoBM, and 25% for both 5MoBM and 10MoBM are observed during this phase change. Higher increase in BET SA in 5MoBM and 10MoBM may suggest migration of some of the anchored bulky MoO_3 species at the mouth of the pores moving deeper into the channels as they are converted to a smaller and orderly structured Mo-carbide species.

In the case of external SA, no change is observed for 3MoBM, whereas but both 5MoBM and 10MoBM experience an increase of about 29 and 26% respectively. This may imply that, for 3MoBM most of the MoO_3 species are well distributed on the external surface [3-7]. In the case of 5MoBM and 10MoBM the MoO_3 species are well distributed on the surface and the pore mouth and in some cases in the pore channel of the catalyst [5].

Going from the activated to the spent catalyst phase (after 20hours TOS), it can be seen that the BET SA decrease very steeply for both 3MoBM (-45%) and 5MoBM (-28%). In the case of 10MoBM the decrease is only 3%. This suggests that coke deposition in 10MoBM is well dispersed over the catalyst resulting in reduced blocking at the pore mouths or channels. In the case of both 3MoBM and 5MoBM, the dispersion of coke is more concentrated around the pore mouth or channels of the zeolite. This resulted in reduced BET SA and at the same time reduced activity as shown in Table 4.1.

In the case of external SA, the trend is similar to BET SA. The main difference being in the % decrease when going from activated to the spent catalyst phase. 3MoBM decreased by 60 %, while 5MoBM and 10MoBM decreased by 44 and 8 % respectively. From these observations it can be suggested that 10MoBM has better coke deposition management or better dispersion than the others.

4.2.3.10 Elemental Analysis

Table 4.5 examines the elemental constituent of the Mo/HZSM-5 catalyst at different phase changes ranging from calcination to activation and finally to the spent catalyst and its effect with Mo loading. The elemental analysis for Mo was carried out by ICP-AES as explained in Chapter 2.

Table 4.5 Elemental Analysis on Mo loading

Catalyst Type	Mo Content (wt %)		
	Calcined	Activated	Spent
3MoBM	2.82	2.78	2.76
5MoBM	4.76	4.69	4.65
10MoBM	9.08	7.92	7.80

The initial impregnated mixture for 3MoBM, 5MoBM and 10MoBM were calculated as 3.0, 5.0 and 10.0 wt% Mo. From Table 4.5, it can be noticed that all 3 catalysts lost < 10% of its Mo on calcination.

For 3MoBM and 5MoBM the loss in Mo content is < 3% when going from calcined to spent stage. This is within the ICP-AES accuracy. This is also in accordance to Iglesia et al [13] and Lin et al [8] observations whereby mixtures containing monolayer coverage lose minimum Mo content from

sublimation during calcinations. This indicates that the Mo species are tightly held within the zeolite.

The same is not true for 10MoBM, where a loss of 12.8% in Mo content is observed when going from calcined to activated stage. The extra loss experienced by 10MoBM may be as a result of sublimation of Mo since it is in excess of a monolayer [3,8].

On comparing the activated with spent catalyst, no significant loss of Mo content is observed for all the 3 catalysts studied. These observations suggest on activation the MoO_3 (more volatile) were converted to Mo_2C (less volatile) species and becomes strongly bonded and well distributed on/in the HZSM-5 catalyst. This is apparent from the observation made with regards to 10MoBM.

4.2.3.11 X Ray Diffraction Analysis

XRD can be used to investigate the possibility of material held within the channels of the zeolite. HZSM-5 structure is known to change from orthorhombic to monoclinic upon incorporation of sorbed molecules [13,14]

Figure 4.8 illustrates the XRD patterns for freshly calcined 3MoBM, 5MoBM and 10MoBM, represented by 3MoBMCal-Fr, 5MoBMCal-Fr and 10MoBMCal-Fr respectively. From the XRD pattern it can be seen that there are no significant phase change between the 3 studies. The MoO_3 peak (2θ values at 33.8, 39.0 and 49.3°), $Al(MoO_4)_3$ (2θ value at 45.7°) and doublet (2θ at 44 to 47°) are isolated and analyzed further .

From the Figure 4.8, it can be seen clearly that MoO_3 peak increases with increase in Mo loading as would be expected.

The doublet (2θ = 44 to 47°) split peak resolution for 5MoBM is not as well defined as that of 3MoBM and 10MoBM. A well split peak resolution is an indication of retention of the zeolite crystallinity as in the case of 3MoBM and to a certain extent 10MoBM. In the case of 5MoBM, the doublet is less resolved and leads to indicate that the zeolite is in the process of changing symmetry from orthorhombic to monoclinic or as a result of sorption of organic molecules or bulky ions occlusion of MoO_3[12,13] could be possible. This may be the cause of inferior performance for 5MoBM in the MDA reaction.

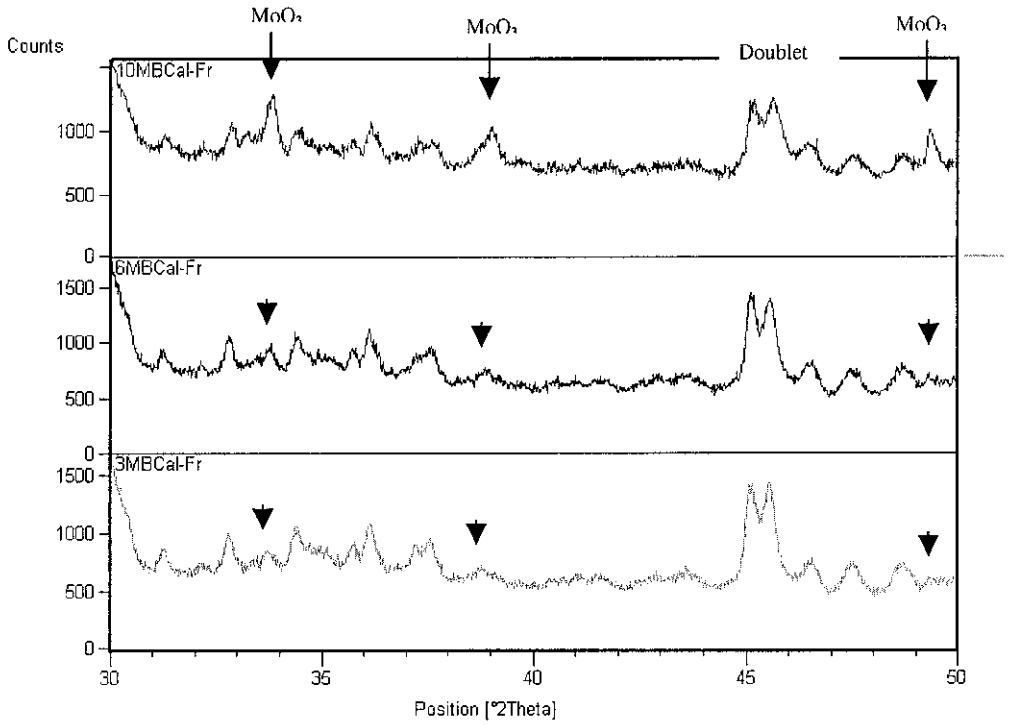

Figure 4.8 XRD Pattern of Calcinated Catalyst

To have an understanding of the transformation of phase from uncalcined right up to reacted catalyst phase, the XRD pattern of 10MoBM catalysts are highlighted in Figure 4.8. The usual suffix is used to differentiate between the different phases of the catalyst to gives the XRD pattern for 10MoBM catalysts.

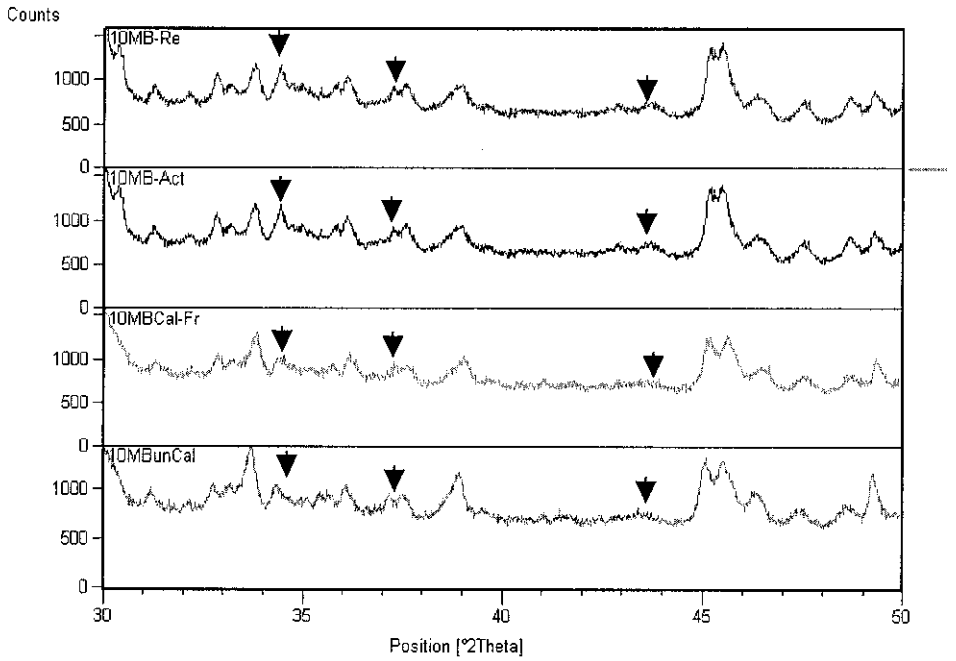

Figure 4.9 XRD Pattern on the Phase Change of 10MoBM Catalyst

The position of Mo_2C peaks (2θ = 34.7, 37.3 and 39.5°) are highlighted by arrow head to show its progressive emergence from uncalcined, calcined, activated and finally to reacted phase of the catalyst. It should be noted that the doublet (2θ = 44 to 47°) is showing difference in peak shapes between the different phases. The peak seems to become narrower when changing

from the uncalcined to the reacted phase. This shows that the transformation of 10MoBMCal-Fr moving away from zeolite crystallinity.

4.3 Calcination

4.3.1 INTRODUCTION

It has been established that preparation and pretreatment of the catalyst can affect the channel structure and acidity of zeolite as well as the location of the Mo species on/in HZSM-5 [2,4,8]. This chemical environment can be significantly altered as a result of high temperature calcination (treatment under air atmosphere). Calcination temperatures are usually carried out between 450 to 700°C [22-25]

Lunsford et al [4] using ion scattering spectroscopy (ISS) measurements concluded that the extent of Mo occupancy inside the channel of the zeolite depended on the calcination temperature. Based on their study using 2wt % Mo, they found that when the sample was calcined below 700°C, insignificant loss of Mo was encountered, whereas calcining at greater than 750°C, significant loss of greater than 5% Mo was observed. They also observed that when the temperature was increased from 500 to 800°C decrease in BAS resulted.

During slurry or incipient wetness impregnation of the HZSM-5 catalyst with ammonium heptamolybdate (AHM), the main portion of the heptamolybdate species (HMS) are adsorbed, not exchanged on the positive site of the HZSM-5 as a result of charge interaction [26]. Based on Xu et al [11] studies by IRS and DTA analysis, they suggested that AHM decomposes in air at 327 to 477°C to MoO_3 crystallites on the external zeolite surface. On increasing the calcination temperature to 500°C, these MoO_3 crystallites dispersed more readily on the external surface of the

zeolite. Some of these MoO_x species even migrated and exchanged within the zeolite channels via vapor or surface diffusion and ultimately anchored at the cation exchange sites by replacing protons in the HZSM-5. As a result of this exchange process, deallumination and loss of HZSM-5 crystallinity occured resulting in loss of acidic protons [13]. Calcination at 700°C results in strong interaction between the Mo species and framework aluminum resulting in the formation of MoO_4^{2-} species which is detrimental to methane activation [7]

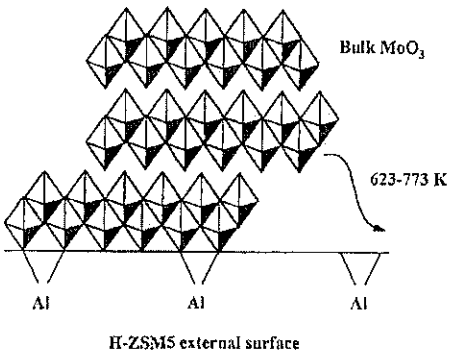

Figure 4.10 Structure of Bulk MoO_3 and Solid –State Migration on H-ZSM-5 Surface (Extract Taken from Ref. 13)

Migration of MoO_3 occurs during calcination. The driving force for MoO_3 migration in this reaction is the Al_2O_3 acid site of the zeolite. On reaching the Al_2O_3 acid sites, MoO_3 species becomes immobile and forms strong bonds with the Al_2O_3 acid sites (Figure 4.10).

The strong Al-O-Mo interaction during calcination led to the spreading of MoO_3 on the external site of the zeolite. This minimised MoO_3 sublimation during the exchange. During this treatment H_2O is evolved. The rate of H_2O evolved per Al depends on the rate of Mo species and the number of

channels of the HZSM-5 made available for transport. At temperatures between 477 to 577°C, the zeolite channels became accessible for external MoO_3 exceeding a monolayer. The rate of migration of MoO_3 species are limited by its degree of condensation whereby allowing the incorporation of more than a monolayer into the zeolite channels [13].

The MoO_3 species within the zeolite channels are believed to be the active sites required for MDA reactions. This MoO_3/HZSM-5 catalyst showed very low initial methane aromatization rates. To improve the aromatization rates, these highly dispersed MoO_3 species on the HZSM-5 must be reduced and carburised into Mo-carbide by methane. The initial products during this transformation are CO_x, H_2 and H_2O. On completion of this reduction and caburisation reaction, benzene, naphthalene and ethylene becomes the most abundant products. Reduction and carburisation processes usually takes about 0.2 to 1.0 hour on stream to complete [23,24]. Significant methane conversion reaction takes place at 700°C [4,5].

From the above explanation it can be inferred that the main function of calcination is to redistribution the MoO_3 species over the catalyst surface and into the channels or pore of the zeolite. This results in stronger interaction between the MoO_3 species and the zeolite's active sites. This effect led to a more stable chemical environment which reduces or prevented the sublimation of MoO_3 species [13].

4.3.2 EXPERIMENTAL

From the previous section it was noticed that 10MoBM was the better catalyst than either 3MoBM or 5MoBM. Based on this, 10MoBM was

selected as a suitable candidate for studying the effect of calcination temperatures of MDA reactions.

Based on the discussion in section 4.3.1, the ideal calcination temperatures would be between 500 to 650°C. Since the initial 10MoBM was calcined ex-situ at 600°C, two additional temperatures were selected for this study, i.e. one below and one above 600°C. The lower temperature selected was 500°C, as at this temperature enhance MoO_3 species dispersion takes place more readily on the external surface [13]. The higher temperature selected was 650°C, as 700°C as is said to deactivate the catalyst [7].

Calcination were carried out on HZSM-5 modified by impregnation of 10 wt % of Mo at 500, 600 and 650°C ex-situ as described in subsection 2.1.3 and the characterisation tests in section 2.4 of Chapter 2, unless otherwise stated.

4.3.3 RESULTS AND DISCUSSIONS

4.3.3.1 Methane Conversion

Figure 4.2.1 represents the effect of calcination temperature (500, 600 and 650°C) on the catalytic performance with respect to methane conversion on 10Mo/HZSM-5 catalyst over 20 hours TOS.

From Figure 4.11, it can be seen that the calcination temperature of 600°C gives the best methane conversion of the three studied. From the same figure, the methane conversion for 1st hour TOS for 600 and 650°C are similar. After 3 hours TOS, methane conversion rates for 650°C decreases at a much faster rate than 600°C. In the case of 500, methane conversion starts at a lower rate than both 600 and 650°C, but after 3 hours TOS, 500°C has a similar methane conversion rate as that of 650°C.

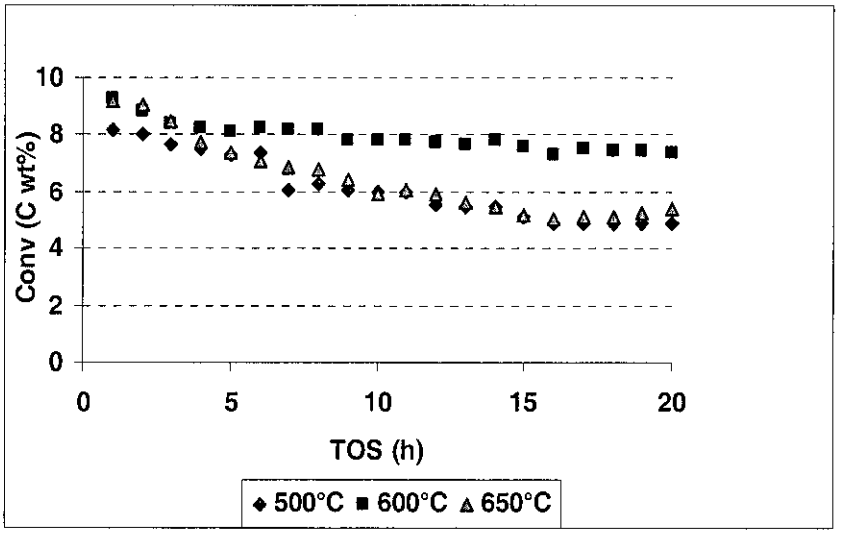

Figure 4.11 Effect of Calcination Temperature on Methane Conversion

4.3.3.2 MDA Product Distribution

The main products from MDA are aromatics, aliphatic hydrocarbons and coke. Figure 4.12 shows the effect of calcination temperature on these product yields in mmol over 20 hours TOS for the 10Mo/HZSM-5 catalysts.

From Figure 4.12, it can be seen that the catalytic activity at 600°C is highest among the three temperatures studied. Calcination at 600°C is 123% and 131% more reactive than that at 500 and 650°C respectively.

Calcination at 600°C produces more aromatics than either 500 or 650°C for the same duration of time. This yield amounted to 227 and 353% more aromatics than that at 500 and 650°C respectively. The coke yield on the other hand attain highest yield at 650°C and lowest at 600°C. No significant yield changes is noticed for the aliphatic fraction at the three different calcination temperature studied.

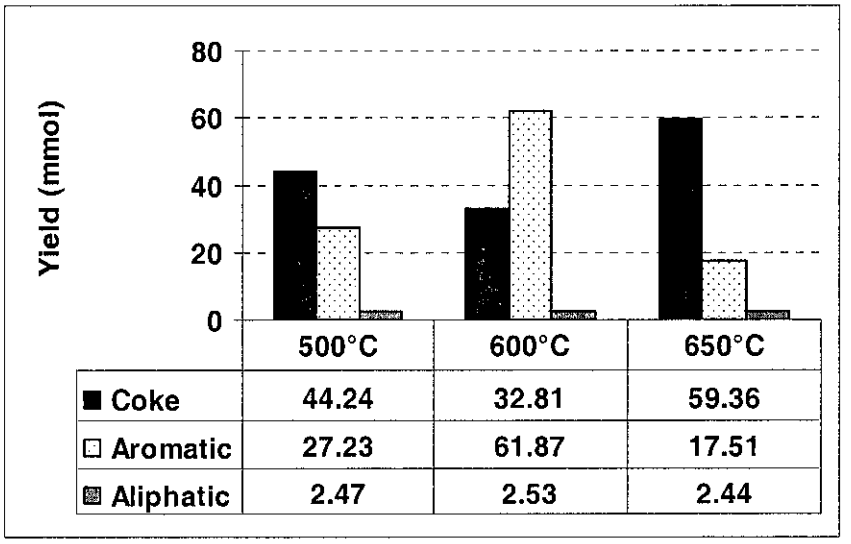

	500°C	600°C	650°C
■ Coke	44.24	32.81	59.36
□ Aromatic	27.23	61.87	17.51
▨ Aliphatic	2.47	2.53	2.44

Figure 4.12 Effect of Calcination Temperature on MDA Product Distribution

In the case of product selectivity, 600°C has 64% for aromatic and 34% for coke. Both 500 and 650 have 37 and 22% for aromatic and 60 and 75 % for coke respectively.

From the above observations, calcination at 600°C has the highest catalytic activity, selectivity and yield for aromatics, and very much lower for coke yield and selectivity as compared to 500 and 650°C. In other words, 600°C is the best calcination temperature for MDA under the specified conditions.

4.3.3.3 Aromatic Product Selectivity

Figure 4.13 represents the effect of calcination temperature on aromatic product selectivity over 20 hours TOS. Benzene and naphthalene represent the major products and its % selectivity is represented on the primary y-axis, while toluene and xylene, the minor products which account for <6 wt %, is represented on the secondary y-axis.

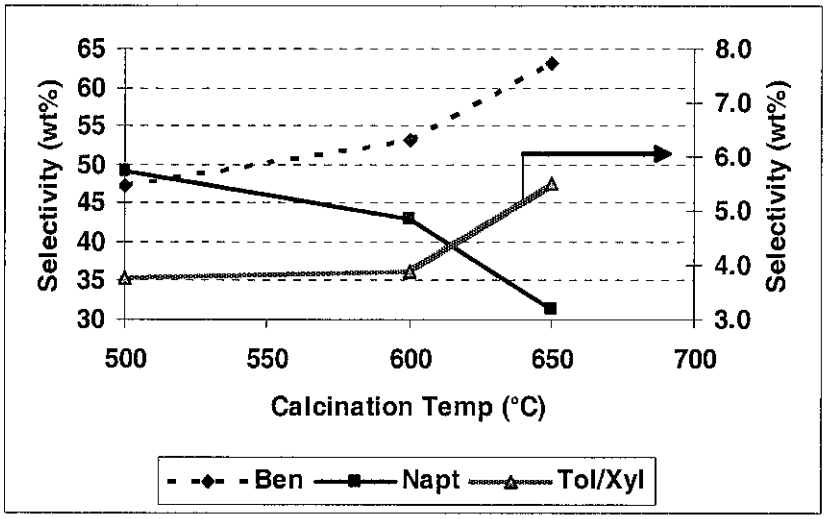

Figure 4.13 Effect of Calcination Temp on Aromatic Fraction Selectivity

From Figure 4.13, it can be seen that both benzene and toluene and xylene group selectivity increased with increase in calcination temperature, whereas for naphthalene the reverse is observed.

Based on the above observations, it suggests that both naphthalene and benzene follow a similar intermediate [20]. Increase in calcination temperature favours benzene selectivity over naphthalene. From Figure 4.12, it was noticed that above calcination temperature of 600°C, the selectivity for coke increases. Analysing Figures 4.12 and 4.13, it may be suggested that calcination at 650°C will induce naphthalene condensation resulting in coke build up leading to catalytic deactivation. As a result naphthalene yield decreases, while benzene increases, with increase in calcination temperature.

4.3.3.4 Coke Yield

The ROF of coke is illustrated in Figure 4.14. As mentioned previously excess coke deposition is the main cause of catalytic deactivation.

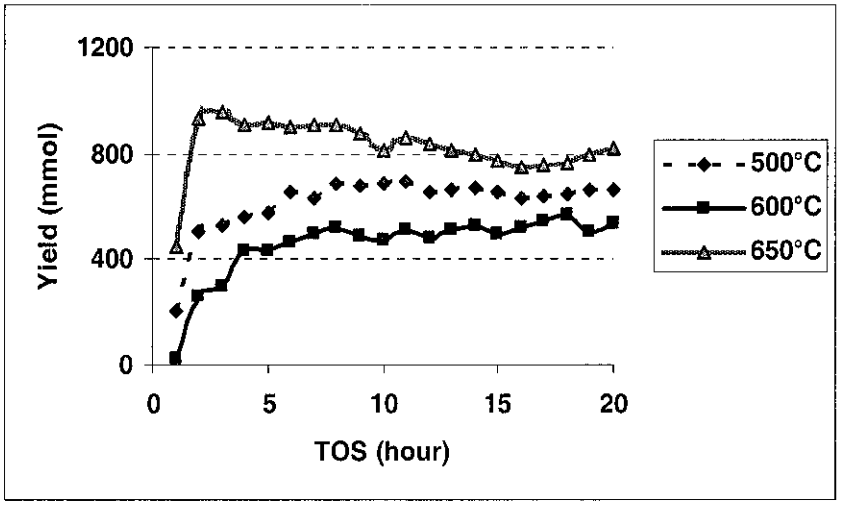

Figure 4.14 Effect of Calcination Temperature on ROF of Coke

From Figure 4.14, it can be noticed that for ROF for coke at various calcination temperature started at a low value which builds up steeply within the first 2 hours TOS. In the case of 500 and 600°C, after 2 hours TOS, the increase in ROF of coke became very gradual and attains a constant value after 7 to 8 hours TOS. For 650°C, the ROF for coke after the initial increase during the 1st hour, decreases gradually thereafter and became almost constant for 16 hours.

From Figure 4.14, it can be seen that calcination temperature at 600°C is the most preferred temperature of the three, because it has least ROF for coke over the 20 hours TOS. Calcination at 650°C is the least preferred, as it has the highest ROF for coke overall. The steep increase in ROF for coke at calcination temperature of 650°C after 1st hour TOS, accounts for the high degree of catalytic deactivation.

Aliphatic components (ethane and ethylene) make up about 3% of the total MDA product fraction. The aliphatic yields are divided into % selectivity of

ethylene and ethane to have a meaningful evaluation and are shown in Table 4.6.

Table 4.6 Effect of Calcination Temp on Ethylene and Ethane Selectivity

Calcination Temp (°C)	Selectivity (wt %)	
	Ethane	Ethylene
500	20.8	79.2
600	35.9	64.1
650	15.4	84.6

Since it is a well documented that aliphatic component is the precursor for aromatics [2], the debate is inconclusive as to whether ethylene or ethane is the main precursor for the aromatic product in MDA reaction.

From Figure 4.12, it can be seen that calcination at 600°C produces the highest yield for aromatic and 650°C the lowest. Based on this input, it can be observed that ethylene yield selectivity decreases with increase in aromatic formation. This observation favour ethylene over ethane for aromatic production.

4.3.3.5 Deactivation Rate

The rate of catalytic deactivation was derived by plotting the natural logarithm of rate of formation of benzene against TOS [20, 21]. The negative gradient gives the rate of deactivation.

From Figure 4.15, it can be seen that the rate of deactivation (kd) is the lowest for calcination temperature at 600°C and highest at 650°C. This suggests that the catalyst calcined at 650°C undergoes much faster catalytic deactivation than both 500 and 600°C, i.e. 600°C being the more stable

catalyst. This is in agreement with all the observations seen in Figures 4.12 and 4.13.

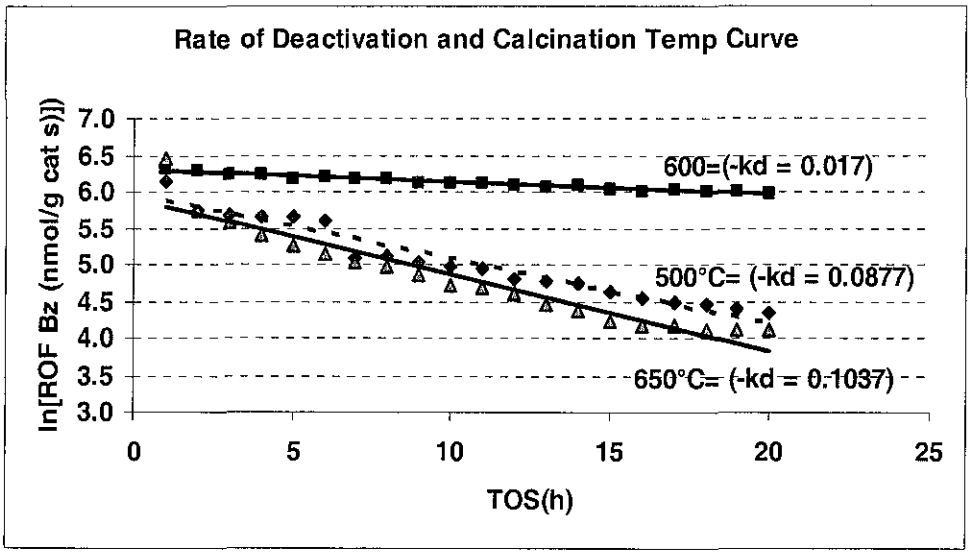

Figure 4.15 Rate of Deactivation with Calcination Temperature

In summary, the catalytic evaluation based on calcination temperature over 20 hours TOS at the set MDA parameters shows that 600°C is the preferred temperature, since it produces the highest yield and selectivity for aromatics and the more stable catalyst of the three studied.

From the above observations it can be suggested that the catalytic activity increases from calcination temperature of 500°C until it reaches a maximum activity at 600°C. As the calcination temperature approaches 650°C the catalytic activity decreases. This may be probably due to sintering of the active Mo species. This is in agreement with findings by Liu et al [8] and Xu et al [11]

4.3.3.6 Surface Analysis

Table 4.7 shows the results from surface analysis of the parent HZSM-5 and the effect of calcination temperature on a 10 wt% Mo modified HZSM-5 catalyst. It also shows the changes in surface properties as the catalyst phase changes from calcination to activation and finally spent (after 20 hours of reaction). The losses in surface properties during these periods as compared to the parent zeolite are shown in brackets in Table 4.7 below.

Table 4.7 Effect of Calcination Temperature on Surface Properties

$S_{BET}(m^2/g)$			
Calcination Temp (°C)	**Calcination (HZSM-5 to Cal)**	**Activation (Cal To Act)**	**Reacted (Act to React)**
500	**199.8 (- 50%)**	**279.7 (-30%)**	**196.0 (-51%)**
600	**193.0 (-52%)**	**287.3(-28%)**	**274.5 (-31%)**
650	**232.6 (-42%)**	**267.5 (-33%)**	**167.2 (-58%)**
HZSM-5	**398.8**		
$S_{Ext}(m^2/g)$			
500	**72.10 (- 50%)**	**98.13 (-32%)**	**45.20 (-69%)**
600	**65.83 (-54%)**	**104.2 (-28%)**	**93.15 (-35%)**
650	**96.50 (-33%)**	**111.0 (-23%)**	**69.40 (-52%)**
HZSM-5	**143.8**		
d_{BJH} (nm)			
500	**62.28 (-14 %)**	**49.82 (-31%)**	**13.59(-81%)**
600	**57.77 (-20%)**	**58.49 (-19%)**	**63.40 (-12%)**
650	**69.03 (-5%)**	**79.38 (+10%)**	**49.61 (-32%)**
HZSM-5	**72.44**		

It can be observed from Table 4.7, that the BET SA increases with increase in calcination temperature. This observation may suggest that spreading of Mo species increases with increasing calcination temperature.

Upon activation from calcination an increase in BET SA is observed for all three catalysts. This was expected as the bulky MoO_3 species are converted to the smaller and orderly Mo-carbide [23, 24]. From Table 4.7, the activated 600 and 500°C catalysts have a much higher BET SA than that at 650°C. This suggests higher spreading of the small uniform Mo-carbide for both 500 and 600°C calcined catalyst, unlike 650°C which has limited migration tendency. Upon reaction, the 600°C activated catalyst loses less BET SA (3%), than either 500 (21%) and 650°C (25%). This further supports better dispersion of the Mo-carbide species at 600°C as compared to the other two temperatures. This is apparent from the low coke deposition observed from catalyst evaluation from Figure 4.12 above.

The same type of effect as BET SA is noticed for the external SA when the catalyst changes from calcinated to activated and finally ends at the spent phase. It is interesting to note that the catalyst calcined at 600°C has a higher external SA after reaction as compared to those at 500 and 650°C. Since coke is generally deposited on the external surface and in the vicinity of Mo-carbide species [5,13], this further suggest that the spreading of Mo species at 500 or 650°C is not as highly dispersed as those at 600°C. It may also suggest that calcination temperature of 500°C is not as efficient as 600°C in dispersing the Mo species.

On examining the calcined catalysts' pore diameter from Table 4.5 it can be noticed that all the three catalysts have lower values than the original HZSM-5 zeolite. This suggests that the pore mouths or the channels may be partially blocked by the migrating Mo species. The highest loss is shown by the catalyst calcined at 600°C and the lowest at 650°C.

On activation, the pore diameter of catalyst calcined at 650°C increases more than the HZSM-5 zeolite. This may suggest that on activation, the pore mouths or channels at 650°C could have been damaged by the excessive Mo species spreading into the pores or channels and reacting with the BAS present there. As for catalyst at 500°C, there was a further decrease in pore diameter suggesting that the blockage at the pore mouth of the catalyst may be the most probable cause. In the case of 600°C there is a slight increase in pore diameter. This may suggest the probable reduction or narrowing of the channels by the transformation of the bulky Mo species to smaller Mo-carbide species.

For the spent catalyst, a decrease in pore diameter is observed in all those studied. This may had resulted from coke depositions which are usually found at the vicinity of the active Mo sites and BAS. This coke deposition may have also occurred at the pore mouth or at the pore channels.

4.3.3.7. Thermo Gravimetric Analysis

Table 4.8 depicts the type of coke present on the catalyst which was derived from kinetic studies from TGA results obtained from freshly activated and spent catalyst. TGA was carried out as in Chapter 2 section 2.4.2 to determine the coke species namely coke I and coke II as in Chapter 3 subsection 3.4.4.2 [29].

Table 4.8 Carbon Deposit Analysis Based on TGA

Calcination Temp	500°C		600°C		650°C	
	Activated	Spent	Activated	Spent	Activated	Spent
Coke I (mg/g cat)	3.0	143.7	3.4	111.1	3.6	211.1
Coke II (mg/g cat)	0.21	0.26	0.36	0.40	0.32	0.55
T. Coke (mg/g cat)	3.32	143.94	3.76	111.5	3.92	211.6

From Table 4.6 it can be seen that coke I and coke II of the activated catalyst increases with increase in calcination temperature. In the case of the spent catalysts, the coke I yield pattern differs with different calcination temperatures. 650°C shows the highest coke I deposit and 600°C the lowest. This is in agreement with catalyst product evaluation discussed above.

Coke II on the other hand, is much smaller than coke I. The coke II species are usually found near BAS or in the channels of zeolite. Coke II of the spent catalyst increases with increase in calcination temperature. The increase in coke II is highest at calcination temperature of 650°C and lowest at 600°C. The high increase in coke II at 650°C may have resulted from increases in acid sites being created with increasing calcination temperature [30].

In the case of total coke content, 650°C has the highest and 600°C the lowest. This suggests lower catalytic activity at higher calcination temperature may have come about by the destruction BAS sites [27]. This is in agreement with results obtained by catalyst evaluation studies above.

Table 4.9 Total Coke Content Using Different Methods

	Total Coke Content (wt%)		
	TGA	Ele. Analysis	MDA
10BC500	14.39	15.16	15.93
10BC600	11.15	11.43	11.81
10BC650	21.17	21.26	21.37

Comparing total coke content determined by elemental analysis and MDA to that obtained by TGA is shown in Table 4.9. It can be seen that all the three different methods show similar coke yield patterns. From the same table, it

can be seen that MDA result shows higher values than the other two analysis methods.

4.3.3.8 Mo Content Elemental Analysis

Table 4.10 shows the effect of Mo content (measured by ICP-AES as in Chapter 2) and its changes with calcination temperature with the different phase changes (activation and spent). From the same table, it can be seen that Mo content during calcination treatment results in a decrease with increase in calcination temperature. During the calcination stage, the loss in Mo for both 500 and 600°C are quite similar, but 650°C experience an extra loss of 5 wt% when compared to the former two.. This may have resulted from increase volatisation of Mo at higher calcination temperature.

Table 4.10 Effect of Calcination Temperature on Mo loading

Calcination Temp (°C)	Mo Content (wt%)		
	Calcination	Activation	Reacted
500	9.08	7.95	7.67
600	9.08	7.92	7.81
650	8.70	7.65	7.62

On activation, the losses of Mo between the three catalysts are between 12-13%. This was expected as explained by to Iglesia et al[13] and Lin et al [8] for more than a monolayer loading for Mo. Further loss of Mo from the reacted catalyst thereafter becomes minimal for all the three studied. This indicates a strong bonding between the Mo species and the active sites of the HZSM-5 zeolite.

The observation made above further strengthens the findings whereby at higher calcination treatment more Mo species are drawn into the zeolite

channels where most of the BAS are found. This is in agreement with Edwards et al. [29] who reported partial diffusion of Mo species into subsurface regions of the catalyst is highly possible during elevated calcination temperature conditions.

4.3.3.9 X-Ray Diffraction Analysis

Figure 4.16 illustrates the XRD patterns for freshly calcined catalyst represented by 10BC500, 10BC600 and 10BC650 is for 500, 600 and 650°C. The arrow heads on the XRD pattern represent the MoO_3 peak (2θ values at 33.8, 39.0 and 49.3°), $Al(MoO_4)_3$ (2θ value at 45.7°) and doublet (2θ at 44 to 47°) are identified and analyzed further .

From the Figure 4.16, it can be seen clearly that MoO_3 peaks for 10BC600 are much more resolved than either 10BC500 or 10BC650. The doublet (2θ = 44 to 47°) split peak resolution for 10BC600 is much better defined than either 10BC500 or 10BC650. A well split peak resolution is an indication of retention of the zeolite crystallinity as in the case of 10BC600 and to a certain extent 10BC650. In the case of 10BC500, the doublet is less resolved and leads to believe or indicate that the zeolite is in the process of changing symmetry from orthorhombic to monoclinic or as a result of sorption of organic molecules or bulky ions occlusion [29, 16] could be possible.

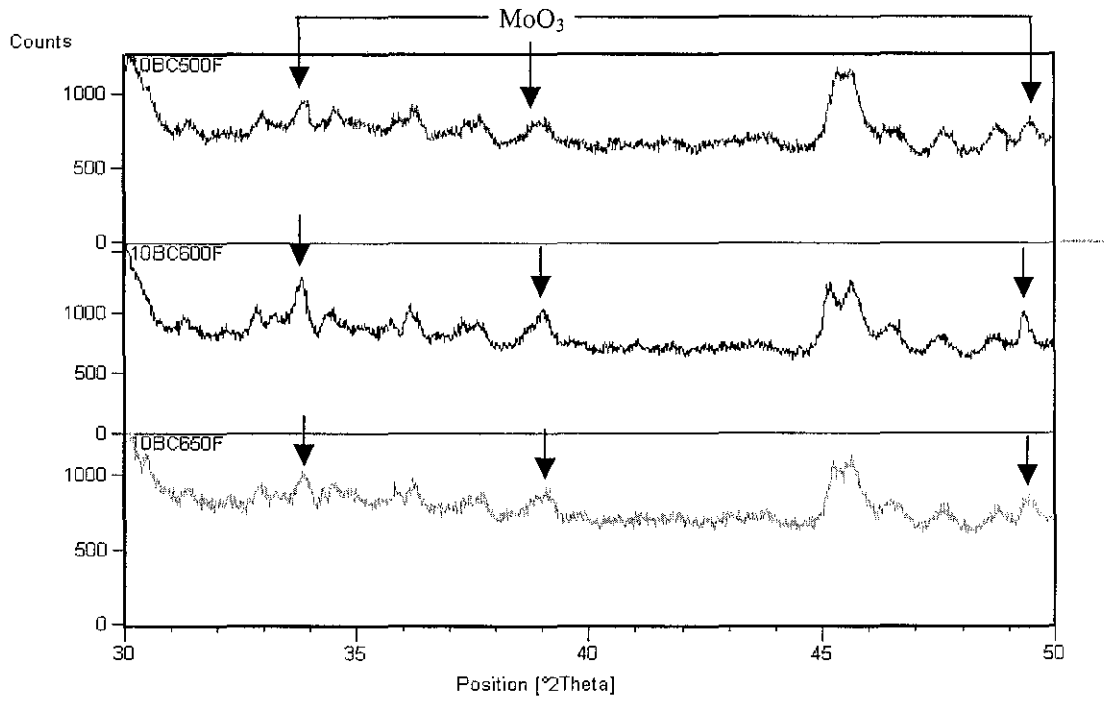

Figure 4.16 XRD Patterns for Freshly Calcined Catalyst

4.4 Reduction and Carburisation Studies

4.4.1 INTRODUCTION

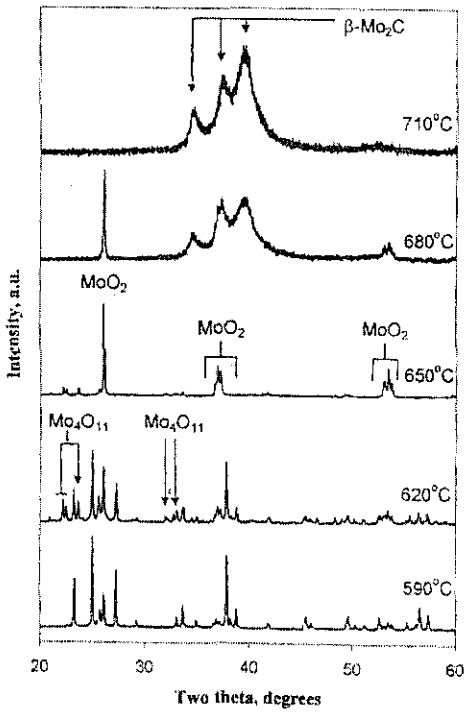

MoO_x/HZSM-5 catalysts after calcination show very low CH_4 aromatisation rates at 700°C. In order to improve the CH_4 aromatisation reaction, the highly dispersed MoO_x species must be converted to Mo-carbide, the active form of the catalyst. This Mo-carbide can be formed by the reaction of MoO_x species with CH_4. The subsequent reduction and carburisation step results in Mo-carbide.

Figure 4.17 In-situ XRD of MoO_3 Carburisation (Taken from Ref. 31)

Bouchy et al [31] studied the transformation of pure MoO_3 when carburised under pure methane feed using in situ XRD. Figure 4.17 represents the in-situ XRD pattern of MoO_3 carburisation under pure methane.

MoO_3 have an orthorhombic layered structures which are held together by weak van der Waals interaction in a <010> direction. Oxygen atoms are removed from the MoO_3 during reduction at 590°C leaving behind anionic vacancies. As the number of these vacancies increases, the structure collapses and reorganizes into a more dense monoclinic Mo_4O_{11} suboxide structure followed by the formation of MoO_2 intermediate.

When the temperature was raised to 650°C, reduction of MoO_3 to MoO_2 is complete. No traces of the original MoO_3 are observed at this stage. At 680°C the development of hcp β-Mo_2C is observed together with the MoO_2 peak. At 710°C complete disappearance of the MoO_2 peak leaving behind the main β-Mo_2C species.

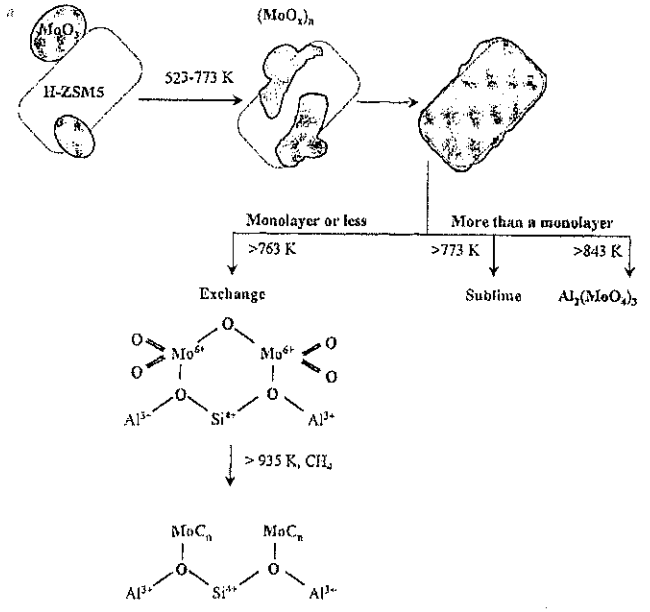

Figure 4.18 Formation of Mo/HZSM-5 Active Sites from MoO_3/ HZSM-5 Physical Mixture (Extract Taken From Ref. 12)

A schematic of the phase changes for the TPR carburisation is given below.

$$MoO_3 \rightarrow Mo_4O_{11} \rightarrow MoO_2 \rightarrow \beta\text{-}Mo_2C$$

During the initial reduction and carburisation period the main products are CO_x, H_2, and H_2O. The formations of hydrocarbon product are only observed after 0.2 to 1 hour TOS. This is because the reduced Mo species must be pacified by the formation of the carbide species before they are able to desorb the reaction products and complete a turnover [13]. This suggests that the active sites, Mo-carbide are created by the reduction and

carburisation. A schematic of this is presented in Figure 4.18. For more detail on the mechanism refer to Ref. 2.

4.4.2 INITIAL ACTIVATION TEMPERATURE STUDIES

An initial activation temperature of 650°C was selected for this study. The study was performed on a 10wt % Mo/HZSM-5 calcined ex situ at 600°C. The procedure for this catalytic evaluation was similar to that described in Chapter 2. Based on this study it was found that the conversion was very low. The methane conversion reduces to almost 2% after only 5 hours TOS. Heavy coking of the catalyst was the main cause of catalytic deactivation. Table 4.11 highlights the results obtained from this study.

From Table 4.11 it can be seen that the methane conversion is very poor and the main product was carbon. Due to the large production of carbon the catalyst was completely deactivated after 7 hours on stream.

Table4. 11 Catalytic Evaluation of 10wt % Mo/HZSM-5 Activation Temperature 650°C

TOS (hour/s)	CH4 Conv (wt %C)	Aromatic (wt %C)	Carbon (wt% C))	Aliphatic (wt% C)
1	4.1	30.5	50.6	18.9
2	3.2	19.5	63.1	17.6
2	3.1	16.5	70.5	13.0
4	2.5	8.7	80.6	10.7
5	2.2	4.3	90.3	5.4
6	2.0	2.5	95.4	2.1

Due to the poor results obtained, the study on variation of activation temperature was discontinued, but study on reduction and carburisation

mixture was then considered. This came about based on the study on unsupported MoO_3 route to produce high surface area Mo_2C as highlighted by Boudart et al [32]. Anderson [15] used this technique introduced by Boudart et al [32] on Mo-modified HZSM-5 catalyst and claim that it has enhance catalytic performance due to its higher catalytic surface area.

4.4.3 Reduction and Carburisation Medium

4.4.3.1 INTRODUCTION

Boudart et al [32] come up with an improved version for the catalyst activation described by Wang et al. [1]. They claimed to have produced a more efficient higher surface area β-Mo_2C (hcp) catalyst which could be prepared from MoO_3 using CH_4/H_2 reaction. Based on their observations from TPD by GC and XRD (Figure 4.19A), they concluded that reduction starts at 430°C and full carburisation completes at 660°C. Based on their work, they produced a graph (Figure 4.19B) relating thermodynamic equilibrium at atmospheric pressure with the reactions given below:

$$CH_4 = C(\text{graphite}) + 2H_2$$

$$2Mo + CH_4 = Mo_2C + 2H_2$$

Together with this relationship they were able to predict a successful caribusation conditions needed. From the same figure the highest CH_4/H_2 ratio permitted before preferred thermodynamic graphite set in can be determined.

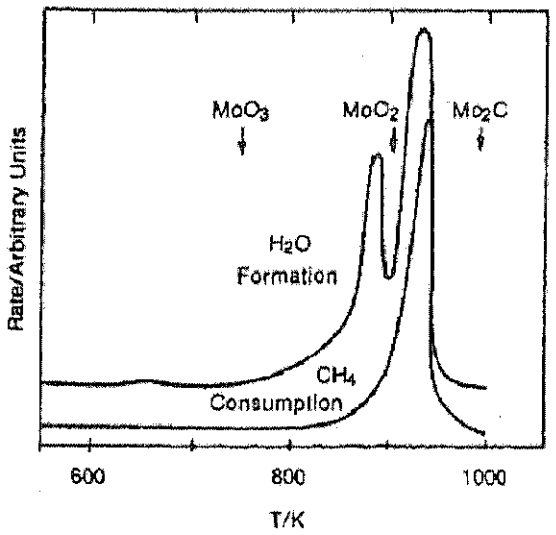

Figure 4.19A TPR Traces of Co-Reduction/Carburisation of Unsupported MoO3 in a 20% CH_4/H_2 (vol/vol) Mixture

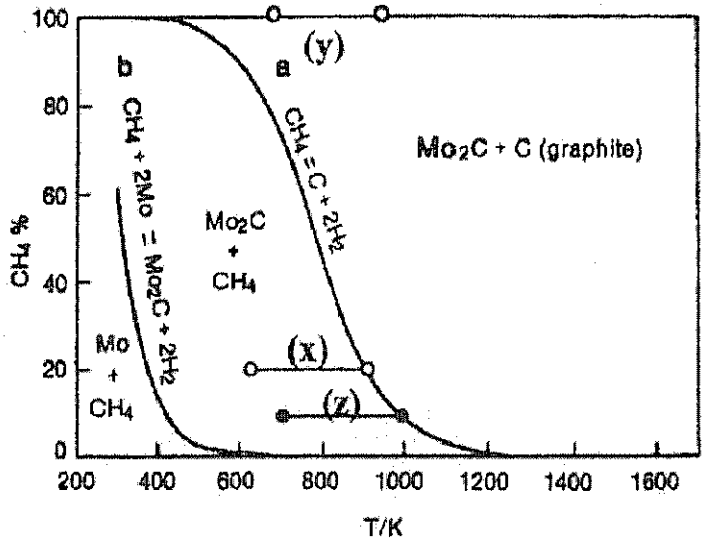

Figure 4.19B Equilibrium Relationships at Atmospheric Pressure Based on Given in Equation 1 and 2

Both the Figures 4.19A and 4.19B are data taken from reference 32. X and Y represent the operation lines for 20% CH_4/H_2 and 10% CH_4/H_2 activation mixture respectively.

Anderson [15] in his PhD thesis further analysed this method proposed by Boudart et a [32]. From the thermodynamic graph produced by Boudart et al [32], it can be seen that in order to avoid the formation of graphitic carbon and allow the caburisation to finish at 700°C, the highest allowable CH_4 content is 10%.

Based on the results/reports above, Anderson [15] proposed his method for the activation of Mo/HZSM-5 for the MDA reaction.

To complement studies made by Anderson, a catalytic evaluation study similar to his was undertaken. Calcination was conducted ex situ as in Chapter 2 section 2.1.3. The micro reactor conditions, variables and operations differ slightly from that mentioned in Chapter 2. The main variation includes the reduction and carburisation mixture, where methane is diluted to 10% by hydrogen. This new mixture now consists of 10%CH_4 in hydrogen with a flow rate of 50 ml/min was introduced at 400°C, i.e. immediately after the drying stage and ramped to 700°C at a rate of 5°C/min. At 700°C, reduction and carburisation mixture was replaced by He scrubbing stage with a flow rate of 10ml/min with a dwell time of 10 mins. This was performed to remove any traces of the reduction and carburisation mixture. After 10 minutes, helium was replaced by the reactant mixture of 3 v/v% Ar in CH_4. This stage marks the activation period where Mo-carbide catalytic functions are optimised together with the BAS of the zeolite. It also marks the end of reduction and carburisation period. From this stage onwards catalytic evaluation as in Chapter 2 will be is followed.

A schematic representation of the reactor/reaction temperature profile is given in Figure 4.20. The above method varied slightly from the original

Anderson method in that, the flow rate during the drying stage and the catalyst activation and reaction stage was set at 7.5ml/min. This was done to complement the space velocity optimised in Chapter 3.

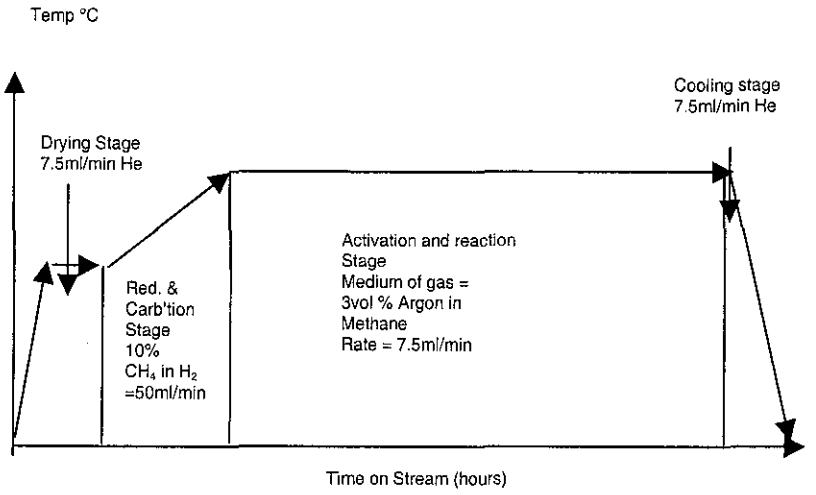

Figure 4.20 Schematic Representation of Reaction Condition

The effect of Mo loading on 3, 5 and 10% were against revisited with the new activation mixture of 10 %(v/v) methane in hydrogen to check for any catalytic activity and selectivity enhancement as claimed by Anderson in his PhD thesis [15]. For simplicity the Mo loading of 3wt%, 5wt% and 10wt % will be referred to as 3MoBMH, 5MoBMH and 10MoBMH respectively hereafter.

4..4.3.2 Catalytic Evaluation

The catalysts for this study selected were the uncalcined 3, 5 and 10 wt% Mo/HZSM-5 similar to that used in section 4.1. These stock catalysts were all calcined at 600°C ex-situ as described in Chapter 2 section 2.1.3. For catalytic evaluation study a comparison between the optimised Mo loadings as in section 4.1 is compared to the new method described above. For the

optimised method in section 4.1 where the reduction and carburisation (R & C) mixture was only methane will be represented as 'MoBM'. For the new R & C mixture (10%CH_4/H_2), a new identification tag 'MoBMH' will be used with the usual prefix used for the various Mo loading as described in earlier chapters. For example Mo loading of 10 wt% will be represented as10MoBMH.

4.4.4 RESULTS AND DISCUSSIONS

4.4.4.1 Methane Conversion

Figure 4.21 shows the methane conversion on a carbon wt % basis. This figure represents the calculated average methane conversion over a 20 hours TOS for each catalyst at the specific Mo loading. It is represented by 2 curves, one by MoBM group and the other by the MoBMH.

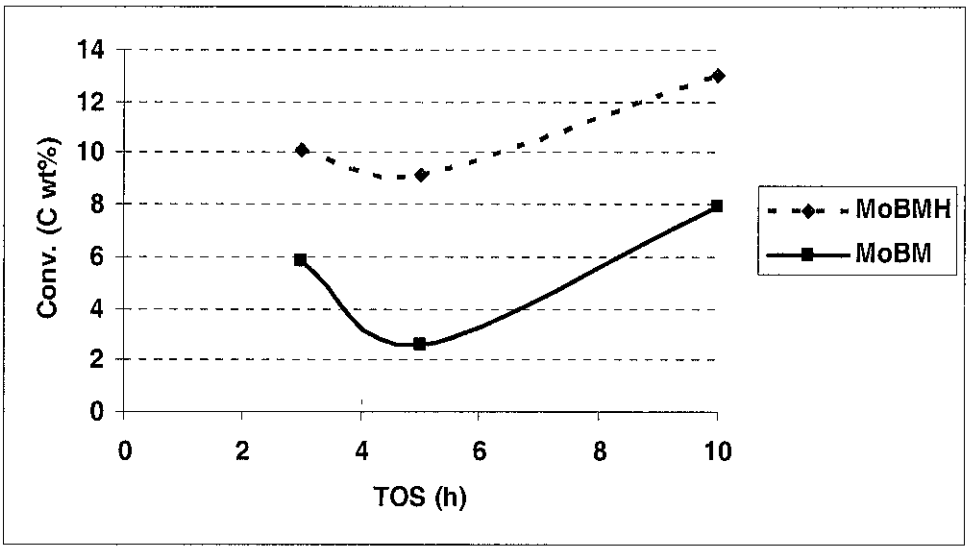

Figure 4.21 Comparison of Methane Conversion Using Different Reduction and Carburisation Mixture

From the Figure 4.21 it can be clearly seen that the new R & C mixture i.e. MoBMH give superior methane conversion or a much higher catalytic activity as compared to MoBM. Methane conversion for 3, 5 and 10 Mo loading has improved by 172, 350 and 153 % respectively. This shows a vast improvement especially for Mo loading of 5 wt%. This result complements works by Anderson [15].

4.4.4.2 MDA Product Yield

It will be interesting to see how the improvement in methane conversion has affected the product distribution especially the aromatic and coke yield. Table 4.11 represents coke and aromatic yield produced over 20 hours TOS. The same table also compares the coke and aromatic yield produced by the two R & C mixtures at the specific Mo loading. Columns 4 and 7 represent the increase percentage in yield for coke and aromatic respectively when shifting the R & C mixture from methane to methane/ hydrogen.

Table 4.12 MDA Product Yield Over 20 Hours Time on Stream

	3MoBMH		5MoBMH		10MoBMH	
Yield (20 hours)	mmol	%	mmol	%	mmol	%
Coke	93.66	75.7	74.46	66.4	73.12	45.9
Aromatic	23.27	18.8	30.40	27.1	80.17	50.3
Aliphatic	6.76	5.5	7.32	6.5	6.16	3.9
Catalyst Activity	123.70		112.18		159.45	
	3MoBM		5MoBM		10MoBM	
Yield (20 hours)	mmol	%	mmol	%	mmol	%
Coke	29.66	41.26	18.95	58.21	32.8	33.7
Aromatic	36.95	51.41	9.84	30.21	61.8	63.5
Aliphatic	5.27	7.33	3.14	9.64	2.5	2.6
Catalyst Activity	71.89		32.56		97.4	

From the Table 4.12, the coke yield is very much higher for MoBMH than MoBM catalyst. Mo loading of 3, 5 and 10 for the MoBMH catalyst has increased by 316, 393 and 223% respectively to that of MoBM.

In the case of aromatic yield, 3MoBHM experience a decrease of 37% compared to its 3MoBM counterpart, while both 5MoBMH and 10MoBMH has improved by 309 and 130% respectively to its MoBM counterpart.

From Table 4.12 it can be seen that for the MoBMH catalyst, the coke yield and selectivity decreases with increase in Mo loading, whereas for the aromatics, the reverse to that of coke is observed. A similar observation as MoBMH is expected for MoBM catalysts. The discrepancy lies in 5MoBM due to its inferior catalytic activity.

In the case of aliphatic yield MoBMH has higher yield than its MoBM counterpart. In both group of catalyst the aliphatic yield is below 10% selectivity.

From the above observation it can be seen that MoBMH has higher catalytic yield as compared to the MoBM group. Further the yield for the entire MDA product is higher than the corresponding MoBM catalyst; except for the aromatic yield from 3MoBMH which is lower that the 3MoBM catalyst. The higher catalytic yields for the MoBMH catalysts are favouring more coke rather than the aromatic selectivity. Taking 10MoBMH and 10MoBM for example, the coke yield for 10MoBMH increases by 223% whiles that for aromatic increases by 130% above the 10MoBM catalyst. In both the groups of catalyst it can be seen that Mo loading of 10% is the preferred catalyst. Another interesting point to note is that, in the case of MoBMH, Mo loading of 5 wt% is a more promising catalysts than the 3wt%. The reverse is true for MoBM group of catalyst.

4.4.4.3 Aromatic Fraction Distribution

Since the optimization of aromatic is the main priority of the optimization study, it is important to know how the R & C mixture effects the distribution of aromatic products with respect to benzene, naphthalene, toluene and xylene. Table 4.13 displays the distribution of these aromatic products yield for both MoBMH and MoBM catalysts. Individual aromatic product for each of the catalyst was calculated as yield in mmol over a 20hours TOS.

Table 4.13 Aromatic Product Distribution from MDA Reaction

	3MoBMH		5MoBMH		10MoBMH	
Yield	mmol	%	mmol	%	mmol	%
Benzene	16.40	70.5	21.34	70.2	59.50	74.2
Naphthalene	5.07	21.8	6.92	22.7	15.45	19.3
Toluene	1.36	5.9	1.64	5.4	4.32	5.4
Xylene	0.44	1.9	0.50	1.7	0.90	1.1
	3MoBM		5MoBM		10MoBM	
Yield	mmol	%	mmol	%	mmol	%
Benzene	18.28	49.4	5.50	55.9	32.86	53.1
Naphthalene	16.84	45.6	3.68	37.5	26.60	43.0
Toluene	1.84	5.0	0.65	6.6	2.39	3.9
Xylene	0.00	0	0.00	0	0.02	0.0

From Table 4.13 it can be seen that, for all MoBMH catalysts, increase in Mo loading results in the increase in the entire aromatic fraction. This is not the same in the MoBM catalysts because of the poor catalytic activity of 5MoBM. Further xylene yield was observed in MoBMH whereas in MoBM catalysts it was undetectable.

Benzene selectivity makes up more than 70 % of the aromatic fraction in MoBMH catalysts, whereas it is much lower for MoBM (49 to 56%). Further the benzene yield increases with increase in Mo loading in MoBMH.

10MoBMH produces 363 and 279% more benzene than 3MoBM and 5MoBM.

Naphthalene contributes about 19 to 23% of the aromatic fraction in the MoBMH and 38 to 46% for MoBM catalysts. This shows that the MoBM produces more naphthalene than MoBMH counterpart.

Both toluene and xylene are minor products of the MDA reaction make up 5 to 6% and 1 to 2% of the aromatic fraction in MoBMH and MoBM catalyst respectively.

From the above observation, MoBMH produces more aromatic yield than the MoBM catalysts. MoBMH is more selective towards benzene and less selective towards naphthalene. MoBM on the other hand has almost similar selectivity towards benzene and naphthalene. The low selectivity in naphthalene in MoBMH catalyst may have reduced due to condensation as a result of increase catalytic activity and low desorption of naphthalene from the catalyst. This effect could have increased the coke yield as seen from Table 4.13

4..4.4.4 Deactivation Rate

The deactivation rate [20,21] for MoBMH catalyst can be calculated from Figure 4.22 given below. The negative slope of the curves give the deactivation constant k_d. It should be noted that a lower k_d value denotes a more stable catalyst.

From Figure 4.22 it can be seen that the deactivation constant for 10MoBMH is lower than either 5MoBMH or 3MoBMH which renders

10MoBMH the more stable catalyst. In other words 10MoBMH is about 3 times more stable than either 5MoBMH or 3MoBMH. The stability of 5MoBMH and 3MoBMH catalyst is about the same.

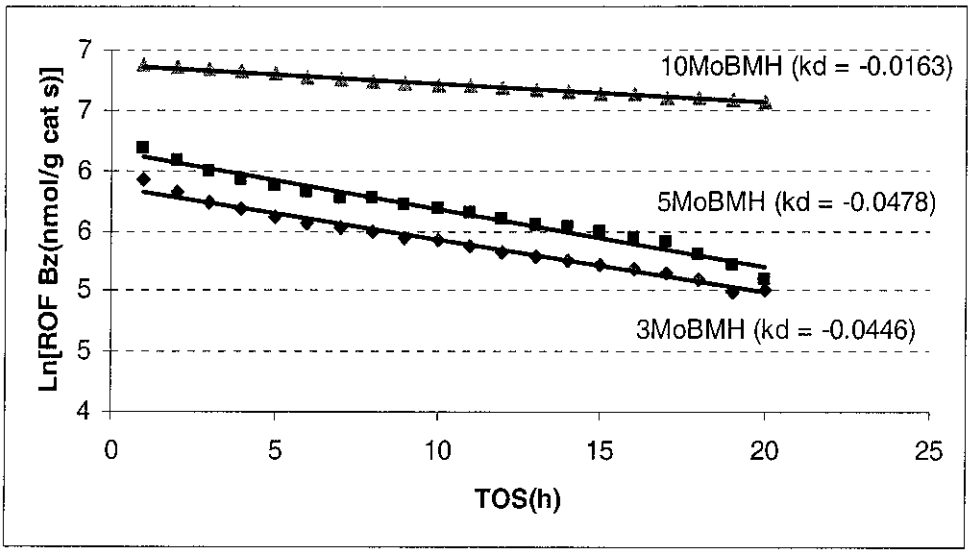

Figure 4.22 Catalytic Evaluations on the Rate of Deactivation Constant
(note: that the deactivation rate is independent of the reactions concentration)

Based on the same reaction condition concept it will be interesting to find how MoBM catalyst compares with MoBMH. Table 4.14 presents the kd value for the different types of catalyst. The stability factor is calculated by dividing the highest kd value (base) by each kd value for the given catalyst. The base kd value is this case is taken from 5MoBMH. This stability factor gives an approximate indication of the stability of each catalyst.

Table 4.14 Catalytic Stability Comparison

Catalyst	3MoBMH	3MoBM	5MoBMH	5MoBM	10MoBMH	10MoBM
-kd *	0.045	0.026	0.048	0.043	0.016	0.017
Stability Fact	1.1	1.8	1.0	1.1	3.0	2.8

* Rate of Deactivation Constant

From Table 4.14, it can be seen that for a Mo loading of 10% the stability is still very high. Stability of this catalyst is least affected by changes in R & C mixture. In the case of Mo loading of 5wt%, no significant changes in stability of the catalyst are noted with changing R &C gaseous phase. On the other hand with Mo loading of 3wt% a drop in stability is noted when the R & C gaseous phase is changed from methane to hydrogen/methane mixture. This observation suggest that the stability of the catalyst with low Mo loading (<3wt%) is not suitable for hydrogen/ methane R & C gaseous phase.

4.4.4.5 Aliphatic and CO Product Distribution

Apart from coke and aromatic products, the product distribution from MDA reaction also contains aliphatic (ethane and ethylene) and carbon monoxide fraction. Although these are minor products, they are important because aliphatic fraction formed on the Mo-carbide sites are primary products which are converted to benzene and higher homologue of aromatic fractions via oligomerization, cracking and cyclization reactions [13].

Table 4.15 gives the yield of ethane, ethylene and CO measured in mmol over a 20 hours TOS. The last row gives the ratio of ethylene and ethane. For the purpose of simplicity it is assumed the reaction is void of thermal cracking.

Table 4.15 Aliphatic and CO Product Distribution

Catalyst Group	MoBM			MoBMH		
Mo Loading (wt%)	3	5	10	3	5	10
Ethylene(mmol)	3.93	2.73	1.63	5.62	6.02	4.14
Ethane (mmol)	1.34	0.41	0.90	1.14	1.30	2.02
Carbon Monoxide (mmol)	0.41	0.63	0.17	0.65	0.86	0.24
$C2^{=}$/C2 Ratio	2.9	6.7	1.8	4.9	4.6	2.0

From Table 4.15, it can be seen that both ethylene and ethane fractions in the MoBMH catalyst are higher then that in the MoBM counterpart at the same Mo loading. Ethylene makes up the major portion of the aliphatic fraction in both types of catalysts.

With MoBMH catalyst it can be seen that with increase in Mo loading, both ethane fraction increases. The reverse affect is observed for the MoBM catalyst (5MoBM is excluded because of its poor catalytic activity). It is also noticed that the ethylene/ethane fraction in both type of catalysts decreases with increase in Mo loading. This indicates more ethylene is consumed with increase in Mo loading

Since ethylene and ethane are initial products of MDA reaction, ethylene which is formed by dehydrogenation is the main precursor for benzene production in the MDA reaction [11]. Increase in ethylene yield favours benzene selectivity. Since MoBMH has higher ethylene yield than MoBM catalyst, higher selectivity for benzene can be anticipated for MoBMH catalyst type. With increase in Mo loading preferential consumption of ethylene is observed (decrease in ethylene/ethane ratio), as a result selectivity to benzene increases with Mo loading. This conclusion complements the findings of aromatic fraction seen in Table 4.12 where, the benzene selectivity for MoBMH catalyst is in the above 75%.

CO yield is a process where the carbon deposit is release from the catalyst by abstracting lattice oxygen from the zeolite framework [5]. Increase in CO content can deplete the lattice oxygen which may eventually lead to structural collapse. From Table 4.12, it can be seen that Mo loading of 10 wt% for both MoBMH and MoBM produces least CO yield which may

indicate reduction in abstraction of lattice oxygen from the zeolite, as a result more of the active catalyst will be retained.

4.4.4.6 Surface Analysis

Table 4.16 gives the raw data on activated catalyst surface properties of MoBM and MoBMH catalysts using an ASAP 2000 Surface analyser. This table highlights the surface areas and pore characteristics with changes in R & C gaseous mixture using different Mo loading. Every 3rd row in the table represents the changes in surface properties between MoBMH and MoBM for the particular Mo loading. The changes are calculated in % difference between MoBM (base) and MoBMH catalyst.

Table 4.16 Surface Properties for Activated MoBM and MoHBM

	Surface Area		Pore Volume		Pore
	BET (m^2/g)	External (m^2/g)	BJH (m^2/g)	Micro (m^2/g)	Diameter (nm)
10MoBM-Act	287.3	104.2	0.182	0.082	69.49
10MoBMH-Act	293.9	116.4	0.186	0.079	68.32
Changes in Surf Prop (10Mo)	2%	12%	2%	-4%	2%
5MoBM-Act	305.8	103.0	0.189	0.090	71.71
5MoBMH-Act	340.7	128.4	0.186	0.094	69.63
Changes in Surf Prop (5Mo)	11%	25%	-2%	4%	2%
3MoBM-Act	318.4	99.61	0.172	0.097	73.44
3MoBMH-Act	381.0	138.8	0.211	0.108	71.23
Changes in Surf Prop (3Mo)	20%	39%	10%	10%	2%
HZSM 5 (Fresh)	398.8	143.8	0.217	0.113	72.44

From Table 4.16, it can be clearly seen that both the surface areas (BET and external) and BJH pore volume of MoBMH is much higher than MoBM counterpart for similar loading at similar phases. As for the pore diameter

and micro-pore, MoBM has higher value than MoBMH catalyst for similar phases. Similar observation is also noticed in the case of Mo loading. Increase in Mo loading for both catalyst results in decrease in surface areas and BJH pore volume. These observations again complement the findings of Anderson [15]. In the case of micro-pore volume, increase in Mo loading leads to decreases micro-pore volume. Not much difference is noticed in the case of pore diameter.

The increase in BET and external SA in the MoBMH catalyst may be one of the reasons for the increase in methane conversion for MoBMH against MoBM catalyst as observed in Table 4.16

It can also be seen from Table 4.16 that the freshly activated MoBMH catalyst has higher BJH pore volume (reflects the meso and inter catalyst channels) than MoBM counterpart. This suggest the MoBMH catalyst being more porous, in turn may have better access for the reactants to the active sites and for the product from the catalyst when compared to MoBM catalyst. This improved reactant and product accessibility may contribute to higher rate of formation of products or higher yield of MDA products for MoBMH as compared to MoBM as observed in Table 4.16.

From the same table, micro-pore volume is observed to be slightly higher in MoBMH catalyst than its MoBM counterpart, except in the case of 10 wt% Mo loading. Decrease in micro-pore volume may results in increase in coke deposition [5] this is reflected in Table 4.16 above.

Pore diameter is higher in MoBM than the MoBMH catalyst. Increase in Mo loading does not have much affect on the pore diameter.

From the above observation it can be seen that the MoBMH catalysts has higher surface areas and could be considered as more accessible to reactants and products than the MoBM counterpart.

4.4.4.7 Thermo-gravimetric Analysis

Table 4.17 gives the TGA derived results for activated and spent or reacted MoBMH and MoBM catalyst. The same table compares the changes in type of coke deposit on these 2 groups of catalysts with increasing Mo loading.

Coke I is equated with coke deposit and generally deposit on the external surface, whereas coke II is the active coke associated with Mo active sites usually found near the BAS [5]. Total coke is the sum of both coke I and coke II. As for the activation energy it represents the nature of the coke species present or the binding strength of the coke species to the active sites on the zeolite or catalyst framework. Increase in activation energy means more tightly bounded coke species

From Table 4.17, it can be seen that for both MoBMH and MoBM activated type catalyst, coke I and coke II increases with Mo loading. MoBMH activated catalyst has higher coke I and coke II values than the MoBM counterpart.

Comparing coke II of the activated catalysts of MoBMH and MoBM, it can be seen that former has about 3 times more coke II at the same Mo loading than the latter. The Mo active sites which are usually found in the channels of the zeolite influences the coke II deposition. Since Coke II amount in MoBMH is higher than MoBM catalysts, this increase in the former may suggest that the Mo species for the former have higher penetration and better

dispersion than the latter species. This is also visible from Table 4.16 and results obtain by Boudart et Al [32] and Anderson [15], where similar activated methods as that of MoBMH catalyst, has a much higher BET and external SA than the MoBM catalyst. Further works by Naccache et al [33] suggest that higher catalytic activity can be associated with increased Mo dispersion

Table 4.17 TGA Results for Activated/Reacted MoBMH and MoBM

	Activated MoBMH Group			Activated MoBM Group		
Mo Load (wt %)	3	5	10	3	5	10
Coke I (mg/g cat)	13.26	20.13	26.61	2.4	2.8	3.40
Coke II (mg/g cat)	0.45	0.60	0.94	0.14	0.23	0.36
Total Coke (wt %)	1.4	2.1	2.8	0.26	0.32	0.39
Act. Energy	98.5	98.5	98.9	100.4	100.4	100.5
	Reacted MoBMH Group			Reacted MoBM Group		
Mo Load (wt %)	3	5	10	3	5	10
Coke I (mg/g cat)	203.1	259.5	259.0	98.9	68.1	111.1
Coke II (mg/g cat)	0.24	0.35	0.46	0.15	0.25	0.40
Total Coke (wt %)	20.3	26.0	26.0	9.91	6.84	11.15
Act. Energy (kJ/Mol)	89.7	89.8	93.3	98.5	98.5	98.9

As for the reacted catalyst, it can be seen coke II for MoBMH catalyst has lower yield than the activated one. The loss for the whole range of Mo loading (MoBMH) averages around 50%. In the case of MoBM, although an increase of less than 10% is noted over the whole range of Mo loading, it can be considered as minimal.. Although MoBMH lose more coke II from activated to reacted phase, but still the coke II yield for reacted MoBMH is much higher than the corresponding MoBM. This may suggest that coke II in MoBM is more tightly bound than MoBMH counterpart.

Reacted MoBMH catalysts have higher total coke II deposition than its MoBM counterpart. On analysing this observation, it may suggest that MoBMH should be less active than MoBM catalysts. On the contrary, the above assumption is not true, because MoBMH have higher activity than MoBM catalysts. Since from surface analysis studies it clearly shows that MoBMH have higher surface area than MoBM counterpart and at the same time high catalytic activity for the former, this suggest higher dispersion of Mo species for the MoBMH over the MoBM catalysts. In other words, the coke for MoBMH catalyst has bigger surface area to be dispersed as compared to MoBM resulting in prolonged catalytic activity and stability for the former.

With increasing Mo loading for reacted MoBMH catalyst, the activation energy increases. This may indicate that for MoBMH catalyst with higher Mo loading, the coke II is less concentrated and highly dispersion with less accumulation as compared to the lower Mo loadings. High dispersion and loosely bounded coke II species leads to higher catalytic activity as observed for MoBMH and MoBM catalysts, where the former has higher catalytic activity than the latter.

4.5 Conclusions

From the study on Mo loading for MoBM catalyst, it can be concluded that Mo loading of 10wt % is the preferred catalytic loading for MDA reaction. It gives the highest catalytic activity with a high average methane conversion of 7.9%. It also has the highest aromatic yield and selectivity. Further 10MoBM is more stable than either 3MoBM or 5MoBM.

Based on calcination temperature studies for 10MoBM at the set parameters, calcination at 600°C is the preferred temperature for MDA reaction as it has the highest catalytic activity and produces the highest yield and selectivity for aromatics and lowest coke yield and selectivity. Further it is most stable catalyst of those studied.

The effects of carburisation and reduction mixture on these catalyst type were investigated. The carburisation and reduction of 10% CH_4 in H_2 is classified under MoBMH group while that with CH_4 only as MoBM. Based on this study it was found that in general, the MoBMH has higher catalytic yields for all MDA products than that of the MoBM group. The higher MDA product yields for the MoBMH catalysts arise from both aromatics and coke yields, but the coke yield is more predominant than the aromatic. For both the MoBM and MoBMH the preferred Mo loading is 10%.

As for the aromatic fraction MoBMH is more selectively towards benzene and less selective towards naphthalene. MoBM on the other hand has almost similar selectivity towards benzene and naphthalene.

The external and BET surface area for the activated and spent 10MoBMH are higher than the corresponding 10MoBM, the increase in surface area results in increase in catalytic activity.

4.6 Chapter 4 Reference

1. Wang, L., Tao, L., Xie, M., Xu,G., Huang,J., and Xu,Y., Catal. Lett.21 (1993) 35
2. Xu, Y., and Lin, L, Appl Catal A, 188 (1999) 53
3. Xu, Y,.Liu, S, Wang, L., Xie, M., and Guo, X., Catal Lett. 30 (1995) 135
4. Solymosi, F., Cserenyi, J., Szoke, A., Bangsagi, T., and Dszko, A., J Catal 165 (1997) 150
5. Wang, D., Lunsford, J.H., and Rosynek, M.P., J Catal 169 (1997) 347
6. Zhang, J.Z., Long, M.A, Howe, R.F., Catal Today 44 (1998) 293
7. Xu, Y., Liu, W., Wong, S., Wang, L., and Guo, X., Catal Lett. 40 (1996) 207
8. Lin, W., Xu, Y, Wong, S.T., Wang, L., Qiu, J., and Yang, N., J Catal. A 120 (1997) 257
9. Chen, L., Lin, L., Xu, Z., Li, X., and Zhang, T., J Catal. 157 (1995) 190
10. Xu, Y., Liu, S., Wang, L., Xie, M., and Guo, X., Catal. Lett. 30 (1995) 135
11. Xu, Y., Shu, Y., Liu, S., Huang, J., and Guo, X., Catal. Lett. 35 (1995) 23
12. Mestl, G., and Knozinger, H., Langmuir (1998) 14 3964
13. Borry III, R.W., Kim, Y.H, Huffsmit, A.,Reimer, J.A. and Iglesia, E., J Phys. Chem. B 1999 103, 5787.
14. Liu, H, Li T., Tian, B., and Xu, Y., Appl. Catal. A 213(2001) 103.
15. Anderson, J.R., Phd Thesis, University of Liverpool, UK (2001).
16. Liu, H., Su, L, Wang, H., Shen, W., Bao, X,, and Xu, Y., Appl. Catal. 236 (2002) 263

17. Koerts, T, Deelen, M.J.AG., and van Santen, R.A. J.Catal. 138 (1992) 101
18. Szoke, A, and Solymosi ,F, Appl. Catal. 142 (1996) 361
19. Solymosi, F, Cserenyi, J, Szoke, A, Bansagi, T, and Oszko A, J. Catal. 165 (1997) 150
20. Wang, H., Hu, G., Lei, H., Xu, Y., and Bao, X, Catal. Lett. 89 (2003) 75
21. Levenspiel, O., J. Catal. 25 (1972) 265
22. Wang, L., Tao, L., Xie, M., and Xu, G., Catal. Lett. 21 (1995) 35.
23. Solymosi, F., Erdohelyi, A., and Szoke, A., Catal. Lett. 32 (1995) 43
24. Wang, D., Lunsford, J.H., and Rosynek, M.P., Topic Catal. 3, (1996) 289
25. Liu, S., Dong, Q., Ohnishi, R., and Ichikawa, M., J. Chem. Soc. Chem Commum. (1997) 1455
26. Stakheev, A.Y., Khodakov, A.Y., Kustov, L.M., Kazansky, V.B., and Minachev, K.M., Zeolite 12 (1992) 866
27. Lo, W., Meitzner, G.D., Borry III, R.W., and Iglesia E., J. Catal. 191 (2000) 373
28. Campbell, S.M., Bibbly, D.M.,. Coddington, J.M, Howe R.F., and Meinhold, R.H., J. Catal. 161 (1996) 338
29. Edwards, J., Adams, R., and Ellis, P., J Am. Chem. Soc. 112 (1990) 8349,
30. Wang, L., Tao, L., Xie, M., and Xu, G., Catal. lett. 21 (1995)35
31 Bouchy, C, Schmidt, I., Anderon, J.R, Jacobsen, C.J.H., Derouane-Abd Hamid, S.B, and Derouane, E.G., J Mol. Catal A163 (2000) 283-296
32. Lee, J.S. Oyama, S.T., and Boudard, M.J., J. Catal. 106, (1987) 125

33. Ha, T.V.T.T., Tiep,L.V., Meriaudeau, P., and Naccache, C., J Mol Catal. A 181 (2002) 283

34. Liu,,S., and Ichikawa, M., J. Catal. 181 (1999) 175

CHAPTER 5
ALPHA MOLYBDENUM CARBIDE / HZSM-5

5.1 Effect of Mo Loading

5.1.1 INTRODUCTION

Two thermodynamically stable molybdenum carbide phases, namely β-Mo_2C with a hexagonally close packed (hcp), and the α-MoC_{1-x} with a face centred cubic (fcc) structure have shown catalytic performances for hydro-treating reactions, comparable with the commercial hydro-treating reactions [1-4]. Ranhotra et al [5] showed that both the alpha and beta form of the Mo carbide exhibit different catalytic properties for the hydrogenolysis of ethane. The beta-form of the Mo carbide has been widely reported for MDA reaction as described in the previous Chapter. The alpha form of the Mo carbide was first reported for MDA reaction by Bouchy et al [6].

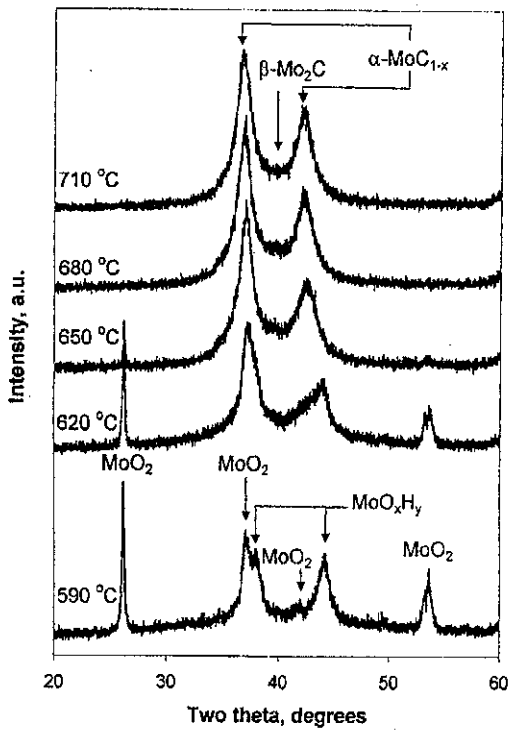

Figure 5.1 XRD Pattern on pure MoO_3 In-Situ Study (Extract from Ref. 6)

Several different routes for the preparation of the fcc α-MoC_{1-x} form have been reported. Two of these include (i) a 2-step process reported by Volpe et al [7] which involves initial nitridation of MoO_3 by ammonia

followed by the carburisation of γ–Mo_2N nitride and (ii) a one step reaction by Lee et al which involves direct carburisation of MoO_3 impregnated with Pt [8]. Based on the latter [8] route, Bouchy et al [6] modified it by pre-reducing the MoO_3 with butane and then by direct carburisation with methane to produced α-MoC_{1-x} catalyst on acidic zeolites namely HZSM-5. This latter report by Bouchy et al [6] is of interest to the present study.

Using in situ XRD, Bouchy et al [6] studied the phase changes involved when pure MoO_3 were subjected to H_2 reduction at 350°C for 24 hours. From their studies they observed that MoO_3 was reduced into a mixture of MoO_2 suboxide and MoO_xH_y oxyhydride. This reduction is brought about under mild conditions by the slow diffusion of hydrogen atom into the lattice structure of MoO_3, resulting in preferential collapse of the MoO_3 structure along the <000> direction. The role of hydrogen atom insertion in the above process is to stabilise the structure from collapsing due to weakening created by the oxygen vacancies in the process of forming MoO_2. The resultant lateral reorganisation gives rise to the fcc oxyhydride (MoO_xH_y), an intermediate which is a template for the formation of fcc α-MoC_{1-x} catalyst.

A schematic of the phase change involved is given below.

$$MoO_3 \rightarrow MoO_xH_y\ (MoO_2\ \text{trace}) \rightarrow \alpha\text{-}MoC_{1-x}\ (\beta\text{-}Mo_2C\ \text{trace})$$

From the same study [6] they observed that carburisation for the transformation to α-MoC_{1-x} starts at 620°C and completes at 680°C. Traces of β-Mo_2C was also observed at the final stages together with the α–MoC_{1-x} resulting from initial traces of partial structural collapse of MoO_2 which on carburisation forms the fcc β-Mo_2C phase [6].

Based on the above report, a method was devised for the preparation of α-MoC_{1-x} supported on HZSM-5. A summary of the preparation is given below.

5.1.2 EXPERIMENTAL

5.1.2.1 Preparation of fcc α-MoC_{1-x} supported on HZSM-5

The α-MoC_{1-x} supported on HZSM-5 the catalyst was prepared by wet impregnation of AHM on to the HZSM-5 support and calcined to 600°C as described in Chapter 2 section 2.1.2

The calcined catalyst obtained was then dried with helium at a flow rate of 12.2ml/min by heating the catalyst from room temperature to 400°C and maintained at this temperature for 30 minutes.

At the end of the 30 minutes, the helium gas was replaced by an activation mixture of a v/v hydrogen/butane gas mixture in a ratio of 11:1 with a total flow rate of 63 ml/min. The activation temperature was raised to 650°C at a ramp rate of 5°C/min and held at this temperature for an hour.

At the end of dwell period, the activation mixture was again replaced by helium at a flow rate of 7.5ml/min. At this stage the temperature was still held at 650°C for an additional 10 minutes for scrubbing purposes.

At the end of the 10 minutes, helium scrubbing gas was replaced by methane with a similar flow rate of 7.5ml/min (GHSV of 1500 h^{-1}) and the temperature was then raised to 700°C and held at these conditions and temperature for 21 hours (1 hour for induction period and 20 hours for reaction time). Thereafter the catalytic process run and data collection were performed as described in Chapter 2.

For the purpose of identification, the fcc α-MoC_{1-x} supported on HZSM-5 catalyst the identification tag 'XMoA' will be used, where the prefix **X** represents the Mo loading and MoA the catalyst type. The present Chapter will cover the investigation on: affect of Mo loading and calcination temperature. At the end of the chapter a comparison study between the MoA, MoBM and MoBHM will be carried out.

5.1.3 RESULTS AND DISCUSSIONS

5.1.3.1 Catalyst Evaluation

Figure 5.2 represent the methane conversions for 3, 5 and 10 MoA catalyst based on percentage carbon number conversion over 20 hours time on stream (TOS).

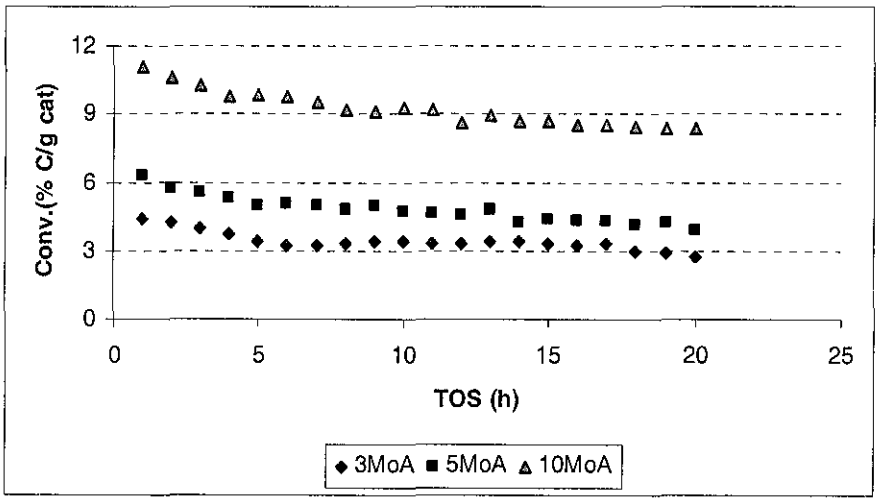

Figure 5.2 Effect of Methane Conversion with Mo loading

From Figure 5.2, it can be seen that with increase in Mo loading, increase in methane conversions are observed. For 10MoA, 5MoA and 3MoA the 1st hour conversions are 11.1, 6.3 and 4.5 C/g cat respectively. The methane conversions drop to 8.4, 3.9 and 2.8% for 10MoA, 5MoA and 3MoA respectively after 20 hours TOS. These represent a reduction of 25% for 10MoA and 38% for both 5MoA and 3MoA.

The average methane conversions for 3MoA, 5MoA and 10MoA are 3.4, 4.8 and 9.2% respectively. This shows that the catalytic activity of 10MoA is 271 and 192% higher than 3MoA and 5MoA respectively.

51.3.2 MDA Product Yield and Selectivity

Figure 5.3 shows the MDA product group yield in mmol obtained over 20 hours TOS for each of the 3 Mo loadings. The main fractions in this MDA reaction are coke and aromatics, while aliphatics make up the minor fraction.

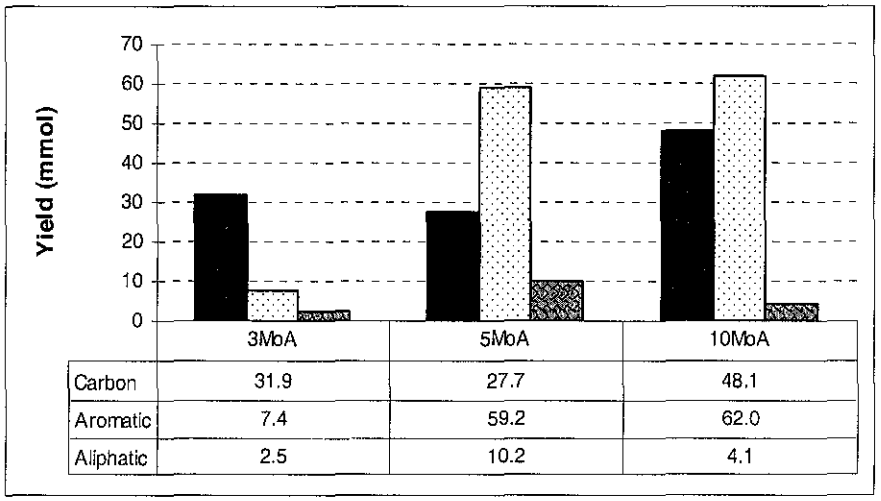

	3MoA	5MoA	10MoA
Carbon	31.9	27.7	48.1
Aromatic	7.4	59.2	62.0
Aliphatic	2.5	10.2	4.1

Figure 5.3 Product Yield with Mo Loading

From Figure 5.3, it can be seen that 10MoA is the most active catalyst of the three studied. Further it has the highest yield for both of the major product i.e., coke and aromatics with the selectivity being 42% for coke and 55% for aromatics. 10MoA also produces 106 and 838% more aromatic than 5MoA and 3MoA respectively. Of the three catalysts, 5MoA produces the lowest coke yield. Its selectivity towards coke and aromatics are 27 and 61% respectively. On the other hand 3MoA is the least active catalyst. Its selectivity for aromatics are 18 % and for coke 76%.

The aliphatic fraction is the main precursor for the formation of aromatic fraction [9-12]. From Figure 5.3 it can be seen that 5MoA has the highest aliphatic content of the three catalysts. This may be one of the reasons for its superior aromatic and low coke producing properties.

From the above discussion, it can be seen that 10MoA is the most reactive catalyst with good aromatic yield. 5MoA is a good catalyst for aromatic production with low coke yield and selectivity whereas 3MoA is basically a coke producing catalyst.

5.1.3.3 Coke Product

Figure 5.4 shows the rate of formation of coke with TOS. It can be seen that 10MoA starts with a low ROF for coke which increases sharply from the 1st to 3rd hours TOS. After the 3rd hour TOS it pseudo stabilises thereafter. 3MoA on the other hand differs from 10MoA in that it starts with initial slightly high ROF which pseudo-stabilises after the 2nd hour TOS. In the case of 5MoA it starts with a slightly lower ROF for coke which pseudo stabilise thereafter for the next 20 hours TOS. This shows that coke deposition in all three catalysts reaches pseudo-steady state after 3 hours TOS.

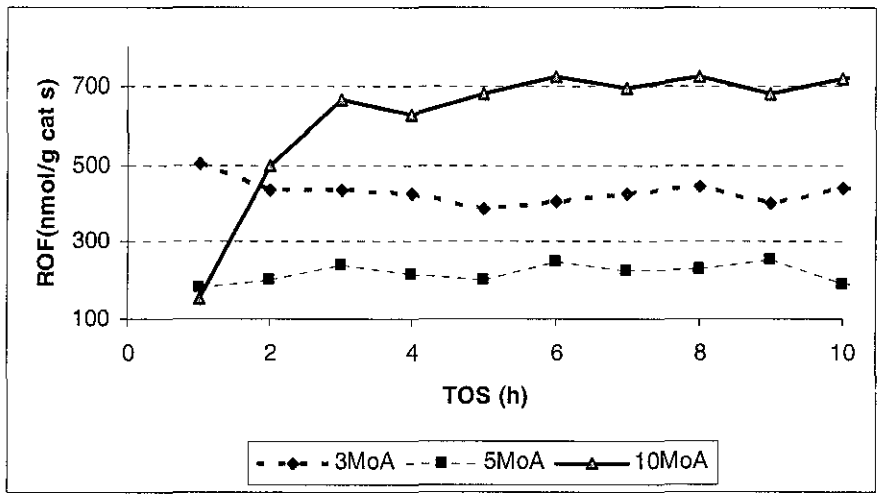

Figure 5.4 ROF of Carbon with Mo loading

5.1.3.4 Aromatic Product

Figure 5.5 represents the breakdown of aromatic fractions from the MDA reactions for the MoA type catalyst. From this figure, it can be seen the benzene and naphthalene are the most dominant products with the former selectivity higher than the latter for all three catalysts studied.

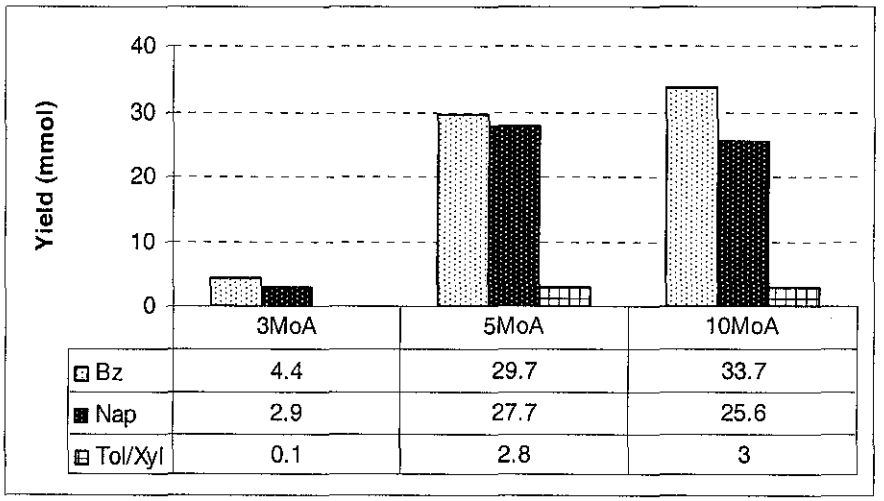

	3MoA	5MoA	10MoA
Bz	4.4	29.7	33.7
Nap	2.9	27.7	25.6
Tol/Xyl	0.1	2.8	3

Figure 5.5 Effect of Mo Loading on the Aromatic Fraction

From the above results, it can see that with increase in Mo loading, the lighter aromatics like benzene, toluene and xylene yield increases. The heavier aromatic component namely naphthalene decreases after reaching an optimum production at 5MoA. Further increase in Mo loading results in a decline in the yield of naphthalene.

Baring 3MoA it can be noticed that the selectivity for benzene increases with increase in Mo loading, while that for naphthalene it is the reverse. Selectivity for benzene for 5MoA and 10MoA are 49.3 and 54.1%, and for naphthalene it is 46.0 and 41.1% respectively.

5.1.3.5 Aliphatic Product

Figure 5.6 represents the effect of ROF of aliphatic (ethane and ethylene) fraction with changing Mo loadings and TOS. From this figure, it can be seen the ROF of ethylene is the more dominant fraction of the two.

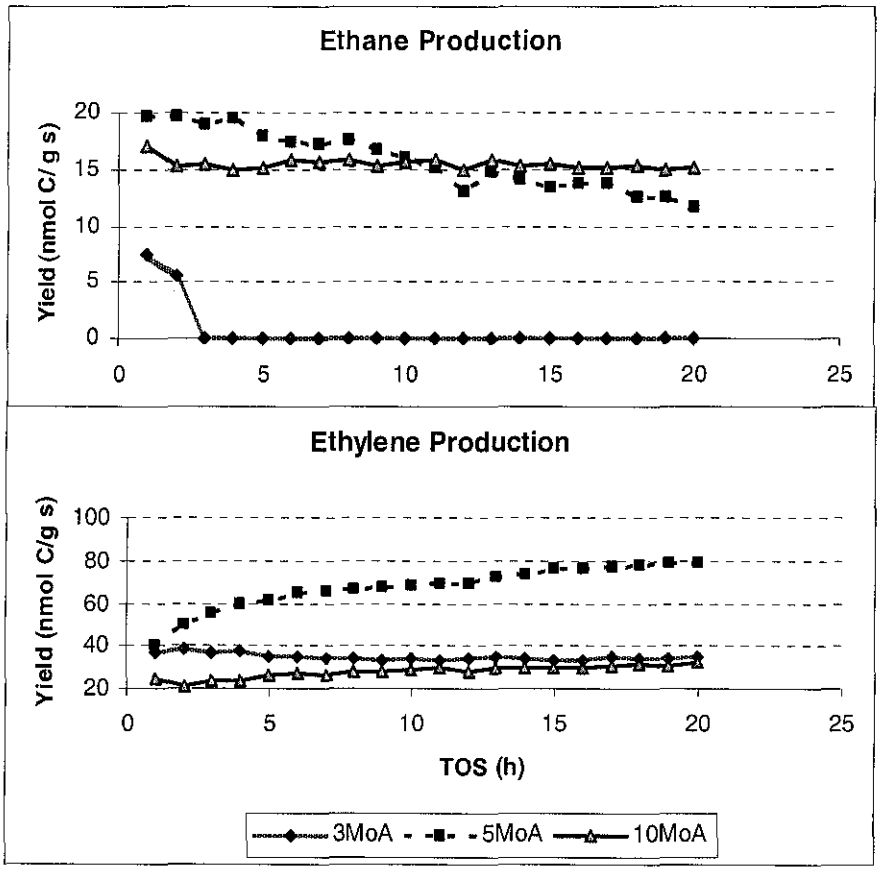

Figure 5.6 Effect of Mo Loading on the Aliphatic Fractions

From Figure 5.6 it can be seen that for both 3MoA and 10MoA the ROF of ethane drops with TOS. The same is not true for 5MoA, where it is unaffected by TOS. In the case of 3MoA, it can be seen that the ROF for ethane ceases production within 3 hours of TOS. As for 10MoA the ROF for ethane decreases by about 25% over 20 hours TOS.

The changes in ROF for ethylene are different from that of ethane. From Figure 5.6, the ROF for ethylene from 3MoA is unaffected with increases

in TOS, unlike 5MoA and 10MoA where an increase in TOS results in an increase in ROF for ethylene. This increase ROF for ethylene for both 10MoA and 5MoA amounts to 25 and 50% respectively over 20 hours TOS.

The above observations seem to support ethylene as the primary product. This is supported by the observation that ethane can be completely eliminated from the product list at low MDA conversion. This observation is in agreement with findings by Xu et al [16,17]. However there is still an ongoing debate as to whether ethylene or ethane is the primary product [18]. From Figure 5.6, it is obvious that both ethane and ethylene do not seem to have a common intermediate. This is because with the elimination of ethane, no increase in ethylene is observed in the case of 3MoA catalyst.

5.1.3.6 Coke Species

The coke species were obtained and calculated by TGA method as described Chapter 3 sub heading 3.4.4.2 is shown in Table 5.1. To recall coke I (TGA temp 260 to 380°C) is associated with Mo species and coke II (TGA Temp 380 to 700°C) is burn-off coke usually present on the external surface [13]. Total Coke is the sum of both coke I and coke II

Table5.1 Carbon Deposit Analysis Based on TGA Results

	Coke I (mg/g)	Coke II (mg/g)	Act Ener (kJ/Mol)	Total Coke (wt%)
3MoA-Act	9.65	0.23	99.5	0.99
3MoA-Re	108.8	0.27	96.5	10.9
5MoA-Act	9.83	0.36	99.6	1.02
5MoA-Re	95.5	0.39	96.6	9.59
10MoA-Act	10.4	0.69	99.7	1.11
10MoA-Re	160.5	0.53	96.8	16.1

Results from Table 5.1 shows that both coke I and coke II for the activated catalyst increased with increase in Mo loading. This was expected as increase in Mo loading increases Mo species which are directly responsible for methane activation [13-15]. As for the reacted catalysts, the changes in coke I and coke II are different from that of the activated catalyst.

From the same table, it can be observed that 10MoA-Re catalyst produces 148 and 168% more coke I than 3MoA-Re and 5MoA-Re respectively. This is in accordance to that observed Figure 5.4.

Upon reaction, coke II increases for both 3MoA and 5MoA, but for 10MoA it decreases. Increase in coke II may have resulted from reduced access of reactant in and aliphatic product out from the Mo active site. In the case of 3MoA, 5MoA and 10MoA, the changes in coke II are +15, +8 and -23%. Based on this, 3MoA should have the lowest and 10MoA the highest catalytic activity. This corresponds well with MDA product yield discussed above. The surface properties may increase our knowledge in changes in coke II yield and will be discussed later.

The activation energy between the activated and the reacted group of catalyst are minimal as can be observed from Table 5.1. This strongly indicates that the coke species present in all the above catalysts do not vary much from each other.

Table 5.2 Coke Yield Comparison

	Total Coke (wt%)			
	TGA	MDA	Ele. Anal	Average
3MoA-Re	10.90	11.48	11.06	11.15
5MoA-Re	9.59	9.97	9.83	9.80
10MoA-Re	16.10	17.32	16.30	16.57

Table 5.2 represent the total coke yield over 20 hours TOS of the MoA spend catalyst calculated from TGA, MDA and elemental analysis. This table is used for comparison purpose only. From the same table, it can be seen that the coke yield follows a similar yield pattern. Further it can be seen that the average result between the three methods do not vary by more than 8%.

5.1.37 Surface Analysis

Figure 5.7 shows the surface properties fresh HZSM, activated and reacted MoA catalysts. The surface properties are shown in the form of a bar chart for the external and BET surface area and the pore diameter of these catalysts.

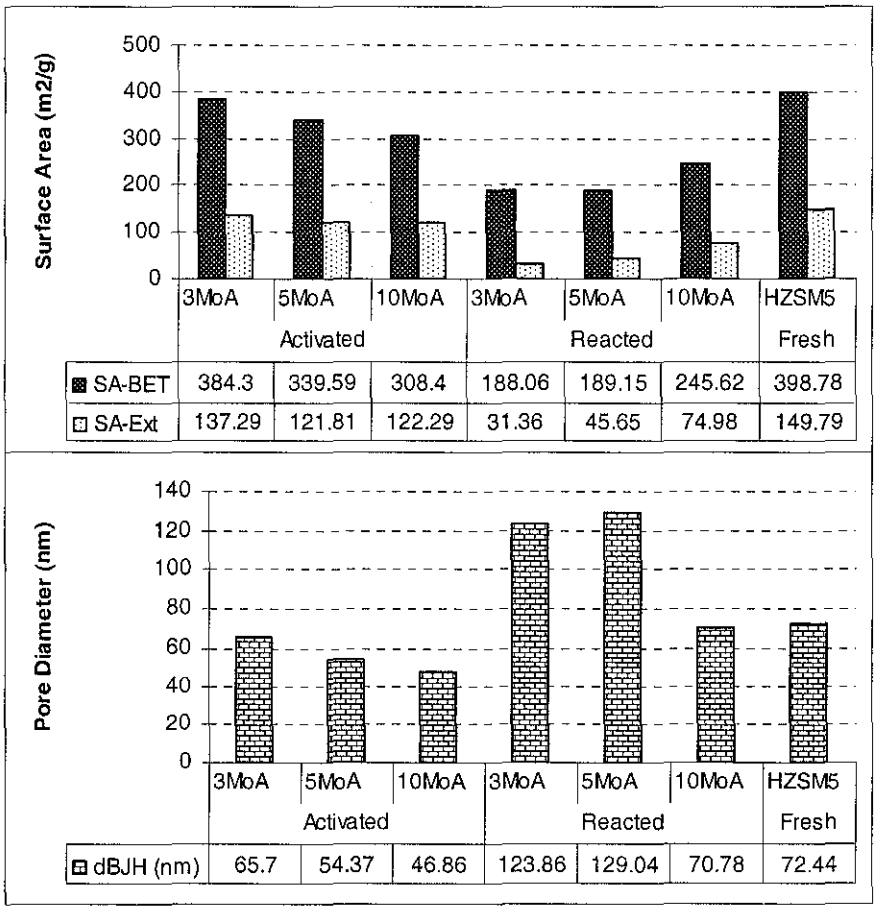

Figure 5.7 Changes in Surface Properties versus Mo Loading

From Figure 5.8, on comparing the freshly activated catalysts to the parent HZSM-5 catalyst, it can be seen that the BET and external surface area decreases with increase in Mo loading from 3 to 10wt%. This decrease amounts to between 3.6 and 22.7% for BET and 8.3, and 18.7% for external SA respectively for 3 to 10% Mo loading. It is interesting to note that, the external SA are similar for both 5MoA and 10MoA activated catalysts, but the BET SA varies by 8 % for the same catalyst. This observation on SA may suggest that the Mo species for 10MoA-Act are well dispersed in the zeolite channels. This is apparent from the increase catalytic activity of 10MoA as observed in the catalyst evaluation section above. Further the 10MoA-Re shows higher BET and external SA than the others. This may be one of the main reason for the robustness of 10MoA although it produces more coke than the others.

From Figure 5.7 it can be seen that, with increase in Mo loading from 3 to 10 wt % for the activated catalyst, a decrease in the BJH pore diameter between 9 and 35% is observed when comparing with parent HZSM-5. This decrease is expected as the migration of the MoO_x species into channels of the HZSM-5 for higher Mo loading takes place on activation [9,15].

When the activated MoA catalyst undergoes MDA reaction, it can be seen that all the reacted MoA catalyst experience an increase in pore diameter. For 3MoA-Re, and 5MoA-Re a huge increase ranging between 171 and 178% respectively of the parent zeolite is observed. This observation suggests that both 3MoA-Re and 5MoA-Re may have undergone some kind of reconstruction of the zeolite support. Gao et al [18] suggest from his studies that partial destruction of pore volume can result in the increase in pore diameter.

In the case of 10MoA-Re the pore diameter has increased by about 51% as compared to 10MoA-Act. This is expected for MDA reactions which resulted from the bulky MoOx species being converted to the smaller fcc MoC_{1-x} species. This conversion result in reduced constriction on the pore volume resulting in increase in pore diameter. It should also be noted that, the pore diameter for 10MoA-Re is still smaller than the HZSM-5 zeolite support. This is because coke deposition reduces pore diameter. Based on the observation made earlier on the SA, it seems to indicate that most of the coke deposition is directed to the external surface. This is in agreement with Derouane et al [19].

5.1.3.8 Elemental Analysis

Table 5.3 shows the element content of MoA catalyst carried out using ICP-AES method as described in Chapter 2. The table represents the changes of Mo wt % on undergoing various treatment conditions. The results in brackets represent the loss in Mo wt% as compared to the amount impregnated initially

Table 5.3 Elemental Mo Analysis

Catalyst Type	Mo content in wt % (loss wt %)			
	Impregnated	Calcined	Activated	Reacted
3MoA	3.0	2.82 (-6.0%)	2.79 (-7.0%)	2.75 (-8.3%)
5MoA	5.0	4.76 (-4.8%)	4.72 (-5.6%)	4.70 (-6.0%)
10MoA	10.0	9.08 (-9.2%)	8.15 (-18.5%)	8.01(-19.9%)

From Table 5.2, it can be seen on activation the calcinated catalyst of 3MoA and 5MoA experience low loss of < 2%, while 10MoA experience a high loss of 10% for the same treatment. This loss in Mo content in 10MoA according to Iglesia et al [15] is due it sublimation of Mo if present above the monolayer threshold [15,17]. Upon reaction of the activated catalyst, the loss is minimal suggesting at this conditions the

Mo species are attached tightly to the Al framework of the zeolite preventing further sublimation of Mo content [15].

Although the loss of Mo in 10MoA is high, the catalytic activity is the still the highest when compared to the other two. This is due to the initial multilayer configuration of the Mo species approaching as close as possible to a monolayer configuration. In doing so, the Mo species are driven further into the channels resulting in better spreading in the form an 'unrolling carpet' mechanism as proposed by Knozinger et al [20]. Better spreading results in increase catalytic reactivity [24].

5.1.3.9 X-Ray Diffraction Analysis

Figure 5.8 reveals the powder XRD pattern for calcined 10Mo, and activated and reacted 10MoA catalyst. The markings A, B, and * represent fcc α-MoC_{1-x}, hcpβ-Mo_2C and MoO_2 species respectively.

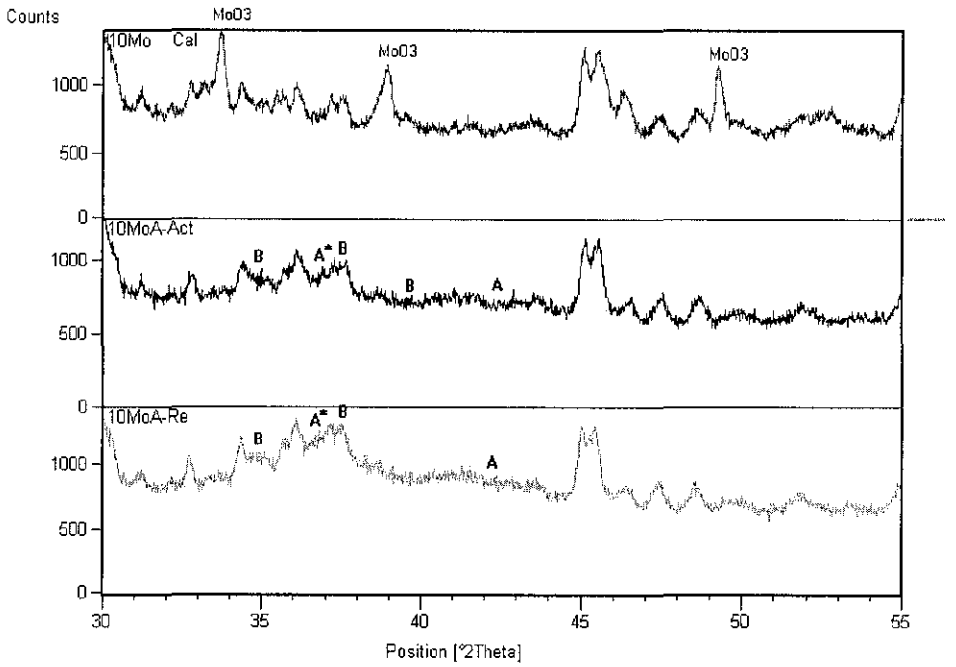

Figure 5.8 Powder XRD Patterns for 10MoA Catalyst

From Figure 5.8 the scan for activated 10Mo catalyst shows clearly the diffraction peak at 2θ =33.8, 38.5 and 49.3° for MoO_3, the precursor for the Mo carbide species. On reduction and carburisation (activated) it can be noticed that the MoO_3 peaks disappears, indicating transformation of these peaks. From literature [6,21,22] the XRD pattern for fcc α-MoC_{1-x}, for 2θ = 36.7 and 42.2°, hcp β-Mo_2C 2θ = 34.7,37.3 and 39.5° and MoO_2 2θ = 36.9 and 53.5°.

From Figure 5.8, notice that doublet at 2θ =36.5 to 37.3° on the calcined Mo catalyst become distorted and broader as it undergoes activation. The fcc α-MoC_{1-x}, scan pattern is represented at 2θ = 36.7°, the hcp β-Mo_2C at 2θ = 37.3° and that of MoO_2 species at 2θ = 36.9°. This observation shows that the activated species does contain all three Mo species mention above, but due to reasons of interference of diffraction peaks from the zeolite, broadening of peaks and limitation of the XRD detection pattern the resolution for these peaks are poor. Broadening of these peaks on the other hand indicates high dispersion [6]. This is in agreement with the findings discussed above and findings by Anderson [22].

5.1.4 CONCLUSIONS

From the above discussion it can be seen that 10MoA is the most reactive catalyst with good aromatic yield. 5MoA is comparable to 10MoA in catalytic activity; it has high aromatic and low coke yield and selectivity which is suitable for an aromatic producing catalyst. As for the aromatic fraction, the selectivity for benzene increases with increase in Mo loading, while that for naphthalene the reverse is observed.

5.2 Effect of Calcination Temperature

5.2.1 INTRODUCTION

The following study investigates the effect of calcination temperature on the 10MoA /HZSM-5 catalyst. The calcination temperatures chosen are 500, 600 and 650°C and same reaction conditions as in sub-section 5.1.3 will be used. The treated calcined catalysts are denoted as 10MoAC500, MoAC600 and MoAC650 to indicate these catalysts were calcined at 500, 600 and 650°C respectively. The usual treatment notation such as 'Cal' ,'Act' and 'Re' will indicate calcined, activated and reacted respectively or unless stated otherwise. Based on these calcination temperatures, similar catalyst evaluation will be conducted as in Section 5A.

5.2.2 RESULTS AND DISCUSSIONS

5.2.2.1 Methane Conversion

Figure 5.9 shows the effect on methane conversion based on a carbon wt % basis and its effect to calcination temperature for the MoA catalysts with TOS.

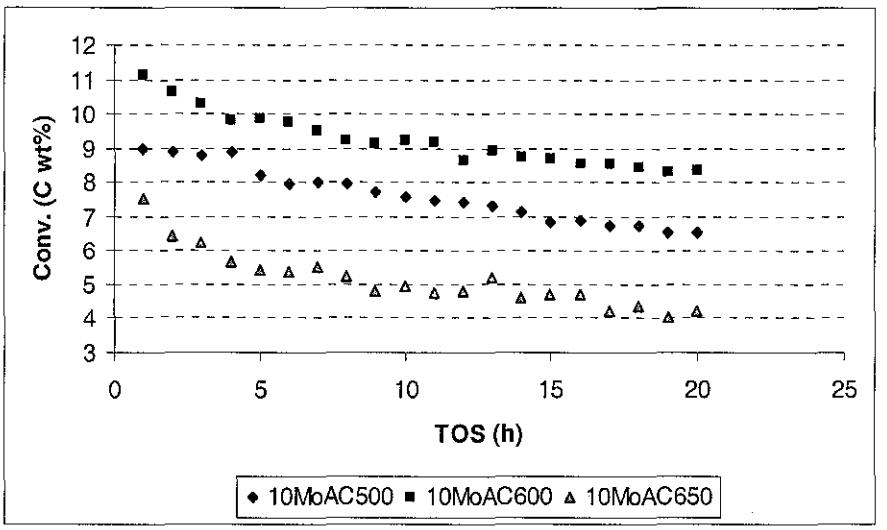

Figure 5.9 Effect Calcination on Methane Conversion

From this Figure 5.9 it can be seen that 10MoAC600 has the highest conversion of the three calcination temperature studied. 10MoAC600 has a 1st hour conversion of 11.1% and after 20 hours TOS this conversion drops to 8.3%. This amounts to a drop of 25 wt% C in methane conversion over 20 hours TOS which average out to 9.2% for the same period.

In the case of 10MoAC500, the drop in methane conversion amounts to 27 wt% C (1st hour 9.0 and the 20th hour being 6.6 wt% C) and an overall average of 7.6 C wt%.

The least competitive of the three for methane conversion is 10MoAC650. A large drop of 44% in methane conversion is observed from the 1st hour (7.5%) to the 20th hour (4.2%) with an overall average of 5.1%.

5.2.2.2 Product Yield

Figure 5.10 shows the effect on product yield obtained from varying the calcination temperature. The main product fractions obtained from the MDA reaction are coke, aromatics and aliphatics. The total yields obtained for each fraction in Figure 5.10 are calculated based on 20 hours TOS and measured in mmol.

From Figure 5.10 it can be seen that all three catalysts have higher selectivities towards aromatic than either coke or aliphatics. The selectivity shown for aromatic yield for 10MoAC500, 10MoAC600 and 10MoAC650 are 83, 55 and 54% respectively, thus making 10MoAC500 the most selective catalyst for aromatics production. For 10MoAC500 aromatic yield amounts to 125 and 230% more than either 10MoAC600 or 10MoAC650 respectively.

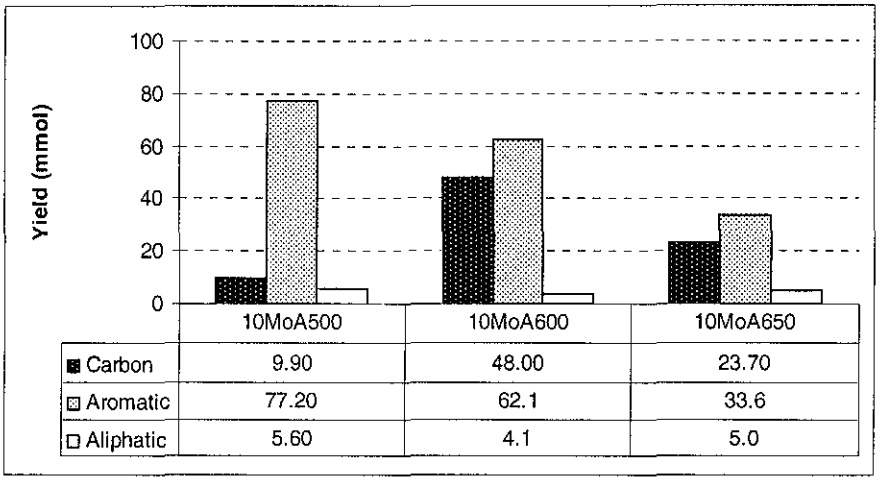

	10MoA500	10MoA600	10MoA650
Carbon	9.90	48.00	23.70
Aromatic	77.20	62.1	33.6
Aliphatic	5.60	4.1	5.0

Figure 5.10 Effect of Calcination Temperature on MDA Product Yield

In the case of coke yield, the highest yield is exhibited by 10MoAC600. It produces 485 and 202% more coke than either MoAC500 or 10MoAC650 respectively. 10MoAC500 on the other hand exhibits the most productive aliphatic fraction yield. It produces 180 and 112% more aliphatic yield than either 10MoAC600 or 10MoAC650 respectively.

From the observations made above in Figure 5.10, it can be seen that the 10MoAC600 is the most active catalyst of the three. Unfortunately this advantage for high activity is lost due to its high coke selectivity. 10MoAC500 appears to be the more favourable catalyst for the title reaction due to its high selectivity towards aromatics (83%) with comparable catalytic activity to10MoAC600.

It is also interesting to note that both 10MoAC600 and 10MoAC650 have high and similar coke selectivity.

5.2.2.3 Coke Product Yield

Although the coke yield is undesirable, it is important because it gives an indication on the stability of the catalyst with TOS.

Figure 5.11 shows how the rate of formation of coke is affected with varying calcination temperature. The ROF for coke is measured in nmol per gram catalyst per second at the respective time during TOS.

From Figure 5.11 it can be seen that, the ROF of coke for 10MoAC500 starts with a low production rate at the 1st hour and then increases steeply until the 3rd hour thereafter does not change with increase in TOS. The same pattern of ROF for coke is noticed for both 10MoAC600 and 10MoAC500, the main difference being higher yields for the former. 10MoAC650 on the other hand, has an entirely different coke yield pattern. It starts at a high ROF for coke at the 1st hour, decreases steeply until the 4th hour, thereafter gradually decreases with increase in TOS.

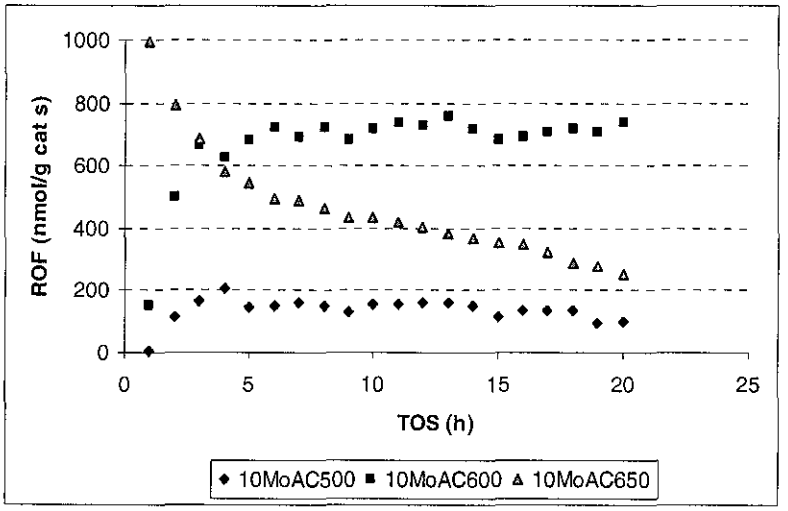

Figure 5.11 Effect of ROF of Coke with Calcination Temperature

From the above observation, it can be seen that ROF for coke for both 10MoAC500 and 10MoAC600 have low initial. This observation may account for the high catalytic activity of these two as discussed in methane conversion and product yield distribution above. In the case of 10MoAC650, the high initial ROF for coke may reduce the chances of it becoming a more active catalyst due to the coke's deactivation

properties. This may be one of the reason for the low catalytic activity exhibited 10MoAC650 with increase TOS.

5.2.2.4 Aromatic Product Yield

From the above discussion on product yield, it was clear that the 10MoA catalyst have better selectivity towards aromatic than the other MDA products. How does this high selectivity affect the aromatic product fraction? Figure 5.12 addresses this question.

From Figure 5.12, it can be seen that the major aromatic component for all three catalyst is benzene. Further the total yield of each individual aromatic component decreases with increasing calcination temperature. The selectivity for benzene from the same figure shows that, 10MoAC500, and 10MoAC650 has similar selectivity of 57%, whereas 10MoAC600 has a slightly lower benzene selectivity of 54%. In the case of naphthalene, the selectivity is slightly lower than benzene. 10MoAC500 and 10MoAC650 shows similar selectivity for naphthalene which is 38%, but 10MoAC600 has a slightly higher value of 41%. The toluene and xylene content for all three show the same selectivity of 5%.

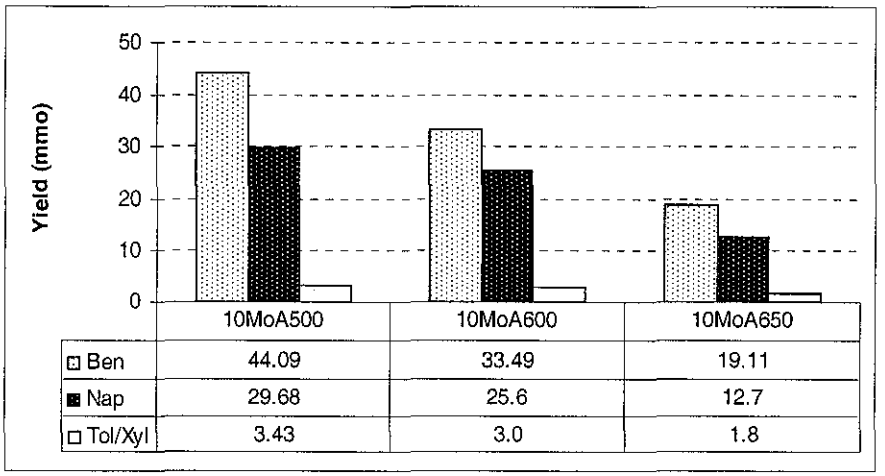

	10MoA500	10MoA600	10MoA650
Ben	44.09	33.49	19.11
Nap	29.68	25.6	12.7
Tol/Xyl	3.43	3.0	1.8

Figure 5.12 Effect of Calcination Temp on Aromatic Fraction

In summary from Figure 5.12, it can be seen that with increasing calcination temperature, a decrease in aromatic content is noted. Of the aromatic component, benzene is the most abundant component. Calcination has little effect on selectivity of the aromatic product component. However, increase in calcination temperature results in decrease in ROF of the entire individual aromatic fractiont yield.

5.2.2.5 Aliphatic Product Yield

Table 5.4 represents the yield of ethane and ethylene fraction in mmol over 20 hours TOS. From the same table the ethylene to ethane ratio is calculated. The main component of the aliphatic fraction is observed to be ethylene.

From Table 5.4, it can be seen that ethane decreases with increase in calcination temperature. In the case of ethylene the highest yield is observed at calcination temperature of 650°C and lowest at 600°C.

Table 5.4 Effect of Aliphatic Yields with Calcination Temperature

Calcination Temp °C	Ethane (mmol)	Ethylene (mmol)	Ethylene/Ethane Ratio
500	1.66	3.95	2.38
600	1.20	2.9	2.42
650	0.82	4.17	5.09

The ethylene to ethane ratio gives an estimate on the consumption of ethylene in general. Low value indicates an increase in ethylene consumption. From Table 5.4, it can be seen that 500°C has the highest consumption of ethylene which is comparable to that at 600°C. Calcination at 650°C has the lowest ethylene consumption. Since ethylene is believed to be the precursor for benzene [15], increase consumption of ethylene results in higher yield for benzene. This

observation supports the increase aromatic yield for 10MoAC500 and 10MoAC600 over 10MoA650 as seen in subheading 5.3.2 above.

5.2.2.6 Catalytic Deactivation

Figure 5.13 shows the rate of catalytic deactivation for all three catalysts. It is based on the plot of the natural logarithm of the ROF of benzene with TOS [3].

From this figure, it can be seen that 10MoAC500 has the lowest rate of deactivation of the three catalysts studied. The rate of deactivation of 10M0AC600 and 10MoAC650 is 1.2 and 1.5 times higher than that of 10MoAC500. This suggests that with increase in calcination temperature the rate of deactivation for MDA reaction increases. Thus, from the above catalytic evaluation studies, it follows that an increase in methane conversions do not necessarily indicate that the catalyst has a lower deactivation rate.

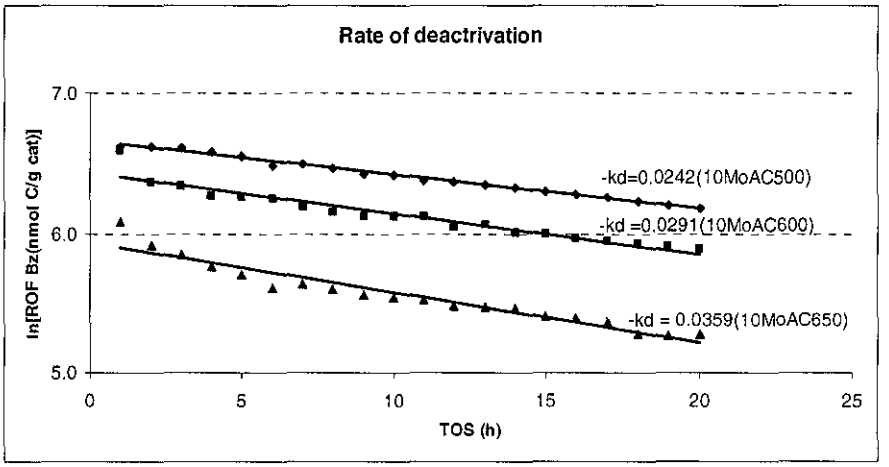

Figure 5.13 Effect of Rate of Deactivation with Calcination Temperature

5.2.2.7 Surface Analysis

The surface characterisation of the parent zeolite, the activated and the reacted catalyst for 10MoAC500, 10MoAC600 and 10MoAC650 is

shown in Table 5.5. The results in brackets represent the changes in percentages with respect to the parent zeolite.

From Table 5.5, it can be seen that 10MoAC600 (-22.7%) shows the lowest and 10MoAC500 (-38.1%) the highest decrease in BET surface area upon activation. Upon reaction of the activated catalyst, it can be seen that for the BET SA, 10MoAC500 undergoes a further decrease of 6.2%, whereas 10MoAC600 and 10MoAC650 loses a further 15.7 and 20.9% respectively.

Table 5.5 Effect of Calcination Temperature on Surface Properties

	Activated			
	HZSM-5	**10MoAC500**	**10MoAC600**	**10MoAC650**
SBET(m2/g)	**398.8**	**246.7 (-38.1%)**	**308.4 (-22.7%)**	**277.6 (-30.4%)**
SExt (m2/g)	**149.8**	**110.1(-26.5%)**	**122.3 (-18.4%)**	**114.4 (-23.7%)**
dBJH (nm)	**72.44**	**39.91 (-44.9%)**	**46.86 (-35.3%)**	**65.60 (-9.4%)**
VBJH(cm3/g)	**0.219**	**0.118(-46.2%)**	**0.131 (-40.2%)**	**0.170 (-22.2%)**
	Reacted			
SBET(m2/g)	**398.78**	**222.1 (-44.3%)**	**245.6 (-38.4%)**	**194.2 (-51.3%)**
SExt (m2/g)	**149.79**	**93.55 (-37.5%)**	**74.98 (-49.9%)**	**77.71(-48.1%)**
dBJH (nm)	**72.44**	**63.26 (-12.7%)**	**70.78 (-2.3%)**	**75.41 (+4.1%)**
VBJH(cm3/g)	**0.219**	**0.163 (-25.5%)**	**0.126 (-42.5%)**	**0.138 (-37.0%**

In the case of the external surface area, it follows the same trend as BET SA for the activated catalyst but at a much lower loss. Upon reaction the external SA shows similar trend as BET but the loss for the former is much higher than the later. These losses in the external SA after reaction is double that of the corresponding BET SA.

Comparing the accessible pore volume of the BJH from Table 5.5 with the parent HZSM-5, it can be seen that on activation 10MoAC500 experience a huge loss of 46% whereas both 10MoAC600 and 10MoAC650 loses 40.2 and 22.2% respectively. When the catalyst from the activated phase goes to the reacted phase, it can be seen that

10MoAC500 gains 20.7% of the pore volume, whereas 10MoAC600 and 10MoAC650 loses a further 2.3 and 10.8% respectively.

From Table 5.5 for the activated catalysts, it can be seen that the BJH pore diameter loss decreases with increase in calcination temperature. The same observation pattern is seen for the reacted catalyst. For all the catalyst except 10MoAC650-Re, the pore diameter is below the parent HZSM-5 zeolite. This suggests that there is minimum reconstruction of the zeolite structure [4].

Based on the above observations from BET and external SA, it may suggest that the 10MoAC600 activated catalyst has the highest surface areas for both the BET and the external SA. This may suggest minimum blockage or better spread by Mo species on the external surface for 10MoAC600-Act. Upon reaction, it can be seen that 10MoAC500 experience lower loss than either 10MoAC600 or 10MoAC650. This may suggest that 10MoAC500 has lower coke deposition or is less vulnerable to coke deposition. This is in agreement with findings above on the product yield from MDA reaction.

In the case of accessible pore volume, 10MoAC500 regains 20.7% of its pore volume when going to the activation to the reacted stage. This suggests improved accessibility and better reaction pathway leading to lower coke deposition. This is in agreement with the above findings.

5.2.2.8 TGA Analysis

Table 5.6 represents the TGA analysis on the coke species present in the activated and reacted catalyst based on the method proposed by Liu et al [13]. From the Table 5.6 it can be seen that both coke I and coke II increases with increase in calcination temperature for the activated catalyst. The same is not true with the reacted catalyst. For the reacted

catalyst MoAC600 shows the highest and10MoAC500 the lowest coke I and II yield. This observation is in agreement with findings of coke deposit yield and selectivity discussed above.

Table 5.6 Carbon Deposit Analysis Based on TGA Results

	Activated (mg/ g cat)			Reacted (mg /g cat)		
	MoAC500	MoAC600	MoAC650	MoAC500	MoAC600	MoAC650
CokeI	8.2	10.4	11.8	25.67	160.5	79.06
CokeII	0.35	0.69	0.74	0.33	0.53	0.35
T.Coke	0.86 %	1.19%	1.25%	2.3%	16.1 %	7.9%

Coke II on the other hand does not follow the yield pattern of coke I. From Table 5.6, it can be seen that 10MoAC500 loses a small fraction (which is minimal) of its coke II when going from the activated to reacted stage. This may suggest that optimised performance by the Mo- carbide species for 10MoAC500 accounts for its low coke yield. For 10MoAC600 and 10MoAC650 the loss from activated to reacted stage amounts to 23 and 53%. This big loss in both 10MoAC600 and 10MoAC650 may suggest that both of them are trying to reach optimum concentration as that of 10MoAC500 by losing excess coke II.

5.2.2.9 Elemental Analysis

The elemental analysis of the Mo content from the calcined to activated to reacted stage is showed in Table 5.7. The results in brackets represent the loss of Mo as compared to the calcined stage. From the same table it can be seen that the loss in Mo content from activated to reacted stage is minimal. This suggests that sublimation of Mo is minimised and the Mo species are tightly held in the catalyst.

Table 5.7 Elemental Analysis of Molybdenum

	Calcined (wt%)	Activated wt%)	Reacted (wt%)
MoAC500	9.08	8.24 (-9.3%)	8.13 (-10.5%)
MoAC600	9.08	8.15 (-10.2%)	8.01 (-11.8%)
MoAC650	8.70	7.94 (-8.7%)	7.83 (-10.0%)

5.2.2.10 X-Ray Diffraction Analysis

The powder XRD pattern in Figure 5.14 was obtained by the XRD analyser Philips PW1710 using CuK α radiation operating at 30kV and 20mA with a scanning speed of 0.05° per sec and room temperature. The powder XRD pattern from Figures 5.14 compares the parent HZSM-5 and the freshly activated 10MoA catalysts at the designated calcination temperature.

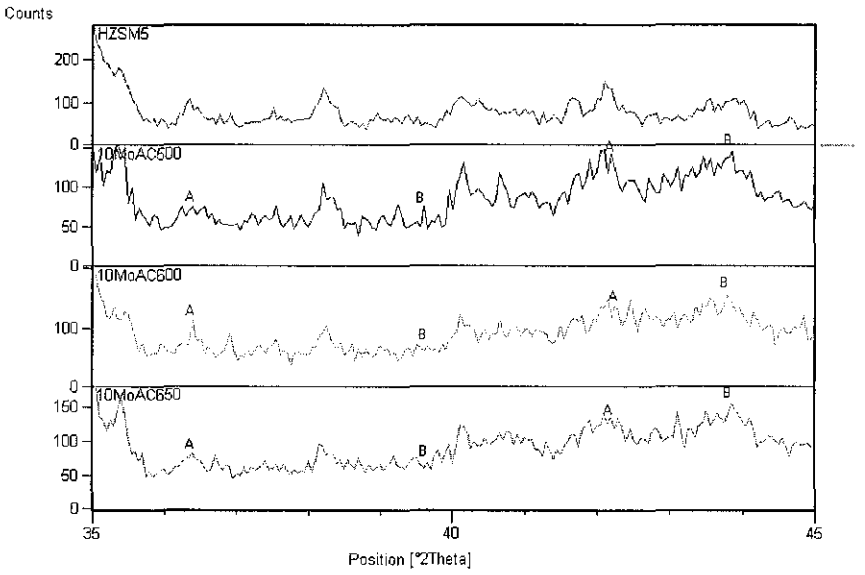

Figure 5.14 XRD Pattern for Freshly Activated 10MoA Catalyst

The diffraction pattern range for 2θ was taken between 35 to 45° to identify possible hcp β-Mo_2C and fcc α-MoC_{1-x} pattern and are represented by the letter 'A' and 'B' respectively on the XRD pattern scan. For fcc α-MoC_{1-x} the 2θ value is taken at 36.33 and 42.20° whereas

for the hcp β-Mo_2C the 2θ value is taken at 39.47 and 43.67°. This value is extracted from the Xpert plus library for the powder XRD. For this powder XRD analysis the data was from Figure 5.14 it can be seen that the all three calcination temperatures have both the fcc α-MoC_{1-x} and the hcp β-Mo_2C patterns. The fcc α-MoC_{1-x} pattern at 2θ= 36.33° appears partially resolved for 10MoAC500 and become more distinctly resolved for 10MoAC600, at 10MoAC650 it broaden out again. The fcc α-MoC_{1-x} pattern at 2θ= 43.67° show almost similar resolution for all three calcination temperatures.

In the case of the hcp β-Mo_2C at 2θ = 39.47°C, it is well resolved for 10MoAC500, which broadens with further increase in calcination temperature. The hcp β-Mo_2C at 2θ = 43.67° is slightly split at 10MoAC500 and becomes more resolved with increase in calcination temperature.

From the above observations, it can be seen that when the fcc α-MoC_{1-x} peak patterns becomes broad, the corresponding hcp β-Mo_2C peak patterns becomes more resolved. Broadening of peaks indicates high dispersion [6]. Based on this observation from the XRD patterns from Figure 5.14, it can be seen in the case of 10MoAC500, the fcc α-MoC_{1-x} peak is highly dispersed as compared to the hcp β-Mo_2C peak. The reverse is observed for the 10MoAC600. In the case of the 10MoAC650, both the hcp β-Mo_2C peak and the fcc α-MoC_{1-x} peak are better dispersed than both 10MoAC500 and 10MoAC600. This observation may suggest that a well dispersed hcp β-Mo_2C phase makes the catalyst more active and less selective, whereas a well dispersed fcc α-MoC_{1-x} phase increases the selectivity to aromatics at the expense of catalyst activity.

5.2.3 CONCLUSIONS

From the observations made on calcinations, 600°C produces the most active catalyst. This increase in activity is attributed to the increase in coke yield. The lower calcination temperature of 500°C accounts for reduce catalytic activity but increases in selectivity and yield for aromatic at the expense of coke yield. Further increase in calcination temperatures had no significant effect on the aromatic fraction selectivity.

5.3 hcp β-Mo_2C and fcc α-MoC_{1-x} COMPARISON

5.3.1 INTRODUCTION

The final section of this chapter compares the catalytic activity of the most promising catalysts for the fcc α-MoC_{1-x} and hcp β-Mo_2C phases. The comparison will be discussed on methane conversion and the aromatic yield and selectivity only. The catalytic characterisation however will not be considered.

For the hcp β-Mo_2C group of catalyst, 10MoBMC600 and 10MoBHMC600 are selected and they will be labelled as MoBM and MoBHM respectively. In the case of the fcc α-MoC_{1-x} group of catalyst, 10MoAC600 and MoAC500 are selected and will be labelled as MoAC6 and MoAC5 respectively. The following catalyst label tag will be hereafter be used for summary purposes only unless stated otherwise.

5.3.2 RESULTS AND DISCUSSIONS

5.3.2.1 Methane Conversion

Figures 5.15 compares the total methane conversion calculated on a % C conversion. From the same figure, it can be seen that MoBHM is the most active and MoAC5 the least active of the four catalysts compared. The average methane conversion of MoBHM, MoBM, MoAC6 and MoA5 are 13.0, 9.2, 7.9 and 7.6% respectively. These show that

MoBHM is 141, 165 and 171% more active than MoBM, MoAC6 and MoAC5 respectively.

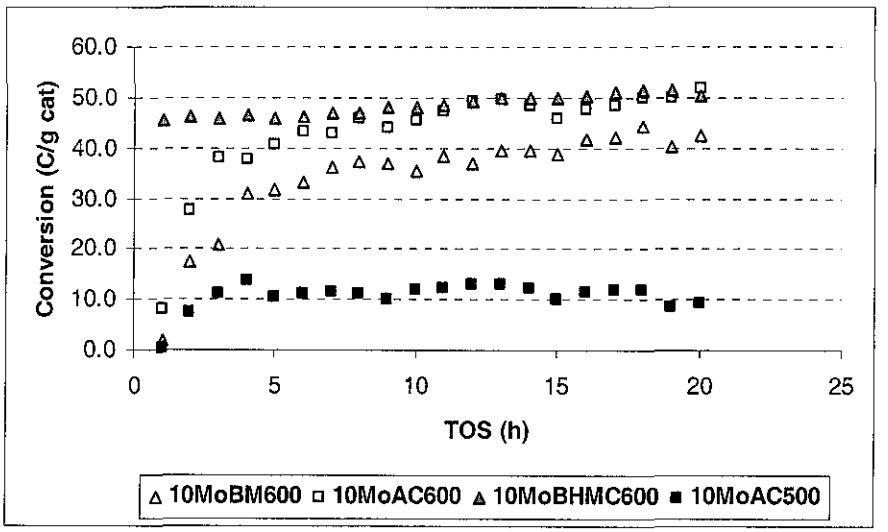

Figure 5.15 Methane Conversion

5.3.2.2 Product Yield

Figure 5.16 compares the product yield obtained after 20 hours TOS for the four catalysts.

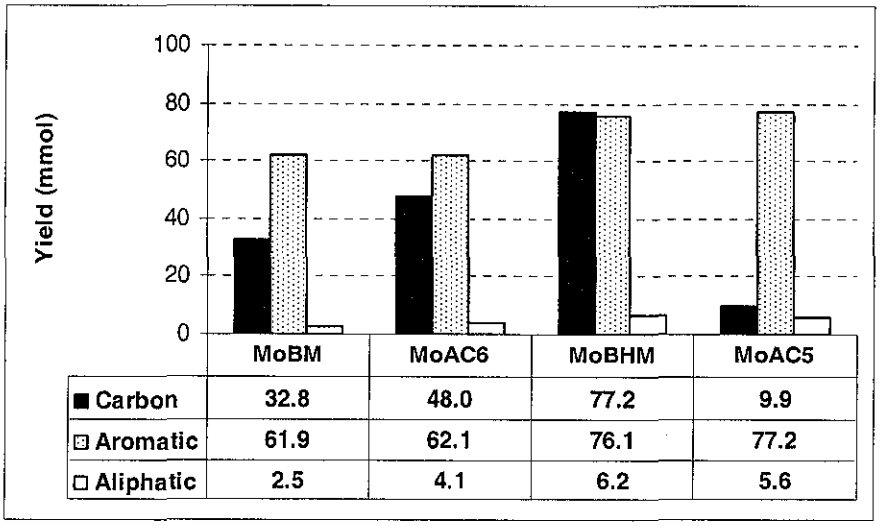

	MoBM	MoAC6	MoBHM	MoAC5
■ Carbon	32.8	48.0	77.2	9.9
⊡ Aromatic	61.9	62.1	76.1	77.2
□ Aliphatic	2.5	4.1	6.2	5.6

Figure 5.16 MDA Product Yield Comparisons

From Figure 5.16, it can be seen that MoAC5 is the least active of the four catalysts, but has the highest yield and selectivity for aromatics. MoHBM also have high yields for aromatics which is only slightly superseded (1.4%) by MoAC5, but it has a much lower selectivity to aromatic at 47.7% as compared to 83.3% for MoAC5.

In the case of coke yield, the highest yield comes from MoBHM, followed by MoAC6, MoBM and the lowest MoAC5. From the same figure, it can be seen that MoBHM, produces 235, 161 and 779% more coke than MoBM, MoAC6 and MoAC5 respectively.

From Figure 5.16 and studies of calcination effects for both the fcc α-MoC_{1-x} and hcp β-Mo_2C catalysts, it can be clearly seen that the fcc α-MoC_{1-x} catalyst have higher selectivity for aromatics than its hcp β-Mo_2C counterpart. Although the hcp β-Mo_2C seems to be more active than its fcc α-MoC_{1-x} counterpart, the extra activity is more coke selective.

5.3.2.3 Aromatic Product Fraction

Figure 5.17 shows the comparison between the aromatic product yield (benzene, naphthalene, and toluene & xylene) as a result of 20 hours TOS for the 4 catalysts.

From the Figure 5.17 it can be seen that MoBHM has the highest yield and selectivity for benzene. MoBHM produces 183, 180 and 136% more benzene than MoBM, MoAC6 and MoAC5 respectively. In terms of benzene selectivity MoBHM has a very high selectivity of 79% as compared to the others which are 53, 54 and 57% for MoBM, MoAC6 and MoAC5 respectively. Toluene/Xylene also follows a similar trend distribution as that of benzene.

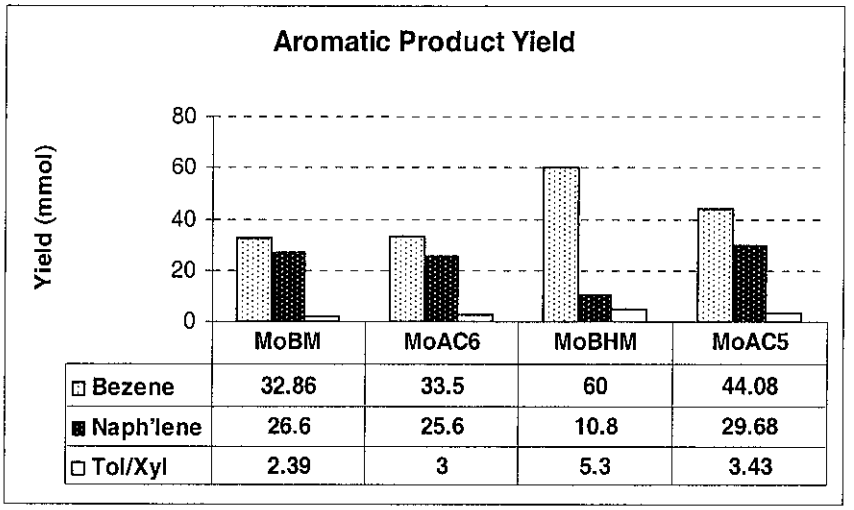

	MoBM	MoAC6	MoBHM	MoAC5
Bezene	32.86	33.5	60	44.08
Naph'lene	26.6	25.6	10.8	29.68
Tol/Xyl	2.39	3	5.3	3.43

Figure 5.17 Aromatic Fraction Yield Comparisons

Naphthalene on the other hand, the next major product after benzene in the MDA reaction has the lowest yield and selectivity for MoBHM. All the others have a more or less even distribution of naphthalene.

5.4 Conclusions

From the above observations it can be seen that the hcp β-Mo_2C have higher methane conversion than the fcc α-MoC_{1-x} group of catalysts. The higher methane conversion for hcp β-Mo_2C catalyst is attributed to the higher coke deposition as compared to its fcc α-MoC_{1-x} counterpart.

In the case of aromatic content it can be seen that the fcc α-MoC_{1-x} have higher yield and selectivity at lower calcination temperature (500°C). Increase in calcination temperature results in increase in coke yield.

The hcp β-Mo_2C on the other hand has increase catalytic activity. The extra catalytic activity results with an increase in ROF of coke at the expense of aromatics, since both coke and aromatics have a common intermediate [25]. Increasing the surface area of this catalyst increases

catalytic activity resulting in increase benzene selectivity and yield for the aromatic fraction.

Based on the above discussion it can be seen that for the hcp β-Mo_2C group of catalyst, the most promising one is the 10MoBHM calcined at 600°C and for the fcc α-MoC_{1-x} group it is 10MoAC500 which is calcined at 500°C.

5.5 References Chapter 5

1 Lee, J.S., and Boudart, M., Appl Catal. 19 (1985) 207

2 Markel, E.J., and van Zee, J.W, J. Catal. 126 (1990) 643

3 Choi, J.G., Brenner, J.R, and Thomson, L.T., J. Catal. 154 (19995) 33

4 Li, S., Lee, J.S., Hyeon, T., and Suslick, K.S, Appl. Catal. 184 (1999) 1

5 Ranhotra, G.S., Bell, A.T., Reimer, J.A., J. Catal. 108 (1987) 40

6 Bouchy, C., Deouane-Abd Hamid, S.B., and Derouane, E.G.. Chem. Commum. 2 (2002) 125

7 Volpe, L., and Boudart, M., J. Solid State Chem. 59 (1985) 348

8 Lee, J.S., Volpe, L., Ribero, F.H., and Boudart, M., J. Catal. 112 (1988) 44

9 Zhang, J.Z., Long, M.A., and Howe, R.F., Catal. Today 44 (1998) 293

10 Us, Y., Liu, W., Wong, S., Wang, L., and Guo, X., Catal. Lett. 40 (1996) 207

11 Lin, W., Us, Y., Wong, S.T., Wang, L., Qiu, J., and Yang, N., J. Catal. A 120(1997) 257-265

12 Liu, S., Wang, L., Ohnishi, R., and Ichikawa, M., J. Catal. 181 (1999) 175

13 Liu, H., Li, T., Tian, B., and Xu, Y., Appl. Catal. A 213 (2001) 103

14 Liu, H., Su, L., Wang, H., Shen, W., Bao, X., and Xu, Y., Appl. Catal. 236 (2002) 263

15 Borry III, RW, Kim, Y.H, Huffsmit, A., Reimer, J.A and Iglesia E.J., Phys. Chem. B (1999) 103, 5787

16 Wong, S., Us, Y., Wang, L., Liu, S., Li, G., Xie, M., and Guo, X., Catal. Lett. 38 (1996) 39

17 Chen, L., Lin, L., Us, Z., Li, X., and Zhang, T., J. Catal. 157 (1995) 190

18 Li, Z., Gao, L., and Zhang, S., Appl. Catal. 236 (2002) 163

19 Derouane-Abd Hamid, S.B., Anderson, J.R., Schmidt, I., Bouchy, C., Jacobsen, C.J.H., and Derouane, E.G., Catal. Today 63 (2000) 461

20 Mestl, G., and Knozinger, H., Langmuir 14 (1998) 3964

21 Yuan, S., Derouane-Abd. Hamid, S.B.H., Li, Y., Ying, P., Xin, Q., and Derouane, E.G., and Li, C., J. Mol. Catal. A Chem. 184 (2002) 257

22 Anderson, J.R., PhD thesis (2001) University of Liverpool., UK

23 Solymosi, F., Cserenyi, J., Szoke, A., Bansagi, T., and Oszko, A., J. Catal. 165 150 (1997)

24 Wang, D., Lunsford, J.H., and Rosynek, M.P, J. Catal 169 (1997) 347

25 Wang, H., Hu, G., Lei, H., Xu, Y., and Bao, X., Catal. Lett. 89 (2003) 75

CHAPTER 6
CATALYTIC STABILISATION STUDY

6.1 Effect of CO dosing on Beta Mo /HZSM-5

6.1.1 INTRODUCTION

The main obstacle for catalytic stability in any MDA reaction is from the gradual build up coke deposition with TOS [1-5]. Coke deposition is unique [6-8] in that, apart from deactivating the catalyst, it also required for MDA reaction. Ichikawa et al [6] concluded that coke accumulation on the catalyst surface is the main obstacle which limits the practical utilisation of MDA reaction. Iglesia et al [7] attributes deactivation to the strongly adsorbed carbonaceous deposit such as large unsaturated hydrocarbon residues caused by unrestricted chain growth. This coke deposit blocks both the Mo-carbide and the Bronsted acid site responsible for MDA reaction [9-12]. The former is necessary for methane activation and the formation of ethylene, which is the main precursor for aromatics formation. The latter is believed to be responsible for aromatics formation

Xu et al [2], based on their study of carbonaceous deposit of Mo/HZSM-5 using NMR technique, showed that there are two kinds of carbonaceous deposit, one located on the acid sites and the other on partially reduced Mo species. Build-up of this carbonaceous material usually takes place on the surface of the catalyst preferably near the acid sites [2]. This is undesirable as it leads to blockage of the active sites. Apart from this, pore sizes and channel structures of the zeolite are also crucial for enhancing catalytic activity and catalytic deactivation.

Restricting the chain growth of this carbonaceous deposit, or efficient suppression can promote catalytic stability. Ichikawa et al [11] claim that the addition of CO and/or CO_2 enhances the catalytic stability and also

improves the ROF of benzene and naphthalene. They demonstrated this by using ^{13}CO isotopic labelling and TPO experiments and suggested that CO and/or CO_2 added to the methane feed acts as a carbon and oxygen donor which dissociate on the catalyst and are efficiently incorporate into the aromatic product. CO and/or CO_2 also aid in the removal of surface coke. According to Ichikawa et al [12] suggested the following mechanism as in Figure 6.1 below:

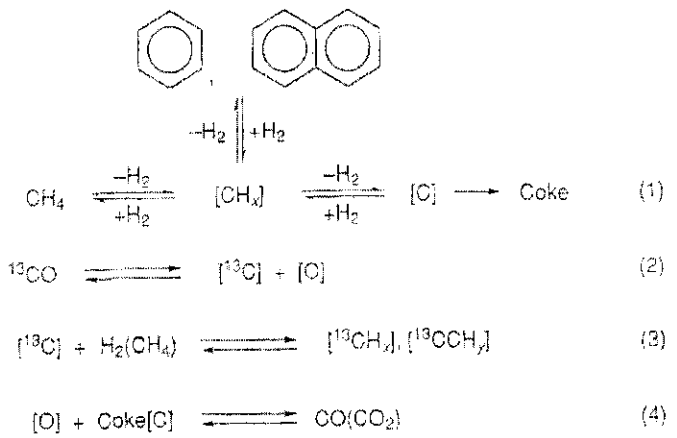

Figure 6.1 Mechanism of CO Dissociation on Mo/HZSM-5 (Extract taken from Ref. 12)

- The 1st stage of the transformation involves the probable dissociation of CO and CH_4 on the Mo active side of Mo/HZSM-5 catalyst to form the active surface species [C], [O] and CH_x as given in equation 2 and 3.
- The active carbon species [C] from CO is hydrogenated to $[CH_x]$ fragments as illustrated in equation 3.
- The $[CH_x]$ derived from CH_4 then undergoes oligomerisation to form the higher hydrocarbon i.e. the benzene and naphthalene as in equation 1.
- The dissociated oxygen species [O] from CO as in equation 2 react with the surface inert carbon species (coke) to regenerate

CO as in equation 4. This results in the suppression of coke formation on the catalyst.

Based on the above probable mechanism, an experiment was devised to study the promotional effects of CO.

6.1.2 EXPERIMENTAL

The promotional effect of CO was conducted on the 10MoBM type catalyst. The catalytic evaluation are based on the CO dosing of 2, 4, 8 and 12 v/v % by a Brooks mass flow controller to the methane feed to make up a flow rate of 7.5ml/min. For the catalytic evaluation test for 10MoBM catalyst, the procedure was conducted as mentioned in Chapter 2 and 4 for each CO addition over a reaction TOS of 20 hours. The actual flow rate of methane was than normalised to 7.5ml/min for calculating the yield of the product in all CO dosing. Assumptions were made that CO is not consumed in the MDA reaction as claimed by Ichikawa et al [12].

The CO dosing was conducted on the 10MoBM catalyst originating from the 10Mo/HZSM-5 stock catalyst pre-calcined at 600°C. For each CO dosing the spent catalyst will be designated with a suffix suggesting its CO vol % dosing. Example 2 v/v% CO dosing will be known as 10MoBMCO2. The same label tagging will be follows for the other CO dosing of 0, 4, 8 and 12 v/v %. This labelling will be used through this chapter or otherwise stated differently. All CO dosing percentage into the methane feed is measured on a vol to vol % basis unless stated otherwise. The 0% CO dosing will be taken as base value of catalytic evaluation hereafter.

6.1.3 RESULTS AND DISCUSSIONS

6.1.3.1 Methane Conversion

Figure 6.2 represents the effect of CO dosing on the average methane, coke and aromatic conversion based on carbon number conversion using 10MoBM catalyst over 20 hours TOS. The methane or overall carbon conversion for the MDA reaction represented in this figure is further broken up to highlight the average of aromatic, carbon and aliphatic conversion at the specific CO addition. Since the aliphatic fraction is small when compared to the carbon or aromatic, it will not be discussed under the carbon conversion sub-heading, but will be discussed later.

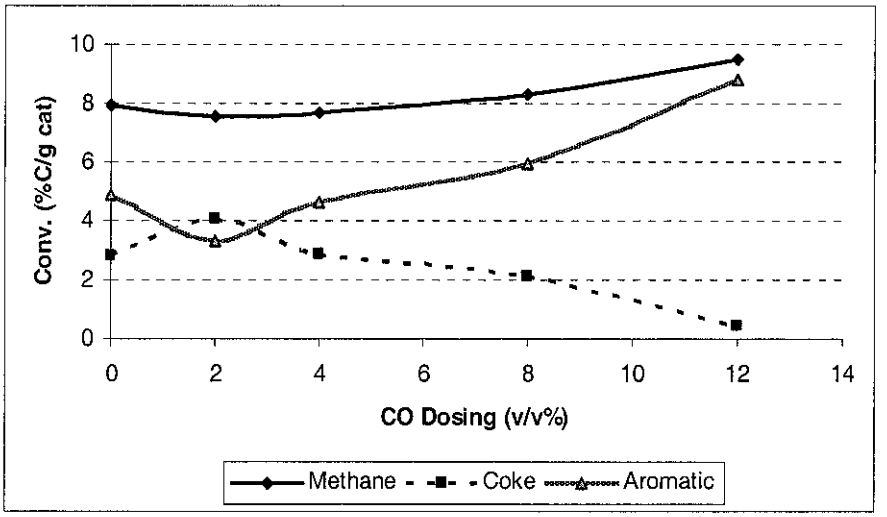

Figure 6.2 Effect of CO Dosing on Carbon Conversion

From Figure 6.2, it can be seen that with increasing CO dosing from 2 to 12%, an increase in the average methane conversion is observed.

From Figure 6.2 it can be seen that methane conversion is only affected with CO dosing above 4%. CO dosing above 4% results in an increase in methane conversion. Coke conversion has an initial increase with an introduction of 2% CO. Higher than 2 % CO dosing results in substantial decrease in the coke conversion. The aromatic conversion on the other

hand shows a reverse pattern to that of coke conversion for similar dosing.

6.1.3.2 Product Yield

Figure 6.3 shows the product yields obtained from MDA reaction on 10MoBM catalyst at different % of CO dosing. From the Figure it can be seen that CO dosing of 12% gave the highest catalytic and aromatic yield, but the lowest coke yield. From the same figure it can also be seen that the aromatic yield increases while the coke content decreased with increase in CO dosing.

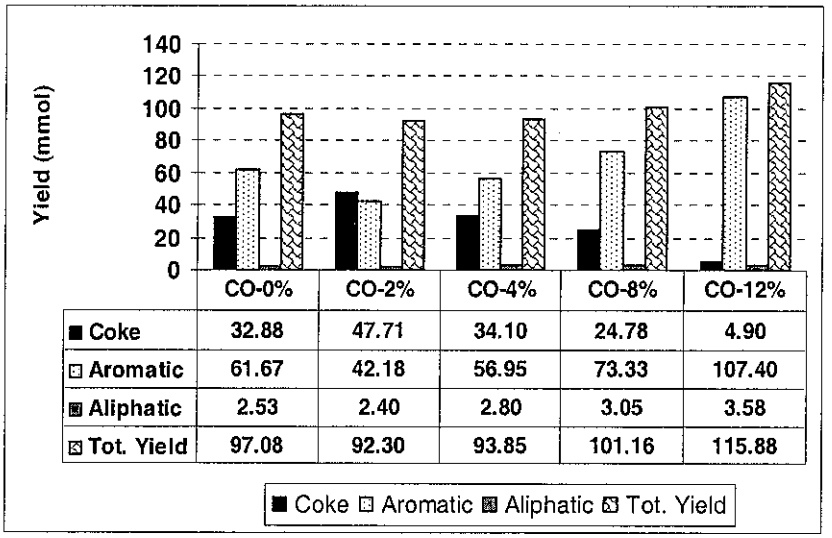

	CO-0%	CO-2%	CO-4%	CO-8%	CO-12%
Coke	32.88	47.71	34.10	24.78	4.90
Aromatic	61.67	42.18	56.95	73.33	107.40
Aliphatic	2.53	2.40	2.80	3.05	3.58
Tot. Yield	97.08	92.30	93.85	101.16	115.88

Figure 6.3 Effect of CO Dosing on 10MoBM Product Yield

Table 6.1 represents the average product selectivity obtained from Figure 6.3 and CO product yield % from the same reaction. It should be noted that the CO product in column 2 is the net % observed after deduction of CO dosing. Further the product CO is part of coke of column 3.

Table 6.1 MDA Product Selectivity

CO Dosing (% v/v)	MDA Product Distribution (%C)			
	CO	Coke	Aliphatic	Aromatic
0	0.80	33.87	2.61	63.52
2	0.02	51.70	2.60	45.70
4	0.65	36.34	2.99	60.68
8	1.05	24.50	3.02	72.48
12	1.50	4.23	3.09	92.68

From Table 6.1 it can be seen that small CO dosing of 2 % results in an initial increase of 17.8 % coke selectivity above the base. By increase the CO dosing above 2%, a decrease in coke selectivity was observed. A decrease of 9.4 and 29.6% coke selectivity is observed at 8 and 12% CO dosing. On the other hand the aromatic selectivity follows a striking reverse pattern to that of coke selectivity. In the case of aliphatic selectivity, increase in CO dosing results in a steady increase in aliphatic selectivity.

It is interesting to note that at lower than 4% CO dosing, the CO product selectivity is much lower than the base suggesting consumption of CO. Higher than 8% results in an increase in CO product selectivity above base value suggesting coke being scavenged with high CO dosing.

From the above observations it can be seen that CO dosing has a significant influence on aromatic and coke selectivity. CO dosing greater than 4% favours aromatic production and suppresses carbon deposition [6,10,12]. At 2% CO dosing, aromatic decreases while coke selectivity increases. This observation may be explained as scrambling of CO and methane on the catalyst surface [12] which creates competitive impact between the two for the active sites [13], as a result coke increases at the expense of aromatic selectivity. With increase in CO dosing to 4%, a slight increase in aromatic but reduction in coke is noticed, but still lower than the base value. This may suggest that, apart from competing with

active sites, some scavenging of surface coke is taking place at 4% CO dosing. With further increase to 8 and 12%, the scavenging of surface coke becomes more predominant compared to the competition for active sites, as a result an increase in aromatics and a decrease in coke is observed. This resulted in an increase in CO-product and aliphatic selectivity during this CO dosing. Since aliphatic component is believed to be the precursor for aromatic especially benzene [14-16], it is therefore supports that with the increase in CO addition, part of the surface coke which blocks the active site is scavenged by the CO. As a result the aliphatic components have better flexibility and excess to the active site. This action create a positive impact on the catalyst as a result increase in aromatic production at the expense of coke is preserved.

6.1.3.3 Aromatic Yield

Figure 6.4 compares the effect of aromatic product yield with variable CO dosing. The primary y-axis in this figure represent the major aromatic component i.e. benzene and naphthalene, while the secondary y-axis represents the total of the minor aromatic component i.e. the sum of toluene and xylene fraction.

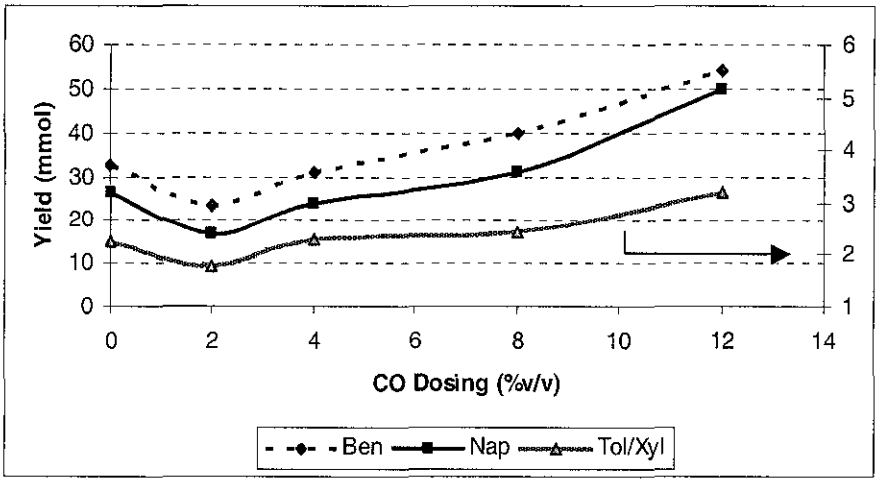

Figure 6.4 Effect of CO Dosing on Aromatic Fractions Yield

From Figure 6.4 it can be seen that for all three aromatic components compared follow a similar yield pattern with increase in CO dosing. This observations suggest that the selectivity of the aromatic components are least effected by CO dosing at the studied range. Further benzene is seen to be the major fraction with an overall average selectivity of 53.6% followed by naphthalene with 42.8% and toluene and xylene with the remainder 3.6%. This finding is similar to that observed by Ichikawa et al [12].

6.1.3.4 Aliphatic Yield

Figure 6.5 shows the effect of CO dosing on the aliphatic product yield. Aliphatic fraction shown in this figure comprises of ethane and ethylene.

From the Figure 6.5 it can be seen that the ethane yield is least effected by CO dosing. It is the ethylene fraction and thus the aliphatic yield which shows changes with variation in CO dosing.

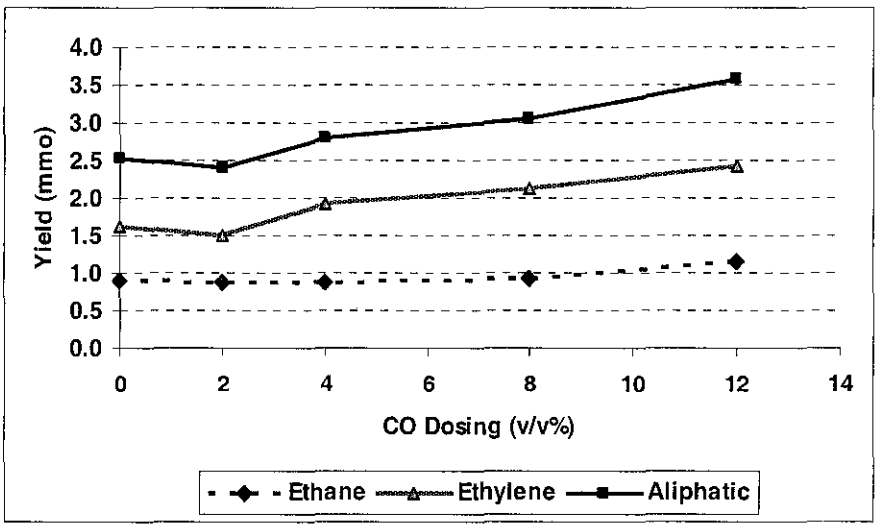

Figure 6.5 Effect of CO Dosing on Aliphatic Products Yield

From the same figure, it can be seen that CO dosing greater than 2% induces a positive effect, i.e. a steady increase of ethylene across the board is observed. This increase results in an increase aromatic selectivity and yield.

6.1.3.5 Coke species

Figure 6.6 shows the effect or changes in coke species with variation in CO dosing. The primary y-axis represents the yield changes for coke I and the secondary y-axis for changes in coke II with variation in CO dosing.

From Figure 6.6 it can be seen that coke I increases initially with initial dosing rate of 2% CO. This increase amounts to 128% higher than the base. On further increasing the CO dosing rate to 4, 8 and 12%, a positive decrease in coke 1 results. This decrease in coke 1 amounts to 101, 77, and 19% respectively to that of the base yield. In other words coke 1 yield decreases with increasing CO dosing greater than 2%.

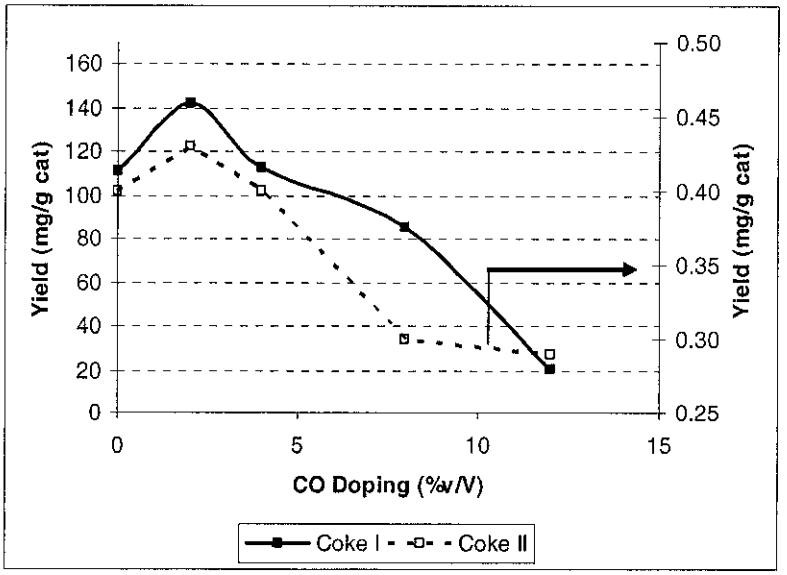

Figure 6.6 Effect of CO Dosing on Coke Species

In the case of coke II, a similar yield pattern is observed, although the loss is not as significant as coke I. CO dosing from 0 to 4% does not

show any significant changes in coke II. When the CO dosing is increased to 8% a significant decrease in coke II is observed. Between 8 and 12% CO dosing no affect on coke II yield was observed.

The above observations and findings may suggest that CO dosing above 8% is required for coke I to be actively scavenged by CO. This scavenging imposes a positive effect to the catalyst by improving accessibility of the methane feed to the Mo active sites resulting in improved catalytic activity favouring aromatic production.

6.1.3.6 Elemental Analysis

Table 6.2 shows the Mo, C and H content on a wt% basis. Table 6.2 also compares the total carbon content analysis performed by TGA and elemental analysis. From the table it can be seen that both method have similar trend, but the result from elemental analysis is higher than TGA across the board.

From the Table 6.2 it can also be seen that CO dosing does not significantly affect Mo loading or the hydrogen content

Table 6.2 Elemental Analysis of C, H and Mo

CO Dosing (v/v %)	ICP-AES (wt%)	TGA (wt%)	Elemental Analysis (wt%)		MDA (wt%)
	Mo	Carbon	Carbon	Hydrogen	Carbon
0	7.80	11.15	11.37	0.21	11.84
2	7.82	14.21	15.65	0.22	16.83
4	7.82	11.13	11.22	0.21	11.78
8	7.84	8.55	8.66	0.18	8.21
12	7.76	2.06	2.81	0.17	1.55

It can be seen that CO dosing only affect C content. It should be noted that the C yield measured by the different methods are used as a mode of comparison only. From the same table, it can be noticed that a similar trend exist between the different mode of carbon analysis with variable CO dosing.

6.1.3.7' Surface Properties

To further understand as to the effect of CO dosing on MDA reaction, the surface properties of the spent catalyst at the various CO dosing were analysed. These properties were compared to the parent HZSM-5 zeolite and the percentage increase or decrease in surface properties with CO dosing were recorded as in Figure 6.7.

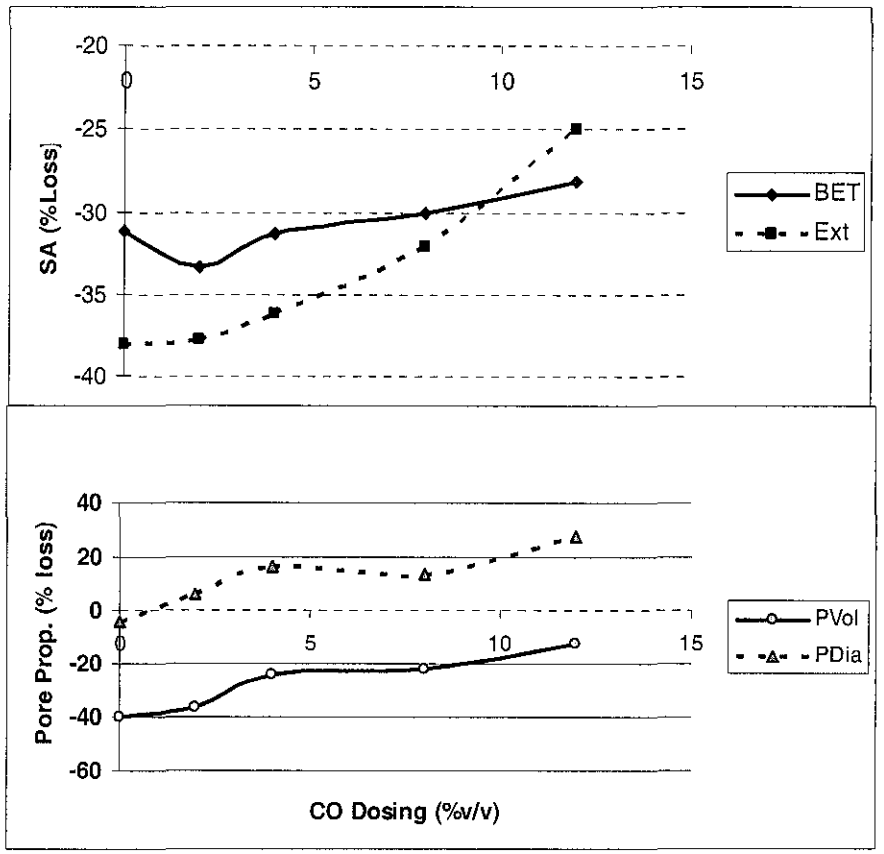

Figure 6.7 Effect of CO Dosing on Surface Properties

From Figure 6.7 it can be seen the BET SA experiences an initially decrease at 2% CO dosing. After the initial decrease at 2%, further increase in CO dosing results in a gradual improvement in BET SA. CO dosing has positive effect on the external SA. Increase in CO dosing results in improvement in external SA overall. This improvement in external SA is marked with a gradual increase from 0 to 4% CO dosing. CO dosing from 4 to 12 % results in a steep improvement of the SA. It is interesting to note that CO dosing has significant effect on the external SA as compared to the BET SA.

From Figure 6.7 it can be seen that the both the BJH pore volume and pore diameter increases with increasing CO dosing. The similar step shape graph is observed for both these pore properties with increase in CO dosing. For the proceeding discussion the effect of CO dosing is compared to the base. It should be noted that in all the case studies above, the BJH pore volume does not exceed the parent HSM5 zeolite's BJH pore volume.

The significant improvement of external SA over BET SA suggests that the CO scavenging is more an external surface phenomena. This observation is similar to that suggested by Ichikawa et al [5,11] and Iglesia et al [6]. As for the BJH pore volume which is associated with meso pores and inter-catalytic channels and the pore diameter, increase in CO dosing has positive effect. The step like improvement suggests threshold CO partial pressure is required to aid in suppressing or reducing the coke build up on the catalyst especially at the BJH pores which includes the inter and intra pores. At the same time, this optimum pressure of CO should not exceed a value which could bring about the destruction of the pore structure or adverse reconstruction of pore

channels [19]. The suppression in coke build up may be brought about by the scavenging properties of CO.

6.1.3.8 X- Ray Diffraction Analysis

Figures 6.8 represent the diffraction pattern for the spent 10MoBM calcined at 600°C and compare it to the same stock catalyst exposed to CO dosing at various CO concentrations. The diffraction pattern ranges between $2\theta = 35$ to 45° was taken to identify the possible hcp β-Mo_2C pattern and is represented by the letter 'B' on the XRD pattern scan. For the hcp β-Mo_2C the 2θ value is taken at 39.87 and 43.67°. This value is extracted from the Xpert plus library software. For this powder XRD analysis, the data was performed by the XRD analyser Philips PW1710 using CuKα radiation operating at 30 kV and 20mA with a scanning speed of 0.05° per sec and room temperature. The scans obtain from the XRD analyser were reprocessed using XPert Plus, a powder XRD software.

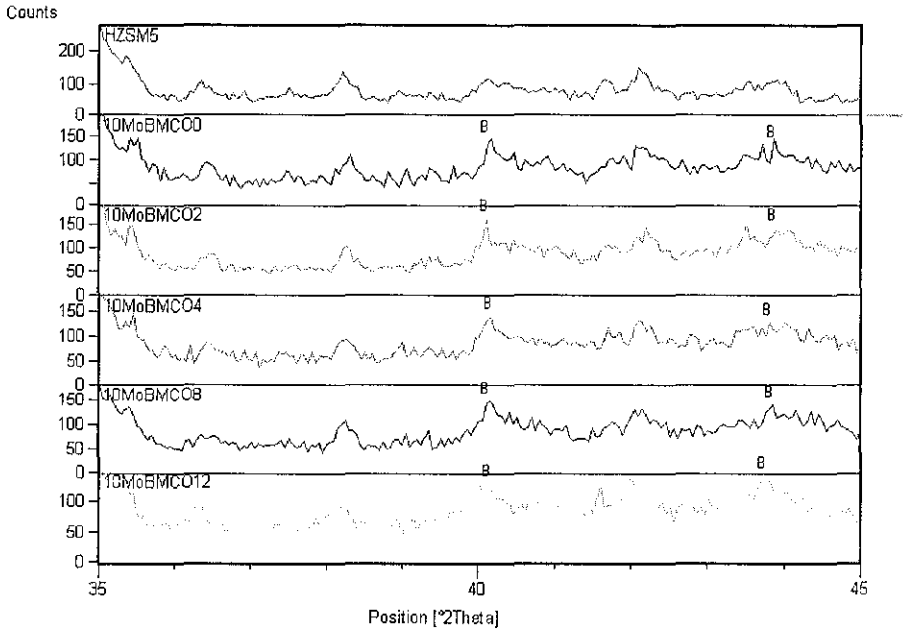

Figure 6.8 XRD Pattern for 10MoBM-Re Dosed With CO

From Figure 6.8 it can be seen that the XRD scans of the spent catalysts do not differ much from the parent HZSM-5 zeolite. This observation indicates minimum structural damage to the zeolite structure under similar MDA process conditions or when subjected to CO dosing.

The main attention in this study will be focus on the changing of hcp β-Mo_2C peak pattern present at 2θ value of 39.87 and 43.67° as shown in Figure 6.8.

From Figure 6.8, focussing on 2θ value at 39.87° it can be seen that the peak becomes more resolve when going from 10MoBMCO0 to 10MoBMCO2. On further dosing with CO, this peak pattern becomes less resolve or broadend and at 10MoBMCO12 and eventually gets split into 2 peaks. Broadening of peaks indicates high dispersion [21].

The second hcp β-Mo_2C peak pattern at 2θ =43.67° is more resolved at 10MoBMCO0, further dosing results in a drop in resolution. At 10MoBMCO4 it splits into 2 peaks. At 10MoBMCO8 this split peak recombines and the resolution improves further with increase CO dosing as can be observed at 10MoBMCO12.

From the above observations it can be concluded that CO dosing within the scope of study does not destroy the HZSM-5 zeolite crystallinity. Further it can be seen that the CO dosing aids in the redistribution of the Mo carbide species to try to attain better spread. This may explain the lack lustre performances of dosing at 2% CO and the improvement at 8 to 12% CO dosing

6.2 Effect of CO Dosing on Alpha Mo /Carbide/HZSM-5

6.2.1 INTRODUCTION

In the previous section the effect of carbon monoxide dosing on the beta form of 10 Mo modified HZSM 5 catalyst was studied. In this section under the same set of CO dosing conditions the alpha form of the catalyst will be investigated. This is performed because both the alpha and the beta form of Mo carbide exhibit different catalytic properties as shown earlier in Chapters 4 and 5. Further Rathotra et al[1] showed that both the alpha and beta form of Mo-carbide differ in the reaction on the hydrogenesis of ethane.

6.2.2 EXPERIMENTAL

For this study the stock sample of the 10Mo/HZSM-5 calcined at 600°C as described in Chapter 2 was used. 10Mo/HZSM-5 calcined at 500°C was not be used, although it proved to be the better catalyst as shown in the Chapter 5. This is done so as to have a more meaningful comparison for CO dosing with 10MoBM catalyst.

To prepare the alpha form of the 10Mo modified HZSM-5 catalyst the same method as described in Chapter 5 section 1.1 was followed. As for the CO dosing test the same dosing rate of 0, 2, 4, 8 and 12 % will be used. The catalyst evaluation studies and catalyst characterisation test will be conducted in a similar manner to that of MoBM study unless otherwise stated.

To differentiate between the alpha from the beta form, the alpha form of the catalyst will be tagged as MoA. As for the CO dosing the same suffix will be followed as in the previous section. Therefore 10Mo alpha modified on HZSM-5 with a CO dosing of 4 will be identified as

10MoACO4 and so forth for the other dosing rates. The following identification tags will apply unless stated otherwise.

6.2.3 RESULTS AND DISCUSSIONS

6.2.3.1 Methane Conversion

Figure 6.9 shows the average carbon conversion for the 10MoA catalyst at various CO dosing rate. The carbon conversion included in this figure is methane, coke or carbon deposition and the aromatic conversion. It should be noted that the methane conversion is the sum of the overall coke, aromatic and aliphatic conversion.

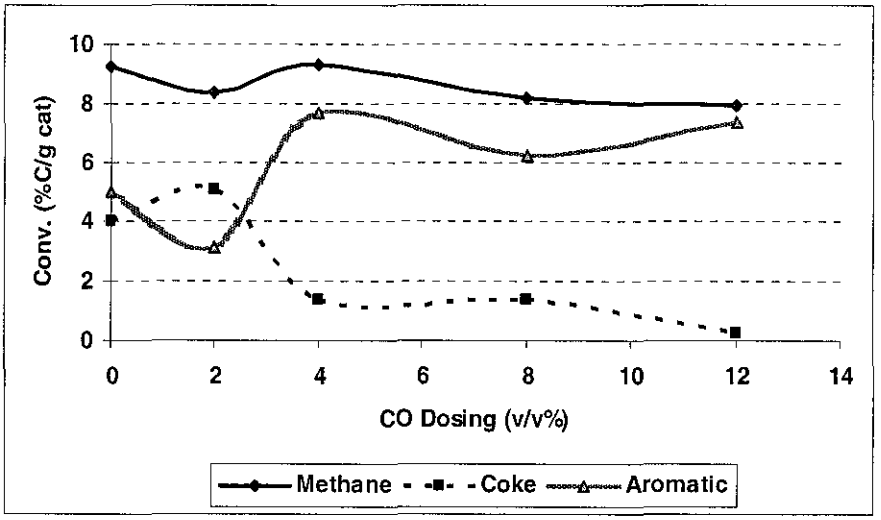

Figure 6.9 Effect of CO Dosing on Carbon Conversion for 10MoA

As for the aliphatic conversion because of it very low conversion, it will not be included in Figure 6.9 but will be discussed later. For the purpose of standardisation, the base of the CO dosing study will be 10MoACO0 or 0% CO dosing.

From Figure 6.9 it can be seen that the average methane conversion decreases by about 10% with the introduction of 2% CO, but on increasing the CO dosing to 4%, the methane conversion increases by

about 1% above the base. Further dosing of CO to 8 and 12% undergoes a carbon conversion loss of 11 and 14% respectively to the base value. At 12%, the methane conversion is at its lowest, compared to the whole range of CO dosing studied.

From Figure 6.9 it can be seen that both aromatic and coke have striking reverse conversion pattern. This is an indication of a common intermediate. With the introduction of 2% CO dosing, the coke yield experiences an increase, while the aromatic yields decreases. When the CO dosing is increased to 4%, it can be seen that the coke conversion decreases sharply. This loss in coke conversion is replaced by a sharp increase in the aromatic conversion. Going from 4 to 8% CO dosing, coke conversion remains the almost same as in 4% CO dosing, whereas the aromatic conversion experience a loss. On further increasing to 12% CO dosing, it can be seen that the aromatic conversion now has increase above the 8% but still lower than 4%CO dosing level, whereas the coke has reduced to its lowest level.

From the above observations it can be seen that CO dosing at 4 and 12% gives promising results. Dosing with 4% CO yields the highest catalytic activity and aromatic conversion with low coke, while the 12% yield the lowest coke with reduced catalytic activity which is highly selective to aromatics.

6.2.3.2 MDA Product Yield

Figure 6.10 shows the effect of CO dosing on the average product yield of 10MoA over 20 hours TOS. The product yield shown in this figure has been normalised and recalculated to represent the yield that would otherwise be obtained when the flow rate is 7.5ml/min. The product selectivity at the respected CO dosing is shown in Table 6.3 together with the CO product from the same MDA reaction. Further it should be noted

that CO product yield from Table 6.3 is the net yield observed after deduction of CO dosing and is a part of the coke yield in the same table. It should be also be noted that the catalytic activity is the net yield of the MDA product which comprises of aromatic, coke and aliphatic fractions.

From the Figure 6.10 and Table 6.3 it can be seen that in general CO dosing reduces catalytic activity excluding 4% which is an exception. Among the CO dosed catalysts, 4% has the highest catalytic activity which is similar to base value. As for the other three CO dosed feed, which include 2, 8 and 12% exhibits in a loss of 12, 14 and 18% respectively to that of the base value.

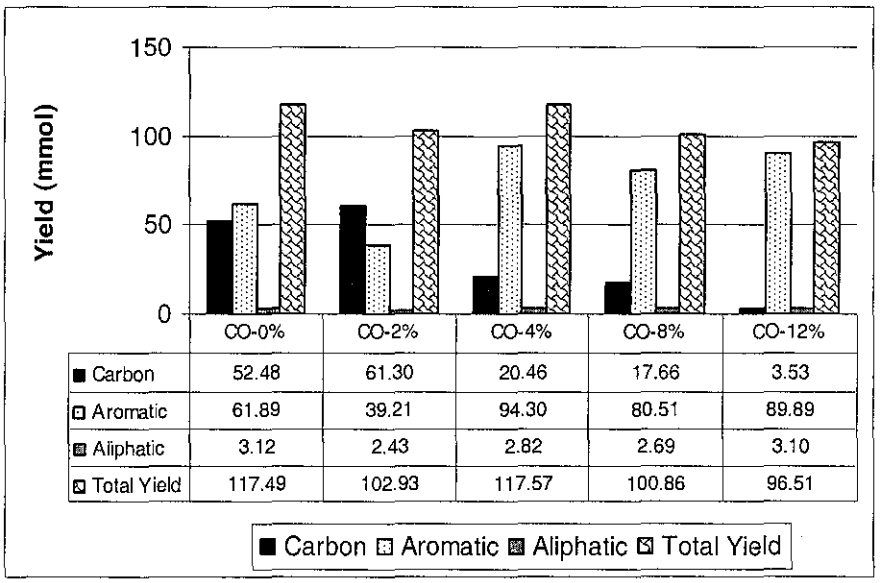

	CO-0%	CO-2%	CO-4%	CO-8%	CO-12%
Carbon	52.48	61.30	20.46	17.66	3.53
Aromatic	61.89	39.21	94.30	80.51	89.89
Aliphatic	3.12	2.43	2.82	2.69	3.10
Total Yield	117.49	102.93	117.57	100.86	96.51

Figure 6.10 Effect of CO Dosing on Product Yield for 10MoA

The aromatic yield and selectivity has an initial decrease at 2% CO dosing, thereafter increases with increasing CO dosing. CO dosing of 4, 8 and 12% results in an increase in aromatic yield of 152, 130 and 145% above the base. The coke yield on the other hand follows a reverse yield pattern to that of the aromatics.

Table 6.3 Effect of CO Dosing on Product Yield for 10MoA

CO Dose	0 %	2 %	4 %	8 %	12 %
Aromatic	52.7 %	38.1 %	80.2 %	79.7 %	93.13 %
Coke	44.7 %	59.6 %	17.4 %	17.0 %	3.66 %
Aliphatic	2.65 %	2.36 %	2.40 %	2.86 %	3.21 %
CO	0.22 %	0.31 %	0.33 %	0.43 %	3.47 %

The aliphatic yield of the CO dosed catalyst is lower than the base value, but increase in CO dosing results in an increases in both the yield and selectivity. As for the CO product, it is much lower than the aliphatic yield. The CO product increases with increase in CO dosing.

From the above observations it can be seen that, CO dosing improves aromatic and reduces coke yield and selectivity (apart from 2% CO dosing which loses 37% of its aromatic yield as compared to the base) in general higher than the base. This improvement in aromatic (yield and selectivity) is a result of the CO scavenging properties in effect as seen by the increase in CO product yield with the increase in CO dosing. For further information on this matter please refer to section 6.1.3. The catalytic activity in general decreases with CO dosing apart from CO dosing at 4%. Dosing with 2% CO produces the lowest aromatic yield, but has the highest coke yield. CO dosing at this level (2%) is undesirable. The 4% CO dosing produces the highest catalytic activity and aromatic yield of the catalyst investigated. Dosing the CO at 8% has high aromatic and low coke yield. Its catalytic activity is moderate. As for 12% CO dosing, it produces the lowest coke yield and high aromatic (2^{nd} to CO 4%), but has the lowest catalytic activity of those studied. From the above discussion it can be seen that both 4 and 12% CO dosing exhibit promising results for the 10MoA.

6.2.3.3 Aromatic Product

Figure 6.11 shows effect of CO dosing on the aromatic product yield. To highlight the minor aromatic products namely toluene and xylene which make less than 5% of the total aromatic yield, a secondary y-axis was created to represent it. The primary y-axis represents the yields obtained form benzene and naphthalene, the major aromatic products.

From Figure 6.11 it can be seen that the aromatic selectivity is not seriously affected by CO dosing. The average aromatic selectivity is quite consistent from 0 to 8% CO dosing. The average % selectivity for benzene, naphthalene and toluene/xylene fraction makes up 54, 42 and 4% respectively. When the dosing of CO was increased to 12% the rate of benzene and toluene/xylene decreases to 47 and 3% respectively whereas naphthalene increases to 50%.

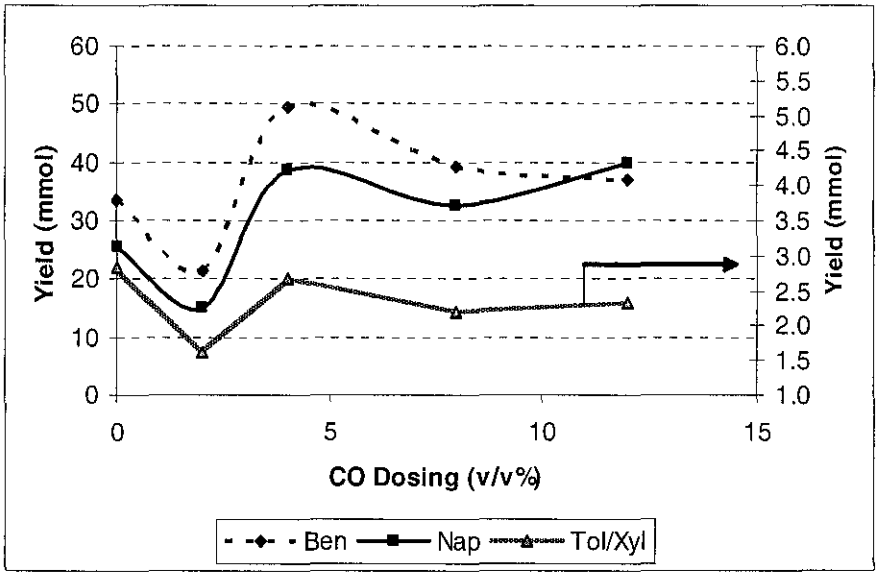

Figure 6.11 Effect of CO Dosing on Aromatic Fraction for 10MoA

From the above observations, it can be concluded that below CO dosing of 8% no significant changes in aromatic fraction % selectivity is

observed, but with the increase of CO dosing to 12%, the selectivity tends towards naphthalene.

6.2.3.4 Aliphatic Product

Figure 6.12 shows effect of CO dosing on aliphatic product yield. From the same figure it can be seen that the selectivity of both ethane and ethylene and thus the total aliphatic is unaffected with CO dosing. The average yield selectivity for ethane and ethylene are 35 and 65% respectively.

From the same figure it can be seen that CO dosing has no influence on the % selectivity of ethane and ethylene, but influences the yield produced. Increase in CO dosing rate results in an increase in ethane and ethylene yield. It should be also be noted that the yield obtain with the entire CO dosing rate does not exceed the base yield for both ethane and ethylene.

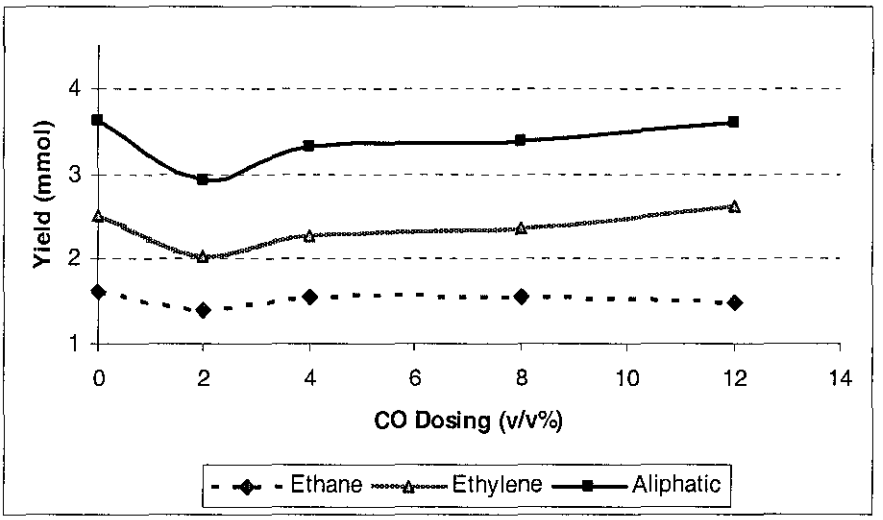

Figure 6.12 Effect of CO Dosing on Average. Aliphatic Fraction for 10MoA

6.2.3.5 Coke Species

Figure 6.13 shows the effect of CO dosing on the carbon species present on the active catalyst. The carbon species identified is based on the studies of Xu et al [18]. The usual notation applies for coke I and coke II. Due to the huge difference in quantity between the two types of coke, the primary y-axis will represents coke 1 and coke II is represented by the secondary y-axis.

From Figure 6.13 it can be seen that CO dosing in general suppresses coke I build-up and slightly reduces coke II. It should also be noted that the coke II species are formed during activation stage, whereas the coke I builds up during reaction stage. From the same figure it can be seen that coke II is least affected by CO dosing, while coke I experiences huge loss with increase in CO dosing. This correlates well to the coke yield as in section 6.2.2.2

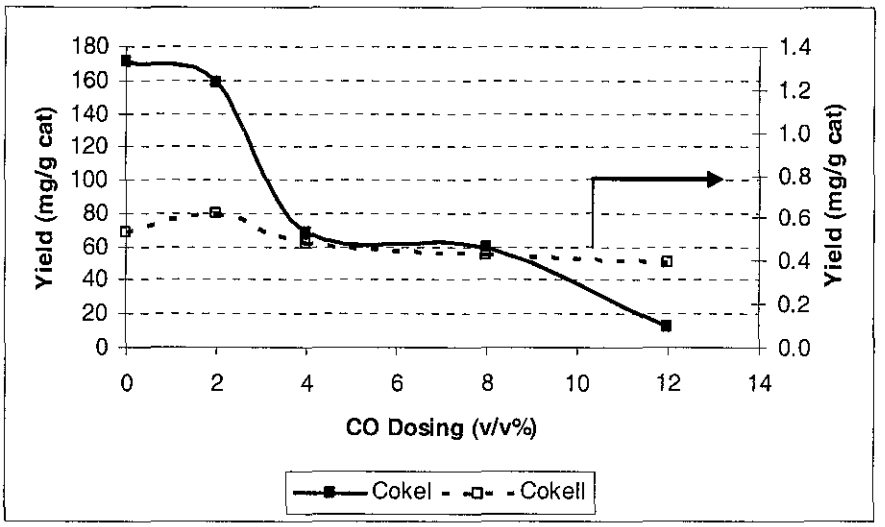

Figure 6.13 Effect of CO Dosing on Coke Species

From the above observation it can be seen that with increase in CO dosing, more of the surface coke or coke I build up is suppressed. This

allows more flexibility and accessibility of the feed to reach the active site for MDA reaction. It should also be noted that coke II which is responsible for methane activation is not as greatly affected as that of coke I. The lack of scavenging power by CO towards coke II may be due to its position in the catalyst and its strong affinity towards Mo species. This reduces the scavenging effect of CO towards it.

6.2.3.6 Elemental Analysis

Table 6.4 shows the carbon and hydrogen content by elemental analysis and coke yield from other analytical techniques.

Table 6.4 Elemental Analysis of C, H and Mo (10MoA)

CO Dosing (v/v %)	ICP-AES (wt%)	TGA (wt%)	Elemental Analysis (wt%)		MDA (wt%)
	Mo	Carbon	Carbon	Hydrogen	Carbon
0	9.42	17.10	18.05	0.28	18.89
2	9.38	15.91	15.88	0.30	16.80
4	9.40	6.88	6.95	0.28	7.07
8	9.36	5.99	6.01	0.23	5.85
12	9.35	1.29	1.60	0.25	1.12

Similar to the 10MoBM catalyst in the previous section, it was noticed that CO dosing does not affect the Mo or hydrogen content of the catalyst. As for the total coke content, the elemental analysis follows a similar trend as experienced in TGA and MDA, but the values are slightly higher for the latter two. It should be emphasised that the main purpose is for comparison only.

6.2.3.7 Surface Properties

The catalytic surface properties of the 10MoA spent catalysts were analysed to study the effect of CO dosing and are shown in Figure 6.14. This figure analyses the surface areas (BET and External) and the pore properties (BJH pore volume and Pore Diameter)

Figure 6.14 represents the changes in the above surface properties in terms of percentages loss with respect to the parent HZSM-5zeolite. Similar calculations were followed as in the previous section.

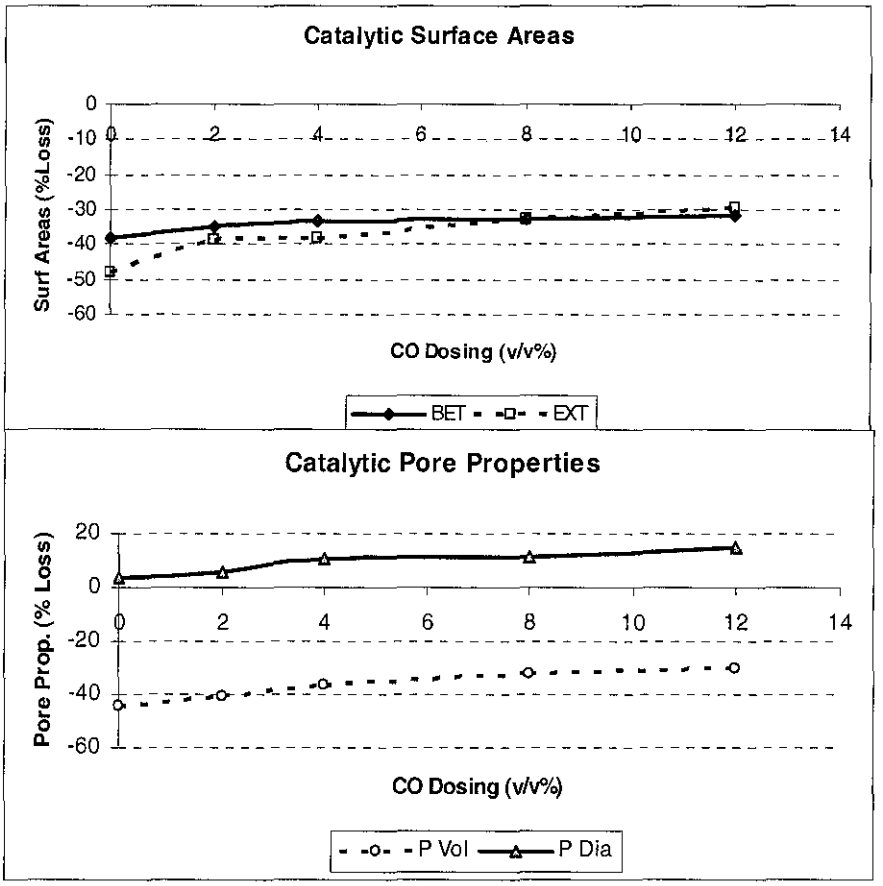

Figure 6.14 Effect of CO Dosing on Catalytic Surface Properties

From Figure 6.14, on analysing the BET surface area it can be seen that no significant change are observed. With an initial dosing of 2% CO an

increase of 6.3 % of the BET SA is observed. On further CO dosing from 2 to 12% any further improvement in BET SA is limited to less than 3%.

On the other hand, when comparing the external surface area, the changes are more significant. With the introduction of 2% CO an improvement of 9.4% is observed. On further increment of CO dosing from 4, 8 and 12% improvement of 9.7, 15.1 and 18.3% respectively are observed.

With a CO dosing of 12% an improvement of the pore diameter can be observed as shown in Figure 6.14. Some improvements are observed from 0 to 4% CO dosing, higher then 4% CO dosing does not indicate any significant changes.

In the case of BJH pore volume, a gradual improvement is noticed with increase in CO dosing. Improvement between 3.8 to 14.3% are observed from 2 to 12% CO dosing when compared to the base.

From the above observation it can be seen both the external and BJH pore are significantly improved with CO dosing. Surface cokes are usually found on the external, pore mouth and intra catalytic particles areas. Based on the above observations it can be seen that CO dosing can efficient suppress inactive surface coke present on surface.

6.2.3.8 X- Ray Diffraction Analysis

The XRD pattern on the spent 10MoA catalysts were carried out by similar methods and condition as explained in the previous section as in the MoBM catalyst. The diffraction pattern range between $2\theta = 35$ to 45° was taken to identify possible hcp β-Mo_2C and α-fcc $Mo_{1-x}C$ pattern are represented by the letter 'A' and 'B' respectively on the XRD pattern

scan. For the hcp β-Mo_2C the 2θ value is taken at 35.18° and 43.67°, whereas for the α-fcc Mo $_{1-x}$ C, it was taken at the 2θ value of 36.45° and 42.22°

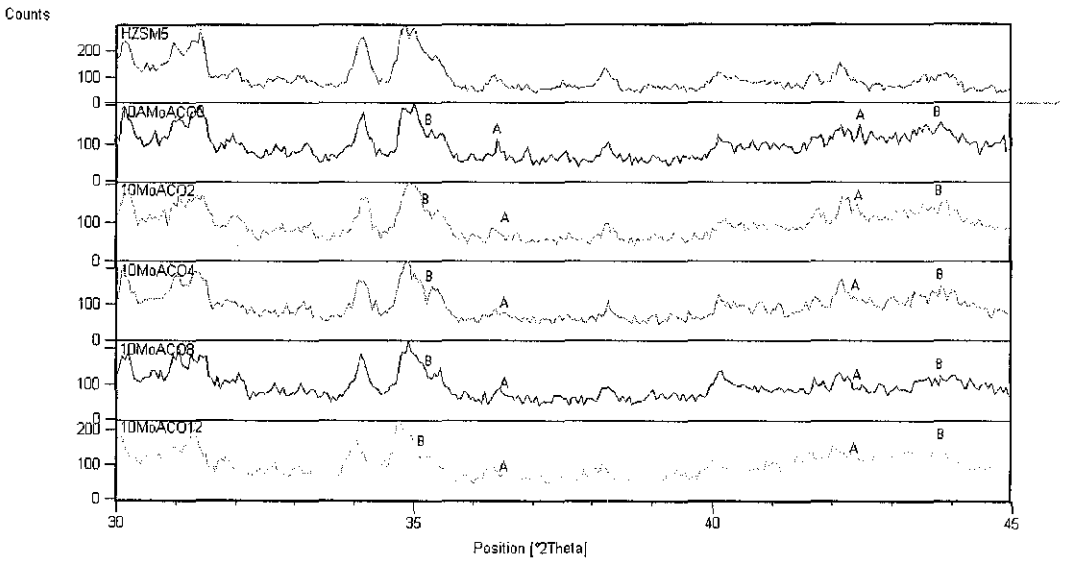

Figure 6.15 XRD Pattern for 10MoA Catalyst Dosed With CO

From Figure 6.15 it can be seen from the XRD pattern the crystallinity of the HZSM parent catalyst is unaffected by CO dosing. From the same figure it can be seen that both the α and the β Mo-carbide are present in the 10MoA CO dosed catalyst. This is expected as explained in Chapter 5. On analysing both the α and β peak for the base it can be seen that both sets of peak are well resolved. On introduction of CO dosing to 2, 4, 8 and 12% it can be seen that the peak resolution decreases or broadens. Broadening of peaks indicates high dispersion [21]. Thus it can be seen that CO addition not only scavenges or suppress coke build up but also aid in the high dispersion of Mo carbide species. This finding is complements Lunsford et al [13] who suggested that pre-treatment with CO can influence the dispersion of transition metal ions. This may also one of the main reasons for the increase in aromatic yield observed with increase in CO dosing.

6.3 Overall Comparison between MoBM and MoA series

6.3.1 INTRODUCTION

To conclude the effect of CO dosing on both the MoBM and MoA series further catalytic evaluation tests were conducted on the 3MoA and 3MoBM using similar process conditions and CO dosing as those of 10MoA and 10MoBM respectively. The purpose of this was to investigate the effect of Mo loading on CO dosing. The main areas of discussion will be concentrated on the methane conversion, the aromatic product yield and the catalytic stability or coke yield. At the end of this chapter the most promising and it respective optimum CO dosing will be recommended.

The main properties or focus of the selection will be based on high yield for aromatics with low carbon or coke deposition.

6.3.2 METHANE CONVERSION

Figure 6.16 compares the methane conversion for all the four catalysts and its effect with CO dosing rate of 0, 2 4 8 and 12%. From the same figure, it can be seen that methane conversion are higher for higher Mo loading.

On observing the effect of CO dosing on the MoBM series it can be seen that for 10MoBM, increase in CO dosing results in an increase in methane conversion, but the 3MoBM follows a reverse pattern to that of 10MoBM i.e. methane conversion decreases with increase in CO dosing. The highest methane conversion recorded 10MoBM is 9.53% with a CO dosing of 12%, whereas for 3MoBM the highest conversion is 6.4% recorded with a CO dosing of 2%.

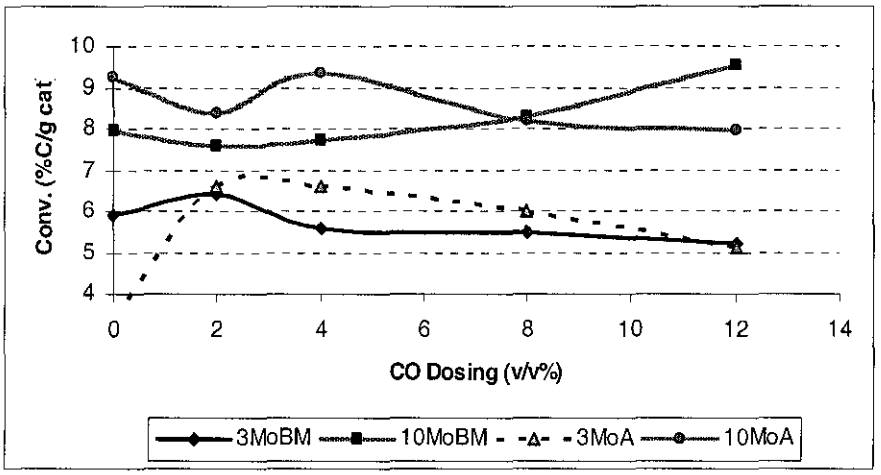

Figure 6.16 Effect of CO Dosing on Methane Conversion

On analysing the MoA series, it can be seen that 10MoA starts with a high methane conversion at 0% CO dosing, which drops slightly at 2% before reaching a maximum at 4% with a methane conversion value of 9.33%. Further dosing results in decrease in methane conversion. 3MoA on the other hand starts at a very low conversion which peaks between 2 and 4 % CO dosing with a methane conversion of 6.40%, thereafter methane conversion decreases with increase in CO dosing. This observation is similar to that observed for 10MoA. In other words MoA catalysts have maximum conversion values from 2 to 4 CO dosing rate. With increase in Mo loading the peak shifts more towards the higher CO dosing value.

6.3.3 COKE

Coke yield is a detrimental in MDA reaction. Lower coke yield increases catalytic stability. The coke yield shown in Figure 6.17 was calculated based on a 20 hours TOS. Figure 6.17 investigates the effect of CO dosing on coke yield.

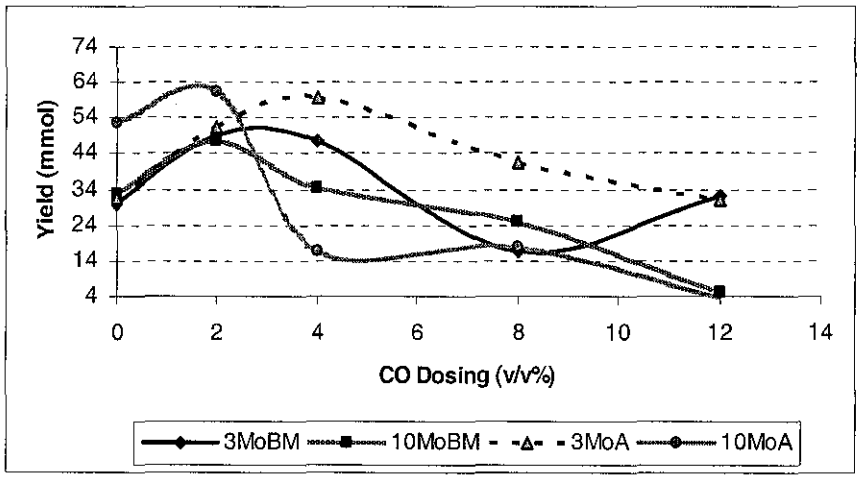

Figure 6.17 Effect of CO Dosing on Coke Yield

From the Figure 6.17, it can be seen that for all four catalyst analysed, initial introduction of 2% CO dosing results in an increase in coke yield. For both the higher Mo loading catalysts of 10MoBM and 10MoA, further addition of CO results in a sharp decrease in coke yield.

The same is not true for the lower Mo loading catalysts of 3MoBM and 3MoA. For these two catalysts the coke peak shifts between 2 and 4% CO dosing before dropping. Except for 3MoBM, the other three catalysts (3MoA, 10MoA and 10MoBM) have lowest coke content at 12% CO dosing. 3MoBM has its lowest coke value at 8% CO dosing, but this increases with further addition of CO dosing. The lowest coke recorded for 3MoBM, 10MoBM, 3MoA and 10MoA are 16.8, 4.9, 31.1 and 3.5% respectively.

From the above observation it can be seen that the positive affect of CO dosing favours higher Mo loading catalysts i.e. 10MoA and 10MoBM.

6.3.4 AROMATIC YIELD

The main product in this study to be optimised is the aromatic yield. Figure 6.18 shows the aromatic yields obtain over 20 hours TOS under the influence of various CO dosing.

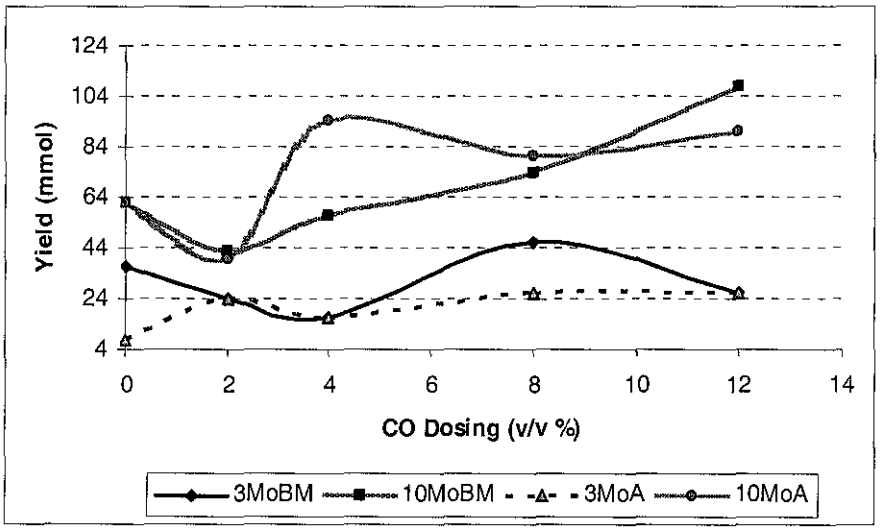

Figure 6.18 Effect of CO Dosing on the Aromatic Yield

Figure 6.18 compares the aromatic yields obtain for the 4 catalysts and its effect with CO dosing. From the same figure, it can be seen that the both the 10Mo loaded catalysts have higher aromatic yields as compared to the 3Mo loading counterparts. This may suggest that higher Mo loadings enhance aromatic production yields. It is interesting to see that 10MoA has a reverse yield pattern to that of 3MoBM while 10MoBM has a reverse yield pattern to that of 3MoA.

Analysing the both 10MoBM and 10MoA catalyst it is interesting to see that the aromatic yield follows a similar yield pattern to its respective methane conversion. 10MoA which records its highest aromatic yield of 94.3 mmol at 4% CO dosing, whereas for 10MoBM it is 73.3mmol obtained at 12% CO dosing.

In the case of 3MoA, the aromatic yield increases sharply at 2% CO dosing. Increasing the CO dosing to above 2% results in a steady increase which becomes almost constant at 8 and 12% CO dosing. 3MoBM on the other has a wave like curve with a minimum at 4% and a maximum at 8% CO dosing. Above 8% CO dosing results in further decrease in aromatic yield.

6.3.4.1 Benzene and Naphthalene Selectivity

Figure 6.19 shows the combined figures of the benzene and naphthalene yield in mmol per gram catalyst over 20 hours TOS.

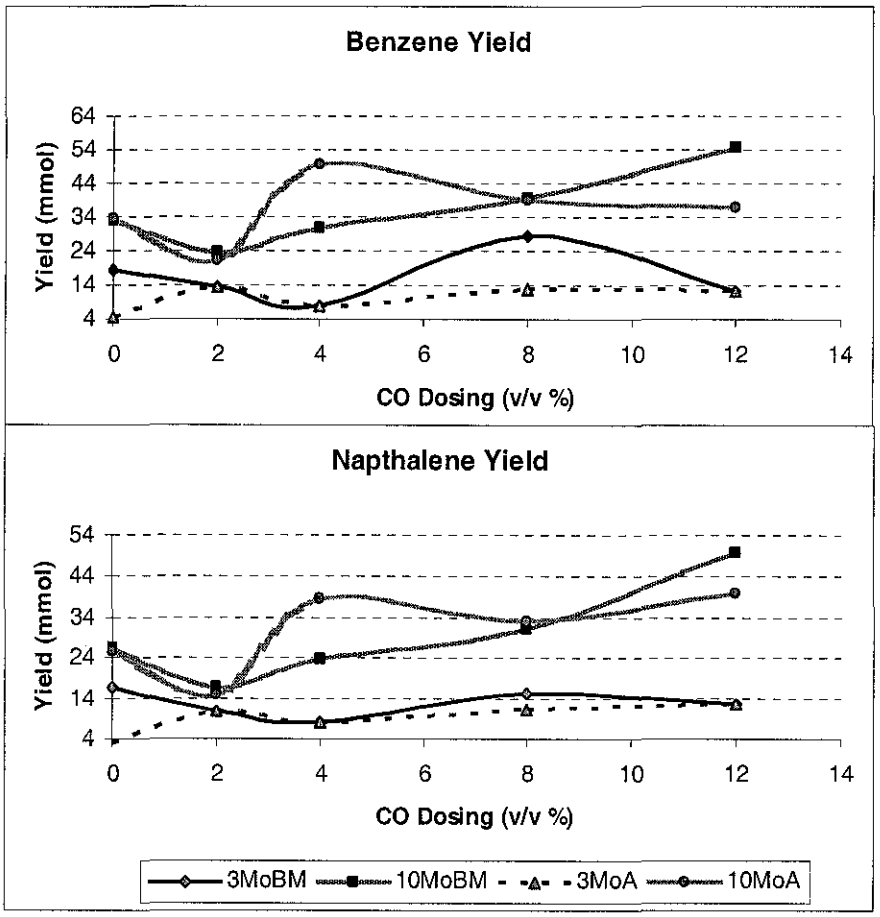

Figure 6.19 Effect of CO Dosing on the Benzene and Naphthalene

Both the benzene and naphthalene are combined in a single figure so as the have a clearer picture on the selectivity of aromatic product fractions under the influence of CO dosing. It can be seen that both the benzene and naphthalene yield follow a similar yield pattern for each of the individual catalyst at the specific CO dosing. The only discrepancy observed between the two sets of figures is the yield of benzene for 3MoBM at 8% CO dosing. Here the increase in benzene yield is sharper than the naphthalene yield from the same catalyst and at the same CO dosing. Other than that all the others follow similar yield pattern.

From these observations it can be concluded that CO dosing do not interfere with the aromatic product fraction % selectivity. Further it can be noticed that benzene yield is higher than the naphthalene counterpart.

6.4 Conclusions

From the above observation and analysis based on the above set of conditions, it can be seen that both that 10Mo loaded catalysts are more suitable than 3Mo counterparts for MDA reaction. Correct CO dosing does improve the catalytic activities and stability. The most suitable CO dosing rate for 3MoBM, 3MoA is 8%, while for 10MoA and 10MoBM it is 4 and 12% respectively. Among the four catalysts and CO dosing, the most promising catalyst in terms of aromatic yield and stability for MDA reaction is exhibited by 10MoBM and 10MoA catalyst with CO dosing of 12% and 4% respectively.

CO dosing at 2% seems to decrease catalytic activity due to increase coke build up, but CO dosing greater than 4% is believed suppress surface coke build up, as a result increase catalytic activity and aromatic yield and selectivity at the expense of coke is observed. CO dosing does not significantly alter the aromatic fraction selectivity. Further it does not

alter the catalytic component significantly, but increases catalytic yield and stability.

6.5 Chapter 6 References

1. Wechkhuysen, B.M., Rosynek, M.P., and Lunsford, J.H., Catal. Lett. 52 (1998) 31
2. Jiang, H., Wang, L., Cui, W., and Xu, Y.,. Catal. Lett. 57 (1999) 95
3. Liu, W., Wang, L., Ohnishi, R., and Ichikawa, M.,. J. Catal. 181, (1999) 175
4. Anderson, JR, Phd Thesis (2001) University of Liverpool., UK
5. Wang, L., Ohnishi, R., and Ichikawa, M., J. Catal 190 (2000) 276
6. Ohnishi, R., and Ichikawa, M., Catal. Surveys Japan Vol. 5, No.2 (2002) 103
7. Liu, Z., Nutt, M.A., and Iglesia, E., Catal. Letts. Vol 81, No 3-4 (2002) 371
8. Borry III, RW., Kim, Y.H., Huffsmith, A., Reimer, J.A., and Iglesia, E., J. Phys. Chem. B 103 (1999) 5787.
9. Ding, W., Meitzner, G.D., Marler, D.O., and Iglesia, E., J. Phys. Chem. B 105 (2001) 506
10. Ohnishi, R., Liu, S., Dong, Q., Wang, L., and Ichikawa, M., J. Catal. 182 (1999) 35.
11. Shu, Y., Ohnishi, R., and Ichikawa, M,. J. Catal 206 (2002) 134
12. Liu, S., Dong, Q., Ohnishi, R., and Ichikawa, M,. Chem. Commum. (1998) 1217
13. Weckhuysen, B.M., Wang, D., Rosynek, M.P., and Lunsford, J.H., J. Catal. 175 (1998) 338
14. Zhang, Z., Long, M.A., Howe, R.F., Catal. Today 44 (1998) 293

15. Us, Y., Liu, W., Wong, S., Wang, L., Guo, X., Catal. Lett. 40 (1996) 207
16. Lin, W., .Xu, Y., Wong, S.T., Wang, L., Qiu, J., Yang, N., J. Catal. A 120 (1997) 257
17. Xu, Y., and Lin, L., Appl. Catal. A Gen. 188 (1999) 53
18. Lin, H., Li T., Tian, B., and Xu, Y., Appl. Catal. A Gen. 213 (2001) 103
19. Li, Z., Gao, L., and Zhang, S., Appl. Catal. 236 (2002) 163
20. Ranhotra, G.S., Bell, A.T., and Reimer, J.A., J. Catal. 108 (1987) 40
21. Bouchy, C., Deouane-Abd Hamid, S.B., and Derouane,.E.G., Chem. Commum. 2 (2002) 125

CHAPTER 7 REGENERATION

7.1 Introduction

Regeneration of Mo modified HZSM-5 by oxygen dosing has not been highly pursued in MDA reaction. Most of the research done in this area is overshadowed by the effect of addition of small amounts of CO or CO_2 to remove coke during the MDA reaction which is claimed to significantly enhance catalytic stability [1-4]. Others include H_2 [4-6] which are believed to lower rates of deactivation during the methane pyrolysis reaction. Oxygen and sometimes nitrogen oxide [3,6,7] are added into the methane feed to prolong the catalyst life.

Ichikawa et al [4] conducted catalyst regeneration on 6 fwt% Mo/HZSM-5 by removal of coke from spent catalyst using temperature – programmed oxidation and pulse dosing experiments. They concluded that deposited coke can be removed by oxidation combustion at 550°C over 2 hours under a mixture of 20% oxygen in helium. Based on their findings they implied that the ROF of benzene could be restored, but not possible for naphthalene. Unfortunately their results were based on 3 hours TOS.

For the present study, the main scope will cover the effect of in situ regeneration of spent 3wt% β-Mo/HZSM-5 catalyst with air, the main source of oxygen and its catalytic evaluation in terms of conversion, yield and selectivity of product together with aromatic fraction. A look at the changing BET and external surface area will also be included. 3MoBM catalyst was chosen for this investigation as it has moderate conversion for aromatic and coke yield compared to the others in the same group as investigated in Chapter 4.

7.2 Experimental

For the regeneration study, the 3MoBM catalyst as described in Chapters 3 and 6 was used. Approximately 5.0 gram of the freshly activated 3MoBM was subjected to MDA reaction at methane space velocity of 1500 h^{-1} over 48 hours at a temperature of 700°C using similar setup technique as used for calcination purposes as described in Chapter 3.

The coke catalyst was cooled under a flow of helium to room temperature and dried at 120°C overnight which was then cooled to room temperature in a desicator without desiccant and stored for further testing. For all regeneration testing here after, the 3MoBM coked catalyst described above will be used, unless otherwise stated.

7.3 Preliminary Testing

A preliminary test was carried out to find the right oxygen dosing rate. The reactor setup for this preliminary test was similar to that described in Chapter 3. For each testing 0.2 gram of the catalyst was used.

The coked catalyst was nestled in the centre of the reactor by two layers of quartz wool. A mixture of helium and air was then introduced to this coked catalyst by means of Brooks mass flow controller at a specific flow rate. The source of oxygen in the mixture is provided by compressed air. For the present study a couple of assumptions were made on the composition of air: it is assumed that the oxygen content in air is 20 v/v% and the other components in the air mixture do not interfere with the regeneration process.

The air was then blended together with helium at various proportions to give an oxygen mixture of 2.5, 5 and 10 v/v %. The gas flow rate into the reactor was introduced by Brooks mass flow controllers as described in Chapter 3 and was fixed at a constant 8 ml/min.

The reactor and its contents were heated from room temperature to 650°C at a constant rate of 10°C per minute and maintained at this temperature for an hour. After the dwell period, the air was discontinued but, still maintaining helium flow. The reactor and its contents were then heated to 700°C at a rate of 10°C/min. At 700°C, helium was replaced by methane at a flow rate of 5 min/min signifying a GHSV of $1500h^{-1}$. Thereafter the same procedure as described in Chapter 3 was followed.

From the preliminary test conducted above the most promising oxygen dosage which comes close in regaining the initial catalytic activity will be selected. After selecting the most promising oxygen dosing %, a GHSV investigation will be conducted to select the best oxygen regeneration rate.

7.3.1 PRELIMINARY TESTS

After the regeneration treatment but before proceeding with the MDA reaction, the catalyst was cooled down to room temperature. On cooling the freshly regenerated catalyst bed was visually inspected. From the inspection it was noticed that for the 2.5% oxygen dosing the catalyst bed was divided into 2 sections, the top section was white in colour while the bottom section was black. For the 10 v/v % oxygen the whole catalyst bed was white in colour. It was only for the 5% v/v oxygen treatment which had a single grey colour catalyst bed.

After the inspection the catalyst was subjected to MDA reaction for 20 hours TOS. The entire preliminary test described above was carried out in a similar manner for better comparison. From the preliminary catalyst evaluation studies Figure 7.1 was derived.

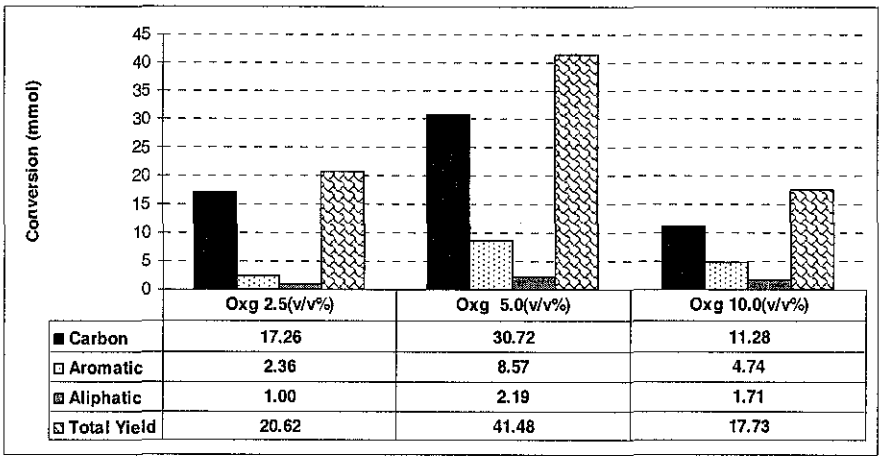

	Oxg 2.5(v/v%)	Oxg 5.0(v/v%)	Oxg 10.0(v/v%)
■ Carbon	17.26	30.72	11.28
□ Aromatic	2.36	8.57	4.74
▨ Aliphatic	1.00	2.19	1.71
▧ Total Yield	20.62	41.48	17.73

Figure 7.1 Preliminary Regeneration Studies

Figure 7.1 shows the results from the preliminary regeneration studies. In this figure the yield distribution over 20 hours TOS is shown. From the same figure it can be seen that 5v/v% oxygen gives the most promising effects of the three regeneration dosing rates studied. Apart from having a high catalytic activity it also has the highest aromatic yield of the 3 studied. Further from the visual inspection it was noticed that the 2.5% oxygen dosing was not enough to complete regeneration. The 10% oxygen dosing on the other hand successfully removes most if not all of the carbon deposit from the coked catalyst. Coke, the main cause for catalytic decay, is also necessary for catalytic activities as shown in previous Chapters.

Having selected the required oxygen dosing rate, the next step was to select the most promising regeneration flow rate. It has been recommended that a high flow rate and reasonably low oxygen dosing are most favoured for regeneration studies [5].

For this study, the volume % of oxygen into the regeneration mixture was fixed but the flow rate was varied to represent the various GHSV. The GHSV studied was between 2400 to 7200 h^{-1}, maintained for 0.5 hours

and 1 hour. The GHSV selected for this study was kept at 2400, 4800 and 7200 h^{-1}.

7.4 Results and Discussions

7.4.1 GAS HOURLY SPACE VELOCITY (GHSV) STUDIES

Table 7.1 shows the average methane conversion (% conversion of C per gram catalyst) after the coked catalyst as explained above has been subjected to regeneration conditions with different GHSV and dwell time. The table is divided into three parts, one representing the average 1st 10 hours named as part 1 the 2nd 10 hours (11th to 20th hour) as Part 2 and the 3rd the average over 20 hours TOS as overall. The control represented in this figure is the carbon conversion derived from freshly activated 3MoBM catalyst which has not undergone any regeneration process. The results in bracket represent % changes in methane conversion. Part 1 and Part 3 the results in brackets are methane conversion compared to control at the respective parts. For Part 2 it is the loss in methane conversion for the specific catalyst.

Table 7.1 Regeneration Study and Methane Conversion

	Methane Conversion in % C/g cat					
	Control	**R2400(0.5h)**	**R4800(0.5h)**	**R7200(0.5h)**	**R2400(1h)**	**R4800(1h)**
Part 1	6.24 (100%)	6.62 (106%)	6.11 (98%)	2.77 (44%)	6.76 (108%)	6.95 (111%)
Part 2	5.49 (-12%)	4.51 (-32%)	4.97 (-19%)	-	5.18 (-23%)	4.98 (-28%)
Overall Average	5.86 (100%)	5.57 (95%)	5.54 (95%)	-	5.97 (102%)	5.96 (102%)

Before conducting the MDA reaction with methane the freshly regenerated catalysts were visually examined. From this visual examination it was noticed apart from R7200 (0.5h) all the other freshly regenerated catalyst were either grey [R4800 (0.5h)and R2400(0.5h)] or

dark shade of grey [R2400(1h) and R4800(1h)]. As for R7200(0.5h) catalyst it was cream in colour. This may indicate that R7200(0.5h) may have been over oxidised.

On comparing the GHSV with ½ hour dwell time from Table 7.1 it can be seen for the 1st 10 hours conversion R2400(0.5h) has 6% higher conversion than the control, whereas R4800(0.5h) loses 2% and R7200(0.5h) loses 56% as compared to the control value. The low methane conversion observed with R7200 (0.5h) is expected as highlighted from the visual observation. Based on this information R7200 (0.5h) will not be discussed any further. Comparing the 2nd 10 hours methane conversion, it can be seen that control loses 12%, whereas R2400 (0.5h) and R4800 (0.5h) loses 32 and 19% respectively. As for the overall average methane conversion over 20 hours TOS both R2400 (0.5h) and R4800 (0.5h) loses 5%.

From Table 7.1 on comparison with the control it can be seen that for both R24800 (1h) and R4800 (1h) the methane conversion has increased by 8 and 11% respectively for the 1st 10 hours. For the 2nd 10 hours for the same it has reduced to 23 and 28 % respectively over 10 hours TOS. This is much higher than the control which loses only 12%. The overall methane conversion for both R24800 (1h) and R4800 (1h) had improved by 1.8 % above the control.

From the above observation, it can be seen that increase in regeneration dwell time increases in methane conversion for both R2400 (1h) and R4800 (1h). Furthermore the overall methane conversion does not seem to be affected by GHSV between the 2 ranges namely 2400 to 4800 h^{-1}. Although both R24800 (1h) and R4800 (1h) start at a higher average methane conversion during the 1st 10 hours, but it drastically loses the advantage with increase in TOS.

Table 7.2 shows the yield obtained and the selectivity after the regeneration of the coked catalyst for the various regenerated catalysts. The data in brackets represent the selectivity of the MDA products from the different regeneration conditions.

Table 7.2 Regeneration Studies – MDA Product Yield

	Yield in mmol over 20 hours TOS				
	Control	R2400(1h)	R4800(1h)	R2400(0.5h)	R4800(0.5h)
Coke	29.66 (41%)	55.96 (76%)	49.36 (67%)	55.91 (82%)	47.32 (70%)
Aromatic	36.95 (52%)	12.96 (18%)	18.74 (26%)	8.96 (13%)	16.18 (24%)
Aliphatic	5.27 (7%)	4.31 (6%)	4.99 (7%)	3.27 (5%)	4.44 (6%)
Total yield	71.88	73.23	73.09	68.14	67.94

From the Table 7.2 it can be seen that for all the regenerated catalyst the coke yield is much higher than the control. Between the regenerated catalysts it can be seen that for the R2400 pair produces more coke than its counterpart R4800 pair. In other words, lower the GHSV h^{-1} results in higher coke yield. Furthermore, it can be noticed that the selectivity for coke between the 2 sets of GHSV h^{-1} decreased with increased dwell time.

The aromatic content on the other hand, seem to favour higher GHSV as can be seen from Table 7.2, where both the R4800 sets have higher yield than R2400 counterpart. For the R4800 set, increase in dwell time results in an increase in aromatic content. The same is the reverse for the R2400 set.

Aliphatic content on the other hand seems to increase with GHSV and dwell time.

in coke content may be one of the reasons for the decline in naphthalene content.

7.5 Catalyst Characterisation

7.5.1 SURFACE AREA

The catalyst characterisation for the surface properties, in particular the BET and external surface areas were carried out using the surface analyser ASAP 2000, as described in method of Chapter 2 and is presented in Table 7.4. The regenerated catalyst chosen for this study is the R4800 (0.5h) and R4800 (1h) as these 2 are the most promising ones from the regeneration studies.

Table 7.4 Regeneration Studies and Surface Area Measurements

		BET Surface Area		External Surface Area	
		BET (m2/g cat)	Loss (%)	Ext. (m2/g cat)	Loss (%)
Regen Stock	Coked Cat	189.2	-50.0	35.07	-75.0
R4800(0.5h)	Regenerated	316.8	-16.0	118.3	-15.0
	Spend	205.2	-46.0	40.89	-71.0
R4800(1h)	Regenerated	352.1	-8.0	120.4	-13.0
	Spend	209.7	-46.0	42.16	-70.0
Control	Activated	381.0	0.0	138.8	0.0
	Spend	204.6	-46.0	49.7	-64.0

Taking the freshly activated value for BET and external SA of the control as base, the % loss was calculated for all the rest.

From Table 7.4 it can be seen that the BET SA for R4800 (0.5h) and R4800 (1h) can be successfully regenerated to retain 84 and 92% respectively of the original activated value. The retainable external SA for R4800 (0.5h) and R4800 (1h) on the other hand is slightly less than the BET SA which amounts to 87 and 85% respectively.

From these observations it can be seen that the BET and external SA can be quite easily regained at high GHSV and with dwell time of 1 hour. This may explain the increased catalytic activity for these regenerated catalysts.

As for the spent catalyst from Table 7.4, a different scenario is observed for the BET and external SA. Loss in BET SA for all three types of spent catalyst are quite similar, but for the external SA the loss in higher in the regenerated catalyst than that of the control. This may be one of the reasons for the high coke yield seen for the regenerated catalysts.

7.6 Conclusions

From the above process conditions, observation and evaluation, it can be seen that it is possible for the regenerated catalyst to regain its initial catalytic activity, but the product selectivity is favoured more towards the coke formation rather than the favoured aromatic yield and selectivity.

7.8 Chapter 7 References

1. Liu, S., Don, Q., Ohnishi, R., and Ichikawa., Chem. Commun, (1998) 1217
2. Ohnishi, R., Liu, S.T., Dong, Q., Wang, L.S., and Ichikawa, M., J. Catal.182 (1999) 92
3. Shu, Y., Ohnishi, R., and Ichikawa, M., J. Catal. 206 (2002) 134
4. Ma, H., Ohnishi, R., and Ichikawa.,M., Catal. Letts. 89 (2003) 143
5. Liu, Z., Nutt, M.A., and Iglesia, E., Catal. Lett. 81 (2002) 271
6. Yuan, S., Li, J., Hao, Z., Feng, Z., Xin, Q., Ying, P., and Li, C., Catal. Letts. 63 (1999) 73
7. Tan, P.L., Leung, Y.L., Lai, S.Y., and Au, C.T., Catal. Lett. 78 (2002) 251

CHAPTER 8 General Conclusions

Since reported by Wang et al in 1993 on the direct conversion of methane under non-oxidative conditions, a number of facts have been established. Mo modified HZSM-5 prepared by impregnation by ammonium heptamolybdate tetrahydrate [$(NH_4)_6Mo_7O_{24}.4H_2O$] is the best route to prepare the catalyst. It is also believed that the Mo/HZSM-5 catalyst is a bi-functional catalyst. The active component is believed to be the Mo-carbide which is capable in activating methane and the Bronsted Acid Sites which oligomerise and dehydrocyclise the intermediate species produced by methane activation to aromatics. Mo-carbide is believed to provide the high stability required for this high temperature reaction and also balances the hydrogenolysis and dehydrogenation functions of the catalyst. Catalytic deactivation is thought to occur by the deposition of unreactive coke usually in the vicinity of the acid sites, which hinders or blocks the zeolite pores. Based on this, the conclusion of the present study is broken down into 4 different sections:

8.1 Optimisation of process variables

8.2 Interaction between the active Mo species and the zeolite support

8.3 Active sites (active phases)

8.4 Role of CO on carbonaceous deposits and regeneration

8.1 OPTIMISATION OF PROCESS VARIABLES

8.1.1 Gas Hourly Space Velocity (GHSV)

For the MDA reaction optimisation of aromatic and minimising coke build up is the main criterion. Coke deposition deactivates the catalyst by blocking pore access of the reactant and product to the active site, at the same time it also deactivates the catalytic active sites leading to low aromatic yield. In order to have a good balance between the aromatic

production and reduced coke build-up in the system, a good GSHV is important. From the present study a GHSV of 1500 h^{-1} was most promising, because apart from being more reactive it produces high aromatic yield and moderate coke deposit. Further it does not affect the structure of the catalyst based on XRD studies.

8.2 INTERACTION BETWEEN THE ACTIVE Mo SPECIES AND THE ZEOLITE SUPPORT

8.2.1 Mo Loading

The interaction of active Mo species with the HZSM-5 zeolite is crucial for optimization of catalytic activity. A good balance between the dehydrogenation component i.e. the Mo active species and the Bronsted acid sites is also important. Altering the % of Mo content or the Si/Al ratio of the HZSM-5 zeolite will also alter the BAS in the catalyst system. Improved catalytic activity can be achieved by having well dispersed active Mo species on/within the zeolite which also improves catalytic stability. The driving force for Mo dispersion is closely related to the acidity of the zeolite. Low Mo loading results in minimum interaction leading to low methane conversion. Too high Mo loading will result in extraction of framework aluminium to form extra framework Al first and then $Al_2(MoO_4)_3$ crystallite which is believed to be inactive for MDA reaction. Based on the present investigation on the hcp β-Mo_2C and fcc α-MoC_{1-x}, a Mo loading of 10wt% is found to be the most favourable catalytic loading for MDA for both systems.

8.2.2 Calcination

The main function of calcination is the redistribution of MoO_3 species over the catalyst surface and into the channels or pore of the zeolite. The degree of MoO_3 crystallites migration and disperse depends on the calcination temperature. Optimum calcination temperatures will results

in good dispersion of MoO_3 species and stronger interaction between them and the HZSM-5 zeolite. This will lead to a more stable chemical environment which reduces or prevents the sublimation of MoO_3 species. Low calcination temperature limits MoO_3 migration, whereas high temperature can result in de-alumination and loss of HZSM-5 crystallinity resulting in loss of acidic protons which is detrimental to methane activation. Effect of calcination temperatures on the Mo modified HZSM-5 zeolite was carried out on 2 kinds of the active Mo-carbide species namely the hcp β-Mo_2C and fcc α-MoC_{1-X} for MDA reactions. For the hcp β-Mo_2C 600°C was the desired calcination temperature while for the α-MoC_{1-X} it was 500°C.

8.3 ACTIVE SITES (OR ACTIVE PHASES)

Reduction and carburisation of the Mo species follows after calcination. This step is important to convert the MoO_3 species to the Mo carbide species which is known to be responsible for methane activation. During this process the active species may be contaminated with carbon which may result in site blockage of the methane feed. Improved catalytic activity and stability can be achieved by improve excess of reactants to the active sites and to the surface of the catalyst. Two kinds of Mo carbide have been reported to be active, namely the hcp β-Mo_2C and the fcc α-MoC_{1-X}. Alpha and beta forms can be produced by different preparation routes. It was observed that the hcp β-Mo_2C have higher methane conversion than the fcc α-MoC_{1-x} group of catalysts under the same reaction conditions. The higher catalytic activity for hcp β-Mo_2C catalyst is attributed by the higher coke formation as compared to its fcc α-MoC_{1-x} counterpart which has lower coke yield and selectivity but higher aromatic yield and selectivity at lower calcination temperature

8.4 CATALYTIC STABILITY AND REGENERATION

8.4.1 Effect of CO Dosing

The main cause of deactivation in MDA reaction is coke build up on the catalyst. The exact nature of the coke deposit which causes catalytic deactivation is still unclear. The general consensus is that restricting coke build up can delay catalytic deactivation and at the same time enhanced catalytic activity as claimed by some researchers. One of the techniques used to suppress coke build up is to co-feed CO with methane. From the analysis based on preset of conditions, it can be seen that correct CO dosing does improve the catalytic activities and stability but it has a higher positive effect towards higher Mo of 10wt% rather than for lower loading of 3wt%. The optimum CO dosing level for the 10wt% α-MoC_{1-x} is 4%, while for 10 wt% hcp β-Mo_2C is 12% based on the scope of study.

8.4.2 Regeneration

In order for a reaction to be extended to industrial prospect, a suitable or economical catalytic regeneration system is necessary. This area is the least investigated topic in MDA reactions. Regeneration can be carried out by incorporating air as a source of oxygen. From the investigation, it was found that regenerating the coked catalyst with 5% oxygen at a GHSV of 4800h^{-1} over 1 hour made it possible for the catalyst to regain its initial catalytic activity, but the product selectivity is favoured more towards that of coke formation rather than the favoured aromatic yield.

Appendix 1

Table Released: October 19, 2005

Next Release: When updated proved reserve estimates become available.

Notes and Sources for Table of World Proved Oil and Natural Gas Reserves, Most Recent Estimates

Important Note on Sources of Foreign Reserve Estimates

Reserve estimates for oil, natural gas, and coal are very difficult to develop. The Energy Information Administration (EIA) develops estimates of reserves of oil, natural gas, and coal for the United States but does not attempt to develop estimates for foreign countries. As a convenience to the public, EIA makes available foreign fuel reserve estimates from other sources, but it does not certify these data. Please carefully note the sources of the data when using and citing estimates of foreign fuel reserves.

Notes and Sources

[1] Proved reserves are estimated quantities that analysis of geologic and engineering data demonstrates with reasonable certainty are recoverable under existing economic and operating conditions.

[2] BP p.l.c., BP Statistical Review of World Energy June 2005, except United States. Oil includes crude oil, gas condensate, and natural gas liquids. United States oil data, including both crude oil and natural gas liquids, and United States natural gas data are from the Energy Information Administration, Advance Summary, U.S. Crude Oil, Natural Gas, and Natural Gas Liquids Reserves, 2004 Annual Report, DOE/EIA-0216(2004) Advance Summary (September 2005). BP notes that "the figure for Canadian oil reserves includes an official estimate of Canadian

oil sands "under active development"." BP says of its data sources for oil reserves that "the estimates in this table have been compiled using a combination of primary official sources, third-party data from the OPEC Secretariat, World Oil, Oil & Gas Journal and an independent estimate of Russian reserves based on information in the public domain. Likewise for natural gas reserves, BP states that "the estimates in this table have been compiled using a combination of primary official sources, third-party data from Cedigaz, the OPEC Secretariat and Oil & Gas Journal. BP also notes that "the reserves figures shown do not necessarily meet the United States Securities and Exchange Commission definitions and guidelines for determining proved reserves nor necessarily represent BP's view of proved reserves by country."

[3] PennWell Corporation, Oil & Gas Journal, Vol. 102, No. 47 (December 20, 2004). Oil includes crude oil and condensate. Data for the United States are the same as those from the Energy Information Administration, Advance Summary, U.S. Crude Oil, Natural Gas, and Natural Gas Liquids Reserves, 2004 Annual Report, DOE/EIA-0216(2004) Advance Summary (September 2005). Oil & Gas Journal's oil reserve estimate for Canada includes 4.3 billion barrels of conventional crude oil and condensate reserves and 174.5 billion barrels of oil sands reserves.

[4] Gulf Publishing Co., World Oil, Vol. 226, No.9 (September 2005), except United States. Oil includes crude oil and condensate but excludes natural gas liquids. Data for the United States are from the Energy Information Administration, Advance Summary, U.S. Crude Oil, Natural Gas, and Natural Gas Liquids Reserves, 2004 Annual Report, DOE/EIA-0216(2004) Advance Summary (September 2005). World Oil's Canadian oil reserve estimate "does not include 174 billion bbl [barrels] of oil sands reserves."

[5] Centre International d'Information sur le Gaz Naturel et tous Hydrocarbures Gazeux (CEDIGAZ), Natural Gas in the World, Major Trends for the Gas Industry July 2005 (Electronic Database), except United States. Data converted from cubic meters to cubic feet at 35.315 cubic feet per cubic meter. United States data are from the Energy Information Administration, Advance Summary, U.S. Crude Oil, Natural Gas, and Natural Gas Liquids Reserves, 2004 Annual Report, DOE/EIA-0216(2004) Advance Summary (September 2005).

[6] Reserve estimates for Kuwait and Saudi Arabia include one-half of the reserves in the Neutral Zone, if separately reported.
Sum of components may not equal total due to independent rounding.